Exploring the divergence: the neurovascular unit in the eye and brain in diabetes and Alzheimer´s disease

Noëlle Bakker

ISBN: 978-94-6537-248-8

The research described in this thesis was financially supported by the RECOGNISED consortium, that has received funding from the European Union's Horizon 2020 research and innovation programme; Algemene Nederlandse Vereniging ter Voorkoming van Blindheid; Leidse Stichting voor Blinden en Slechtzienden; Stichting Oogfonds that contributed through UitZicht; the Rotterdamse Stichting Blindenbelangen; Stichting tot Verbetering van het Lot der Blinden; European Research Council; the Encouraging European Research (EER) regulation of The Dutch Research Council. Printing of this thesis was financially supported by Koninklijke Stichting Blindenhulp and Landelijke Stichting voor Blinden en Slechtzienden.

Cover: immunofluorescence staining of human retinal vasculature. The vasculature was stained for laminin and pericytes were stained for platelet-derived growth factor receptor beta and alpha-smooth muscle actin.

Lay-out and cover design: Noëlle Bakker
Printing: Ridderprint |www.ridderprint.nl

Exploring the divergence: the neurovascular unit in the eye and brain in diabetes and Alzheimer´s disease

ACADEMISCH PROEFSCHRIFT

ter verkrijging van de graad van doctor
aan de Universiteit van Amsterdam
op gezag van de Rector Magnificus
prof. dr. ir. P.P.C.C. Verbeek
ten overstaan van een door het College voor Promoties ingestelde commissie,
in het openbaar te verdedigen in de Agnietenkapel
op donderdag 30 april 2026, te 16.00 uur

door Noëlle Bakker
geboren te Alkmaar

Promotiecommissie

Promotor:	prof. dr. R.O. Schlingemann	AMC-UvA
Copromotores:	dr. I. Klaassen	AMC-UvA
	prof. dr. C.J.F. van Noorden	AMC-UvA
Overige leden:	prof. dr. E.M.A. Aronica	AMC-UvA
	prof. dr. C.J.M. de Vries	AMC-UvA
	prof. dr. H. Tan	Vrije Universiteit Amsterdam
	prof. dr. E.A.J. Reits	AMC-UvA
	prof. dr. E.T. van Bavel	AMC-UvA
	prof. dr. F.A.C. le Noble	Karlsruhe Instituut of Technology

Faculteit der Geneeskunde

Table of contents

Chapter 1

General introduction and scope of the thesis

The blood-retinal barrier and blood-brain barrier

The retina and brain are the most energy-demanding tissues in the body due to the high metabolic requirements of neuronal tissue and the dark adaptation function of the rod photoreceptors [1-3]. In addition, neuronal tissues require a tightly regulated microenvironment for proper function. For this purpose, the retina and brain possess specialized blood vessels with a highly selective barrier that ensures adequate delivery of oxygen, glucose and other blood-borne components, removal of waste products, and protection of neuronal tissue by limiting the free transport of molecules and cells across the barrier. The barriers in the retina and brain are called blood-retinal barrier (BRB) and blood-brain barrier (BBB), respectively, and they are formed by cellular and extracellular components [2, 4, 5]. In the retina, there is an outer and inner BRB. The outer BRB is guaranteed by tight junctions between the retinal pigment epithelial cells that separate the neural retina from the choroid. The inner BRB and BBB consist of capillary endothelial cells that form the vasculature and are also interconnected by tight junctions, lack fenestrations and have few pinocytotic vesicles.

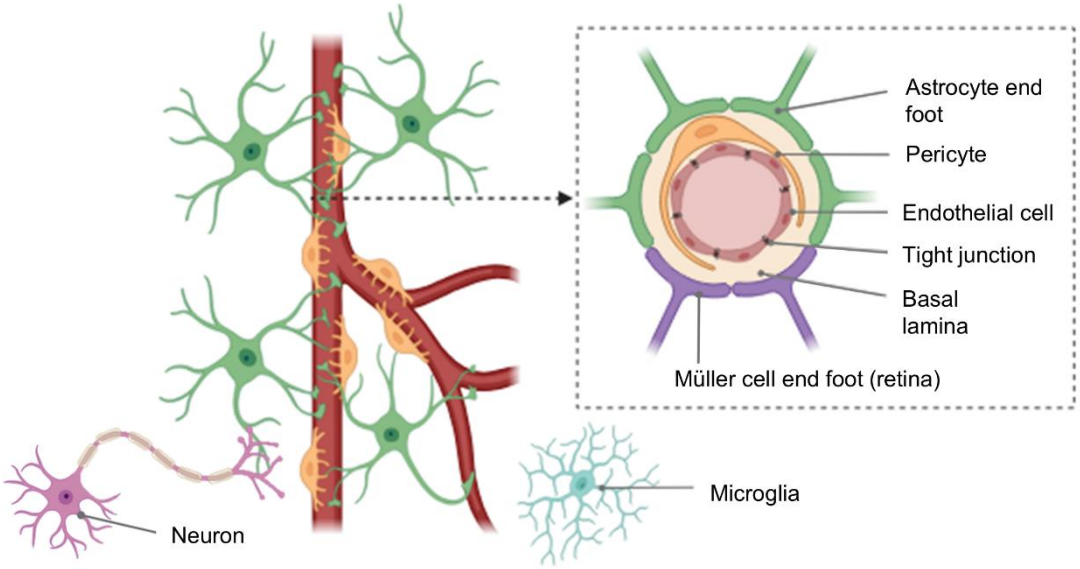

Figure 1. Schematic illustration of the neurovascular unit in the eye and brain. The blood-retinal barrier and blood-brain barrier are formed by endothelial cells that are connected by tight junctions. Endothelial cells are lining capillaries and are surrounded by pericytes, sharing the basal lamina. End feet of astrocytes and Müller cells (retina) are projected onto the capillaries. Endothelial cells, pericytes, macroglia (astrocytes and Müller cells), microglia, and surrounding neurons together form the neurovascular unit. Created with BioRender.com.

The neurovascular unit in the eye and brain

The barrier properties are regulated by the neurovascular unit (NVU), a complex, multicellular structure composed of endothelial cells, pericytes, macroglia, microglia, and neurons (Figure 1) [4-9]. Pericytes are perivascular cells that tightly wrap around capillaries, thereby partially covering the capillary wall [5, 10-15].

Pericytes are surrounded by basal lamina and share the basal lamina with endothelial cells. Pericytes form direct contacts with endothelial cells through peg-socket contacts and

adhesion plaques and communicate through autocrine and paracrine regulation and modulation of the basal lamina [10]. Pericytes are crucial for vascular development, maturation, remodelling and maintenance, for regulation of blood flow, for clearing of harmful metabolites in the extracellular matrix and for regulation of transcytosis, astrocyte end feet polarization, and tight junction protein expression. The importance of pericytes in the eye and brain is reflected by the high prevalence of pericytes in the retina and brain in comparison with other organs. The pericyte-to-endothelial cell ratio ranges from 1:1 to 1:3, in contrast to the ratio of 1:10 to 1:100 observed in other capillaries throughout the body [10, 16].

Macroglia project their end feet onto the basal lamina that is directly surrounding pericytes [5, 7]. In the brain NVU, macroglial cells are represented by astrocytes, while in the retina, both astrocytes and Müller cells are present, with Müller cells being exclusive to the retinal tissue [5, 7, 17-19]. Müller cells have radial processes that span the width of the neural retina. Astrocytes are mostly located in the nerve fibre layer of the retina and are the most abundant cell type in the human central nervous system. Macroglia are considered to play a critical role in barrier permeability regulation, structural support for neuronal cells and maintenance of the balance of water, ions, and neurotransmitters. Additionally, macroglia are involved in the regulation of immune cell entry, blood flow, the supply of nutrients, and the removal of waste products.

Microglia, which are unrelated to macroglia, are the resident immune cells of the central nervous system [4, 6]. Microglia perform continuous surveillance in the tissues and remove dying cells and metabolic debris by phagocytosis. Microglia produce anti-inflammatory cytokines and neurotrophic factors to protect neuronal tissue but can also secrete high levels of pro-inflammatory cytokines during pathology.

Neurons in the retina include photoreceptors, ganglion cells, bipolar cells, horizontal cells, and amacrine cells [6, 20]. The light signals are converted into electrical signals by photoreceptors, and the other retinal neurons process and transmit these signals to the brain via the optic nerve. In the brain, there is a wide variety of neuronal types classified by function, structure, and molecular signatures [21]. To ensure an adequate supply of nutrients and oxygen, both organs regulate local blood supply in response to neuronal activity, which is called neurovascular coupling [22, 23]. Neurovascular coupling involves complex interactions between neurons, astrocytes, Müller cells, endothelial cells, smooth muscle cells, and pericytes. Neurons can directly act on pericytes of capillaries and smooth muscle cells of arterioles via the production of nitric oxide, leading to vasodilation. Upon activation, neurons can also release vasoactive agents. Astrocytes and Müller cells detect the neuronal activity and transmit signals to smooth muscle cells and pericytes through a series of molecular events. Specifically, these cells initiate a cascade of signalling pathways that lead to hyperpolarization of their end-feet on the vascular wall, resulting in the relaxation of capillaries and arterioles. Taken together, the NVU in both the eye and brain exhibit similar structural and functional characteristics.

The eye and brain in diabetes

Diabetes is characterized by abnormal glucose metabolism having deleterious effects on the systemic vasculature [24]. A common microvascular complication associated with chronic

hyperglycaemia is diabetic retinopathy (DR) [25], a leading cause of blindness among the working-age population. DR is characterized by retinal vascular abnormalities, including increased vessel tortuosity, capillary occlusion and dropout, microaneurysms, haemorrhages, lipid exudates, increased vascular permeability, cotton-wool spots and in a later stage neovascularization [26-28]. Prior to the appearance of these overt abnormalities, subtle changes occur in the BRB, including basal lamina thickening, loss of pericytes and endothelial cells, disruption of tight junction complexes, and an increase in the number of transport vesicles within endothelial cells [5, 29-31]. Macular edema can develop early and late in DR and can lead to significant vision loss [32]. In addition to microvascular complications, DR is also characterized by neurodegeneration [26, 29, 33], particularly ganglion cell apoptosis in the inner retina [29, 34]. Notably, neuronal and Müller cell death precede the loss of pericytes and endothelial cells [29, 35-43], although these changes are not visible with optical coherence tomography until they become more widespread in the retina [36-39, 44-46]. Neurovascular coupling dysfunction is also a common feature in DR [23] and may form a link between the neurodegenerative and vascular features.

Despite the similarities in the NVU between the eye and brain, and their shared embryonic origin [47], there is no equivalent of DR in the brain, the reasons of which are still unclear. Possible explanations are specific metabolic or vascular characteristics of the retina, and/or activation of compensatory mechanisms in the brain that prevent the development of DR-like changes. In diabetes, cerebral vascular abnormalities are generally limited to capillary basal lamina thickening [48-51] and alterations in vessel tortuosity and capillary density [49, 52]. Microbleeds [53], white matter lesions, and lacunes [54] have been reported in the brains of diabetic individuals, but these may represent vascular damage of larger order vessels. A correlation has been reported between retinal vessel density and structural abnormalities in cerebral vasculature in individuals with type 2 diabetes [55]. However, no direct association has been identified between retinal microvascular changes/DR and such small vessel dysfunction in the brain [56]. Moreover, no evidence of pericyte loss, a hallmark of DR, has been observed in the cerebral vasculature of diabetic patients [57, 58]. Hyperglycaemia and insulin resistance can induce oxidative stress and inflammation in the brain, contributing to neuronal apoptosis [59, 60]. Atrophy has been observed in several brain regions in diabetic patients [61-67], and may represent an equivalent of the neurodegeneration known to occur in the retina independently from DR. In line with this, type 2 diabetes is also associated with cognitive impairment, including deficits in attention, memory, executive function, and emotional processing, and is a known risk factor for true dementia, including Alzheimer's disease (AD) [4, 68]. This increased risk persists even after adjusting for vascular risk factors [69, 70]. The precise mechanisms underlying these functional and structural changes in the brain, whether due to microvasculopathy [53, 71-74], direct hyperglycaemic effects [75, 76], or fluctuations in glucose levels [77], remain debated. Differences in glucose uptake rates between endothelial cells in the retina and brain may contribute to the distinct pathologies observed in these tissues [78-80]. However, the biological mechanisms driving these changes in the brain remain incompletely understood.

The eye and brain in Alzheimer's disease

AD is an age-related neurodegenerative disorder characterized by progressive cognitive decline [81, 82]. With the increasing life expectancy, the number of patients suffering from AD is expected to rise worldwide, posing a major health and societal burden [81]. Heritability

accounts for 60-80% of the risk for developing AD [83, 84], with type 2 diabetes also identified as a risk factor [4]. However, it is unknown whether the presence of DR is an additional risk factor, and the relationship between DR and AD remains debated [85-87]. Pathological changes in the brain, including extracellular accumulation of amyloid-beta (Aβ) plaques and intracellular tau tangles, begin long before clinical symptoms of AD emerge [88-91]. Aβ plaques and neurofibrillary tangles can cause synaptic dysfunction and neuronal loss [90, 91]. However, these pathological hallmarks have also been found in normal aging [92]. Significant atrophy of the cerebral cortex, amygdala, hippocampus and parahippocampus is associated with AD because of high susceptibility to neuronal degeneration in these regions [91, 93-95]. In contrast, regions like the striatum and cerebellum do not show similar neuronal pathology, although these regions show some degree of plaque formation. Cerebral vascular alterations also occur in AD, including changes in vascular density, basal lamina thickening, BBB dysfunction, and cerebral amyloid angiopathy, contributing to microbleeds, lacunes, and infarcts [4, 96, 97]. In addition, widespread astrocyte activation [98-101] and pericyte loss across multiple brain regions [14, 101-108] have been observed in the human AD brain.

Although less widely recognized, both vascular abnormalities and neurodegeneration occur in the retina of patients with AD. Retinal vascular abnormalities in AD include narrowing of the veins [109] and venules [110], altered venular structure [110, 111], reduced blood flow [109, 112], and both increased [110, 113] and decreased [111] tortuosity have been suggested. Some studies reported an association between alterations in the retinal vasculature and vascular dementia, but not between alterations in the retinal vasculature and AD [114-116]. Retinal vascular changes have been previously associated with retinal Aβ plaque burden [111]. In several mouse models of AD, Aβ and tau accumulations have been observed in the retina, but findings in human studies are inconsistent [117], questioning the relevance of retinal findings in these mouse models. Retinal neurodegeneration, such as retinal ganglion cell loss and thinning of the retinal nerve fibre layer, has been identified in AD [117-120]. A better understanding of the biological mechanisms underlying AD pathology in both the retina and brain, and in particular the role of the microvasculature and the blood-tissue barriers, is essential for improving understanding of AD, its diagnosis, monitoring, and for expanding treatment options.

Scope of the thesis

The studies presented in this thesis are primarily aimed at understanding changes in the NVU in the retina and brain in the context of type 2 diabetes and its increased risk of AD. First, we have worked on improving and developing new model systems in this context. For this purpose, zebrafish are an ideal *in vivo* model for studying changes within the NVU due to their optical transparency, small size, rapid reproduction, and suitability for genetic editing, offering advantages over larger animal models for real-time studies and high-throughput research. In **Chapter 2**, we describe a zebrafish model which represents a multimodal toolbox for visualizing and quantifying barrier permeability, protein expression, and ultrastructure in the brain. It provides a valuable foundation for using a zebrafish model to investigate the molecular mechanisms of BBB disruption in various pathological conditions, with direct implications for studies of diabetic macular edema and other neurovascular diseases. Such animal models facilitate longitudinal studies of the structure and function of the NVU, as demonstrated in **Chapter 3**, which details alterations in the retina of an

established transgenic AD mouse model during disease progression, with a focus on changes in the JNK signalling pathway, synaptic integrity, gliosis, and amyloid pathology. In the following chapter, the focus shifts to a broader examination of retinal and cerebral neurovascular changes in human AD as well as type 2 diabetes. **Chapter 4** describes human retinal and cerebral neurovascular changes in type 2 diabetes and AD, including assessment of vascular permeability, tight junction integrity, transcytosis, macroglial reactivity and functionality, and pericyte coverage. Increased vascular permeability can be attributed to dysfunctional transcellular and paracellular transport. We further explored the changes in pericytes associated with type 2 diabetes and further progression into DR in the retina, and the brain in type 2 diabetes and AD. **Chapter 5** describes the development of an immunofluorescence staining methodology for 3D reconstruction of pericytes in human retinal flatmounts. Using flatmounts, rather than tissue sections, enhances spatial information by allowing visualisation of pericyte distribution across the entire retinal vascular network. The newly developed immunofluorescence staining protocol is used to examine pericyte characteristics in the retina in type 2 diabetes and further progression into DR, as well as in the brain in diabetes and AD, as described in **Chapter 6**. Immunofluorescence staining for several pericyte markers is performed to assess marker expression, vascular staining coverage, and cellular pericyte density in capillaries. These pericyte characteristics were compared between the retina and brain to explore similarities and differences in pericyte pathology across the studied conditions. **Chapter 7** discusses the novel findings of this thesis in the context of the current literature and outlines potential directions for future research.

References

[1] Bakdalieh A, Khawaja LM, Yu M (2025) Dark Adaptometry as a Diagnostic Tool in Retinal Diseases: Mechanisms and Clinical Utility. J Clin Med 14(11). doi: 10.3390/jcm14113742

[2] Diaz-Coranguez M, Ramos C, Antonetti DA (2017) The inner blood-retinal barrier: Cellular basis and development. Vision Res 139: 123–137. doi: 10.1016/j.visres.2017.05.009

[3] Wong-Riley MT (2010) Energy metabolism of the visual system. Eye Brain 2: 99–116. doi: 10.2147/EB.S9078

[4] Little K, Llorian-Salvador M, Scullion S, Hernandez C, Simo-Servat O, Del Marco A, et al. (2022) Common pathways in dementia and diabetic retinopathy: understanding the mechanisms of diabetes-related cognitive decline. Trends Endocrinol Metab 33(1): 50–71. doi: 10.1016/j.tem.2021.10.008

[5] Klaassen I, Van Noorden CJ, Schlingemann RO (2013) Molecular basis of the inner blood-retinal barrier and its breakdown in diabetic macular edema and other pathological conditions. Prog Retin Eye Res 34: 19–48. doi: 10.1016/j.preteyeres.2013.02.001

[6] Nian S, Lo ACY, Mi Y, Ren K, Yang D (2021) Neurovascular unit in diabetic retinopathy: pathophysiological roles and potential therapeutical targets. Eye Vis (Lond) 8(1): 15. doi: 10.1186/s40662-021-00239-1

[7] O'Brown NM, Pfau SJ, Gu C (2018) Bridging barriers: a comparative look at the blood-brain barrier across organisms. Genes Dev 32(7-8): 466–478. doi: 10.1101/gad.309823.117

[8] Rowsthorn E, Pham W, Nazem-Zadeh MR, Law M, Pase MP, Harding IH (2023) Imaging the neurovascular unit in health and neurodegeneration: a scoping review of interdependencies between MRI measures. Fluids Barriers CNS 20(1): 97. doi: 10.1186/s12987-023-00499-0

[9] Yu X, Ji C, Shao A (2020) Neurovascular Unit Dysfunction and Neurodegenerative Disorders. Front Neurosci 14: 334. doi: 10.3389/fnins.2020.00334

[10] Armulik A, Genove G, Betsholtz C (2011) Pericytes: developmental, physiological, and pathological perspectives, problems, and promises. Dev Cell 21(2): 193–215. doi: 10.1016/j.devcel.2011.07.001

[11] Caporarello N, D'Angeli F, Cambria MT, Candido S, Giallongo C, Salmeri M, et al. (2019) Pericytes in Microvessels: From "Mural" Function to Brain and Retina Regeneration. Int J Mol Sci 20(24). doi: 10.3390/ijms20246351

[12] Ferland-McCollough D, Slater S, Richard J, Reni C, Mangialardi G (2017) Pericytes, an overlooked player in vascular pathobiology. Pharmacol Ther 171: 30–42. doi: 10.1016/j.pharmthera.2016.11.008

[13] Huang H (2020) Pericyte-Endothelial Interactions in the Retinal Microvasculature. Int J Mol Sci 21(19). doi: 10.3390/ijms21197413

[14] Li P, Fan H (2023) Pericyte Loss in Diseases. Cells 12(15). doi: 10.3390/cells12151931

[15] van Noorden CJF, Yetkin-Arik B, Martinez PS, Bakker N, Smallenburg MEV, Schlingemann RO, et al. (2024) New Insights in ATP Synthesis as Therapeutic Target in Cancer and Angiogenic Ocular Diseases. J Histochem Cytochem 72(5): 329–352. doi: 10.1369/00221554241249515

[16] Shepro D, Morel NM (1993) Pericyte physiology. FASEB J 7(11): 1031–1038. doi: 10.1096/fasebj.7.11.8370472

[17] de Hoz R, Rojas B, Ramirez AI, Salazar JJ, Gallego BI, Trivino A, et al. (2016) Retinal Macroglial Responses in Health and Disease. Biomed Res Int 2016: 2954721. doi: 10.1155/2016/2954721

[18] Manu DR, Slevin M, Barcutean L, Forro T, Boghitoiu T, Balasa R (2023) Astrocyte Involvement in Blood-Brain Barrier Function: A Critical Update Highlighting Novel, Complex, Neurovascular Interactions. Int J Mol Sci 24(24). doi: 10.3390/ijms242417146

[19] Wei DC, Morrison EH (2025) Histology, Astrocytes. In: StatPearls, Treasure Island (FL)

[20] Grimes WN, Berson DM, Sabnis A, Hoon M, Sinha R, Tian H, et al. (2025) Layer-specific anatomical and physiological features of the retina's neurovascular unit. Curr Biol 35(1): 109–120 e104. doi: 10.1016/j.cub.2024.11.023

[21] Zeng H, Sanes JR (2017) Neuronal cell-type classification: challenges, opportunities and the path forward. Nat Rev Neurosci 18(9): 530–546. doi: 10.1038/nrn.2017.85
[22] Feng L, Gao L (2024) The role of neurovascular coupling dysfunction in cognitive decline of diabetes patients. Front Neurosci 18: 1375908. doi: 10.3389/fnins.2024.1375908
[23] Garhofer G, Chua J, Tan B, Wong D, Schmidl D, Schmetterer L (2020) Retinal Neurovascular Coupling in Diabetes. J Clin Med 9(9). doi: 10.3390/jcm9092829
[24] Cheung N, Wong TY (2008) Diabetic retinopathy and systemic vascular complications. Prog Retin Eye Res 27(2): 161–176. doi: 10.1016/j.preteyeres.2007.12.001
[25] Wong TY, Sabanayagam C (2019) The War on Diabetic Retinopathy: Where Are We Now? Asia Pac J Ophthalmol (Phila) 8(6): 448–456. doi: 10.1097/APO.0000000000000267
[26] Barot M, Gokulgandhi MR, Patel S, Mitra AK (2013) Microvascular complications and diabetic retinopathy: recent advances and future implications. Future Med Chem 5(3): 301–314. doi: 10.4155/fmc.12.206
[27] Lee H, Lee M, Chung H, Kim HC (2018) Quantification of Retinal Vessel Tortuosity in Diabetic Retinopathy Using Optical Coherence Tomography Angiography. Retina 38(5): 976–985. doi: 10.1097/IAE.0000000000001618
[28] Cai J, Boulton M (2002) The pathogenesis of diabetic retinopathy: old concepts and new questions. Eye (Lond) 16(3): 242–260. doi: 10.1038/sj.eye.6700133
[29] Barber AJ, Gardner TW, Abcouwer SF (2011) The significance of vascular and neural apoptosis to the pathology of diabetic retinopathy. Invest Ophthalmol Vis Sci 52(2): 1156–1163. doi: 10.1167/iovs.10-6293
[30] Hammes HP, Feng Y, Pfister F, Brownlee M (2011) Diabetic retinopathy: targeting vasoregression. Diabetes 60(1): 9–16. doi: 10.2337/db10-0454
[31] Lorenzi M, Gerhardinger C (2001) Early cellular and molecular changes induced by diabetes in the retina. Diabetologia 44(7): 791–804. doi: 10.1007/s001250100544
[32] Cunha-Vaz J, Mendes L, Reste-Ferreira D (2025) Understanding nonproliferative diabetic retinopathy progression using noninvasive imaging. Eye (Lond) 39(14): 2627–2634. doi: 10.1038/s41433-025-03901-3
[33] Simo R, Stitt AW, Gardner TW (2018) Neurodegeneration in diabetic retinopathy: does it really matter? Diabetologia 61(9): 1902–1912. doi: 10.1007/s00125-018-4692-1
[34] Lynch SK, Abramoff MD (2017) Diabetic retinopathy is a neurodegenerative disorder. Vision Res 139: 101–107. doi: 10.1016/j.visres.2017.03.003
[35] Peng RP, Zhu ZQ, Shen HY, Lin HM, Zhong L, Song SQ, et al. (2022) Retinal Nerve and Vascular Changes in Prediabetes. Front Med (Lausanne) 9: 777646. doi: 10.3389/fmed.2022.777646
[36] Vujosevic S, Midena E (2013) Retinal layers changes in human preclinical and early clinical diabetic retinopathy support early retinal neuronal and Muller cells alterations. J Diabetes Res 2013: 905058. doi: 10.1155/2013/905058
[37] van Dijk HW, Verbraak FD, Kok PH, Stehouwer M, Garvin MK, Sonka M, et al. (2012) Early neurodegeneration in the retina of type 2 diabetic patients. Invest Ophthalmol Vis Sci 53(6): 2715–2719. doi: 10.1167/iovs.11-8997
[38] De Clerck EEB, Schouten J, Berendschot T, Goezinne F, Dagnelie PC, Schaper NC, et al. (2018) Macular thinning in prediabetes or type 2 diabetes without diabetic retinopathy: the Maastricht Study. Acta Ophthalmol 96(2): 174–182. doi: 10.1111/aos.13570
[39] van Dijk HW, Verbraak FD, Stehouwer M, Kok PH, Garvin MK, Sonka M, et al. (2011) Association of visual function and ganglion cell layer thickness in patients with diabetes mellitus type 1 and no or minimal diabetic retinopathy. Vision Res 51(2): 224–228. doi: 10.1016/j.visres.2010.08.024
[40] Abu El-Asrar AM, Dralands L, Missotten L, Geboes K (2007) Expression of antiapoptotic and proapoptotic molecules in diabetic retinas. Eye (Lond) 21(2): 238–245. doi: 10.1038/sj.eye.6702225
[41] Mizutani M, Gerhardinger C, Lorenzi M (1998) Muller cell changes in human diabetic retinopathy. Diabetes 47(3): 445–449. doi: 10.2337/diabetes.47.3.445

[42] Villarroel M, Ciudin A, Hernandez C, Simo R (2010) Neurodegeneration: An early event of diabetic retinopathy. World J Diabetes 1(2): 57–64. doi: 10.4239/wjd.v1.i2.57
[43] Simo R, Hernandez C, European Consortium for the Early Treatment of Diabetic R (2012) Neurodegeneration is an early event in diabetic retinopathy: therapeutic implications. Br J Ophthalmol 96(10): 1285–1290. doi: 10.1136/bjophthalmol-2012-302005
[44] Chihara E, Matsuoka T, Ogura Y, Matsumura M (1993) Retinal nerve fiber layer defect as an early manifestation of diabetic retinopathy. Ophthalmology 100(8): 1147–1151. doi: 10.1016/s0161-6420(93)31513-7
[45] van Dijk HW, Kok PH, Garvin M, Sonka M, Devries JH, Michels RP, et al. (2009) Selective loss of inner retinal layer thickness in type 1 diabetic patients with minimal diabetic retinopathy. Invest Ophthalmol Vis Sci 50(7): 3404–3409. doi: 10.1167/iovs.08-3143
[46] Lim HB, Shin YI, Lee MW, Park GS, Kim JY (2019) Longitudinal Changes in the Peripapillary Retinal Nerve Fiber Layer Thickness of Patients With Type 2 Diabetes. JAMA Ophthalmol 137(10): 1125–1132. doi: 10.1001/jamaophthalmol.2019.2537
[47] Cheung CY, Ikram MK, Chen C, Wong TY (2017) Imaging retina to study dementia and stroke. Prog Retin Eye Res 57: 89–107. doi: 10.1016/j.preteyeres.2017.01.001
[48] Kern TS, Engerman RL (1996) Capillary lesions develop in retina rather than cerebral cortex in diabetes and experimental galactosemia. Arch Ophthalmol-Chic 114(3): 306–310. doi: DOI 10.1001/archopht.1996.01100130302013
[49] Mukai N, Hori S, Pomeroy M (1980) Cerebral-Lesions in Rats with Streptozotocin-Induced Diabetes. Acta Neuropathologica 51(1): 79–84. doi: Doi 10.1007/Bf00688853
[50] Frank RN, Dutta S, Frank SE (1987) Cerebral cortical capillary basement membrane thickening in galactosaemic rats. Diabetologia 30(9): 739–744. doi: 10.1007/BF00296999
[51] Johnson PC, Brendel K, Meezan E (1982) Thickened cerebral cortical capillary basement membranes in diabetics. Arch Pathol Lab Med 106(5): 214–217.
[52] Jakobsen J, Sidenius P, Gundersen HJ, Osterby R (1987) Quantitative changes of cerebral neocortical structure in insulin-treated long-term streptozocin-induced diabetes in rats. Diabetes 36(5): 597–601. doi: 10.2337/diab.36.5.597
[53] Woerdeman J, van Duinkerken E, Wattjes MP, Barkhof F, Snoek FJ, Moll AC, et al. (2014) Proliferative retinopathy in type 1 diabetes is associated with cerebral microbleeds, which is part of generalized microangiopathy. Diabetes Care 37(4): 1165–1168. doi: 10.2337/dc13-1586
[54] Sanahuja J, Alonso N, Diez J, Ortega E, Rubinat E, Traveset A, et al. (2016) Increased Burden of Cerebral Small Vessel Disease in Patients With Type 2 Diabetes and Retinopathy. Diabetes Care 39(9): 1614–1620. doi: 10.2337/dc15-2671
[55] Huang Y, Wang S, Cai C, Huang X, Chen Y, Wu X, et al. (2024) Retinal vascular density as a potential biomarker of diabetic cerebral small vessel disease. Diabetes Obes Metab 26(5): 1789–1798. doi: 10.1111/dom.15492
[56] de Leijer JF, Pham SDT, Vissers T, Exalto LG, Schlingemann RO, Siero JSW, et al. (2025) Association between retinal microvasculature and cerebral small vessel function in type 2 diabetes: An ultrahigh field MRI study. Diabetes Obes Metab 27(9): 5346–5350. doi: 10.1111/dom.16546
[57] de Oliveira F (1966) Pericytes in diabetic retinopathy. Br J Ophthalmol 50(3): 134–143. doi: 10.1136/bjo.50.3.134
[58] Addison DJ, Garner A, Ashton N (1970) Degeneration of intramural pericytes in diabetic retinopathy. Br Med J 1(5691): 264–266. doi: 10.1136/bmj.1.5691.264
[59] Akhtar A, Sah SP (2020) Insulin signaling pathway and related molecules: Role in neurodegeneration and Alzheimer's disease. Neurochem Int 135: 104707. doi: 10.1016/j.neuint.2020.104707
[60] van Sloten TT, Sedaghat S, Carnethon MR, Launer LJ, Stehouwer CDA (2020) Cerebral microvascular complications of type 2 diabetes: stroke, cognitive dysfunction, and depression. Lancet Diabetes Endocrinol 8(4): 325–336. doi: 10.1016/S2213-8587(19)30405-X

[61] Mahmood S, Dkhar W, Kadavigere R, Sukumar S, Nayak K, Pradhan A, et al. (2025) An analysis of brain structural changes in type 2 diabetes using advanced MRI techniques. Magn Reson Imaging 121: 110419. doi: 10.1016/j.mri.2025.110419
[62] Hussain S, Mansouri S, Sjoholm A, Patrone C, Darsalia V (2014) Evidence for cortical neuronal loss in male type 2 diabetic Goto-Kakizaki rats. J Alzheimers Dis 41(2): 551–560. doi: 10.3233/JAD-131958
[63] Kodl CT, Franc DT, Rao JP, Anderson FS, Thomas W, Mueller BA, et al. (2008) Diffusion tensor imaging identifies deficits in white matter microstructure in subjects with type 1 diabetes that correlate with reduced neurocognitive function. Diabetes 57(11): 3083–3089. doi: 10.2337/db08-0724
[64] Musen G, Lyoo IK, Sparks CR, Weinger K, Hwang J, Ryan CM, et al. (2006) Effects of type 1 diabetes on gray matter density as measured by voxel-based morphometry. Diabetes 55(2): 326–333. doi: 10.2337/diabetes.55.02.06.db05-0520
[65] Hughes TM, Ryan CM, Aizenstein HJ, Nunley K, Gianaros PJ, Miller R, et al. (2013) Frontal gray matter atrophy in middle aged adults with type 1 diabetes is independent of cardiovascular risk factors and diabetes complications. J Diabetes Complications 27(6): 558–564. doi: 10.1016/j.jdiacomp.2013.07.001
[66] van Duinkerken E, Schoonheim MM, Steenwijk MD, Klein M, RG IJ, Moll AC, et al. (2014) Ventral striatum, but not cortical volume loss, is related to cognitive dysfunction in type 1 diabetic patients with and without microangiopathy. Diabetes Care 37(9): 2483–2490. doi: 10.2337/dc14-0016
[67] Klein JP, Waxman SG (2003) The brain in diabetes: molecular changes in neurons and their implications for end-organ damage. Lancet Neurol 2(9): 548–554. doi: 10.1016/s1474-4422(03)00503-9
[68] Luna R, Talanki Manjunatha R, Bollu B, Jhaveri S, Avanthika C, Reddy N, et al. (2021) A Comprehensive Review of Neuronal Changes in Diabetics. Cureus 13(10): e19142. doi: 10.7759/cureus.19142
[69] Huang CC, Chung CM, Leu HB, Lin LY, Chiu CC, Hsu CY, et al. (2014) Diabetes mellitus and the risk of Alzheimer's disease: a nationwide population-based study. PLoS One 9(1): e87095. doi: 10.1371/journal.pone.0087095
[70] Wang KC, Woung LC, Tsai MT, Liu CC, Su YH, Li CY (2012) Risk of Alzheimer's disease in relation to diabetes: a population-based cohort study. Neuroepidemiology 38(4): 237–244. doi: 10.1159/000337428
[71] van Duinkerken E, Ijzerman RG, Klein M, Moll AC, Snoek FJ, Scheltens P, et al. (2016) Disrupted subject-specific gray matter network properties and cognitive dysfunction in type 1 diabetes patients with and without proliferative retinopathy. Hum Brain Mapp 37(3): 1194–1208. doi: 10.1002/hbm.23096
[72] McCrimmon RJ, Ryan CM, Frier BM (2012) Diabetes and cognitive dysfunction. Lancet 379(9833): 2291–2299. doi: 10.1016/S0140-6736(12)60360-2
[73] Umegaki H (2010) Pathophysiology of cognitive dysfunction in older people with type 2 diabetes: vascular changes or neurodegeneration? Age Ageing 39(1): 8–10. doi: 10.1093/ageing/afp211
[74] van Duinkerken E, Schoonheim MM, Sanz-Arigita EJ, RG IJ, Moll AC, Snoek FJ, et al. (2012) Resting-state brain networks in type 1 diabetic patients with and without microangiopathy and their relation to cognitive functions and disease variables. Diabetes 61(7): 1814–1821. doi: 10.2337/db11-1358
[75] Kodl CT, Seaquist ER (2008) Cognitive dysfunction and diabetes mellitus. Endocr Rev 29(4): 494–511. doi: 10.1210/er.2007-0034
[76] Zhang S, Zhang Y, Wen Z, Yang Y, Bu T, Bu X, et al. (2023) Cognitive dysfunction in diabetes: abnormal glucose metabolic regulation in the brain. Front Endocrinol (Lausanne) 14: 1192602. doi: 10.3389/fendo.2023.1192602

[77] Rizzo MR, Marfella R, Barbieri M, Boccardi V, Vestini F, Lettieri B, et al. (2010) Relationships between daily acute glucose fluctuations and cognitive performance among aged type 2 diabetic patients. Diabetes Care 33(10): 2169–2174. doi: 10.2337/dc10-0389
[78] Rajah TT, Olson AL, Grammas P (2001) Differential glucose uptake in retina- and brain-derived endothelial cells. Microvasc Res 62(3): 236–242. doi: 10.1006/mvre.2001.2337
[79] Tang J, Zhu XW, Lust WD, Kern TS (2000) Retina accumulates more glucose than does the embryologically similar cerebral cortex in diabetic rats. Diabetologia 43(11): 1417–1423. doi: 10.1007/s001250051548
[80] Badr GA, Tang J, Ismail-Beigi F, Kern TS (2000) Diabetes downregulates GLUT1 expression in the retina and its microvessels but not in the cerebral cortex or its microvessels. Diabetes 49(6): 1016–1021. doi: DOI 10.2337/diabetes.49.6.1016
[81] (2025) 2025 Alzheimer's disease facts and figures. In: Alzheimers & Dementia. Vol 21
[82] Grammas P (2011) Neurovascular dysfunction, inflammation and endothelial activation: implications for the pathogenesis of Alzheimer's disease. J Neuroinflammation 8: 26. doi: 10.1186/1742-2094-8-26
[83] Andrews SJ, Renton AE, Fulton-Howard B, Podlesny-Drabiniok A, Marcora E, Goate AM (2023) The complex genetic architecture of Alzheimer's disease: novel insights and future directions. Ebiomedicine 90: 104511. doi: 10.1016/j.ebiom.2023.104511
[84] Gatz M, Reynolds CA, Fratiglioni L, Johansson B, Mortimer JA, Berg S, et al. (2006) Role of genes and environments for explaining Alzheimer disease. Arch Gen Psychiatry 63(2): 168–174. doi: 10.1001/archpsyc.63.2.168
[85] Chai YH, Han YP, Zhang JY, Zhou JB (2024) Diabetic Retinopathy and Brain Structure, Cognition Function, and Dementia: A Bidirectional Mendelian Randomization Study. J Alzheimers Dis 97(3): 1211–1221. doi: 10.3233/JAD-231022
[86] Kopf D, Frolich L (2009) Risk of incident Alzheimer's disease in diabetic patients: a systematic review of prospective trials. J Alzheimers Dis 16(4): 677–685. doi: 10.3233/JAD-2009-1011
[87] Cheung CY, Ong YT, Ikram MK, Chen C, Wong TY (2014) Retinal microvasculature in Alzheimer's disease. J Alzheimers Dis 42 Suppl 4: S339–352. doi: 10.3233/JAD-141596
[88] Grande G, Qiu C, Fratiglioni L (2020) Prevention of dementia in an ageing world: Evidence and biological rationale. Ageing Res Rev 64: 101045. doi: 10.1016/j.arr.2020.101045
[89] Jack CR, Jr., Therneau TM, Weigand SD, Wiste HJ, Knopman DS, Vemuri P, et al. (2019) Prevalence of Biologically vs Clinically Defined Alzheimer Spectrum Entities Using the National Institute on Aging-Alzheimer's Association Research Framework. JAMA Neurol 76(10): 1174–1183. doi: 10.1001/jamaneurol.2019.1971
[90] Almohmadi NH, Al-Kuraishy HM, Albuhadily AK, Al-Gareeb AI, Abdelaziz AM, Alexiou A, et al. (2025) Alzheimer disease: Amyloid peptide controversies and challenges of anti-Abeta immunotherapy. J Pharmacol Exp Ther 392(8): 103639. doi: 10.1016/j.jpet.2025.103639
[91] Vickers JC, Dickson TC, Adlard PA, Saunders HL, King CE, McCormack G (2000) The cause of neuronal degeneration in Alzheimer's disease. Prog Neurobiol 60(2): 139–165. doi: 10.1016/s0301-0082(99)00023-4
[92] Plascencia-Villa G, Perry G (2022) Neuropathologic Changes Provide Insights into Key Mechanisms of Alzheimer Disease and Related Dementia. Am J Pathol 192(10): 1340–1346. doi: 10.1016/j.ajpath.2022.07.002
[93] Krumm S, Kivisaari SL, Probst A, Monsch AU, Reinhardt J, Ulmer S, et al. (2016) Cortical thinning of parahippocampal subregions in very early Alzheimer's disease. Neurobiol Aging 38: 188–196. doi: 10.1016/j.neurobiolaging.2015.11.001
[94] Xiao Y, Hu Y, Huang K, Alzheimer's Disease Neuroimaging I (2023) Atrophy of hippocampal subfields relates to memory decline during the pathological progression of Alzheimer's disease. Front Aging Neurosci 15: 1287122. doi: 10.3389/fnagi.2023.1287122
[95] Punzi M, Sestieri C, Picerni E, Chiarelli AM, Padulo C, Delli Pizzi A, et al. (2024) Atrophy of hippocampal subfields and amygdala nuclei in subjects with mild cognitive impairment progressing to Alzheimer's disease. Heliyon 10(6): e27429. doi: 10.1016/j.heliyon.2024.e27429

[96] Fisher RA, Miners JS, Love S (2022) Pathological changes within the cerebral vasculature in Alzheimer's disease: New perspectives. Brain Pathol 32(6): e13061. doi: 10.1111/bpa.13061
[97] Iadecola C, Gottesman RF (2018) Cerebrovascular Alterations in Alzheimer Disease. Circ Res 123(4): 406–408. doi: 10.1161/CIRCRESAHA.118.313400
[98] Hoozemans JJ, Rozemuller AJ, van Haastert ES, Eikelenboom P, van Gool WA (2011) Neuroinflammation in Alzheimer's disease wanes with age. J Neuroinflammation 8: 171. doi: 10.1186/1742-2094-8-171
[99] Kamphuis W, Middeldorp J, Kooijman L, Sluijs JA, Kooi EJ, Moeton M, et al. (2014) Glial fibrillary acidic protein isoform expression in plaque related astrogliosis in Alzheimer's disease. Neurobiol Aging 35(3): 492–510. doi: 10.1016/j.neurobiolaging.2013.09.035
[100] Vehmas AK, Kawas CH, Stewart WF, Troncoso JC (2003) Immune reactive cells in senile plaques and cognitive decline in Alzheimer's disease. Neurobiol Aging 24(2): 321–331. doi: 10.1016/s0197-4580(02)00090-8
[101] Kirabali T, Rust R, Rigotti S, Siccoli A, Nitsch RM, Kulic L (2020) Distinct changes in all major components of the neurovascular unit across different neuropathological stages of Alzheimer's disease. Brain Pathol 30(6): 1056–1070. doi: 10.1111/bpa.12895
[102] Sengillo JD, Winkler EA, Walker CT, Sullivan JS, Johnson M, Zlokovic BV (2013) Deficiency in mural vascular cells coincides with blood-brain barrier disruption in Alzheimer's disease. Brain Pathol 23(3): 303–310. doi: 10.1111/bpa.12004
[103] Ding R, Hase Y, Ameen-Ali KE, Ndung'u M, Stevenson W, Barsby J, et al. (2020) Loss of capillary pericytes and the blood-brain barrier in white matter in poststroke and vascular dementias and Alzheimer's disease. Brain Pathol 30(6): 1087–1101. doi: 10.1111/bpa.12888
[104] Hase Y, Jobson D, Cheong J, Gotama K, Maffei L, Hase M, et al. (2024) Hippocampal capillary pericytes in post-stroke and vascular dementias and Alzheimer's disease and experimental chronic cerebral hypoperfusion. Acta Neuropathol Commun 12(1): 29. doi: 10.1186/s40478-024-01737-8
[105] Nielsen HM, Ek D, Avdic U, Orbjorn C, Hansson O, Netherlands Brain B, et al. (2013) NG2 cells, a new trail for Alzheimer's disease mechanisms? Acta Neuropathol Commun 1(1): 7. doi: 10.1186/2051-5960-1-7
[106] Halliday MR, Rege SV, Ma Q, Zhao Z, Miller CA, Winkler EA, et al. (2016) Accelerated pericyte degeneration and blood-brain barrier breakdown in apolipoprotein E4 carriers with Alzheimer's disease. J Cereb Blood Flow Metab 36(1): 216–227. doi: 10.1038/jcbfm.2015.44
[107] Baloyannis SJ, Baloyannis IS (2012) The vascular factor in Alzheimer's disease: a study in Golgi technique and electron microscopy. J Neurol Sci 322(1-2): 117–121. doi: 10.1016/j.jns.2012.07.010
[108] Shi H, Koronyo Y, Rentsendorj A, Regis GC, Sheyn J, Fuchs DT, et al. (2020) Identification of early pericyte loss and vascular amyloidosis in Alzheimer's disease retina. Acta Neuropathol 139(5): 813–836. doi: 10.1007/s00401-020-02134-w
[109] Berisha F, Feke GT, Trempe CL, McMeel JW, Schepens CL (2007) Retinal abnormalities in early Alzheimer's disease. Invest Ophthalmol Vis Sci 48(5): 2285–2289. doi: 10.1167/iovs.06-1029
[110] Cheung CY, Ong YT, Ikram MK, Ong SY, Li X, Hilal S, et al. (2014) Microvascular network alterations in the retina of patients with Alzheimer's disease. Alzheimers Dement 10(2): 135–142. doi: 10.1016/j.jalz.2013.06.009
[111] Frost S, Kanagasingam Y, Sohrabi H, Vignarajan J, Bourgeat P, Salvado O, et al. (2013) Retinal vascular biomarkers for early detection and monitoring of Alzheimer's disease. Transl Psychiatry 3(2): e233. doi: 10.1038/tp.2012.150
[112] Feke GT, Hyman BT, Stern RA, Pasquale LR (2015) Retinal blood flow in mild cognitive impairment and Alzheimer's disease. Alzheimers Dement (Amst) 1(2): 144–151. doi: 10.1016/j.dadm.2015.01.004
[113] Williams MA, McGowan AJ, Cardwell CR, Cheung CY, Craig D, Passmore P, et al. (2015) Retinal microvascular network attenuation in Alzheimer's disease. Alzheimers Dement (Amst) 1(2): 229–235. doi: 10.1016/j.dadm.2015.04.001

[114] Baker ML, Marino Larsen EK, Kuller LH, Klein R, Klein BE, Siscovick DS, et al. (2007) Retinal microvascular signs, cognitive function, and dementia in older persons: the Cardiovascular Health Study. Stroke 38(7): 2041–2047. doi: 10.1161/STROKEAHA.107.483586
[115] de Jong FJ, Schrijvers EM, Ikram MK, Koudstaal PJ, de Jong PT, Hofman A, et al. (2011) Retinal vascular caliber and risk of dementia: the Rotterdam study. Neurology 76(9): 816–821. doi: 10.1212/WNL.0b013e31820e7baa
[116] Qiu C, Cotch MF, Sigurdsson S, Jonsson PV, Jonsdottir MK, Sveinbjrnsdottir S, et al. (2010) Cerebral microbleeds, retinopathy, and dementia: the AGES-Reykjavik Study. Neurology 75(24): 2221–2228. doi: 10.1212/WNL.0b013e3182020349
[117] Javaid FZ, Brenton J, Guo L, Cordeiro MF (2016) Visual and Ocular Manifestations of Alzheimer's Disease and Their Use as Biomarkers for Diagnosis and Progression. Front Neurol 7: 55. doi: 10.3389/fneur.2016.00055
[118] Hart NJ, Koronyo Y, Black KL, Koronyo-Hamaoui M (2016) Ocular indicators of Alzheimer's: exploring disease in the retina. Acta Neuropathol 132(6): 767–787. doi: 10.1007/s00401-016-1613-6
[119] Parisi V, Restuccia R, Fattapposta F, Mina C, Bucci MG, Pierelli F (2001) Morphological and functional retinal impairment in Alzheimer's disease patients. Clin Neurophysiol 112(10): 1860–1867. doi: 10.1016/s1388-2457(01)00620-4
[120] Coppola G, Di Renzo A, Ziccardi L, Martelli F, Fadda A, Manni G, et al. (2015) Optical Coherence Tomography in Alzheimer's Disease: A Meta-Analysis. PLoS One 10(8): e0134750. doi: 10.1371/journal.pone.0134750

Chapter 2

A zebrafish multimodal toolbox to study the blood-brain barrier in health and disease

Noëlle Bakker-van Bugnum[1,2,3], Emma E. Snijders[1], Eloise F.E.E. Hogendorp[1], Cornelis J.F. van Noorden[1], Liang Lou[4,5], Marie Vanhollebeke[4,5], Benoit Vanhollebeke[4,5], Anita E. Grootemaat[6], Nicole N. van der Wel[6], Reinier O. Schlingemann[1,2,3] and Ingeborg Klaassen[1,2,3]

[1] Ocular Angiogenesis Group, Department of Ophthalmology, Amsterdam UMC location University of Amsterdam, Amsterdam, The Netherlands.
[2] Amsterdam Cardiovascular Sciences, Microcirculation, Amsterdam, The Netherlands.
[3] Amsterdam Neuroscience, Cellular & Molecular Mechanisms, Amsterdam, The Netherlands.
[4] Laboratory of Neurovascular Signaling, Department of Molecular Biology, ULB Neuroscience Institute, Université libre de Bruxelles (ULB), Gosselies, Belgium.
[5] WEL Research Institute, avenue Pasteur, 6, Wavre, Belgium
[6] Electron Microscopy Centre Amsterdam, Amsterdam UMC location Academic Medical Centre, Amsterdam, The Netherlands.

Accepted for publication in Scientific Reports

Abstract

Vasogenic edema, due to blood-retinal barrier (BRB) disruption, is a major cause of vision loss across various ocular diseases. Similarly, blood-brain barrier (BBB) breakdown is a hallmark of many neurological disorders. However, the precise molecular and cellular mechanisms underlying barrier dysfunction under pathological conditions remain poorly understood. In this study, we aimed to develop a pathological model to investigate the integrity of the BRB and BBB using *in vivo* live imaging in zebrafish larvae, employing hyperglycemia-induced leakage as a proof of concept. Our results show that external glucose exposure elevates internal glucose levels, inducing hyperglycemia. Hyperglycemia increased midbrain blood vessel diameter and tracer leakage, indicative of barrier dysfunction, without affecting overall larval survival. Using fluorescent reporters, we found that hyperglycemia concurrently reduced claudin-5 and increased PLVAP, suggesting compromised tight junction integrity and impeded BBB maturation. Preliminary studies using transmission electron microscopy further revealed ultrastructural defects of junctions and transcellular caveolae. This proof of concept study establishes an *in vivo* protocol for visualizing and quantifying barrier permeability, protein expression, and ultrastructure. It provides a valuable foundation for a zebrafish model to dissect the molecular mechanisms of blood-barrier breakdown, with direct implications for investigations of diabetic macular edema and other neurovascular diseases.

Introduction

In the eye, vasogenic macular edema arises from the breakdown of the blood-retinal barrier (BRB) and is a primary cause of vision loss in patients with diabetic retinopathy, retinal vein occlusions, uveitis, and exudative age-related macular degeneration [1, 2]. Similarly, disruption of the neuroprotective blood-brain barrier (BBB) is a critical and persistent pathological event in various neurological disorders such as brain trauma and brain tumors [1, 3]. Compromised barrier integrity leads to plasma protein extravasation, which contributes to vasogenic edema and is associated with neuronal injury and cell death. The cerebral and retinal vasculatures share structural and functional characteristics, including highly selective transport mechanisms that restrict the passage of proteins and other molecules from the circulation into the neural parenchyma, thereby protecting the delicate neuronal components. Both the BBB and BRB maintain homeostasis through a coordinated interplay of specialized cellular and molecular features. Nevertheless, the precise molecular and cellular mechanisms governing barrier dysfunction under pathological conditions remain incompletely understood. Advancing therapeutic strategies necessitate a comprehensive understanding of disease progression and underlying mechanisms.

The aim of our study was to establish a zebrafish model that can be employed to investigate effects of pathological breakdown of the BBB, serving as a model for both the BBB and BRB. Currently, no such zebrafish model exists. We focused on the BBB because zebrafish larvae lack a BRB similar to humans [4, 5], and as the BRB shares many structural and functional features with the BBB [3]. Rodent models are most commonly used for studying the BRB and BBB, because of their similarity in cell types, transporters and restrained permeability properties as compared to those of the human BBB [6]. However, use of these animal models raises ethical concerns, is expensive and time-consuming, and requires invasive procedures to assess brain gene expression.

In this study, we used zebrafish larvae to study vascular leakage induced by hyperglycemia, as a model for vasogenic edema. Zebrafish are the smallest vertebrate model organisms with a functional endothelial BBB [7-10] that resembles that of humans. The zebrafish model is ideal for vascular biology and therapy development due to its transparency, rapid development, and suitability for live imaging. While it is established that zebrafish larvae develop a functional BBB between 3 and 10 days post fertilization (dpf) [5, 7, 8, 10-12], the precise timing of its maturation remains debated. Some studies posit that BBB development coincides with angiogenesis from 2 dpf onwards [5, 10], while others report a broader maturation window from 3 to 10 dpf based on tracer permeability assays [11]. In addition, BBB development has been assessed through the expression levels of tight junction proteins [5, 10, 12]. Claudin-5 and ZO-1 have been detected in all cerebral blood vessels as early as 3 dpf [5, 10], although one study reported a more gradual upregulation of claudin-5 in the cerebral vasculature, with expression initiating at 3 dpf and becoming widespread across nearly all brain vessels by 5 dpf [12]. Anatomical analysis by transmission electron microscopy (TEM) identified tight junctions at 5 dpf and pericytes and astrocyte endfeet at 10 dpf [11].

In the light of this discussion, as a proof of concept for our model, we investigated whether hyperglycemia disrupts, delays, or alters normal BBB development. We used the *Tg(fli1:EGFP)* transgenic line to visualize the cerebral vasculature *in vivo*. We also employed transgenic

zebrafish lines to visualize expression of claudin-5 and plasmalemma vesicle-associated protein (PLVAP), which are markers of BBB formation [12] and immature and permeable vasculature [8], respectively. These reporter lines allowed for real-time *in vivo* monitoring of gene expression during barrier formation. To investigate BBB integrity and molecular responses, we used these zebrafish reporter lines [8, 12, 13] in combination with techniques including quantification of internal glucose level [14], vascular diameter [15] and fluorescent tracer-based permeability [7], BBB marker expression analysis and TEM. Based on these techniques, we present a multimodal *in vivo* platform for assessing BBB disruption under hyperglycemic conditions.

Results

Increased internal glucose levels in zebrafish larvae without affecting survival or morphology

To establish hyperglycemic conditions in zebrafish, *Tg(fli1:EGFP)* zebrafish were continually immersed in medium supplemented with 60 mM or 130 mM glucose, from 3 to 5 dpf. To confirm the establishment of hyperglycemia, we measured internal glucose levels in larvae after glucose exposure (Figure 1). We observed significant heterogeneity in glucose levels among zebrafish under hyperglycemic conditions. Larvae exposed to 60 mM and 130 mM glucose for 24 h (4 dpf) (Figure 1b) and 48 h (5 dpf) (Figure 1c) showed at least 4-fold higher glucose levels relative to both the non-exposed control group and the 130 mM mannitol group ($P < 0.05$). No differences were observed between the control groups at 24 h and 48 h. These results demonstrate a dose-dependent increase in the total internal glucose levels of zebrafish after 24 h and 48 h of exposure to 60 mM and 130 mM glucose.

Hyperglycemic exposure from 3 to 5 dpf did not significantly affect survival rates (Figure 2a) or cause morphological abnormalities compared to controls (Figure 2b). In summary, immersing zebrafish in medium supplemented with glucose elevates internal glucose levels without affecting survival rates or morphology.

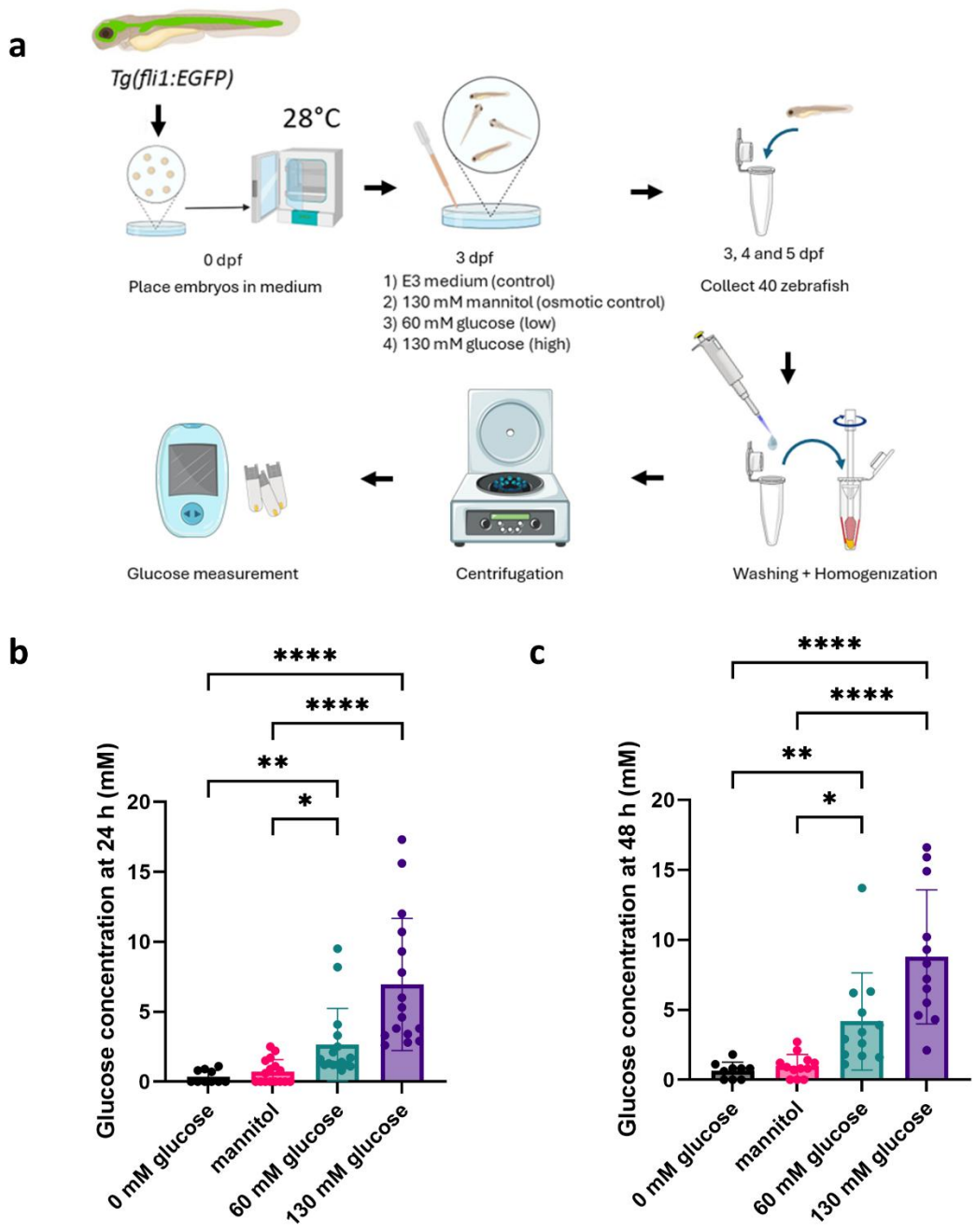

Figure 1. Endogenous glucose level measurements at 5 dpf in zebrafish after exogenous glucose exposure. (a) Experimental design for internal glucose measurements. *Tg(fli1:EGFP)* zebrafish were exposed to 60 mM or 130 mM glucose between 3 dpf and 5 dpf. 0 mM glucose and 130 mM mannitol were included as controls. Forty zebrafish from each experimental group were collected, washed and homogenized. Supernatant was collected after centrifugation and internal glucose levels were measured with a glucose meter. Images adapted from Servier Medical Art (https://smart.servier.com/), licensed under CC BY 4.0 (https://creativecommons.org/licenses/by/4.0/). Internal glucose levels were measured after **(b)** 24 h (4 dpf) or **(c)** 48 h (5 dpf) of exposure to 60 mM or 130 mM glucose. 0 mM glucose and 130 mM mannitol were included as controls. n = 9-16 biological replicates per group. Data are represented as mean ± SD. **P* < 0.05, ***P* < 0.01, *****P* < 0.0001 by Kruskal-Wallis statistical test.

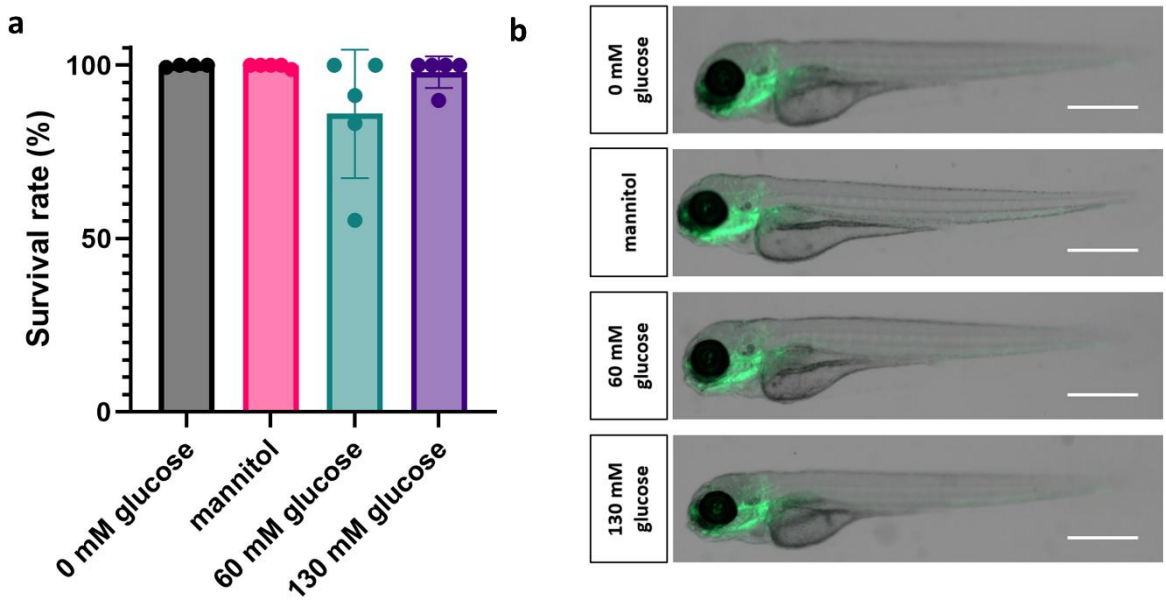

Figure 2. Hyperglycemia effects on survival and morphology in zebrafish larvae of 5 dpf. (**a**) Survival rates after glucose exposure (60 mM or 130 mM glucose) in *Tg(fli1:EGFP)* zebrafish larvae at 5 dpf. 0 mM glucose and 130 mM mannitol were included as controls *(*n = 5 per condition). Data are represented as mean ± SD. (**b**) Morphological differences were not found between control conditions (0 mM glucose and 130 mM mannitol) and glucose-treated *Tg(fli1:EGFP)* zebrafish larvae (60 mM or 130 mM glucose) at 5 dpf. Scale bars: 500 µm.

Increased cerebral tracer permeability under hyperglycemic conditions

To evaluate the effects of hyperglycemia on BBB formation in zebrafish larvae, we performed permeability assays using simultaneous intracardiac co-injections of small (792 Da Cy5) and large (70 kDa Dextran-Texas Red) fluorescent tracers in zebrafish larvae at 3, 4 and 5 dpf. Tracer extravasation was quantified by live-imaging after injection (Figure 3a-d).

At all time points, both tracers were detected in brain parenchyma (Figure 3e, f; Supplementary Figure S1), confirming their extravasation. In control larvae (0 mM glucose), the normalized tracer intensity in the midbrain remained stable throughout development (Figure 3g, h).

Following 48 h of exposure to 130 mM glucose, leakage of both 70 kDa-Dextran (0.78 ± 0.17 intensity; $P = 0.0014$) and Cy5 (0.93 ± 0.21 intensity; $P = 0.026$) was increased compared to baseline. Cy5 leakage showed a 1.6-fold increase relative to the 0 mM glucose control at 5 dpf ($P = 0.011$) (Figure 3h). No differences were found for any other conditions or time points.

These results indicate that 130 mM glucose exposure had a more pronounced effect on tracer leakage than 60 mM glucose for 70 kDa-Dextran, and an even greater effect for the smaller Cy5 tracer. To determine how the BBB itself contributes to this hyperglycemia-induced increase in permeability , we further characterized the developing cerebral vasculature.

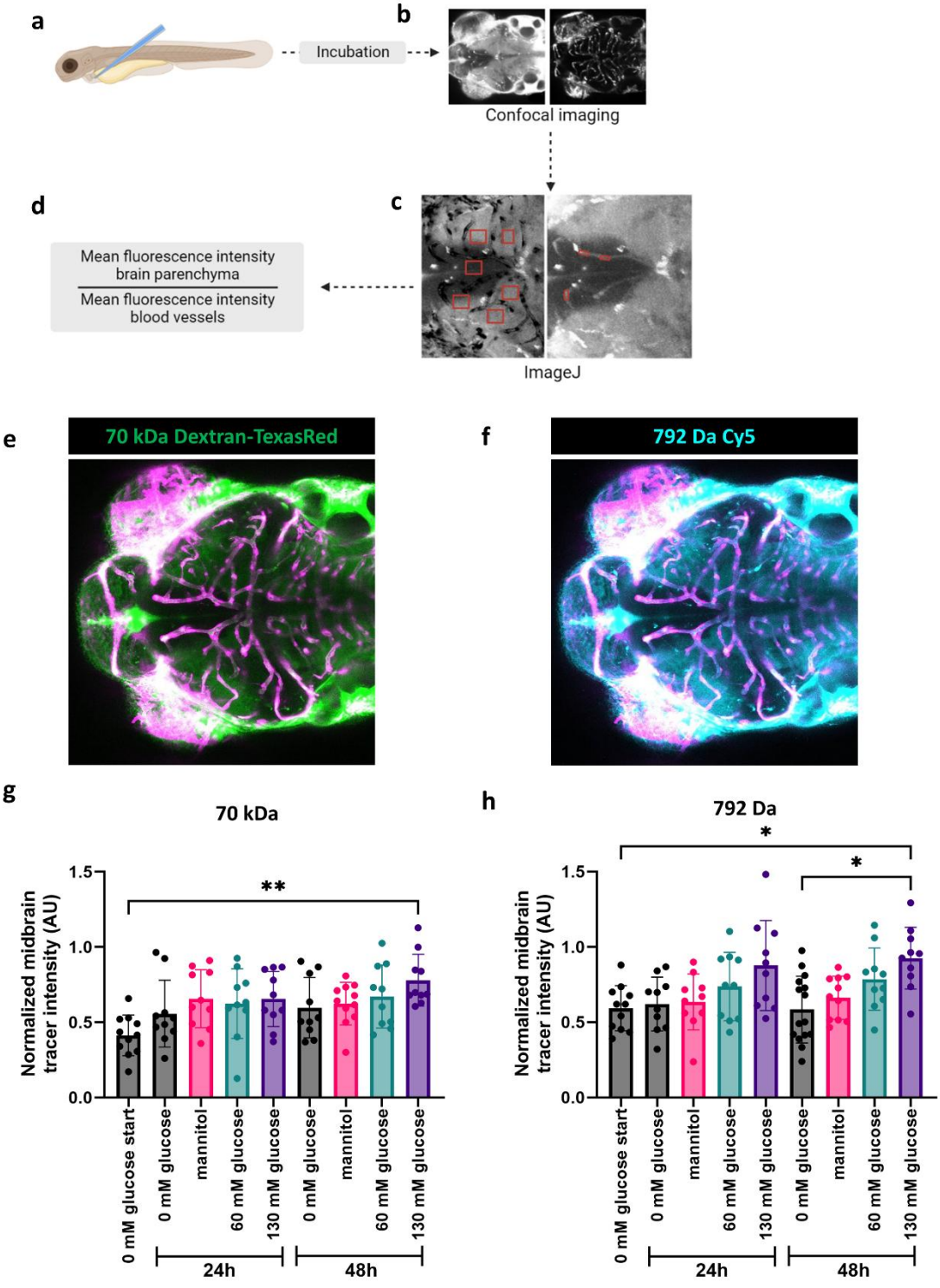

Figure 3. BBB permeability measurements after hyperglycemia in zebrafish larvae. (a-d) Experimental design for the quantification of blood vessel permeability. Created in https://BioRender.com. (**a**) At 3, 4 and 5 dpf, *Tg(fli1:EGFP)* zebrafish larvae were injected into the cardiac sac with fluorescent tracers. (**b**) Confocal microscopy images of a fluorescent tracer (left image) and the fluorescent blood vessels (right image) are shown separately. (**c**) Fluorescence intensity measurements using ImageJ software are shown. Left image: In the tracer channel, the vasculature (GFP) was subtracted from the tracer fluorescence. Tracer fluorescence was measured in

6 regions of brain parenchyma (red rectangles). Right image: In the tracer channel, the fluorescence intensity was measured at 3 regions inside the lumen (red rectangles). (**d**) To normalize the fluorescence intensity, the mean fluorescence inside the parenchyma is divided by the fluorescence intensity inside the lumen. (**e, f**) Examples of vascular leakage in the zebrafish brain (dorsal view) of *Tg(fli1:EGFP)* zebrafish at 4 dpf injected with (e) 70 kDa Dextran-Texas Red (green) and (**f**) 792 Da Cy5 (cyan) under hyperglycemic conditions. Vasculature is shown in magenta. (**g, h**) Quantification of tracer intensity as measured in the midbrain parenchyma at baseline, after 24 h and 48 h of glucose exposure normalized to luminal tracer intensity, both for (**g**) 70 kDa Dextran-Texas Red and (**h**) 792 Da Cy5. n = 10-15 fish per group. Data are represented as mean ± SD. **P* < 0.05, ***P* < 0.01.

Hyperglycemia-induced increase in cerebral vascular diameter

To assess the effects of glucose on cerebral vasculature, we measured the diameter of the middle mesencephalic central artery following 48 h of exposure (5 dpf) (Figure 4a-c). Exposure to 60 mM and 130 mM glucose increased vascular diameter compared to both 0 mM glucose (8.85 µm ± 2.04 µm) and mannitol controls (8.75 µm ± 1.19 µm) (Figure 4d). Specifically, the diameter increased to 11.21 µm ± 2.52 µm with 60 mM glucose ($P < 0.05$) and to 11.42 µm ± 2.05 µm with 130 mM glucose ($P < 0.01$).

Hyperglycemia alters inter-endothelial junctions in zebrafish midbrain

To examine the impact of hyperglycemia on tight junction integrity, we analyzed claudin-5 expression using a *Tg(cldn5a:EGFP)* reporter zebrafish line (Figure 5a, b). In a preliminary small sample set (n = 3 per condition), hyperglycemic larvae showed reduced claudin-5 expression at 5 dpf (Figure 5b).

Ultrastructural analysis by TEM confirmed intact tight junctions in both groups but indicated qualitative morphological changes, with hyperglycemic larvae occasionally displaying widened intercellular spaces at endothelial cell junctions that were largely absent in controls (Figure 5c and 5d).

Higher PLVAP expression in hyperglycemic barrier endothelium

To assess the effects of glucose on the transcellular pathway, we visualized the expression of *plvapb*, a marker of immature and permeable vasculature involved in transcellular transport [8, 16], using a *Tg(plvapb:EGFP)*^{ulb40} transgenic zebrafish line. In this zebrafish line EGFP is controlled by the cis-regulatory sequences of *plvapb*, as defined by Umans et al [8]. *plvapb:*EGFP expression normally decreases during maturation of the endothelial barrier [8]. To evaluate the effect of hyperglycemia on *plvapb* expression in the midbrain and hindbrain vasculature, zebrafish exposed to 0 mM glucose, 130 mM mannitol or 130 mM glucose from 3 dpf onwards were compared at 4 and 5 dpf (Figure 6). *plvapb:EGFP* expression was similar at 4 dpf for all conditions (Figure 6a,b). By contrast, EGFP expression in zebrafish exposed to 130 mM glucose appeared heterogenous with a minor fraction of the larvae exhibiting higher values compared to the untreated control group (Figure 6c,d). These results suggest that hyperglycemia can increase PLVAP expression and consequently upregulate transcytosis in the brain vasculature.

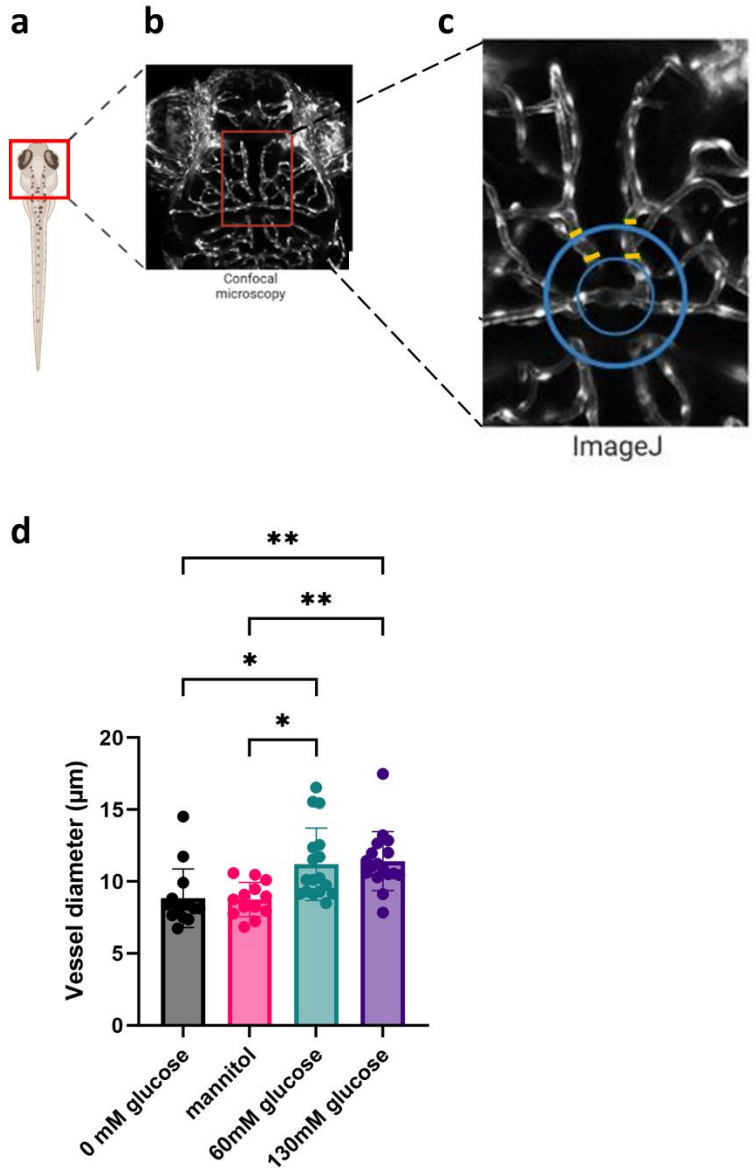

Figure 4. Cerebral artery diameter measurements after hyperglycemia in zebrafish larvae. (a-c) Procedure to quantify cerebral blood vessel diameter. (**a**) The zebrafish head was imaged using confocal microscopy. (**b**) Microscopical fluorescence images at 20x magnification were prepared and the cerebral blood vessel diameter was measured using ImageJ. (**c**) The diameter of middle mesencephalic central artery was determined in 2 branches at 4 sites (orange) on the 2 concentric circles (blue) drawn with the Concentric Circle plugin of ImageJ. Created in https://BioRender.com. **(d)** Quantification of the mesencephalic vein diameter. The diameter of the middle mesencephalic central artery in *Tg(fli1:EGFP)* zebrafish at 5 dpf increased after 48-h exposure to 60 mM and 130 mM glucose as compared to 0 mM glucose and mannitol conditions. An average of the diameter measured at 4 locations on the middle mesencephalic central artery was taken for n = 13-17 fish per group. Data are represented as mean ± SD. **P* < 0.05, ***P* < 0.01.

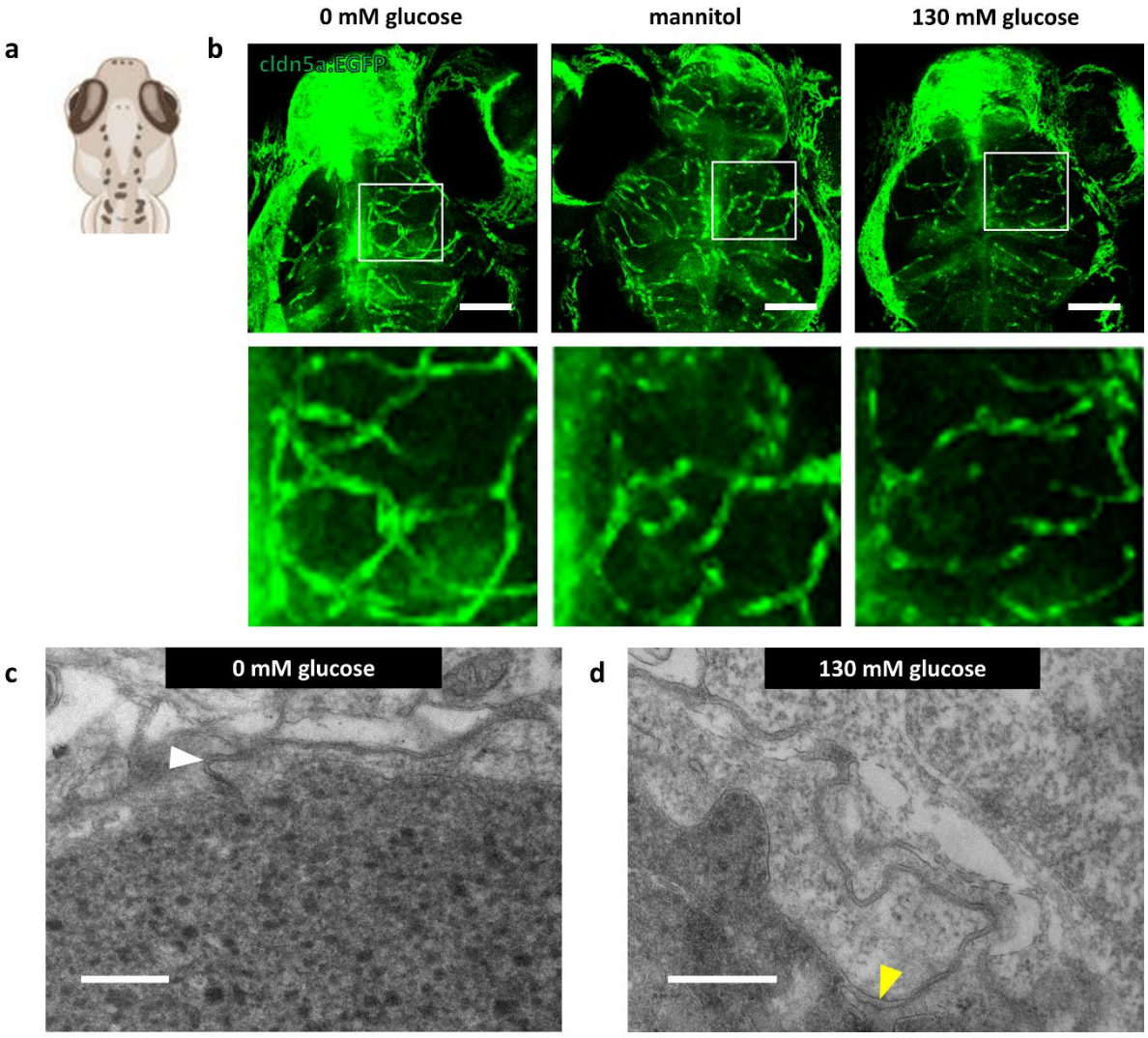

Figure 5. Imaging-based methods to analyze brain endothelial junctions in hyperglycemic zebrafish larvae (**a**) Schematic figure to illustrate the orientation of the zebrafish head for images shown in (**b**). (**b**) Representative maximum intensity projection of a confocal z-stack showing the midbrain (dorsal view) in *Tg(cldn5a:EGFP)* zebrafish larvae at 5 dpf to visualize claudin-5 expression (green) for 0 mM glucose control, mannitol control and after hyperglycemia (130 mM glucose). Lower panel, higher magnification of inset (midbrain boxed in images). (**c, d**) High-magnification TEM images of interendothelial junctions, indicated with arrowheads. The yellow arrowhead indicates an inter-endothelial junction with increased electron-lucent space. Scale bars: 100 µm in **b**; scale bars: 500 nm in **c, d**.

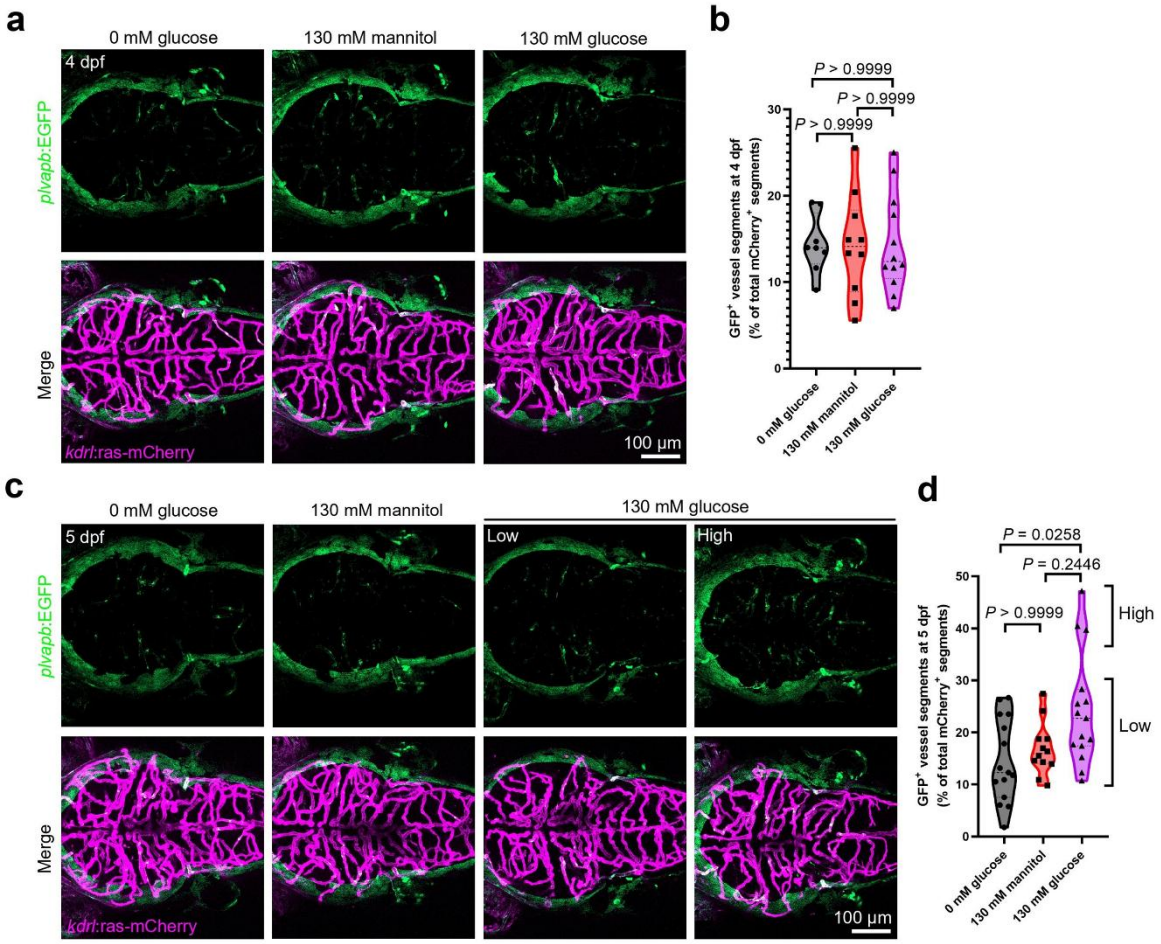

Figure 6. Microscopical analysis of *plvapb:EGFP* expression in larval brains under hyperglycemic conditions. Representative maximum intensity projection of a confocal z-stack showing *Tg(plvapb:EGFP;kdrl:ras-mCherry)* zebrafish larvae at 4 dpf (**a**) and 5 dpf (**c**) to visualize *plvapb:EGFP* expression (green) in 0 mM glucose controls, 130 mM mannitol-exposed larvae and after hyperglycemia (130 mM glucose). Vasculature is shown in magenta. Scale bars: 100 µm. Quantification of vessels segments positive for GFP in the brain parenchymal vasculature, indicating PLVAP expression, at 4 dpf (**b**) and 5 dpf (**d**).

Challenges in ultrastructural analysis of hyperglycemia-induced BBB disruption

To investigate mechanisms of glucose-induced BBB permeability, we assessed endothelial caveolae. Blood vessels were identified in the zebrafish midbrain, of which examples are shown in Figure 7a-c. While caveolae were identifiable in all groups (Figure 7d-f), their overall scarcity made quantification difficult. This limited abundance may be an inherent feature of zebrafish vasculature or a technical artifact.

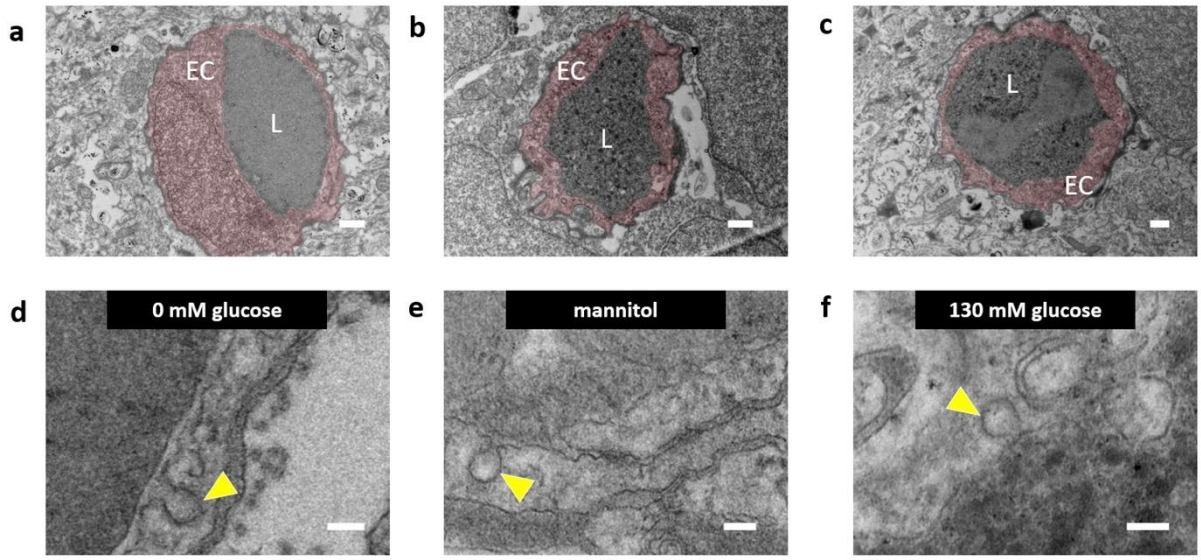

Figure 7. TEM analysis of caveolae after hyperglycemia in zebrafish larval cerebral vasculature. (**a**) Optimized TEM images of individual cerebral blood vessels (cross-sectional) in *Tg(fli1:EGFP)* zebrafish at 5 dpf. Morphology of cerebral blood vessels with endothelial cells (EC) pseudocoloured red, and lumen (L). (**b, c**) Representative TEM images of individual cerebral blood vessels (cross-sectional) in *Tg(fli1:EGFP)* zebrafish at 5 dpf. Morphology of cerebral blood vessels with endothelial cells (EC) pseudocoloured red, and lumen (L). Scale bars in **a-c**: 500 nm. High-magnification TEM images of vascular endothelial cells in *Tg(fli1:EGFP)* zebrafish at 5 dpf for (**d**) 0 mM glucose, (**e**) mannitol, or (**f**) hyperglycemic (130 mM glucose) conditions. Examples of a caveola are indicated with a yellow arrow. Scale bars in **d-f**: 100 nm.

Discussion

This study aimed to establish a zebrafish model to investigate the BBB under physiological and pathological conditions, serving as a model for both the BBB and BRB. Disruption of these barriers, a hallmark of neurological disorders and a major cause of vision loss in retinal diseases [1, 3, 17-19], is poorly understood at the molecular level. Employing hyperglycemia-induced vascular leakage as a proof of concept to validate the model, we used developing zebrafish larvae as an *in vivo* model of vasogenic edema. To this end, we developed a toolbox to comprehensively assess BBB integrity. The techniques include 1) live imaging in *Tg(fli1:EGFP)* zebrafish to visualize the midbrain vasculature and quantify tracer extravasation, 2) fluorescent reporter imaging in transgenic lines to examine claudin-5 and PLVAP expression, and 3) TEM to reveal tight junction structures and incidental transcellular caveolae.

Hyperglycemia altered BBB formation in our zebrafish model between 3 and 5 dpf, resulting in increased extravasation of fluorescent tracers. However, this permeability assay alone is not sufficient to prove BBB disruption. Other barriers in the brain, including the choroid plexus and meninges, could also contribute to the increase in parenchymal tracer intensity. Therefore, additional assays are required to determine whether the BBB is specifically affected under these pathological conditions. To find further evidence that the BBB contributes to the tracer extravasation, we studied the expression of claudin-5 and PLVAP using two transgenic zebrafish lines, *Tg(cldn5a:EGFP)* and *Tg(plvapb:EGFP).* Our preliminary

imaging from the *Tg(cldn5a:EGFP)* line indicates impaired tight junctions in the brain vessels that form a BBB under hyperglycemic conditions. The observed reduction in cerebral claudin-5 expression aligns with reports from diabetic rodents, human co-culture models [20-22] and a prior zebrafish study [23]. These findings collectively suggest that BBB dysfunction is a key contributor to the increased tracer leakage.

Heterogeneous PLVAP expression was observed in zebrafish exposed to high levels of glucose. A minor fraction of larvae in the high-glucose group showed significantly higher expression than the controls, suggesting that high glucose levels can prevent BBB maturation in the cerebral vasculature. The bimodal nature of the PLVAP response is consistent with heterogeneity in internal glucose levels, a possibility that remains to be tested. The observed heterogeneity in internal glucose levels represents a limitation of the current hyperglycemic model and may contribute to variability in other physiological parameters measured in zebrafish in this study. PLVAP expression is regulated by several key pathways. VEGF, a primary regulator, is increased during hyperglycemia and upregulates PLVAP, thereby compromising BBB and blood-retina barrier (BRB) integrity [1, 24-30]. Conversely, the Wnt/β-catenin pathway is essential for maintaining low PLVAP expression and intact BBB/BRB function [31-35]. Sustained Wnt/β-catenin activity is required to suppress PLVAP. Consistent with this, PLVAP expression in the mouse [25] and zebrafish [8] retina, as well as in the mouse and zebrafish brain [8, 31], has been established as a marker of immature or pathological BBB and BRB.

While our model is well-suited to investigate the prevention of BBB formation during development, it may not fully recapitulate the breakdown of a mature barrier. Therefore, future research using adult zebrafish may be more appropriate for investigating BRB and BBB dysfunction in the context of established human disease [36, 37]. The current model replicates compromised barrier integrity and the resulting vasogenic edema, as observed in various human pathologies affecting the BRB [1, 3] and BBB [18, 19]. However, it studies the barrier during its initial formation rather than after its subsequent disruption. Therefore, adult zebrafish may be a superior model for future research, since their larger head size minimizes confounding tracer influx from non-BBB sources.

In addition to increased tracer permeability, we detected vasodilation in the midbrain vasculature of zebrafish exposed to hyperglycemia, with changes in vessel diameter detectable as early as 24 h (4 dpf) after exposure. This early response to hyperglycemia in the brain is in agreement with reports of hyperglycemia-induced vasodilation in retinal blood vessels of diabetic patients [38]. A potential mechanism for the vasodilation is hyperglycemia-triggered VEGF signaling, leading to nitric oxide (NO)-mediated pericyte relaxation [15, 18, 39]. This mechanism is supported by Jung et al. (2016), who demonstrated hyperglycemia-induced NO production in hyaloid-retinal vessels through direct NO measurements [15]. Alternatively, hyperglycemia may induce phenotypic changes in pericytes that impair their maturation and disrupt pericyte-endothelial communication [40-42]. This disruption can lead to both vasodilation [40] and impaired barrier formation in the developing brain [43]. In addition to investigating the role of pericytes, other cell types of the neurovascular unit, such as radial glia cells [10, 44, 45] and microglia [46-50], may be worth investigating for their contribution to BBB formation. Live imaging of these cell types in

transgenic lines would enable detailed investigation of their roles in processes such as vasodilation and vascular permeability.

Elevated VEGF levels could also promote caveolae formation in barrier endothelium, as shown by TEM [2, 26, 51]. In the present study, TEM analysis confirmed the presence of caveolae in endothelial cells at 5 dpf on both the luminal and abluminal sides with morphology consistent with prior reports [7]. However, their quantification was challenged by their frequent indistinctness. It remains unclear if this was due to an intrinsically low density of caveolae in this model or a technical limitation of our image resolution. As a result, the role of caveolar-mediated transcytosis in the hyperglycemia-induced permeability we observed could not be determined. A much higher caveolar density (up to 13-fold) has been reported in other models, such as retinal capillary endothelial cells of monkeys [51], likely reflecting interspecies variation. However, technical limitations in resolution or contrast in our study may also be a factor. Future studies using enhanced TEM protocols with contrast agents like peroxidase tracers [52], may yield more reliable visualization .

In conclusion, we have established a zebrafish model of vasogenic edema and a corresponding toolbox for *in vivo* BBB in assessment. This platform is extendable to other BBB challenges, including inflammatory proteins, and allows for deeper mechanistic insight through the analysis of additional targets like tight junction proteins ZO-1 [10, 53], and the transcytosis inhibitor Mfsd2a [7, 54]. As a proof of concept, our work also underscores the potential of this model for studying long-term BRB and BBB breakdown in adult zebrafish, thereby accelerating the development of therapies for associated eye diseases and neurological complications.

Materials and methods

Zebrafish maintenance

The animal ethics of this study were conducted in accordance with the EU Directive 2010/63/EU on the protection of animals used for scientific purposes. All methods were conducted in compliance with the ARRIVE guidelines (https://arriveguidelines.org). Adult zebrafish were maintained at 28.0 °C in aerated 5 liter tanks with a 14 h light/10 h dark cycle. Embryos were obtained from adult *Tg(fli1:EGFP)*, *Tg(cldn5a:EGFP)* (kindly provided by prof. dr. Wilbert Bitter) and *Tg(plvapb:EGFP;kdrl:mCherry)* and raised in embryonic (E3) media under standard conditions at 28.0 °C. *Tg(fli1:EGFP)* expresses enhanced green fluorescent protein (EGFP) under the control of the promotor of the *fli1* gene, an endothelial cell marker, showing the vasculature [55]. *Tg(cldn5a:EGFP)* was included because of the high homology and synteny of *claudin 5a* with human *CLDN5* and has an inserted EGFP at the translation start site of the *claudin 5a* gene [12]. The *Tg(plvapb:EGFP)*^{ulb40} line was generated in this study, by cloning a 3.083 kb fragment of the zebrafish *plvapb* promoter (ENSDARG00000045003) upstream of EGFP in pTol2, as previously described[8]. The transgenic line was generated by co-injecting 15 pg of the construct with 25 pg of Tol2 transposase mRNA in one-cell stage embryos.

Glucose exposure and measurement of whole-body glucose levels
Tg(fli1:EGFP) zebrafish embryos were placed in 100 mm petri dishes at 3 dpf with 100 embryos per petri dish in E3 media containing either 60 mM or 130 mM D-glucose (Cat. No. 108337; Merck), based on results previously published by Jung *et al*. (2016) and Sing *et al*. (2019) [14, 15]. Media were maintained until 5 dpf and refreshed every day. Survival rates were determined at 3, 4 and 5 dpf. In the following experiments, zebrafish larvae were exposed to 60 mM and 130 mM glucose from 3 to 5 dpf.

Control zebrafish were maintained under identical conditions in E3 medium only. Furthermore, zebrafish were exposed to mannitol (130 mM) (Cat. No. 12.534.21; Janssen Chimica) instead of glucose under identical conditions as a control for hyperosmolarity. Quantitative analysis of glucose levels was performed on whole body lysates at 3, 4 and 5 dpf. Forty zebrafish larvae in each experimental group were placed on ice. The medium was removed and the larvae were washed thrice with E3 medium to remove extracellular glucose. After the E3 medium was aspirated as completely as possible, the zebrafish were homogenized using a hand homogenizer. After centrifugation at 18,407 g for 2 min, 5 µl of the supernatant was placed on parafilm and aspirated by a test strip. Total internal glucose levels were measured with a glucose meter (Accu-Chek Instant, Roche). The procedures are shown in Figure 1a. The average of 3 technical replicates was taken per condition with at least 3 independent biological replicates (n = 3).

Tracer injections
Tg(fli1:EGFP) zebrafish larvae at 3, 4 and 5 dpf were anesthetized using tricaine (0.9 mM; A-5040, Sigma) and placed with their yolk sac facing upwards in a 2% low melting point (LMP) agarose (Cat. No. 16520; Invitrogen) with grooves made with an injection mold. Two nanoliter of 5 mg/ml Cy5 792 Da (Cat. No. 95017-553; Amersham Bioscience) and 5 mg/ml Dextran-Texas Red 70 kDa (D1830; Invitrogen) was injected into the cardiac sac using a FemtoJet (Eppendorf) coupled to an InjectMan NI 2 (Eppendorf) under a Leica DM IRB inverted fluorescence microscope. Following injection, larvae were screened for a beating heart. Those with confirmed cardiac activity were selected, and the timing of their live imaging was randomized within the 30 min to 4 h post-injection window.

Fluorescence microscopy
Injected *Tg(fli1:EGFP)* and non-injected *Tg(cldn5a:EGFP)* zebrafish larvae were anesthetized with tricaine and mounted in 0.8% LMP agarose on a glass bottom imaging dish (Cat. No. 627860; Greiner bio-one) with their yolk sac facing upwards and were imaged within 3 h. Image analysis was performed with a confocal laser scanning microscope (Leica TCS SP8 X/ Leica TCS SP8 SMD/Leica Stellaris 8; Leica DMI 6000) using a 20x dry objective (NA 0.75) and 40x oil immersion objective (NA 1.30). A z-stack of 30 µm was taken with the middle mesencephalic central arteryin the middle of the z-stack to image cerebral blood vessels. *Tg(plvapb:EGFP)^{ulb40};(kdrl:ras-mCherry)^{s896}* larvae were anesthetized with tricaine and mounted in 1% low melting point agarose on a glass bottom imaging dish (MatTek Corporation, Ashland, MA) with their yolk sac facing upwards. Larvae were imaged using the Zeiss LSM900 confocal microscope with 20x dry objective (NA 0.8). A z-stack of 3 µm was taken. Images were analyzed and processed using ImageJ software.

Non-injected *Tg(fli1:EGFP)* zebrafish of 3, 4 and 5 dpf were mounted in 0.8% LMP agarose on a glass bottom imaging dish in a lateral position to assess the zebrafish morphology. Fifteen zebrafish per condition per day were imaged. Brightfield and fluorescence images were generated with an Axio Zoom.V16 microscope (Zeiss).

Quantification of tracer permeability

Permeability of cerebral blood vessels was assessed after tracer injection and imaging of zebrafish heads. Fluorescence images taken at 20x magnification with a z-stack of 30 µm were included for quantification. Fluorescence tracer intensity was measured using ImageJ. After masking and digitally subtracting the vasculature, fluorescence intensity was measured in 6 parenchymal regions. The mean of the parenchymal tracer intensity was then normalized to the mean tracer intensity within the vasculature, that was measured in 3 regions in order to correct for variations in the amount of tracer injected or circulating tracer. The normalized fluorescence intensity was calculated for each fish, with a total sample size of 10-15 fish per experimental condition, originating from at least 3 independent adult crosses. The quantification procedure is shown in Figure 3a-d.

Quantification of blood vessel diameter

Cerebral blood vessel diameter was determined using ImageJ software (National Institute of Health) with the Concentric Circle plugin [56]. Fluorescence images of the zebrafish head were used for quantification of blood vessel diameter. Images were prepared as a z-stack of 30 µm. The diameter of the middle mesencephalic central artery of each fish was measured at 4 different locations on the artery on the concentric circles of which the mean was calculated for every fish. The blood vessel measurement procedures are shown in Figure 4a-c. A total number of 15 ± 2 fish was quantified per experimental condition with at least 3 biological replicates.

Quantification of PLVAP expression

*plvapb:*EGFP expression was quantified using ImageJ. Vessel segments were defined as discrete vascular elements between branching points or endpoints. For each larvae, the proportion of GFP^+ vessel segments relative to the total number of $mCherry^+$ segments at 4 and 5 dpf was calculated from maximum intensity projections of confocal z-stacks. For each experimental condition, a total of 8–15 larvae were analyzed across two independent biological replicates.

Transmission electron microscopy

Tg(fli1:EGFP) zebrafish of 5 dpf were fixed in glutardialdehyde 25% (Sigma, 1.04239) overnight at room temp and post-fixed with 1% osmium tetroxide (OsO4, Electron Microscopy Sciences, Hatfield, PA, USA). Subsequently, the samples were dehydrated in an alcohol series and last steps in 1,2-propylene oxide (Sigma-Aldrich) then embedded into Epon (LX-112 resin Ladd research, Williston, VT, USA). Ultrathin (60 nm) epon sections of the samples were cut and collected on Formvar-coated grids, counterstained with uranyl acetate and lead citrate. All samples were examined and photographed in a Tecnai T12 TEM with a Xarosa camera and Radius software (EMSIS) at the Electron Microscopy Centre Amsterdam.

Statistical analysis

Statistical analysis was performed using GraphPad Prism 8 or 10 (GraphPad Software, Inc.). A Kruskal-Wallis statistical test (with post hoc Dunn's test) was used to determine statistically significant differences between experimental groups and between different ages. $P < 0.05$ was considered statistically significant. No data was excluded from the statistical analyses.

Data availability

The datasets generated during and/or analyzed during the present study are available from the corresponding author on request.

Acknowledgements

The authors acknowledge Theo Verboom, dr. Kinki Jim and the Microscopy and Cytometry Core Facility - location AMC (MCCF-AMC) for their technical assistance. This work was supported by the following foundations: Algemene Nederlandse Vereniging ter Voorkoming van Blindheid, Leidse Stichting voor Blinden en Slechtzienden, Stichting Oogfonds that contributed through UitZicht (UZ2021-27), the Rotterdamse Stichting Blindenbelangen (grant B20220071) and Stichting tot Verbetering van het Lot der Blinden. Work in the B.V. laboratory is supported by the ERC (Ctrl-BBB 865176). This study was published with the help of the Edmond and Marianne Blaauw Fund for Ophthalmology. The funding organizations had no role in the design or conduct of this research. They provided unrestricted grants.

Author contributions

N.B.v.B , E.E.S. and I.K. designed experiments. N.B.v.B., E.E.S., F.E.E.H. and A.E.G. performed experiments and analyzed data. L.L, M.V. and B.V. contributed the *Tg(plvapb:EGFP)* line and data. I.K. supervised the project. N.B.v.B. wrote the manuscript. B.V., L.L., M.V., N.v.d.W, C.J.F.v.N., R.O.S., and I.K. contributed to the discussion and editing of the manuscript. All authors have read and approved the final manuscript.

Additional information

Competing interests

The authors declare no competing interests.

References

[1] Klaassen I, Van Noorden CJ, Schlingemann RO (2013) Molecular basis of the inner blood-retinal barrier and its breakdown in diabetic macular edema and other pathological conditions. Prog Retin Eye Res 34: 19–48. doi: 10.1016/j.preteyeres.2013.02.001

[2] Wisniewska-Kruk J, van der Wijk AE, van Veen HA, Gorgels TG, Vogels IM, Versteeg D, et al. (2016) Plasmalemma Vesicle-Associated Protein Has a Key Role in Blood-Retinal Barrier Loss. Am J Pathol 186(4): 1044–1054. doi: 10.1016/j.ajpath.2015.11.019

[3] Little K, Llorian-Salvador M, Scullion S, Hernandez C, Simo-Servat O, Del Marco A, et al. (2022) Common pathways in dementia and diabetic retinopathy: understanding the mechanisms of diabetes-related cognitive decline. Trends Endocrinol Metab 33(1): 50–71. doi: 10.1016/j.tem.2021.10.008

[4] Alvarez Y, Cederlund ML, Cottell DC, Bill BR, Ekker SC, Torres-Vazquez J, et al. (2007) Genetic determinants of hyaloid and retinal vasculature in zebrafish. BMC Dev Biol 7: 114. doi: 10.1186/1471-213X-7-114

[5] Xie J, Farage E, Sugimoto M, Anand-Apte B (2010) A novel transgenic zebrafish model for blood-brain and blood-retinal barrier development. BMC Dev Biol 10: 76. doi: 10.1186/1471-213X-10-76

[6] Li Y, Chen T, Miao X, Yi X, Wang X, Zhao H, et al. (2017) Zebrafish: A promising in vivo model for assessing the delivery of natural products, fluorescence dyes and drugs across the blood-brain barrier. Pharmacol Res 125(Pt B): 246–257. doi: 10.1016/j.phrs.2017.08.017

[7] O'Brown NM, Megason SG, Gu C (2019) Suppression of transcytosis regulates zebrafish blood-brain barrier function. Elife 8. doi: 10.7554/eLife.47326

[8] Umans RA, Henson HE, Mu F, Parupalli C, Ju B, Peters JL, et al. (2017) CNS angiogenesis and barriergenesis occur simultaneously. Dev Biol 425(2): 101–108. doi: 10.1016/j.ydbio.2017.03.017

[9] Eliceiri BP, Gonzalez AM, Baird A (2011) Zebrafish model of the blood-brain barrier: morphological and permeability studies. Methods Mol Biol 686: 371–378. doi: 10.1007/978-1-60761-938-3_18

[10] Jeong JY, Kwon HB, Ahn JC, Kang D, Kwon SH, Park JA, et al. (2008) Functional and developmental analysis of the blood-brain barrier in zebrafish. Brain Res Bull 75(5): 619–628. doi: 10.1016/j.brainresbull.2007.10.043

[11] Fleming A, Diekmann H, Goldsmith P (2013) Functional characterisation of the maturation of the blood-brain barrier in larval zebrafish. PLoS One 8(10): e77548. doi: 10.1371/journal.pone.0077548

[12] van Leeuwen LM, Evans RJ, Jim KK, Verboom T, Fang X, Bojarczuk A, et al. (2018) A transgenic zebrafish model for the in vivo study of the blood and choroid plexus brain barriers using claudin 5. Biol Open 7(2). doi: 10.1242/bio.030494

[13] Lawson ND, Weinstein BM (2002) In vivo imaging of embryonic vascular development using transgenic zebrafish. Dev Biol 248(2): 307–318. doi: 10.1006/dbio.2002.0711

[14] Singh A, Castillo HA, Brown J, Kaslin J, Dwyer KM, Gibert Y (2019) High glucose levels affect retinal patterning during zebrafish embryogenesis. Sci Rep 9(1): 4121. doi: 10.1038/s41598-019-41009-3

[15] Jung SH, Kim YS, Lee YR, Kim JS (2016) High glucose-induced changes in hyaloid-retinal vessels during early ocular development of zebrafish: a short-term animal model of diabetic retinopathy. Br J Pharmacol 173(1): 15–26. doi: 10.1111/bph.13279

[16] Bosma EK, van Noorden CJF, Schlingemann RO, Klaassen I (2018) The role of plasmalemma vesicle-associated protein in pathological breakdown of blood-brain and blood-retinal barriers: potential novel therapeutic target for cerebral edema and diabetic macular edema. Fluids Barriers CNS 15(1): 24. doi: 10.1186/s12987-018-0109-2

[17] Li X, Cai Y, Zhang Z, Zhou J (2022) Glial and Vascular Cell Regulation of the Blood-Brain Barrier in Diabetes. Diabetes Metab J 46(2): 222–238. doi: 10.4093/dmj.2021.0146

[18] Kadry H, Noorani B, Cucullo L (2020) A blood-brain barrier overview on structure, function, impairment, and biomarkers of integrity. Fluids Barriers CNS 17(1): 69. doi: 10.1186/s12987-020-00230-3
[19] Profaci CP, Munji RN, Pulido RS, Daneman R (2020) The blood-brain barrier in health and disease: Important unanswered questions. J Exp Med 217(4). doi: 10.1084/jem.20190062
[20] Bogush M, Heldt NA, Persidsky Y (2017) Blood Brain Barrier Injury in Diabetes: Unrecognized Effects on Brain and Cognition. J Neuroimmune Pharmacol 12(4): 593–601. doi: 10.1007/s11481-017-9752-7
[21] Carús-Cadavieco M, de la Fuente SG, López IB, Serrano-Lope MA, Aguado B, Guix F, et al. (2024) Loss of Cldn5-and increase in Irf7-in the hippocampus and cerebral cortex of diabetic mice at the early symptomatic stage. Nutr Diabetes 14(1). doi: 10.1038/s41387-024-00325-y
[22] Geng J, Wang L, Zhang L, Qin C, Song Y, Ma Y, et al. (2018) Blood-Brain Barrier Disruption Induced Cognitive Impairment Is Associated With Increase of Inflammatory Cytokine. Front Aging Neurosci 10: 129. doi: 10.3389/fnagi.2018.00129
[23] Chhabria K, Plant K, Bandmann O, Wilkinson RN, Martin C, Kugler E, et al. (2020) The effect of hyperglycemia on neurovascular coupling and cerebrovascular patterning in zebrafish. J Cereb Blood Flow Metab 40(2): 298–313. doi: 10.1177/0271678X18810615
[24] Schlingemann RO, Hofman P, Vrensen GF, Blaauwgeers HG (1999) Increased expression of endothelial antigen PAL-E in human diabetic retinopathy correlates with microvascular leakage. Diabetologia 42(5): 596–602. doi: 10.1007/s001250051200
[25] van der Wijk AE, Wisniewska-Kruk J, Vogels IMC, van Veen HA, Ip WF, van der Wel NN, et al. (2019) Expression patterns of endothelial permeability pathways in the development of the blood-retinal barrier in mice. FASEB J 33(4): 5320–5333. doi: 10.1096/fj.201801499RRR
[26] Hofman P, Hoyng P, vanderWerf F, Vrensen GF, Schlingemann RO (2001) Lack of blood-brain barrier properties in microvessels of the prelaminar optic nerve head. Invest Ophthalmol Vis Sci 42(5): 895–901.
[27] Hofman P, Blaauwgeers HG, Vrensen GF, Schlingemann RO (2001) Role of VEGF-A in endothelial phenotypic shift in human diabetic retinopathy and VEGF-A-induced retinopathy in monkeys. Ophthalmic Res 33(3): 156–162. doi: 10.1159/000055663
[28] Kida T, Oku H, Osuka S, Horie T, Ikeda T (2021) Hyperglycemia-induced VEGF and ROS production in retinal cells is inhibited by the mTOR inhibitor, rapamycin. Sci Rep 11(1): 1885. doi: 10.1038/s41598-021-81482-3
[29] Adamis AP, Miller JW, Bernal MT, D'Amico DJ, Folkman J, Yeo TK, et al. (1994) Increased vascular endothelial growth factor levels in the vitreous of eyes with proliferative diabetic retinopathy. Am J Ophthalmol 118(4): 445–450. doi: 10.1016/s0002-9394(14)75794-0
[30] Aiello LP, Avery RL, Arrigg PG, Keyt BA, Jampel HD, Shah ST, et al. (1994) Vascular endothelial growth factor in ocular fluid of patients with diabetic retinopathy and other retinal disorders. N Engl J Med 331(22): 1480–1487. doi: 10.1056/NEJM199412013312203
[31] Benz F, Wichitnaowarat V, Lehmann M, Germano RF, Mihova D, Macas J, et al. (2019) Low wnt/beta-catenin signaling determines leaky vessels in the subfornical organ and affects water homeostasis in mice. Elife 8. doi: 10.7554/eLife.43818
[32] Liebner S, Corada M, Bangsow T, Babbage J, Taddei A, Czupalla CJ, et al. (2008) Wnt/beta-catenin signaling controls development of the blood-brain barrier. J Cell Biol 183(3): 409–417. doi: 10.1083/jcb.200806024
[33] Laksitorini MD, Yathindranath V, Xiong W, Hombach-Klonisch S, Miller DW (2019) Modulation of Wnt/beta-catenin signaling promotes blood-brain barrier phenotype in cultured brain endothelial cells. Sci Rep 9(1): 19718. doi: 10.1038/s41598-019-56075-w
[34] Zhou Y, Wang Y, Tischfield M, Williams J, Smallwood PM, Rattner A, et al. (2014) Canonical WNT signaling components in vascular development and barrier formation. J Clin Invest 124(9): 3825–3846. doi: 10.1172/JCI76431

[35] Wang Y, Rattner A, Zhou Y, Williams J, Smallwood PM, Nathans J (2012) Norrin/Frizzled4 signaling in retinal vascular development and blood brain barrier plasticity. Cell 151(6): 1332–1344. doi: 10.1016/j.cell.2012.10.042
[36] Kim SY, Cheon J (2024) Senescence-associated microvascular endothelial dysfunction: A focus on the blood-brain and blood-retinal barriers. Ageing Res Rev 100: 102446. doi: 10.1016/j.arr.2024.102446
[37] Knox EG, Aburto MR, Clarke G, Cryan JF, O'Driscoll CM (2022) The blood-brain barrier in aging and neurodegeneration. Mol Psychiatry 27(6): 2659–2673. doi: 10.1038/s41380-022-01511-z
[38] Bek T (2017) Diameter Changes of Retinal Vessels in Diabetic Retinopathy. Curr Diab Rep 17(10): 82. doi: 10.1007/s11892-017-0909-9
[39] Bosma EK, Darwesh S, Habani YI, Cammeraat M, Martinez PS, Smallenburg MEV, et al. (2023) Differential roles of eNOS in late effects of VEGF-A on hyperpermeability in different types of endothelial cells. Sci Rep-Uk 13(1). doi: 10.1038/s41598-023-46893-4
[40] Bergers G, Song S (2005) The role of pericytes in blood-vessel formation and maintenance. Neuro Oncol 7(4): 452–464. doi: 10.1215/S1152851705000232
[41] Chilton R, Iranpour EI, Bloomgarden Z (2024) Deciphering the connection: Diabetes, pericyte dysfunction, and their impact on cardiovascular health. J Diabetes 16(2): e13539. doi: 10.1111/1753-0407.13539
[42] Liu C, Ge HM, Liu BH, Dong R, Shan K, Chen X, et al. (2019) Targeting pericyte-endothelial cell crosstalk by circular RNA-cPWWP2A inhibition aggravates diabetes-induced microvascular dysfunction. Proc Natl Acad Sci U S A 116(15): 7455–7464. doi: 10.1073/pnas.1814874116
[43] van der Wijk AE, Vogels IMC, van Veen HA, van Noorden CJF, Schlingemann RO, Klaassen I (2018) Spatial and temporal recruitment of the neurovascular unit during development of the mouse blood-retinal barrier. Tissue Cell 52: 42–50. doi: 10.1016/j.tice.2018.03.010
[44] Lyons DA, Talbot WS (2014) Glial cell development and function in zebrafish. Cold Spring Harb Perspect Biol 7(2): a020586. doi: 10.1101/cshperspect.a020586
[45] McKeown KA, Moreno R, Hall VL, Ribera AB, Downes GB (2012) Disruption of Eaat2b, a glutamate transporter, results in abnormal motor behaviors in developing zebrafish. Dev Biol 362(2): 162–171. doi: 10.1016/j.ydbio.2011.11.001
[46] Vazquez-Liebanas E, Mocci G, Li W, Lavina B, Reddy A, O'Connor C, et al. (2024) Mosaic deletion of claudin-5 reveals rapid non-cell-autonomous consequences of blood-brain barrier leakage. Cell Rep 43(3): 113911. doi: 10.1016/j.celrep.2024.113911
[47] Silva NJ, Dorman LC, Vainchtein ID, Horneck NC, Molofsky AV (2021) In situ and transcriptomic identification of microglia in synapse-rich regions of the developing zebrafish brain. Nat Commun 12(1): 5916. doi: 10.1038/s41467-021-26206-x
[48] Narra SS, Rondeau P, Fernezelian D, Gence L, Ghaddar B, Bourdon E, et al. (2023) Distribution of microglia/immune cells in the brain of adult zebrafish in homeostatic and regenerative conditions: Focus on oxidative stress during brain repair. J Comp Neurol 531(2): 238–255. doi: 10.1002/cne.25421
[49] Lou L, Yu T, Dai Y, Zhao S, Feng S, Xu J, et al. (2022) Mafba and Mafbb regulate microglial colonization of zebrafish brain via controlling chemotaxis receptor expression. Proc Natl Acad Sci U S A 119(39): e2203273119. doi: 10.1073/pnas.2203273119
[50] Palsamy K, Chen JY, Skaggs K, Qadeer Y, Connors M, Cutler N, et al. (2023) Microglial depletion after brain injury prolongs inflammation and impairs brain repair, adult neurogenesis and pro-regenerative signaling. Glia 71(11): 2642–2663. doi: 10.1002/glia.24444
[51] Hofman P, Blaauwgeers HG, Tolentino MJ, Adamis AP, Nunes Cardozo BJ, Vrensen GF, et al. (2000) VEGF-A induced hyperpermeability of blood-retinal barrier endothelium in vivo is predominantly associated with pinocytotic vesicular transport and not with formation of fenestrations. Vascular endothelial growth factor-A. Curr Eye Res 21(2): 637–645.
[52] Reese TS, Karnovsky MJ (1967) Fine structural localization of a blood-brain barrier to exogenous peroxidase. J Cell Biol 34(1): 207–217. doi: 10.1083/jcb.34.1.207
[53] Wang Y, Pan L, Moens CB, Appel B (2014) Notch3 establishes brain vascular integrity by regulating pericyte number. Development 141(2): 307–317. doi: 10.1242/dev.096107

[54] Wood CAP, Zhang J, Aydin D, Xu Y, Andreone BJ, Langen UH, et al. (2021) Structure and mechanism of blood-brain-barrier lipid transporter MFSD2A. Nature 596(7872): 444–448. doi: 10.1038/s41586-021-03782-y
[55] Delov V, Muth-Kohne E, Schafers C, Fenske M (2014) Transgenic fluorescent zebrafish Tg(fli1:EGFP)y(1) for the identification of vasotoxicity within the zFET. Aquat Toxicol 150: 189–200. doi: 10.1016/j.aquatox.2014.03.010
[56] Schneider CA, Rasband WS, Eliceiri KW (2012) NIH Image to ImageJ: 25 years of image analysis. Nat Methods 9(7): 671–675. doi: 10.1038/nmeth.2089

Supplementary Figure

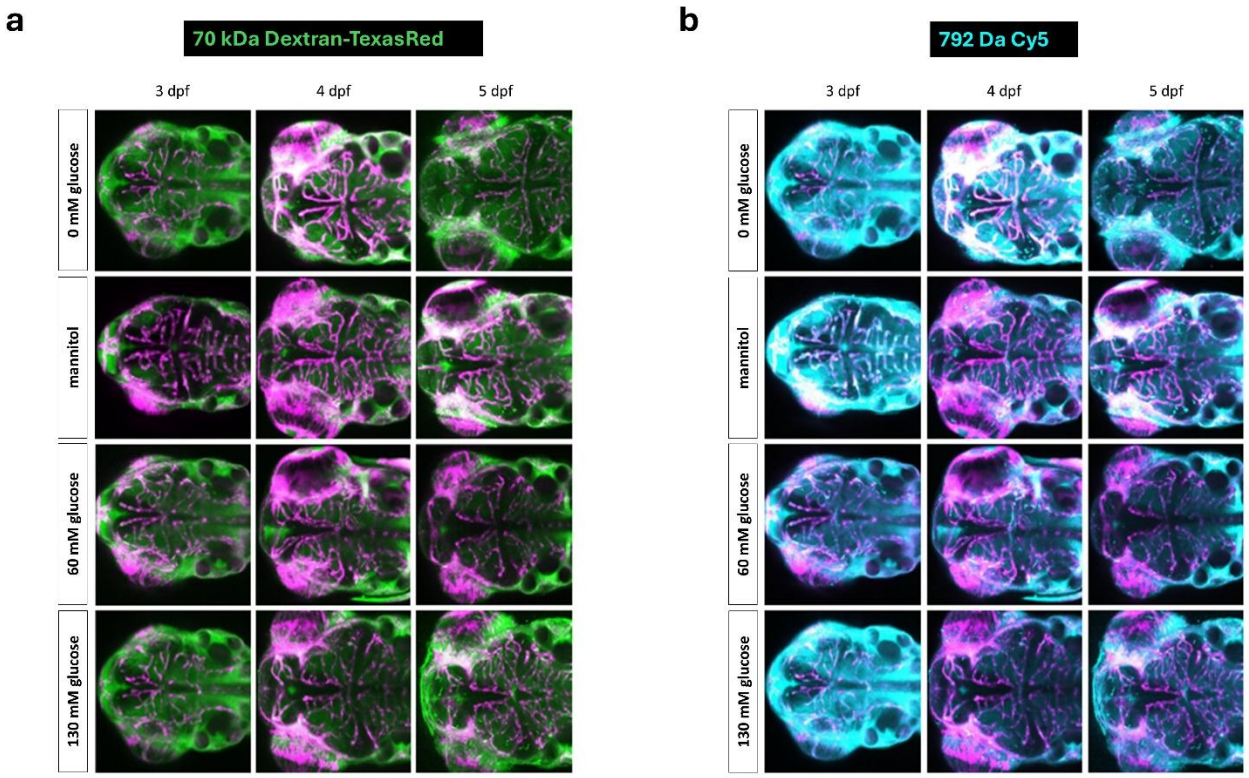

Supplementary Figure S1. Tracer permeability in zebrafish cerebral vasculature. Representative maximum intensity projection of a confocal z-stack showing the brain (dorsal view) of *Tg(fli1:EGFP)* zebrafish injected with (**a**) 70 kDa Dextran-Texas Red (green) and (**b**) 792 Da Cy5 (cyan) at 3, 4 and 5 dpf under hyperglycemic conditions (60 mM or 130 mM glucose). 0 mM glucose and 130 mM mannitol were included as controls. Vasculature is shown in magenta.

Chapter 3

Revealing subcellular retinal alterations in 5xFAD B6SJLF1/J mice

A. Giani[1,2]*, C.A. Musi[1,2]*, E.C. Priori[1,2], S. Turchetti[3,2], M. Passi[1,2], S. Galbiati[4], I. Viganò[4], N. Bakker[5], I. Klaassen[5], G. Zerbini[4] and T. Borsello[1,2†], on behalf of the RECOGNISED consortium

[1] Department of Pharmacological and Biomolecular Sciences, University of Milan, Milan, Italy
[2] Department of Neuroscience, IRCCS-Mario Negri Institute for Pharmacological Research, Milan, Italy
[3] Department of Life and Environmental Sciences, Marche Polytechnic University, Ancona, Italy
[4] Complications of Diabetes Unit, Diabetes Research Institute, IRCCS Ospedale San Raffaele, Milano, Italy
[5] Ocular Angiogenesis Group, Department of Ophthalmology, Amsterdam UMC location University of Amsterdam, Amsterdam, The Netherlands.

* These authors contributed equally to this work.

Manuscript under revision at Experimental Neurology

Abstract

5xFAD mouse model recapitulates key pathological features of Alzheimer's disease (AD). However, it remains unclear whether JNK activation is a common pathogenic mechanism driving both retinal and cerebral neurodegeneration. Establishing this shared pathway would significantly enhance the retina's potential as an accessible central nervous system (CNS) window for monitoring AD progression.

We analyzed total retinal homogenates and postsynaptic-enriched protein fractions from 2, 4, 6, and 10-month-old 5xFAD B6SJLF1/J mice using western blotting and immunofluorescence staining. Key markers of JNK signaling (JNK, p-JNK, JNK3, c-Jun, p-c-Jun) and synaptic integrity (PSD95, p-PSD95) were examined. Additionally, we assessed gliosis (GFAP) and amyloid pathology (APP, p-APP) markers to evaluate retinal AD progression. Finally, we compared retinal layer thickness between 5xFAD and wild-type (WT) mice across these age points.

Although western blotting revealed no significant JNK signaling activation in total retinal homogenates, synaptic dysfunction was evident through increased PSD95 phosphorylation in 5xFAD mice. Immunofluorescence analysis demonstrated elevated JNK3 immunoreactivity and gliosis in transgenic animals compared to controls. Notably, while WT mice exhibited age-related inner nuclear layer (INL) thinning, 5xFAD mice maintained stable INL thickness and showed progressive total retinal thickening.

These findings demonstrate fundamental differences in AD pathology between retinal and brain tissues in 5xFAD B6SJLF1/J mice. The weak JNK activation signature observed in retinal tissue, contrasting with robust brain pathology, suggests current limitations in developing retinal biomarkers for AD detection. Furthermore, our results underscore the necessity of both technical refinement and cautious interspecies interpretation when evaluating the retina's potential as a CNS disease monitor.

Introduction

Alzheimer's disease (AD) is a progressive neurodegenerative disorder characterized by a gradual and irreversible decline in cognitive and functional abilities [1]. Current treatments are primarily symptomatic and aim to slow the progression of the disease rather than provide a definitive solution. Recently, two anti-amyloid therapies have been approved for early-stage Alzheimer's disease, marking a milestone in disease-modifying treatment. Lecanemab (Leqembi) received FDA approval in January 2023, and donanemab (Kisunla) was approved in July 2024. Both are monoclonal antibodies targeting amyloid plaques, aimed at reducing amyloid burden and slowing cognitive decline in patients with early symptomatic AD.

The pathological features of AD include the accumulation in the brain of amyloid β (Aβ) plaques and the formation of neurofibrillary tangles (NFTs) of hyperphosphorylated tau (pTau). These pathological processes drive synaptic dysfunction and neuronal degeneration, ultimately leading to cognitive impairment. The absence of a resolutive cure for AD is primarily due to its multifactorial pathology and the brain's limited accessibility, which makes it difficult to identify the onset and progression of degenerative processes.

Recent evidence suggests that the retina may serve as a window into brain parenchyma. As an extension of the central nervous system (CNS), the retina shares an embryonic origin with the brain and exhibits similar responses to neuronal damage. This connection is reinforced by clinical observations in type 2 diabetes (T2D), where diabetic retinopathy frequently co-exists with cognitive impairment and dementia [2, 3]. Retinal neural degeneration in AD was first reported in 1986 [4], showing ganglion cell loss and optic nerve fiber degeneration in post-mortem AD retinas. Optical coherence tomography (OCT), now the gold standard for retinal imaging, has since revealed AD-related retinal changes, including thinning of the peripapillary retinal nerve fiber layer (pRNFL), ganglion cell-inner plexiform layer (GC-IPL), macula volume, and choroid [5-7]. Similar thinning has been seen in mild cognitive impairment (MCI) patients, correlating with AD severity and cognitive decline [8]. Aβ plaques have also been detected in AD retinas [7]. However, collecting longitudinal data on elderly populations can be challenging. Consequently, transgenic mice serve as a valuable model for studying AD-related changes in the CNS and retina and for assessing drug efficacy [9].

Retinal accumulation of Aβ has been observed in multiple transgenic mouse models of AD, though the timing of plaque formation varies across models [10, 11]. For instance, 5xFAD mice, with a C57BL/6J pure background, exhibit the earliest plaque formation at 2 months, while Tg2576 mice exhibit the latest at 10 months [12-14]. Notably, in APPSWE/PS1△E9 mice, retinal Aβ plaques appear earlier than brain plaques, suggesting retinal changes precede brain pathology [15, 16]. Functional retinal degeneration, including RNFL thinning and ganglion cell activity shifts, be-gins early and progresses with disease severity. Retinal thinning correlates with broader neurodegenerative changes, making the retina a potential early marker for AD progression.

Although evidence is growing, the link between retinal, brain abnormalities and cognitive impairment remains unclear. Identifying shared pathogenic mechanisms and therapeutic targets between the brain and retina is crucial for identifying measurable retinal indicators for brain damage, paving the way for new diagnostic and therapeutic advancements.

c-Jun N-terminal kinase (JNK) plays a critical role in Alzheimer's disease and retinal degeneration. The JNK family consists of three main isoforms, JNK1, JNK2, and the neuron-enriched JNK3, which typically appear at ~46 kDa and ~54 kDa, and collectively regulate stress-responsive signaling pathways highly relevant to neurodegeneration. In AD, JNK contributes to Aβ plaque formation and tau tangle pathology by phosphorylating of APP and tau. Additionally, it disrupts synaptic function through glutamate receptors mislocalization. In the retina, JNK activation is involved in retinal ganglion cell loss, vascular endothelial growth factor (VEGF) expression, and photoreceptor death [17-23]. In the context of AD, the CRND8 AD model showed increased JNK and c-Jun activation in both the retina and the brain [24]. This suggests that JNK activation in both areas is linked to Aβ oligomer production and neuronal degeneration, making JNK a common player in the retina and brain. In the 5xFAD mouse model on B6SJLF1/J hybrid background, amyloid plaque deposition in the brain begins at 2 months, during the presymptomatic phase, while cognitive decline becomes apparent by 3.5 months [25]. In this model, JNK activation also correlates with post-synaptic density alterations and early-stage memory impairment, underscoring its pivotal role in AD pathogenesis.

Using western blotting and immunofluorescence, we examined whether neurodegeneration occurs earlier in the retina in this model and whether JNK activation represents a shared pathogenic pathway in retinal and brain degeneration. We longitudinally analyzed mice using OCT to assess retinal alterations focusing on four different time points to mirror the progression of AD: 2 months of age (pre-symptomatic phase), 4 months of age (prodromic phase), 6 months of age (advanced phase), and 10 months of age (late-stage disease).

Materials and methods

Mice

5xFAD mice (B6SJL-Tg (APPSwFlLon, PSEN1*M146L*L286V) 6799Vas/Mmjax Strain #034840-JAX) on a B6SJLF1/J background were obtained from the Jackson Laboratory. Age-matched wild-type (WT) littermates were used as controls. Hemizygous male mice (not carriers for the Pde6brd1 gene) were bred to B6SJLF1/J female mice (carriers for the Pde6brd1 gene) at the Mario Negri Institute for Pharmacological Research IRCCS animal facility [25]. Procedures involving animals and their care were conducted by national and international laws and policies (Permit Number 4/2021-PR). The experimental design included two groups: Tg-5xFAD B6SJLF1/J mice and WT mice. Blind (homozygous for mutation in the Pde6brd1 gene) and heterozygous mice were not included in the experiment. Both male and female Tg-5xFAD B6SJLF1/J and WT mice were assessed at four ages: 2 months (n = 7 per group), 4 months (n = 7 per group), 6 months (n=7 per group) and 10 months (n = 7 per group). Specifically, for each group (WT and TG), four males and three females were included at each time point. Animals were sacrificed by decapitation and retinas were extracted from the eyes of Tg-5xFAD B6SJLF1/J and WT. Retinal tissues were stored at −80°C until further pro-cessing.

Genotyping

Genotyping was conducted using PCR, using a standard protocol provided by the Jackson Laboratory, using the GoTaq®G2 Flexi DNA polymerase kit (Promega, Madison, WI, USA). Tg-5xFAD B6SJLF1/J and WT mice were tested for APP and Pde6brd1 genes.

Triton X-100 insoluble fractionation (TIF)
Animals were sacrificed and the retina was extracted to perform biochemical analysis. Sub-cellular fractionation was performed as reported in the literature[26, 27], with minor modifications. Briefly, the tissue was homogenized with a glass-glass Potter apparatus in 0.32 M ice-cold sucrose (S0389) buffer containing the following concentrations: 1 mM HEPES (H3375), 1 mM MgCl2 (M8266), 1 mM NaHCO3 (S5761), 10 mM NaF (71519) and 0.1 mM PMSF (P7626) at pH 7.4 (all from Sigma-Aldrich Darmstadt, Germany), with a complete set of pro-tease inhibitors and phosphatase inhibitors (4693124001, 04906837001, Roche Diagnostics, Basel, Switzerland). A portion of the sample was stored at -80°C as total homogenate, while the remaining part was processed for TIF. Samples were centrifuged at 17,900 × g, for 15 min at 4°C and the supernatant was removed. The pellet was resuspended in a buffer containing 75 mM KCl (P5405) 1 mM HEPES, and 1% Triton X-100 (X100) (all from Sigma-Aldrich) plus protease and phosphatase inhibitors. The suspension was ultracentrifuged at 100,000×g for 1 h. After supernatant removal, the final pellet (TIF) was homogenized using a sonicator (SONOPLUS, Bandelin, Berlin, Germany) in 20 mM HEPES (H3375, Sigma-Aldrich) with a complete protease and phosphatase inhibitor cocktail. The homogenate was stored at −80°C until further processing.

Western blot
Protein concentrations were quantified using the Bradford Assay (5000006, Bio-Rad Protein Assay, Hercules, CA, USA): 20 µg of total tissue homogenate and 10 µg of TIF extracted pro-teins were separated by 10% SDS polyacrylamide gel electrophoresis. PVDF membranes (1620177, Bio-Rad) were blocked in PBS-buffered saline with 5% non-fat milk powder (70166, Sigma-Aldrich), and 0.1% Tween20 (P1379, Sigma-Aldrich) (1 h, RT). Primary anti-bodies were diluted in the same buffer and incubated overnight at 4°C with the dilutions listed in Table 1. Blots were developed using horseradish-peroxidase-conjugated secondary antibodies (Santa Cruz Biotechnology, Dallas, TX, USA) and the ECL chemiluminescence system (Bio-Rad). Protein bands were quantified by densitometry using Quantity One software (Bio-Rad). All experiments were performed in at least three independent replicates.

ELISA
The Mouse Aβ42 Elisa Kit (KMB3441, Invitrogen) was used to assess the presence of Amy-loid beta 42 in the tissue homogenate of the retina of WT and Tg-5xFAD B6SJLF1/J mice ac-cording to the manufacturer's instructions. The calibration curve ranges between 3.12 and 200 pg/mL. In case of low values (below the limit of detection), the data were censored and substituted with a constant value, equal to half the limit of detection (1.56 pg/mL).

OCT
In vivo analysis of the retina was carried out as previously described (Zerbini et al., 2023). Briefly: optical coherence tomography of the retina was performed using Micron IV together with Image-Guided 830nm OCT (Phoenix Research Laboratories, Pleasanton, CA, USA). After anaesthesia with intraperitoneal injection of 80 mg/kg Ketamine, 10 mg/kg Xylazine (Sigma-Aldrich, Munich, Germany), mydriatic animals underwent OCT through a bidimensional scan (B-scan) of both eyes and results were finally averaged. Insight software (Phoenix Research Laboratories) was used to perform retinal layer segmentation and quantification [28].

RNA extraction, reverse transcription and droplet digital PCR

RNA was isolated from the retina of 3 WT and 3 Tg-5xFAD B6SJLF1/J mice (4 months old) using the Maxwell® RSC SimplyRNA Tissue Kit (Promega) following the manufacturer's instructions. The RNA was eluted in 50 µL of nuclease-free water and reverse transcribed using the High-Capacity cDNA Reverse Transcription Kit (Applied Biosystems, Waltham, Massachusetts, USA), generating cDNA at a final concentration of 25 ng/µl. Human and mouse APP expression levels were determined by droplet digital PCR (ddPCR) using a QX100 ddPCR platform (Bio-Rad). The final volume of the PCR mix was 20 µL, including 10 µL of ddPCR™ Supermix for Probes (No dUTP, Bio-Rad), 1 µL of probe (Human APP = dHsaCPE5046076 labelled in FAM, mouse APP = dMmuCPE5117707 labelled in HEX, Bio-Rad), and 2 µL (50ng) of cDNA template. The droplet emulsion was thermally cycled using a C1000 Touch Thermal Cycler (Bio-Rad). Cycling conditions were 95°C for 5 min, followed by 40 cycles of amplification (94°C for 30 s and 55°C for 1 min), and ending at 98°C for 10 min, according to the manufacturer's protocol. The concentration of the target was calculated automatically using QuantaSoft™ software version 1.7.4 (Bio-Rad).

Immunofluorescence staining of mouse retina

For immunofluorescence staining of mouse retina, eyes of Tg-5xFAD B6SJLF1/J mice and WT mice were collected. Retinal cryostat sections (10 µm thick) were fixed in 4% (w/v) formaldehyde for 20 min and were washed once in 3x phosphate-buffered saline (PBS). For blocking, sections were incubated for 1h or 30 min (only for APP) at room temperature (RT) with blocking solution composed of either 2% BSA, 0.1% Triton X-100 and 2% normal goat serum (NGS) in PBS (for APP); or 3% BSA, 0.5% Triton X-100 and 2% NGS in PBS (for p-APP); or 0.1% Triton X-100 and 10% NGS in PBS (for p-JNK and glial fibrillary acidic protein (GFAP)); or 0.5% Triton X-100 and 5% NGS in PBS (for JNK3). Directly after blocking, sections were incubated overnight at 4°C with primary antibodies (Table 1).

Table 1. List of antibodies used in Western blots and IF analysis.

Antigen	Host Species	Source	Dilution for WB	Dilution for IF
APP	Rabbit	PA1-4648, Invitrogen	1:1000	1:50
p-APP (Thr668)	Rabbit	3823, Cell Signaling	1:1000	
p-APP (Thr668)	Rabbit	6986, Cell Signaling		1:100
p-JNK (Thr183/Tyr185)	Rabbit	9251, Cell Signaling	1:1000	1:100
JNK	Rabbit	9252, Cell Signaling	1:1000	
JNK3	Rabbit	2305, Cell Signaling	1:1000	1:200
c-Jun	Rabbit	9165, Cell Signaling	1:1000	
p-c-Jun (Ser73)	Rabbit	06-659, Millipore	1:1000	
PSD95	Mouse	004CA10011435-25, Cayman	1:4000	
p-PSD95 (Ser295)	Rabbit	ab2930, Abcam	1:4000	
Actin	Mouse	MAB1501, Millipore	1:5000	
GFAP	Rabbit	Z0034, DAKO		1:500

For negative controls, primary antibodies were omitted. Antibodies were diluted in blocking buffer (APP and p-JNK), in 1% BSA (p-APP) or in normal antibody diluent (AB999, Scytek) (for GFAP and JNK3). Sections were subsequently washed 3 times with PBS for 5 min and

incubated with Isolectin GS-IB4 conjugated to Alexa Fluor™ 488 (I21411, Invitrogen; 1:50) and secondary antibodies goat anti-rabbit Alexa Fluor™ 633 (A21071, Invitrogen; 1:200) or goat anti-rabbit Cy3 (111-165-144, Jackson ImmunoResearch; 1:200). After washing 3 times with PBS for 5 min, sections were mounted with Vectashield antifade mounting medium with DAPI (H-1200–10, Vector Laboratories). Sections were imaged using a confocal laser scanning micro-scope (Leica, SP8) with settings kept constant between experimental groups.

Statistical analysis

Statistical analyses were performed with GraphPad Prism (version 10.2.0). For layer thickness measurements, individual eyes were included as independent samples. Data were assessed using Student's t-test and Mann-Whitney test, with results reported as mean ± standard deviation (SD). A *P* value <0.05 was considered statistically significant.

Results

The JNK signaling pathway is not active in retinal total homogenates of 5xFAD B6SJLF1/J mice

Previous work from our group demonstrated activation of the c-Jun N-terminal kinase (JNK) pathway in cortical total homogenates of 5xFAD B6SJLF1/J mice, with significant JNK activation detectable at 3.5 months of age, followed by induction of the c-Jun-mediated neuronal death pathway by 10 months [25]. In the current study, we investigated whether this pathway is similarly activated in retinal total homogenates. Specifically, we assessed: (1) the ratio of phosphorylated JNK (p-JNK) to total JNK, (2) protein levels of JNK3 (the predominant CNS-specific JNK isoform), and (3) phosphorylation of c-Jun (the principal downstream effector of JNK signaling and a key transcriptional regulator of apoptotic cell death).

In contrast to our cortical findings, retinal analyses revealed no significant activation of JNK or c-Jun in 5xFAD B6SJLF1/J mice compared to wild-type (WT) controls at any examined time point (Fig. 1A, B). JNK3 expression levels also remained unchanged between genotypes and across all ages (Fig. 1A, B), further supporting the absence of JNK pathway engagement in the retina. This tissue-specific difference in JNK signaling dynamics points to intrinsic differences in stress vulnerability between cortical and retinal neurons in neurodegenerative disease.

Altered PSD95 levels in retinal neurons precede JNK activation during disease progression in 5xFAD B6SJLF1/J mice

We have previously demonstrated a disrupted organization of postsynaptic density (PSD) markers in the cortex of 5xFAD B6SJLF1/J mice [25]. To determine whether similar alterations occur in the retina, we analyzed protein levels in the retinal postsynaptic-enriched protein fraction by isolating the Triton-insoluble fraction (TIF), which is known to represent the PSD region [22, 23, 25-27, 29].

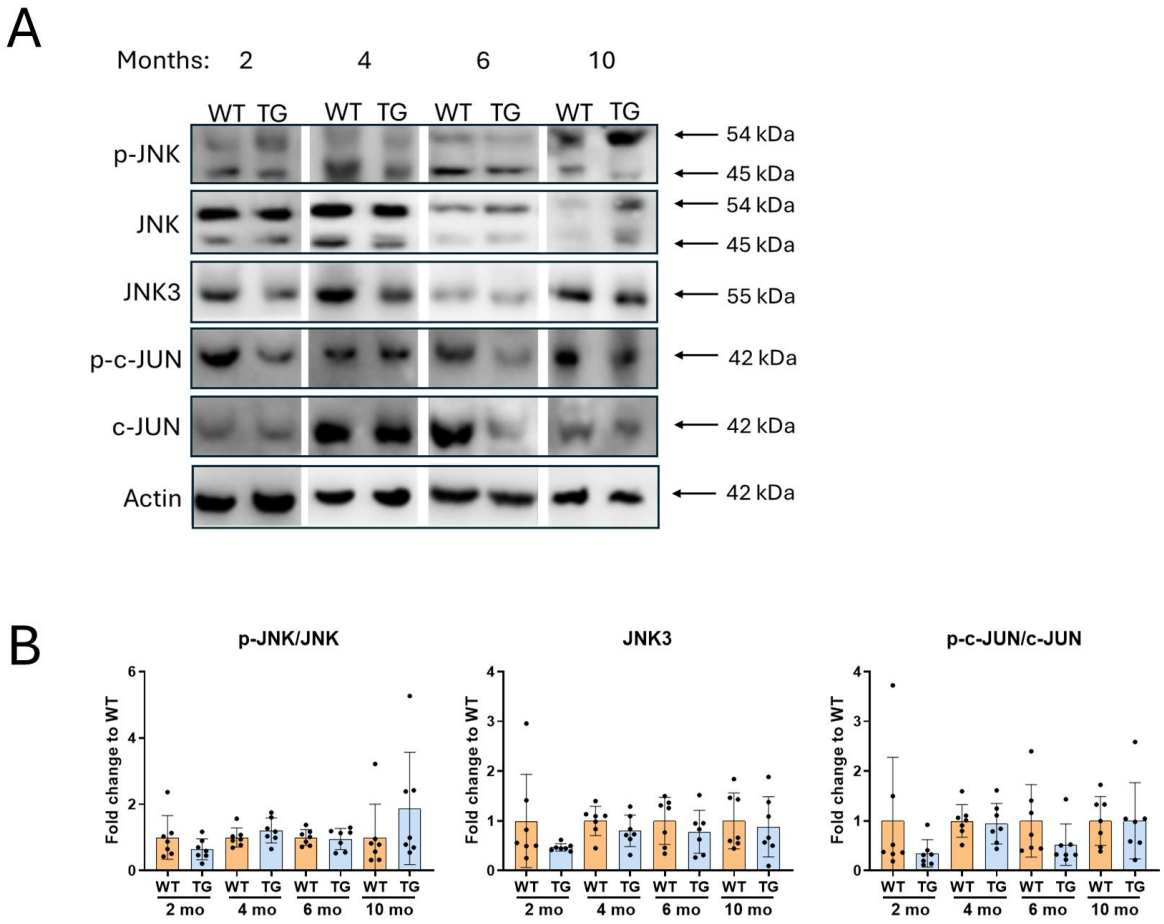

Figure 1. JNK signaling pathway in retinal total homogenates of WT and 5xFAD B6SJLF1/J mice across different ages. **A**) Representative cropped images of Western blots of p-JNK, JNK, JNK3, p-c-Jun, c-Jun and β-actin (loading control) in retinal total homogenates from WT and 5xFAD B6SJLF1/J mice at 2, 4, 6, and 10 months of age. **B**) Quantification of protein levels relative to WT mice, presented as mean ± SD (n = 7 per time point).

We focused on the postsynaptic compartment specifically the postsynaptic density (PSD) fraction to examine molecular changes occurring directly at the synapse, a critical hub for synaptic signaling and plasticity. Enriching for postsynaptic proteins enhances our ability to study PSD-95, a scaffold protein and direct target of JNK. This targeted approach increases sensitivity for detecting subtle, functionally relevant alterations that might otherwise be masked in analyses of total retinal protein, providing a more precise view of early synaptic dysfunction.

To assess whether JNK activation occurs selectively within the PSD region, we examined both: (1) JNK phosphorylation status in the TIF, and (2) JNK-mediated modulation of PSD95, a canonical JNK substrate and essential PSD scaffolding protein that organizes synaptic signaling complexes [30-32]. While our previous work demonstrated early JNK pathway activation in cortical postsynaptic fractions (evidenced by increased p-JNK and p-PSD95 levels from 3.5 months of age), retinal analyses revealed distinct spatiotemporal patterns. At 4 months, we detected elevated p-PSD95 despite the absence of p-JNK (Figure 2). Notably, retinal JNK activation only became apparent at 10 months. Together, these findings suggest a

compartmentalized and delayed JNK-mediated stress response in the retina compared to cortical neurons, highlighting distinct spatiotemporal patterns of neurodegenerative pathology in the CNS of 5xFAD mice.

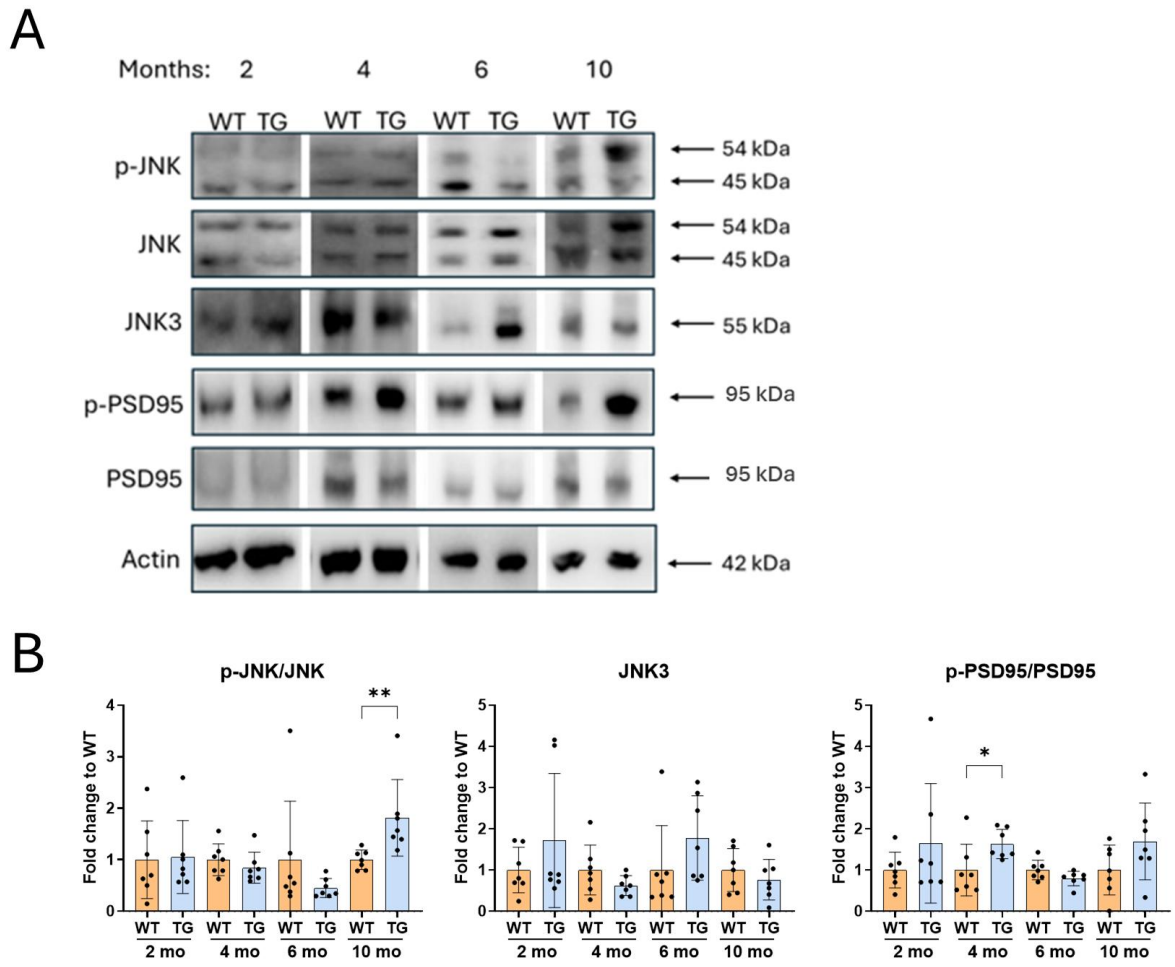

Figure 2. JNK signaling pathway in the retinal postsynaptic-enriched protein fraction. A) Representative cropped images of Western blots of post-synaptic enriched protein fractions of p-JNK, JNK, JNK3, P-PSD95, PSD95, and β-actin (loading control) from WT and 5xFAD B6SJLF1/J (TG) mice at 2, 4, 6, and 10 months of age. B) Quantification of protein levels relative to WT mice, presented as mean ± SD (n = 7 per time point). Statistical analyses were performed using t-tests. Data are expressed as mean ± SD. Statistical significance is indicated as *P < 0.05, **P < 0.01.

Absent JNK3 but persistent gliotic GFAP upregulation in 5xFAD mouse retinas

To evaluate JNK3 and p-JNK expression patterns in 5xFAD B6SJLF1/J retina, we performed immunofluorescence staining (Figure 3A). While JNK3 expression was minimal in WT retinas at 4 months, 5xFAD B6SJLF1/J mice showed enhanced JNK3 immunofluorescent signal specifically in the inner nuclear layer (INL). Notably, this layer-specific intensity is in contrast with Western blot analyses of total retinal homogenates, which showed no genotype-dependent differences in JNK3 levels (Figure 1B).

Immunofluorescence staining revealed nuclear p-JNK expression in the GCL, INL, and outer nuclear layer (ONL) of both WT and 5xFAD B6SJLF1/J mice, with a slightly reduced signal in

5xFAD retinas. GFAP staining showed vascular-associated expression in WT mice, while 5xFAD B6SJLF1/J retinas exhibited more intense GFAP staining in Müller cell radial processes, indicative of reactive gliosis.

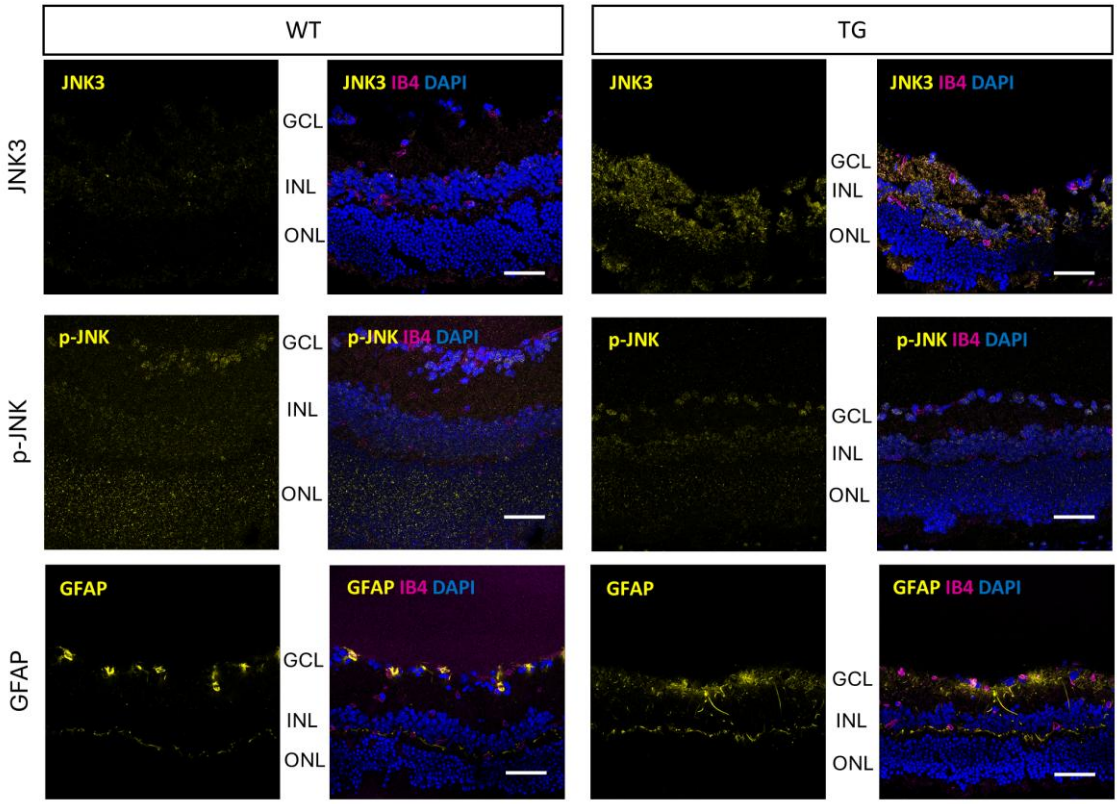

Figure 3. Immunohistochemical analysis of retinal sections in murine samples. Representative IHC images of retinal sections of WT and 5xFAD B6SJLF1/J (TG) mice at 4 months of age (n = 3), showing staining for JNK3, phosphorylated JNK (p-JNK), GFAP, IB4, and DAPI. Scale bars = 50 µm.

5xFAD B6SJLF1/J mice do not exhibit Alzheimer's disease-related marker expression in the retina

Given the absence of clear JNK pathway activation, we next assessed whether 5xFAD B6SJLF1/J retinas exhibit altered AD marker expression. Digital droplet PCR (ddPCR) detect-ed human amyloid precursor protein (APP) expression exclusively in 5xFAD B6SJLF1/J retinas at 4 months (Figure 4A, left), while combined human/murine APP levels (normalized to GAPDH) showed no genotype-dependent differences due to predominant murine APP ex-pression (Figure 4A, right). ELISA analysis revealed comparable amyloid beta 42 (Aβ42) levels between 5xFAD B6SJLF1/J and WT retinal homogenates (Figure 4B).

Western blot analysis of retinal tissue from 2- to 10-month-old mice confirmed no significant differences in either total APP or phosphorylated APP (p-APP) levels between genotypes (Figure 4C). This retinal profile contrasts sharply with our previous findings in brain parenchyma, where both APP and p-APP levels increase progressively during disease progression [25], indicating fundamental differences in APP metabolism between retinal and brain tissues.

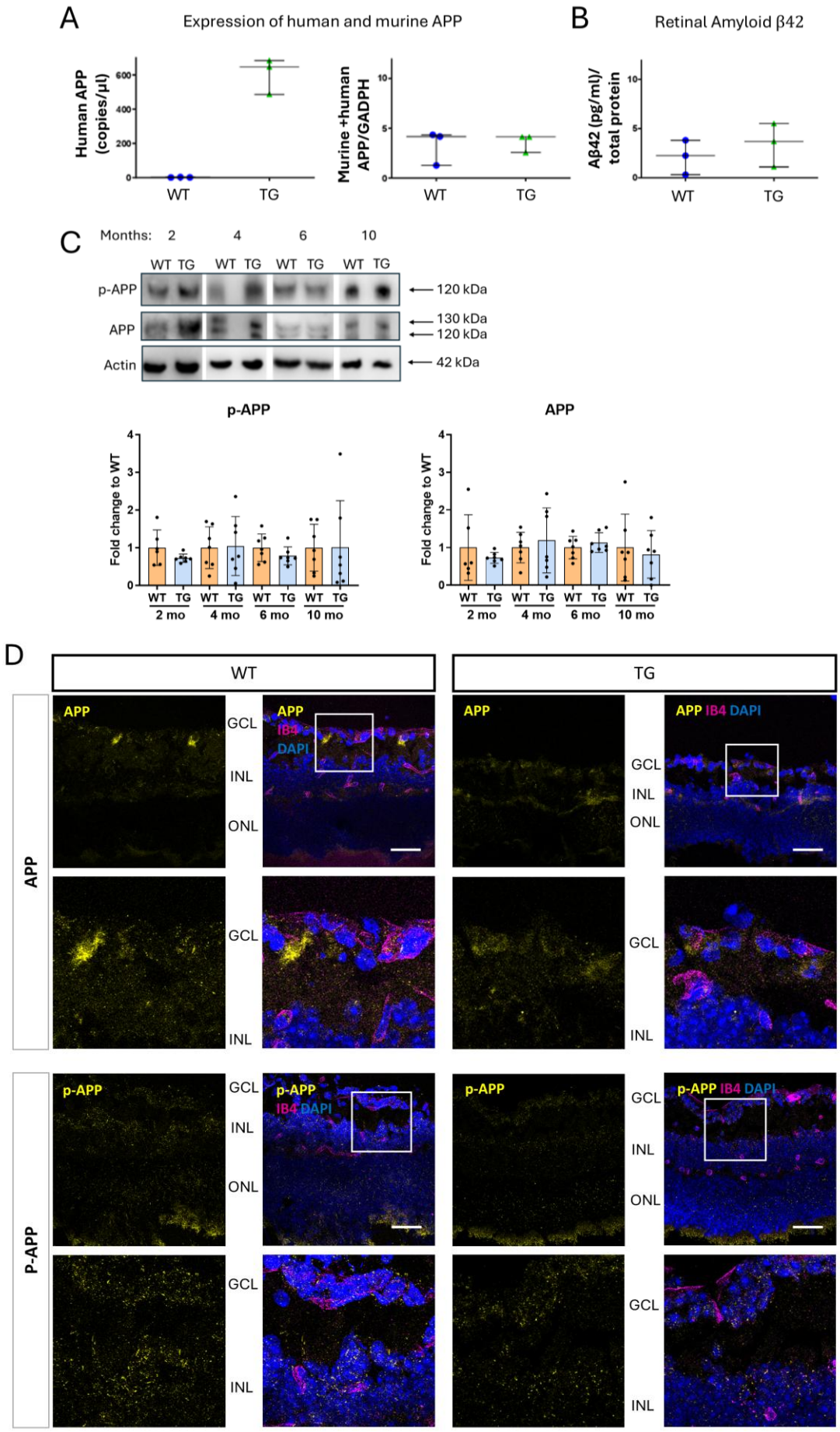
A
Expression of human and murine APP
Human APP (copies/µl)
Murine +human APP/GADPH
WT
TG
B
Retinal Amyloid β42
Aβ42 (pg/ml)/ total protein
C
Months: 2 4 6 10
p-APP
APP
Actin
120 kDa
130 kDa
120 kDa
42 kDa
Fold change to WT
2 mo
4 mo
6 mo
10 mo
D
WT
TG
APP
p-APP
IB4
DAPI
GCL
INL
ONL

Figure 4. Characterization of amyloid pathology in mouse retina. A) Digital PCR analysis of human and murine APP expression levels in retinal samples of 4-month-old mice (n = 3). B) ELISA quantification of Aβ oligomers in retinal tissues from 4-month-old mice (n = 3). C) Representative cropped images of Western blots and quantification of APP and p-APP in 2, 4, 6, 10 months old WT and 5xFAD B6SJLF1/J (TG) mice (n = 7 per time point). Data is presented as mean ± SD. D) Representative immunohistochemistry images of retinal sections and magnifications of 4-month-old WT and TG mice showing APP and p-APP localization, co-stained with IB4 and DAPI (n = 3). Scale bar: 50 μm.

Immunofluorescence analysis of 4-month-old mice confirmed transgenic human APP expression in 5xFAD B6SJLF1/J retinas (Figure 4D). While WT retinas showed vascular-associated APP expression in the GCL, 5xFAD B6SJLF1/J retinas exhibited: (1) widespread APP distribution throughout retinal layers, with reduced vascular localization; and (2) decreased p-APP expression compared to WT controls. In WT mice, p-APP was detected in all nuclear layers (GCL, INL, ONL), whereas 5xFAD B6SJLF1/J retinas showed nuclear-restricted p-APP localization primarily in the GCL and INL. Together, these results demonstrate distinct APP handling between retinal and brain tissues in 5xFAD mice, suggesting tissue-specific protection against Alzheimer's-related protein dysregulation.

5xFAD Mice show total Retinal thickening with stable INL thickness while WT mice develop INL thinning over time

Given the increased immunostaining of JNK3 in the GCL and INL and the presence of gliosis in the transgenic mice (Figure 3), we assessed potential structural changes in retinal layer thickness during the mice 10-month lifespan using OCT (Figure 5A).

The INL was thinner in 5xFAD B6SJLF1/J at 2 months ($P = 0.035$), but thicker at 4 months ($P<0.001$) and 10 months ($P = 0.012$) (Figure 5B). The retinal nerve fiber layer (RNFL), existing of axons of ganglion cells, was thicker in 5xFAD B6SJLF1/J at 4 months ($P = 0.042$), but no differences at other ages. Total retinal thickness was increased in 5xFAD at 4 months ($P = 0.036$) and 10 months ($P = 0.024$). No consistent genotype differences were found in ONL and choroid.

Longitudinal comparison between 2-month and 10-month time points revealed significant age-related thinning of the INL ($P < 0.001$) accompanied by choroidal thickening ($P < 0.001$) in WT mice (Figure 6). In contrast, TG mice exhibited increased total retinal thickness ($P = 0.011$) and similar choroidal thickening ($P < 0.001$), while maintaining stable INL thickness ($P = 0.824$). While both genotypes show choroidal thickening with age, 5xFAD B6SJLF1/J retinas diverge through maintained INL thickness and increased total retinal thickness, indicating genotype-specific differences.

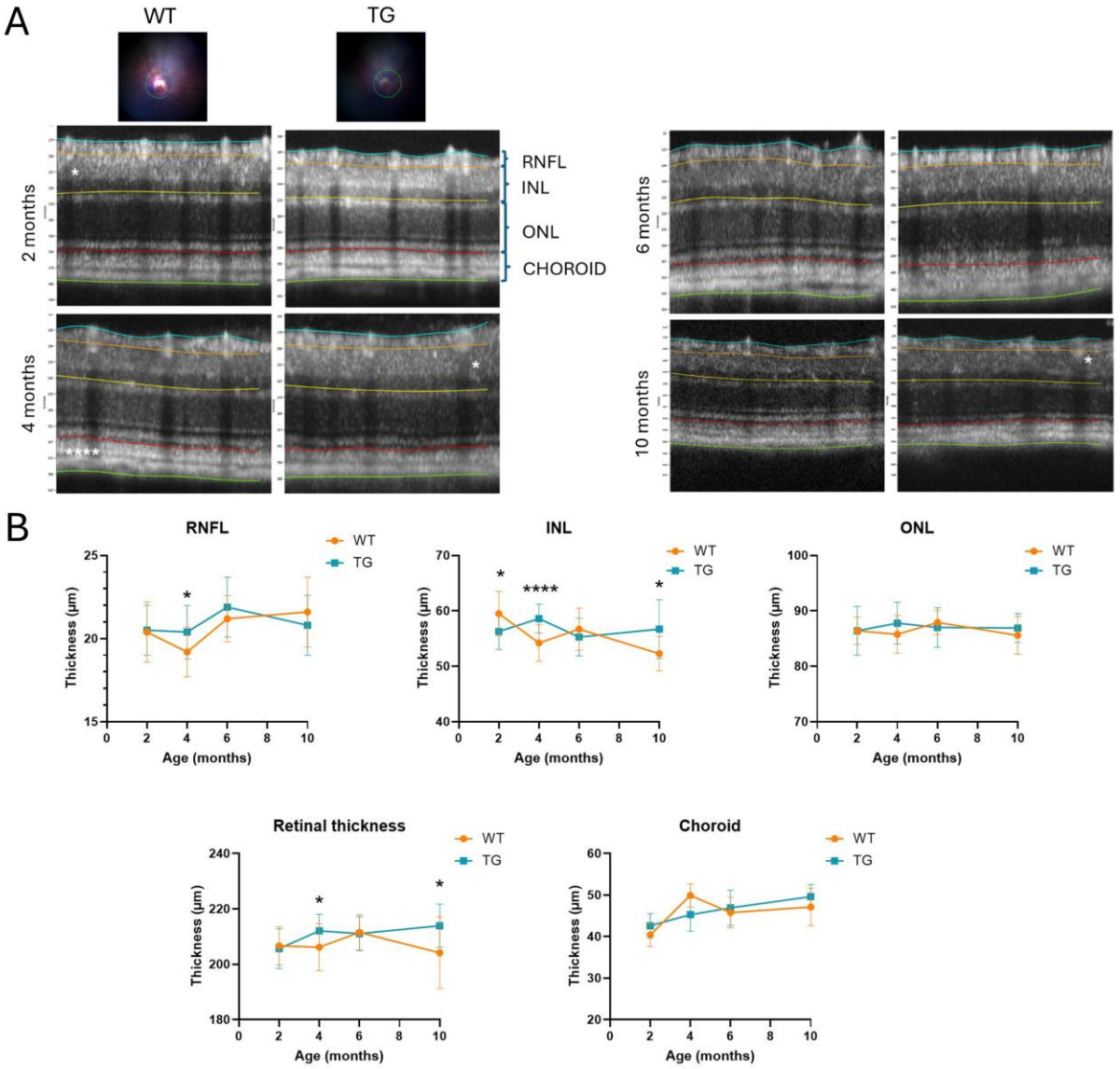

Figure 5. Longitudinal analysis of retinal layer thickness in WT and 5xFAD B6SJLF1/J mice. A) Representative OCT images of the right eye from WT and 5xFAD B6SJLF1/J (TG) mice at 2, 4, 6, and 10 months of age (n = 7 per group). The optic nerve head is indicated with a circle. B) Graphical representation of the longitudinal changes in retinal layer thickness over time for WT and 5xFAD B6SJLF1/J (TG) mice. Statistical analyses were performed using t-tests. Statistical significance is indicated as *P < 0.05, **** P< 0.001. RNFL, Retinal Nerve Fiber Layer; INL, inner nuclear layer; ONL, outer nuclear layer.

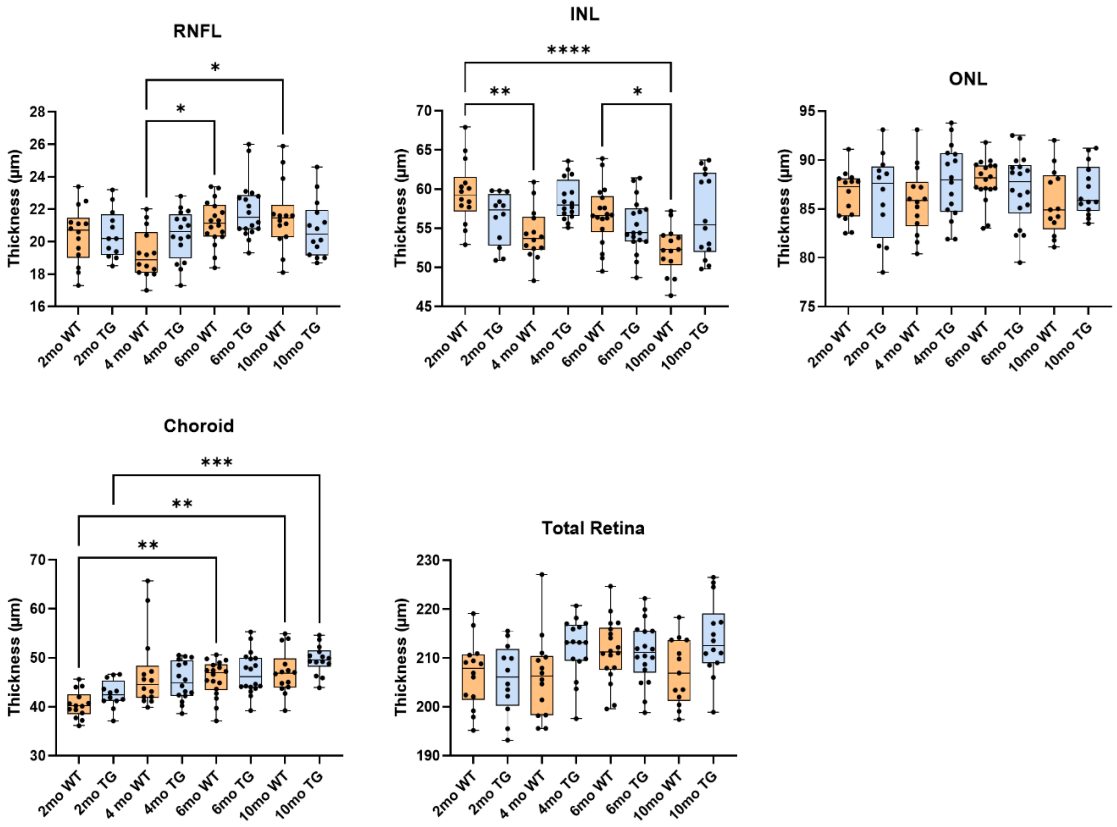

Figure 6. Longitudinal changes in retinal layer thickness. Graphical representation of the longitudinal changes in retinal layer thickness over time for WT and 5xFAD B6SJLF1/J (TG) mice. Statistical analyses were performed using ANOVA. Statistical significance is indicated as *P < 0.05, ** P< 0.01, *** P< 0.001, **** P< 0.0001. RNFL, Retinal Nerve Fiber Layer; INL, inner nuclear layer; ONL, outer nuclear layer.

Discussion

There is increasing evidence that neurodegenerative brain diseases, including AD, often involve retinal pathology, suggesting the retina as a potential "window into the brain" [33]. This is rooted in their shared embryonic origin and structural similarities, including synaptic networks and vascular systems. Recently, in the context of AD, the concept that detectable changes in the retina may mirror, or diverge, from cerebral pathology has emerged. A key advantage of studying the retina is that these alterations can be assessed through non-invasive imaging, offering a promising pathway for early diagnosis.

Emerging studies also reveal that retinal metabolic dysfunction and oxidative stress closely mirror those in the AD brain [34], suggesting overlapping degenerative pathways. To investigate this further, we examined whether retinal neurodegeneration aligns with brain pathology in the 5xFAD B6SJLF1/J mouse model of AD, previously reported in Priori et al., 2023[25] and whether JNK activation is a shared pathogenic mechanism. Retinal changes were tracked across disease progression (2, 4, 6, and 10 months) using OCT imaging, Western blotting and immunofluorescence.

Despite robust cerebral pathology, including amyloid accumulation and JNK activation, the retina of 5xFAD B6SJLF1/J mice showed minimal Aβ oligomer accumulation and no significant APP expression compared to wild-type mice. This corresponded with a lack of JNK pathway activation, as indicated by stable p-JNK/JNK and JNK3 levels assessed by Western blot in the total retinal homogenate.

However, JNK3 is particularly sensitive to changes in the neuronal environment, and immunofluorescence revealed its early, localized upregulation in 4-month-old 5xFAD B6SJLF1/J mice, especially in the ganglion cell layer (GCL) and inner nuclear layer (INL). This technique provides superior spatial resolution, allowing detection of compartment-specific alterations that are not evident in whole-retina lysates. Consistently, PSD-enriched fractions showed early increases in PSD95 phosphorylation without changes JNK activation, suggesting that initial postsynaptic dysfunction can arise independently of detectable JNK signaling at the tissue level. These localized changes likely precede broader pathway activation and may relate to early JNK3 engagement at the synapse. Elevated GFAP in Müller cells further indicated early gliosis and neuroinflammation, reinforcing that localized retinal pathology can occur in the absence of overt global biochemical changes. By 10 months, increased p-JNK/JNK ratios in TIF fractions indicated later-stage, more widespread activation of JNK isoforms, making these changes detectable by Western blot. This temporal progression supports a model in which early, spatially restricted signalling events eventually converge into broader stress pathway activation. Together, these findings emphasize that subcellular and cell-type–specific analyses are essential for detecting early retinal alterations in this model and illustrate how localized molecular changes may precede or even diverge from global pathological readouts.

Strikingly, no retinal Aβ aggregation was detected, strongly contrasting with the Aβ42 accumulation in the brain [25], aligning with some human studies [35]. However, our findings must be interpreted within the context of a complex and sometimes contradictory body of literature on retinal pathology in 5xFAD mice. A key factor underlying these inconsistencies is the influence of genetic background. Although all 5xFAD colonies carry the same transgenes, their backgrounds can markedly modulate Aβ kinetics, inflammatory tone, and neuronal vulnerability. The B6SJLF1/J hybrid background combines C57BL/6J and SJL/J contributions, introducing genetic diversity that better reflects the heterogeneity observed in human populations and potentially broadens the translational relevance of the model. However, this diversity also alters disease expression. Mouse background can influence the timing and extent of amyloid accumulation, retinal thickening, and synaptic alterations, as shown by differences between B6SJLF1/J, C57BL/6J, and SJL/J 5xFAD lines. For instance, Nam et al. (2022) reported delayed Aβ deposition in SJL/J 5xFAD mice, while early Aβ42 accumulation was observed in C57BL/6J strains [36-38]. These discrepancies suggest that the hybrid background may attenuate or delay retinal involvement, even when central pathology is pronounced. Thus, although the B6SJLF1/J background provides valuable genetic heterogeneity, it also highlights important limitations when attempting to model the full spectrum of AD-related retinal changes and underscores the need to consider background-dependent variability when comparing findings across studies. Detection methods should also be taken into ac-count. Using alternative antibodies, Jovanovic Macura et al. (2023) detected Aβ in 5xFAD B6SJLF1/J mice at 4 and 12 months, emphasizing the methodological sensitivity required to detect subtle retinal pathology [39]. In addition, antibody selection,

tissue preparation, imaging resolution, and sample processing can markedly affect the detection of subtle pathological features, including Aβ aggregation and JNK activation. These considerations likely explain why some studies report early retinal amyloid deposits, whereas our data highlight selective synaptic and inflammatory alterations without robust Aβ accumulation.

Unexpectedly, our longitudinal OCT data revealed retinal thickening over time, rather than the expected thinning, potentially reflecting Müller cell swelling and gliotic remodeling. Similar findings have been reported [40], although others observed retinal thinning [41] or no changes [36, 42], further underscoring the influence of strain background and temporal progression [12, 43].

In line with our findings, Zhang and colleagues (2021) also reported early structural retinal changes in 5xFAD mice before the onset of robust functional deficits. They observed thickening of the outer nuclear layer (ONL) at 4 months, followed by general retinal thickening at 6 months, accompanied by glial activation and a modest increase in amyloid plaques. Importantly, they documented that this structural remodelling preceded major functional decline: at 6 months the mice showed impaired visual behaviour (optomotor test) and reduced light responses of retinal ganglion cells (via multielectrode-array), while full-field ERG and pERG remained relatively preserved. These observations parallel our OCT-based detection of retinal thickening at early ages and support the hypothesis that structural changes, rather than synapse loss or massive amyloid deposition, may be among the first detectable retinal pathologies in 5xFAD. On the other hand, while Zhang et al. reported more amyloid plaques (albeit few) in the retina by 6 months, our study found no robust Aβ aggregation at similar or earlier timepoints, suggesting a divergence in the timeline or magnitude of amyloid accumulation [40].

In summary, our study highlights a compartmentalized and non-linear relationship between retinal and cerebral pathology in the 5xFAD model of Alzheimer's disease. While the 5xFAD B6SJLF1/J model faithfully recapitulates cerebral AD phenotypes, including Aβ deposition and JNK activation [25], the retina exhibits a distinct trajectory: early synaptic dysfunction, localized JNK3 upregulation, gliosis, and paradoxical retinal thickening occur in the absence of widespread Aβ aggregation or global JNK activation.

Localized JNK3 activation and gliosis in the retina, alongside paradoxical thickening, suggest a distinct trajectory, possibly driven by alternative stress pathways or compensatory remodeling. It is possible that differences in APP expression and Aβ processing between brain and retina, shaped by regional regulation and strain background, likely underlie these divergent outcomes.

Importantly, our results reconcile previously conflicting reports by demonstrating that subtle retinal alterations may precede overt amyloid pathology and functional deficits, supporting the retina as a sensitive but independent window into neurodegeneration.

These findings support the retina's potential as a sensitive site for monitoring neurodegenerative changes but also emphasize the importance of methodological rigor and

strain con-sideration. The retina does reflect brain pathology, but not as a simple mirror. It may offer an early glimpse into neurodegeneration, albeit through its own molecular lens.

Data availability

The datasets generated during and/or analyzed during the current study are available from the corresponding author upon reasonable request.

Funding

This study was funded by the European Commission (H2020 programme-GA 847749).

Author contributions

The authors have contributed to this article as follows: conception and design (AG, CAM, ECP, TB), experiments and data analysis (AG, CAM, ECP, ST, MP, SG, IV, NB, IK, GZ), scientific discussions (all authors), manuscript writing (all authors), and supervision of the entire study (TB). All authors have read and approved the final manuscript.

References

[1] (2025) 2025 Alzheimer's disease facts and figures. Alzheimers & Dementia 21(4). doi: 10.1002/alz.70235

[2] Kopf D, Frolich L (2009) Risk of incident Alzheimer's disease in diabetic patients: a systematic review of prospective trials. J Alzheimers Dis 16(4): 677–685. doi: 10.3233/JAD-2009-1011

[3] Biessels GJ, De Leeuw FE, Lindeboom J, Barkhof F, Scheltens P (2006) Increased cortical atrophy in patients with Alzheimer's disease and type 2 diabetes mellitus. J Neurol Neurosurg Psychiatry 77(3): 304–307. doi: 10.1136/jnnp.2005.069583

[4] Hinton DR, Sadun AA, Blanks JC, Miller CA (1986) Optic-nerve degeneration in Alzheimer's disease. N Engl J Med 315(8): 485–487. doi: 10.1056/NEJM198608213150804

[5] Doustar J, Torbati T, Black KL, Koronyo Y, Koronyo-Hamaoui M (2017) Optical Coherence Tomography in Alzheimer's Disease and Other Neurodegenerative Diseases. Front Neurol 8: 701. doi: 10.3389/fneur.2017.00701

[6] Jin Z, Wang X, Lang Y, Song Y, Zhan H, Shama W, et al. (2025) Retinal optical coherence tomography intensity spatial correlation features as new biomarkers for confirmed Alzheimer's disease. Alzheimers Res Ther 17(1): 33. doi: 10.1186/s13195-025-01676-z

[7] Gaire BP, Koronyo Y, Fuchs DT, Shi H, Rentsendorj A, Danziger R, et al. (2024) Alzheimer's disease pathophysiology in the Retina. Prog Retin Eye Res 101: 101273. doi: 10.1016/j.preteyeres.2024.101273

[8] Parisi V, Restuccia R, Fattapposta F, Mina C, Bucci MG, Pierelli F (2001) Morphological and functional retinal impairment in Alzheimer's disease patients. Clin Neurophysiol 112(10): 1860–1867. doi: 10.1016/s1388-2457(01)00620-4

[9] Olivares Ordonez MA, Smith RC, Yiu G, Liu YA (2025) Retinal Microstructural and Microvascular Changes in Alzheimer Disease: A Review. Int Ophthalmol Clin 65(1): 59–67. doi: 10.1097/IIO.0000000000000549

[10] Dutescu RM, Li QX, Crowston J, Masters CL, Baird PN, Culvenor JG (2009) Amyloid precursor protein processing and retinal pathology in mouse models of Alzheimer's disease. Graefes Arch Clin Exp Ophthalmol 247(9): 1213–1221. doi: 10.1007/s00417-009-1060-3

[11] Alexandrov PN, Pogue A, Bhattacharjee S, Lukiw WJ (2011) Retinal amyloid peptides and complement factor H in transgenic models of Alzheimer's disease. Neuroreport 22(12): 623–627. doi: 10.1097/WNR.0b013e3283497334

[12] Lim JKH, Li QX, He Z, Vingrys AJ, Chinnery HR, Mullen J, et al. (2020) Retinal Functional and Structural Changes in the 5xFAD Mouse Model of Alzheimer's Disease. Front Neurosci 14: 862. doi: 10.3389/fnins.2020.00862

[13] Salobrar-Garcia E, Mendez-Hernandez C, Hoz R, Ramirez AI, Lopez-Cuenca I, Fernandez-Albarral JA, et al. (2020) Ocular Vascular Changes in Mild Alzheimer's Disease Patients: Foveal Avascular Zone, Choroidal Thickness, and ONH Hemoglobin Analysis. J Pers Med 10(4). doi: 10.3390/jpm10040231

[14] Vandenabeele M, Veys L, Lemmens S, Hadoux X, Gelders G, Masin L, et al. (2021) The App(NL-G-F) mouse retina is a site for preclinical Alzheimer's disease diagnosis and research. Acta Neuropathol Commun 9(1): 6. doi: 10.1186/s40478-020-01102-5

[15] Bevan RJ, Hughes TR, Williams PA, Good MA, Morgan BP, Morgan JE (2020) Retinal ganglion cell degeneration correlates with hippocampal spine loss in experimental Alzheimer's disease. Acta Neuropathol Commun 8(1): 216. doi: 10.1186/s40478-020-01094-2

[16] Chiquita S, Campos EJ, Castelhano J, Ribeiro M, Sereno J, Moreira PI, et al. (2019) Retinal thinning of inner sub-layers is associated with cortical atrophy in a mouse model of Alzheimer's disease: a longitudinal multimodal in vivo study. Alzheimers Res Ther 11(1): 90. doi: 10.1186/s13195-019-0542-8

[17] Du H, Sun X, Guma M, Luo J, Ouyang H, Zhang X, et al. (2013) JNK inhibition reduces apoptosis and neovascularization in a murine model of age-related macular degeneration. Proc Natl Acad Sci U S A 110(6): 2377–2382. doi: 10.1073/pnas.1221729110

[18] Guma M, Rius J, Duong-Polk KX, Haddad GG, Lindsey JD, Karin M (2009) Genetic and pharmacological inhibition of JNK ameliorates hypoxia-induced retinopathy through interference with VEGF expression. Proc Natl Acad Sci U S A 106(21): 8760–8765. doi: 10.1073/pnas.0902659106
[19] Galy A, Roux MJ, Sahel JA, Leveillard T, Giangrande A (2005) Rhodopsin maturation defects induce photoreceptor death by apoptosis: a fly model for RhodopsinPro23His human retinitis pigmentosa. Hum Mol Genet 14(17): 2547–2557. doi: 10.1093/hmg/ddi258
[20] Kang MJ, Chung J, Ryoo HD (2012) CDK5 and MEKK1 mediate pro-apoptotic signalling following endoplasmic reticulum stress in an autosomal dominant retinitis pigmentosa model. Nat Cell Biol 14(4): 409–415. doi: 10.1038/ncb2447
[21] Ploia C, Antoniou X, Sclip A, Grande V, Cardinetti D, Colombo A, et al. (2011) JNK plays a key role in tau hyperphosphorylation in Alzheimer's disease models. J Alzheimers Dis 26(2): 315–329. doi: 10.3233/JAD-2011-110320
[22] Sclip A, Arnaboldi A, Colombo I, Veglianese P, Colombo L, Messa M, et al. (2013) Soluble Abeta oligomer-induced synaptopathy: c-Jun N-terminal kinase's role. J Mol Cell Biol 5(4): 277–279. doi: 10.1093/jmcb/mjt015
[23] Sclip A, Tozzi A, Abaza A, Cardinetti D, Colombo I, Calabresi P, et al. (2014) c-Jun N-terminal kinase has a key role in Alzheimer disease synaptic dysfunction in vivo. Cell Death Dis 5(1): e1019. doi: 10.1038/cddis.2013.559
[24] Buccarello L, Sclip A, Sacchi M, Castaldo AM, Bertani I, ReCecconi A, et al. (2017) The c-jun N-terminal kinase plays a key role in ocular degenerative changes in a mouse model of Alzheimer disease suggesting a correlation between ocular and brain pathologies. Oncotarget 8(47): 83038–83051. doi: 10.18632/oncotarget.19886
[25] Priori EC, Musi CA, Giani A, Colnaghi L, Milic I, Devitt A, et al. (2023) JNK Activation Correlates with Cognitive Impairment and Alteration of the Post-Synaptic Element in the 5xFAD AD Mouse Model. Cells 12(6). doi: 10.3390/cells12060904
[26] Gardoni F, Schrama LH, Kamal A, Gispen WH, Cattabeni F, Di Luca M (2001) Hippocampal synaptic plasticity involves competition between Ca2+/calmodulin-dependent protein kinase II and postsynaptic density 95 for binding to the NR2A subunit of the NMDA receptor. J Neurosci 21(5): 1501–1509. doi: 10.1523/JNEUROSCI.21-05-01501.2001
[27] Musi CA, Agro G, Buccarello L, Camuso S, Borsello T (2020) JNK signaling activation in the Ube3a maternal deficient mouse model: its specific inhibition prevents post-synaptic protein-enriched fraction alterations and cognitive deficits in Angelman Syndrome model. Neurobiol Dis 140: 104812. doi: 10.1016/j.nbd.2020.104812
[28] Zerbini G, Maestroni S, Vigano I, Mosca A, Paleari R, Gabellini D, et al. (2023) Progressive Thinning of Retinal Nerve Fiber Layer/Ganglion Cell Layer (RNFL/GCL) as Biomarker and Pharmacological Target of Diabetic Retinopathy. Int J Mol Sci 24(16). doi: 10.3390/ijms241612672
[29] Biggi S, Buccarello L, Sclip A, Lippiello P, Tonna N, Rumio C, et al. (2017) Evidence of Presynaptic Localization and Function of the c-Jun N-Terminal Kinase. Neural Plast 2017: 6468356. doi: 10.1155/2017/6468356
[30] Musi CA, Marchini G, Giani A, Tomaselli G, Priori EC, Colnaghi L, et al. (2022) Colocalization and Interaction Study of Neuronal JNK3, JIP1, and beta-Arrestin2 Together with PSD95. Int J Mol Sci 23(8). doi: 10.3390/ijms23084113
[31] Coffey ET (2014) Nuclear and cytosolic JNK signalling in neurons. Nat Rev Neurosci 15(5): 285–299. doi: 10.1038/nrn3729
[32] Zhou X, Yi W, Zhi Y, Yu J, Lu D, Luo Z, et al. (2023) Stress-Activated Protein Kinase JNK Modulates Depression-like Behaviors in Mice. Mol Neurobiol 60(5): 2367–2378. doi: 10.1007/s12035-023-03209-x
[33] Simo R, Stitt AW, Gardner TW (2018) Neurodegeneration in diabetic retinopathy: does it really matter? Diabetologia 61(9): 1902–1912. doi: 10.1007/s00125-018-4692-1
[34] Ravichandran S, Snyder PJ, Alber J, Kenny MR, Rothstein A, Brown K, et al. (2024) Quantifying Putative Retinal Gliosis in Preclinical Alzheimer's Disease. Invest Ophthalmol Vis Sci 65(5): 5. doi: 10.1167/iovs.65.5.5

[35] den Haan J, Morrema THJ, Verbraak FD, de Boer JF, Scheltens P, Rozemuller AJ, et al. (2018) Amyloid-beta and phosphorylated tau in post-mortem Alzheimer's disease retinas. Acta Neuropathol Commun 6(1): 147. doi: 10.1186/s40478-018-0650-x
[36] Matei N, Leahy S, Blair NP, Burford J, Rahimi M, Shahidi M (2022) Retinal Vascular Physiology Biomarkers in a 5XFAD Mouse Model of Alzheimer's Disease. Cells 11(15). doi: 10.3390/cells11152413
[37] Parthasarathy R, Chow KM, Derafshi Z, Fautsch MP, Hetling JR, Rodgers DW, et al. (2015) Reduction of amyloid-beta levels in mouse eye tissues by intra-vitreally delivered neprilysin. Exp Eye Res 138: 134–144. doi: 10.1016/j.exer.2015.06.027
[38] Nam Y, Kim S, Kim J, Hoe HS, Moon M (2022) Mesoscopic Mapping of Visual Pathway in a Female 5XFAD Mouse Model of Alzheimer's Disease. Cells 11(23). doi: 10.3390/cells11233901
[39] Jovanovic Macura I, Zivanovic A, Perovic M, Ciric J, Major T, Kanazir S, et al. (2023) The Expression of Major Facilitator Superfamily Domain-Containing Protein2a (Mfsd2a) and Aquaporin 4 Is Altered in the Retinas of a 5xFAD Mouse Model of Alzheimer's Disease. Int J Mol Sci 24(18). doi: 10.3390/ijms241814092
[40] Zhang M, Zhong L, Han X, Xiong G, Xu D, Zhang S, et al. (2021) Brain and Retinal Abnormalities in the 5xFAD Mouse Model of Alzheimer's Disease at Early Stages. Front Neurosci 15: 681831. doi: 10.3389/fnins.2021.681831
[41] Kim TH, Son T, Klatt D, Yao X (2021) Concurrent OCT and OCT angiography of retinal neurovascular degeneration in the 5XFAD Alzheimer's disease mice. Neurophotonics 8(3): 035002. doi: 10.1117/1.NPh.8.3.035002
[42] McCool S, Smith JC, Sladek A, Fan S, Van Hook MJ (2025) Retinal and thalamic alterations in the 5xFAD mouse model of Alzheimer's disease. PLoS One 20(3): e0319397. doi: 10.1371/journal.pone.0319397
[43] Creighton SD, Mendell AL, Palmer D, Kalisch BE, MacLusky NJ, Prado VF, et al. (2019) Dissociable cognitive impairments in two strains of transgenic Alzheimer's disease mice revealed by a battery of object-based tests. Sci Rep 9(1): 57. doi: 10.1038/s41598-018-37312-0

Chapter 4

Retinal and cerebral microvascular changes in diabetes and Alzheimer's disease

Noëlle Bakker-van Bugnum[1,2], Amber Teppema[1], Aïcha A. Croes[1], Eva Prevaes[1], Gwen van de Brug[1], Alexander M. Emeis Escalante[1], Hinke Groeneveld[1], Cornelis J.F. van Noorden[1], Reinier O. Schlingemann[1,2] and Ingeborg Klaassen[1,2], on behalf of the RECOGNISED consortium

[1] Amsterdam UMC, University of Amsterdam, Department of Ophthalmology, Ocular Angiogenesis Group, Amsterdam Cardiovascular Sciences, Meibergdreef 9, Amsterdam, The Netherlands.
[2] Amsterdam UMC, University of Amsterdam, Department of Ophthalmology, Ocular Angiogenesis Group, Amsterdam Neuroscience, Meibergdreef 9, Amsterdam, The Netherlands.

Manuscript in preparation

Abstract

Diabetic retinopathy (DR), the major microvascular complication of diabetes mellitus (DM), is associated with neurovascular unit (NVU) impairment. At the same time, patients with DM are at an increased risk of Alzheimer's disease (AD). However, the mechanisms induced by DM and the potential similarities in NVU pathology between DR and the AD brain remain unexplored. In this study, we examined NVU alterations in the retina of patients with type 2 DM and DR, and in the brain of patients with DM and AD. Immunofluorescence staining of key vascular and glial markers related to NVU functions revealed distinct tissue- and disease-specific profiles. In DM conditions, the retinal vasculature showed disrupted vascular permeability, a feature not observed in the brain vasculature. The DM retina also showed alterations in tight junction integrity, transcytosis, and pericyte coverage that differed from those seen in the brain. Our findings suggest that the mechanisms driving NVU alterations may differ between the eye and brain. However, a common response to DM was also identified: both tissues exhibited macroglial activation, indicating a shared inflammatory response. In AD, we observed similar macroglial activation alongside changes in tight junctions, transcytosis regulation, water and potassium channel expression, and pericyte coverage, collectively impairing blood-brain barrier function. Notably, vascular permeability and tight junction disruption were most severe in patients with both DM and AD, surpassing the damage observed in either condition alone. These results underscore the critical role of microvascular dysfunction in the pathophysiology of DM and AD, and they reveal exacerbated cerebrovascular dysfunction when both diseases are present.

Introduction

Individuals with diabetes mellitus (DM) have an increased risk of developing Alzheimer's disease (AD) [1], but the mechanisms involved are not yet understood [2]. DM is a fast growing global pandemic [3] and diabetic retinopathy (DR) is the most common microvascular complication in diabetic patients, characterized by vascular damage, leakage and angiogenesis in the retina [4]. DR is considered to be a neurovascular disease affecting multiple cell types in the retina. Accumulating evidence indicates that NVU dysfunction in the retina contributes to the development and progression of DR [2, 5]. Likewise, NVU dysfunction in the brain has been implicated in the pathological processes underlying AD [6-8]. The NVU consists of capillaries with a single layer of endothelial cells that are in close communication with pericytes, macroglia, microglia and neurons [9]. In both the retina and brain, the homeostasis of the neuronal microenvironment depends on the NVU, which regulates the permeability of the blood-retinal barrier (BRB) and blood-brain barrier (BBB) [2].

In more detail, specialized endothelial cells in the retina and brain form continuous blood vessels and are tightly linked with tight junctions and adherens junctions to restrict paracellular transport of molecules and cells [10]. Furthermore, transcellular transport via transcytosis is highly suppressed in this healthy barrier endothelium, characterized by a relatively low number of endothelial caveolae, which are preferentially located at the abluminal membrane [11, 12]. Pericytes envelop the capillaries within the shared basal lamina. Pericytes are active signalling partners of the endothelium which locally regulate blood flow, clear harmful metabolites (e.g. lactate) from the endothelial microenvironment, and control endothelial cell proliferation. Importantly, they directly modulate the barrier's functional properties by regulating endothelial transport pathways and by contributing to the basal lamina through the secretion of extracellular matrix proteins [13-18]. Macroglia, astrocytes and Müller cells in the retina, as well as astrocytes in the brain [11], project their endfeet onto this basal lamina that covers pericytes, thereby providing essential structural support and creating a functional interface for metabolic exchange and signalling at the abluminal side of capillaries [9-11, 19]. Macroglia exhibit a polarised distribution of ion channels, including Kir4.1, and water channels, such as AQP4, which are highly concentrated in endfoot membranes and show low expression along somata and processes [20-25]. This polarisation is essential for regulating barrier function, nutrient and waste exchange, and signalling for vascular control. In addition, macroglia secrete basal lamina proteins and neurotrophic factors, regulate extracellular volume and glucose metabolism, participate in visual cycles, release neurotransmitters, and modulate innate immune response [10, 26, 27]. Finally, the NVU is monitored and modulated by microglia, the resident immune cells of the central nervous system [28]. Activated microglia have several functions in the NVU: regulating immune responses by balancing pro- and anti-inflammatory cytokines, releasing neurotrophic factors and enabling neuronal survival, activity and pruning of synapses, and regulating blood flow, degradation of apoptotic cells and protein aggregates, including amyloid-β (Aβ) [29-31].

NVU impairment in the retina in DM and during the different stages of DR has been well-characterized. Both retinal neurodegeneration and vascular lesions occur early in the progression of DR [2]. Early vascular abnormalities include basal lamina thickening, loss of endothelial cells and pericytes, and diffuse impairment of the BRB, which is followed by the

development of acellular capillaries. Progression of DR is associated with retinal haemorrhages, focal profuse leakage, exudate formation, and macular swelling, all of which are sequelae of retinal ischemia caused by widespread capillary loss [2, 32]. During this process, pro-angiogenic factors are upregulated, leading to local vascular leakage and in the more severe form of proliferative DR to abnormal neovascularization. In addition to microvascular complications, DR is also characterized by neurodegeneration [33-35], primarily involving ganglion cell apoptosis in the inner retina [33, 36]. Notably, neuronal and glial activation, as well as Müller cell death occur before the loss of pericytes and endothelial cells [2, 33, 37-45], although these changes are not clinically visible until they manifest more extensively across the retina [38-41, 46-48]. The heritability for DR varies widely across studies, ranging from 6 to 52% [49-51], with higher genetic contributions observed in more severe forms of the disease.

There is no clear equivalent of DR in the brain. In diabetes, cerebral vascular abnormalities include capillary basal lamina thickening [52-55], alterations in vessel tortuosity and capillary density [53, 56], microbleeds [57], white matter lesions, and lacunes [58]. However, pericyte loss, gross dysfunction of the BBB, or widespread capillary damage such as occurs in DR has not been detected in the cerebral vasculature of diabetic patients [59-61]. In contrast, atrophy has been observed in several brain regions in diabetic patients, but is unknown whether this is caused by vascular damage [62-68]. Diabetes is also associated with an increased prevalence of cognitive impairment, including deficits in attention, memory, executive function, and emotional processing, and is a recognized risk factor for dementia [2, 69]. The mechanisms underlying neurodegeneration in the diabetic brain remain debated. It may be secondary to alterations in the microvasculature [57, 70-73], or be a direct effect of hyperglycaemia or insulin resistance [74-77], or a result of fluctuations in glucose levels [78].

AD is typically associated with cerebral neurodegeneration and cognitive decline [2, 79], which correlates with significant atrophy in brain regions such as the cerebral cortex, amygdala, hippocampus and parahippocampus [80-83]. In addition, extracellular Aβ plaques and intracellular tau tangles are pathological hallmarks of AD, appearing long before clinical symptoms emerge [80, 84-86]. Heritability accounts for the majority of the risk (60-80%) in the development of AD [87, 88]. Recent advancements in neuroimaging techniques have demonstrated that increased BBB permeability is an early event in AD patients, independent of Aβ and tau [2]. Vascular alterations in the human AD brain include vascular remodelling, changes in vascular density, basal lamina thickening, and vascular regression [2, 89, 90]. Furthermore, widespread macroglia activation [91-94] and pericyte loss across multiple brain regions [94-102] are consistent neuropathological features. In AD, the brain exhibits higher vascular permeability, yet the contribution of altered paracellular and transcellular transport pathways remains insufficiently explored [2, 103-105]. Cerebral neuropathological hallmarks, along with cognitive assessments and biomarkers in the blood and cerebrospinal fluid, are currently used to diagnose AD [106]. Although less widely recognized, retinal pathology has also been observed in AD patients, including presence of Aβ and tau [107-109], loss of retinal ganglion cells [110], and thinning of the retinal nerve fibre layer [111-116], as well as vascular abnormalities [117-121]. We propose that cerebral NVU dysfunction, possibly caused or aggravated by DM, and possibly similar to the NVU changes in DM or DR, represents a critical mechanism leading to impaired neuronal function and neurodegeneration in AD.

A comprehensive investigation exploring multiple components of the NVU in human retinal tissue in DM. The aim of our present explorative study is to investigate and compare NVU alterations in the human BRB in type 2 DM with or without DR, and in the human BBB in DM and AD. To characterize the structural components and functions of the NVU, we performed immunofluorescence staining of several key markers. These included markers for tight junction proteins, transcellular transport, macroglia and pericytes, and vascular permeability. Our analysis included retinal samples from donors with DM with or without DR, as well as brain tissues from donors with DM, AD, or both conditions.

Materials and methods

Human post-mortem retinal tissue

Human post-mortem eyes from cornea donors were provided by the Corneabank, Beverwijk, the Netherlands. The current research was performed in accordance with all requirements stated in the Dutch law "Wet op orgaandonatie" that describes the use of donor material for research purposes. According to this law, donors provide written informed consent for donation with an opt out of left-over material for related scientific research purposes. Specific requirements for the use for scientific research of left-over material originating from corneal grafting have been described in an additional document formulated by the Ministry of Health, Welfare, and Sport and the BIS foundation (Eurotransplant; Leiden, July 21, 1995; 6714.ht). The eyes were stored anonymously and therefore, approval of their use by the Ethics Committee was not required by Dutch law. The use of human material was also in accordance with the Declaration of Helsinki on the use of human material for scientific research.

Several hours post mortem, eyes were enucleated and the anterior parts of the eye, including the cornea and lens, were dissected. Fundoscopy images of the retina were taken before storage in the freezer and were evaluated by two independent ophthalmologists to determine the ophthalmological status. The eyecup was filled with Tissue-tek (cat# 4583, Sakura, Finetek Europe, Alphen aan de Rijn, The Netherlands) and eyes were snap frozen before being stored at –80 °C. Information on the type and duration of diabetes, when available, was kindly provided by Bio Implant Services Foundation (Leiden, The Netherlands). The retinal tissues were obtained from three patient groups: 1) donors with type 2 DM without DR, 2) donors with DM and DR, and 3) non-diabetic controls. Donor characteristics are summarized in Table 1. For the PLVAP/MFSD2A double staining experiments, tissue from one donor in the DR group was replaced due to reduced quality over time and replaced with a sample from a donor matched for key parameters: age (71 years; average 64 ± 4.9 years), post-mortem interval (10 hours; average 15.8 ± 4.4 hours), and health status. For optimal staining, radial incisions were made in the eyecup prior to processing.

Table 1. Characteristics of retinal tissue donors.

Case	Laser yes/ no	Sex (F/M)	Age at death (y)	Post-mortem delay (h)	Age at diabetes onset (y)	Insulin use (yes/no)	Diagnosis	Cause of death
Control								
1	No	F	68	14		No	Stomach cancer, asthma, COPD, fibrositis syndrome, Meniere's disease	Cancer (stomach)
2	No	F	68	17		No	Myocardial infarction	Myocardial infarction
3	No	F	67	12		No	Atherosclerotic disease, chronic kidney failure, narrowed coronary arteries	Atherosclerotic disease
4	No	M	66	9		No	Melanoma, lung embolism	Melanoma
Mean ± SD			*67 ± 0.8*	*13.0 ± 2.9*				
DM no DR								
5	No	M	67	15	Unknown	No	Vascular disease, leg amputation	Aortic aneurysm
6	No	F	71	18	64	No	Hypertension, hypercholesterolemia, arthrosis, cardiac arrhythmia, vascular disease	Cerebral infarction
7	No	M	62	19	57	Yes	Hypertension, vascular disease, Dupuytren's contracture, basal cell carcinoma	Heart failure
8	No	M	75	16	Unknown	Yes	Unknown	Heart failure
Mean ± SD			*69 ± 4.8*	*17.0 ± 1.6*				
DM + DR								
9	Yes	F	66	19	Unknown	No	Heart failure, hypertension, morbid obesity	Heart failure
10	Yes	F	61	13	<49	Yes	Heart failure, cardiac asthma	Heart failure
11	Yes	M	58	21	31	Yes	Nephropathy	Heart failure
12	Yes	F	71	13	69	Yes	Hypertension, myocardial infarction	Heart failure
Mean ± SD			*64 ± 4.9*	*16.5 ± 3.6*				

DM, diabetes mellitus; *DR*, diabetic retinopathy.

Immunofluorescence staining of human retina

Eye tissue specimens were cut into 10-µm-thick sections at -20°C, using an Microm Cryo Star HM 560 cryostat (Thermo Fisher Scientific), and stored at -80°C until further use. Prior to immunofluorescence staining, tissue cryosections were air dried, at RT for 20 min. The sections were then fixed with 4% formaldehyde (28908; Thermo Fisher Scientific) for 20 min and were washed once in 3× PBS for 10 min. For staining of retinal vasculature using wheat germ agglutinin (WGA), the retinal cryosections were incubated with fluorescent WGA conjugate in PBS for 30 min followed by washing twice in PBS for 5 min. The retinal sections were incubated in blocking buffer containing 0.1% (v/v) Triton X-100 (T-X; T8787; Merck Life Science, Amsterdam, The Netherlands) and 10% (v/v) normal goat serum (006-01; Southern Biotech, Birmingham, AL, USA) or 5-10% normal donkey serum (0030-01, Southern Biotech), depending on the secondary antibodies, in PBS, at RT for 1 h. For double staining of claudin-5 and CD31, the retinal cryosections were incubated in blocking buffer containing 2% (wt/v) bovine serum albumin (BSA; 10735094001; Roche Diagnostics, Mannheim, Germany) and 0.1% T-X in PBS. Directly after incubation with blocking buffer, the sections were incubated with the primary antibodies (Table 2) diluted in Normal Antibody Diluent (phosphate buffered; ABB999; ScyTek Laboratories, Logan, UT, USA) overnight at 4°C. Anti-CD31, PLVAP and MFSD2A antibodies were incubated in 0.2% BSA and 0.01% T-X in PBS. As a negative control, primary antibodies were omitted. After primary antibody incubation, the sections were washed three times with PBS for 5 min. The sections were incubated with secondary antibodies (Table 3), at RT for 1 h. Fibrinogen antibodies directly conjugated with fluorescein isothiocyanate (FITC) were incubated together with secondary antibodies. Following incubation, the sections were washed three times with PBS for 10 min each for staining for claudin-5, CD31, PLVAP and MFSD2A, and 5 min for all other antibodies. Following secondary antibody incubation and washing, the sections were incubated overnight at 4°C with claudin-5 antibodies directly conjugated with Alexa Fluor 488, diluted in Normal Antibody Diluent. This was followed by three 5-min washes in PBS. Finally, the sections were mounted with Vectashield antifading mounting medium containing DAPI (H-1200-10, Vector Laboratories Newark, CA, USA), covered with a cover glass, and sealed with transparent nail varnish.

Table 2. Primary antibodies used in this study.

Antigen	Host species	Source	Working dilution in retina	Working dilution in brain
AQP4	Rabbit	Merck, AB3594	1:10,000	1:200
CD31	Sheep	R&D systems, AF806	1:100/250	1:250
Claudin-5-AF488 (conjugated)	Mouse	Invitrogen, 352588	1:500	1:250
Fibrinogen-FITC (conjugated)	Rabbit	DAKO, F0111	1:200	1:50
GFAP	Mouse	Merck, G3893	1:400	1:400
Kir4.1	Rabbit	Alomone Labs, APC-035	1:200	1:50
Laminin	Rabbit	Abcam, Ab11575	1:750/1000	1:250/1000
MFSD2A	Rabbit	Chenghua Gu, J9590	1:500	1:200

NG2	Mouse	Merck, MAB2029	1:100	1:100
Occludin	Mouse	Invitrogen, 33-1500	1:500	1:100
PDGFRβ	Goat	R&D systems, AF385	1:100	1:60
PLVAP	Mouse	LUMC Pathology, clone: VC3, PAL-E	1:500	-
vWF	Rabbit	DAKO, A0082	1:400	1:600
WGA-AF555 (conjugated)	Wheat germ	Invitrogen, W32494	1:500	1:500/750

AF = Alexa Fluor; AQP4 = aquaporin-4; GFAP = glial fibrillary acidic protein; FITC = Fluorescein isothiocyanate; NG2 = Neural/glial antigen 2; PAL-E, Pathologische anatomie Leiden endothelium; SMA = smooth muscle actin; VWF = Von Willebrand factor; WGA = wheat germ agglutinin. Abcam (Amsterdam, the Netherlands); Alomone Labs (Jerusalem, Israel); DAKO (Santa Clara, CA, USA); Invitrogen (Waltham, MA, USA); R&D Systems (Minneapolis, MI, USA).

Table 3. Secondary antibodies used in this study.

Antibody	Conjugate	Source	Working dilution
Goat anti-mouse IgG	Alexa Fluor 488	Jackson ImmunoResearch Laboratories, 115-545-146	1:400
Goat anti-rabbit IgG	Alexa Fluor 488	Invitrogen, A-11034	1:400
Donkey anti-rabbit IgG	Alexa Fluor™ 488	Invitrogen, A-21206	1:400
Goat anti-mouse IgG	Cy3	Jackson ImmunoResearch Laboratories, 115-165-166	1:50-70
Goat anti-rabbit IgG	Cy3	Jackson ImmunoResearch Laboratories, 111-165-144	1:200
Donkey anti-goat IgG	Cy3	Jackson ImmunoResearch Laboratories, 705-165-147	1:100
Goat anti-mouse IgG	Alexa Fluor 633	Invitrogen, A-21052	1:100/200
Goat anti-rabbit IgG	Alexa Fluor 633	Invitrogen, A-21071	1:100
Donkey anti-rabbit IgG	Alexa Fluor 647	Invitrogen, A-32795	1:800
Donkey anti-sheep IgG	Alexa Fluor 647	Invitrogen, A-21448	1:400-500

Jackson ImmunoResearch Laboratories (West Grove, PA, USA).

Human post-mortem brain tissue

Post-mortem brain samples of the human frontal cortex were provided by the Netherlands Brain Bank, Amsterdam, The Netherlands. Frontal cortex samples were selected, because pathological features [125-127], including vascular pathology [128, 129], appear in the frontal cortex during early stages of dementia. All donors or their relatives provided written informed consent for brain autopsy and the use of brain tissue for research purposes. This usage was also in accordance with the Declaration of Helsinki on the use of human material for scientific research. Brain tissues were collected within several hours post-mortem, dissected, snap frozen in liquid nitrogen and stored at –80°C until sectioning. Donors were classified into four groups: 1) donors with DM type 2, 2) donors with AD, 3) donors with DM type 2 and AD, and 4) non-diabetic non-AD controls. Clinical diagnoses were confirmed by autopsy findings. Donors characteristics are summarized in Table 4. The subject groups were age-matched to control group to account for age-dependent changes in BBB integrity.

Table 4. Characteristics of brain tissue donors.

Case	Sex (F/M)	Age at death (y)	Post-mortem delay (h)	Age at disease onset (y)	Braak stage (0–6)	Vascular pathology in frontal cortex	Neuropathology in frontal cortex	Cause of death
Control								
1	F	66	6.3		1	Slight atherosclerosis	Myelin pallor; only MS plaques; no AD plaques	Cancer
2	M	58	7.7		0	Slight atherosclerosis	Partly absent myelination; no amyloid plaques	Myocardial ischemia
3	F	87	4.6		2	Slight atherosclerosis	No CAA; moderate number of amyloid diffuse plaques; a few classic plaques, no tangles	Pneumonia
4	M	71	5.1		0	Moderate atherosclerosis	Few fuzzy astrocytes (age-related Tau-astrogliopathy); no amyloid beta deposits.	Pancreatic cancer, euthanasia
Mean ± SD		*71 ± 12.2*	*5.9 ± 1.4*					
DM								
5	F	70	6.0	50	2	Slight atherosclerosis, perivascular oedema some iron pigment	Few diffuse plaques; no CAA; no tangles	Kidney failure
6	M	67	9.0	61	1	Slight atherosclerosis	No CAA; moderate to large number of diffuse plaques; no tangles; slight perivascular oedema	Aortic aneurysm, asystole
7	M	65	7.2	Unknown	2	Slight atherosclerosis	No plaques or tangles; some tau-positive cells	Fever, neuroleptic malignant syndrome
8	F	86	7.5	Unknown	2	Slight atherosclerosis, severe perivascular oedema	No CAA; moderate number of plaques; equal numbers of diffuse and classic types; no tangles	Cancer
Mean ± SD		*72 ± 9.6*	*7.4 ± 1.2*					

Table 4. Characteristics of brain tissue donors (continued).

Case	Sex (F/M)	Age at death (y)	Post-mortem delay (h)	Age at disease onset (y)	Braak stage (0–6)	Vascular pathology in frontal cortex	Neuropathology in frontal cortex	Cause of death
AD								
9	F	78	7.5	71	5	Slight atherosclerosis	Moderate CAA; no dysphoric angiopathy; no striking capillary angiopathy; moderate to many amyloid plaques, especially diffuse; many tangles	Dehydration
10	M	75	6.3	66	5	Slight atherosclerosis	Slight CAA; many diffuse and classic plaques; presence of tangles, neuritic plaques, and Lewy bodies	Cachexia
11	M	63	9.8	56	6	Slight to severe atherosclerosis	Slight CAA with dysphoric angiopathy and no capillary angiopathy; many plaques, diffuse types and classic types; many tangles	Dehydration / cachexia
12	M	80	5.5	79	6	No atherosclerosis	CAA present; many diffuse plaques and few classic plaques; presence of tangles and Lewy bodies	Dehydration and pneumonia
Mean ± SD		*74 ± 7.6*	*7.3 ± 1.9*					
DM + AD								
13	M	67	5.4	DM and Dem: unknown	5	Slight atherosclerosis	Many senile plaques, neurofibrillary tangles and many neuropil threads; moderate number of plaques, mainly "classic" plaques with large cores	Cerebral infarction
14	M	71	4.0	DM: 57; Dem: 64	6	Slight atherosclerosis	Large plaques with coarse fibrils of weakly staining amyloid, few diffuse plaques; many neuritic plaques and a moderate amount of tangles	Dementia, delirium and dehydration
15	M	82	8.5	DM: unknown; Dem: 80	5	Perivascular oedema	Many amyloid beta depositions, including diffuse plaques, classic plaques and small depositions; many neuropil threads, tangles and dispersed neuritic plaques; myelination is normal	Heart failure
16	F	77	3.8	DM: 73; Dem: 73	5	Moderate atherosclerosis	Slight to moderate CAA, mostly diffuse plaques, few-to-moderate neuritic plaques; moderate number of tangles; many Lewy inclusions; many Lewy threads	Infection and dehydration
Mean ± SD		*74 ± 6.6*	*5.4 ± 2.2*					

AD, Alzheimer's disease; *CAA,* Cerebral amyloid angiopathy; *DM*, diabetes mellitus; *Dem*, dementia

Immunofluorescence staining of human brain

Brain tissue specimens were cut into 10-µm-thick sections at –20°C, using an Microm Cryo Star HM 560 cryostat, and were stored at –80°C until further use. Prior to immunofluorescence staining, the tissue cryosections were air dried at RT for 20 min. Next, the brain sections were fixed with 4% formaldehyde for 20 min and were washed once in 3× PBS for 10 min. The sections were blocked and permeabilized by incubation in PBS supplemented with (1) 10% normal goat/donkey serum and 0.1% T-X (NG2; PDGFRβ; fibrinogen; occludin and claudin-5; MFSD2A; co-staining Aqp4+GFAP), or (2) 5% BSA and 0.1% T-X (co-staining Kir4.1+GFAP), at RT for 1 hour. Lipofuscin autofluorescence was reduced by incubating the sections in Trueblack [130, 131] (23007; Biotium, Fremont, CA) diluted 20x in 70% ethanol for 30 seconds followed by three times washing in PBS for 10 min each, except for fibrinogen, NG2, Mfd2a staining. The sections were incubated with primary antibodies (Table 2) diluted in 0.2% BSA with 0.01% T-X in PBS (MFSD2A) or Normal Antibody Diluent (ABB999; ScyTek) (all other markers) overnight at 4°C. Fibrinogen antibodies were incubated for 1 h at RT, followed by three times washing in PBS for 5 minutes and incubation with fluorescent WGA conjugate diluted in PBS, at RT for 30 min. As a negative control, primary antibodies were omitted. Following primary antibody incubation, the sections were washed three times with PBS for 5 min. Next, the sections were incubated with secondary antibodies (Table 3) for 1 h at RT in the dark. Following secondary antibody incubation, the sections were washed three times with PBS for 5-10 min. For NG2 and MFSD2A staining, the sections were subsequently incubated with Trueblack diluted 20× in 70% ethanol for 30 seconds followed by three times washing in PBS for 5-10 min each. After secondary antibody incubation and washing, claudin-5 antibodies directly conjugated with Alexa Fluor 488 in Normal Antibody Diluent were incubated for 2 h at RT, followed by three times washing in PBS for 5 min. For co-staining of GFAP and WGA, secondary antibody incubation and washing was followed by incubation with fluorescent WGA conjugate diluted in PBS, at RT for 30 min, and three times washing in PBS for 5 min. Finally, the sections were mounted with Vectashield antifading mounting medium containing DAPI, covered with a cover glass, and sealed with transparent nail varnish.

Microscopical analysis of staining

Retinal and brain tissue sections were imaged using a Leica STELLARIS confocal microscope (Leica Microsystems, Wetzlar, Germany) with a HC APO CS2 40x/1.30 oil-immersion objective. The confocal images were made with bidirectional sequential scanning at 1024x1024 resolution with a scanning speed of 600 Hz and line average of 8. Acquired images were processed and exported from Leica Application Suite X. For each marker, the exposure time and laser intensity were maintained constant for each section, among all patient groups.

Image analysis

Protein expression was quantified using ImageJ software (National Institutes of Health) [132]. Images of at least 3 randomly selected areas per tissue section were analysed for quantification for each donor (n = 3–4 donors for the control group; n = 4 for all other groups).

For the quantification of fibrinogen protein expression, fluorescence intensity outside the vasculature and inside the vasculature was measured as follows: a region of interest (ROI)

was drawn manually around individual blood vessels using WGA as a marker for blood vessels. For extravascular fibrinogen staining, the “Make Band” function in ImageJ was used with a band size customized for each blood vessel to cover all fibrinogen outside of vasculature. For blood vessels without fibrinogen leakage, a band size of 0.1 was assigned. The fluorescence intensity in the vascular ROI and the surrounding perivascular band was measured. The extravascular-to-intravascular ratio was calculated for each blood vessel and expressed either as individual datapoints per donor or as a mean value from all images per donor.

Fluorescence intensity of tight junction proteins was normalized to blood vessel length. Briefly, individual blood vessels were delineated with a manual ROI based on the vascular marker. This ROI was applied to the channel with tight junction staining to measure fluorescence intensity. Vessel length was calculated using ImageJ by tracing the central axis. The fluorescence intensity for each blood vessel was then divided by its length in µm. Results are expressed either as individual datapoints per donor or as the mean intensity per µm blood vessel from all images per donor. In addition to intensity, the tight junction staining was quantified by a semi-quantitative score system based on two distinct approaches. The first approach quantifies the staining as follows: 1. Continuous for border staining as an uninterrupted line; 2. Fragmented for border staining as an interrupted line); 3. Absent for complete loss of border staining. The second approach was as follows: 1. Sharp for border staining; 2. Diffuse for intracellular staining; 3. Absent for complete loss of border staining. The results were summed and the frequency of each score was calculated and plotted. A 3D histogram of for each of the examples of staining pattern was formed using the Surface Plot function in ImageJ after applying Gaussian Blurr (Sigma of 2) as a filter.

For semi-quantification of PLVAP and MFSD2A protein expression, PLVAP and MFSD2A staining was analysed via a semi-quantitative ranking score system on a scale of three categories indicating the fluorescence intensity: high (fluorescence intensity), low, and absent. Semi-quantification was performed in a blinded manner by three independent observers. The results were summed, and the frequency of each score was calculated and plotted.

Global and perivascular GFAP fluorescence intensity as well as the global and perivascular GFAP-positive coverage was measured. To quantify global fluorescence and global coverage in the retina, we included only the retinal layers in each image and excluded other layers in the eye. For the brain, the total tissue area in each image was used for global quantification. A vascular ROI was drawn manually around individual blood vessels using WGA as a marker for blood vessels. A perivascular ROI was defined by drawing a band with a distance of around 5 µm around each vascular ROI. The mean fluorescence intensity and perivascular GFAP coverage was measured in perivascular ROI using ImageJ. Global and perivascular fluorescence intensity for AQP4 and Kir4.1 were measured using the same ROI for global and perivascular GFAP measurements. The ratio of perivascular and global fluorescence intensity for AQP4 and Kir4.1 was calculated for each image. The results were expressed either as individual datapoints per donor or as mean value from all images per donor.
The percentage of vascular area covered by the pericyte marker was quantified. Individual blood vessels were delineated with a manual ROI based on the laminin staining. To select for capillaries, we excluded blood vessels with a diameter larger than 10 µm. This ROI was

applied to the channel with staining for pericyte markers to measure Area Fraction of the NG2 or PDGFRβ channel. The results were expressed as individual datapoints per donor or as mean vascular coverage from all images per donor.

Statistical analysis

Statistical tests were performed using GraphPad Prism v10 (GraphPad Software, La Jolla, USA). A Kruskal-Wallis test was used for comparison between patient groups (n = 4) and data are presented as mean ± standard deviation. A two-way ANOVA with Tukey's multiple comparisons test was used for statistical analysis of the tight junction staining pattern and when using each region of interest (blood vessel / image) as an individual datapoint. These data were presented as median per group. Statistical significance was set at $p < 0.05$. Correlation coefficients were calculated using Spearman's correlation (α = 0.05, CI 95%, two-tailed) and heatmaps were generated in GraphPad Prism v10.

Results

Vascular permeability

Vascular leakage was evaluated by immunofluorescence staining of endogenous fibrinogen in the retina (Fig. 1; Supplementary Fig. S1) and frontal cortex (Fig. 1, Supplementary Fig. S2). In control retinas, fibrinogen was predominantly localised within the retinal intravascular space (Fig. 1A, Supplementary Fig. S1). In contrast, the retina of individuals with DM and DR more frequently showed fibrinogen extravasation than non-diabetic controls. The extent of fibrinogen extravasation was highly variable, both across patient groups and within individual retinas and brains, with not all regions exhibiting leakage. Despite this heterogeneity, quantification revealed a trend toward higher vascular leakage in DM and in particular DR retinas compared with non-diabetic controls (Fig. 1B, C).

In the brain, fibrinogen was predominantly confined to the intravascular space in both control and DM groups (Fig. 1D). Extravasation was observed more frequently in the brains of individuals with DM+AD compared to all other groups. Quantification confirmed this pattern, revealing the lowest level of extravasation in the DM-only group (Fig. 1E, F). DM+AD brains exhibited clearly higher scores of vascular leakage compared to DM-only brains (p = 0.0008; Fig. 1F).

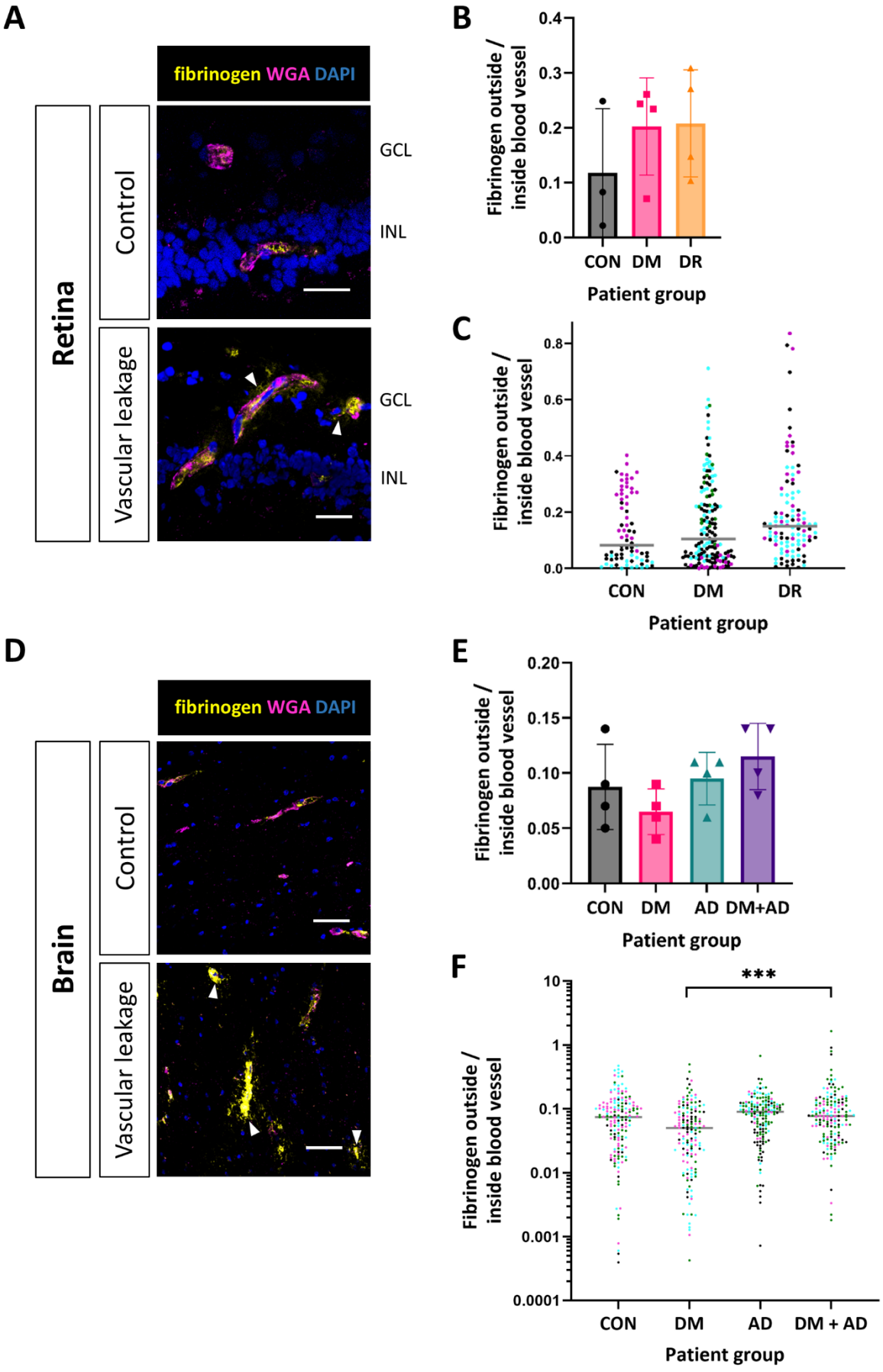
A
fibrinogen WGA DAPI
Retina
Control
Vascular leakage
GCL
INL
GCL
INL
B
Fibrinogen outside / inside blood vessel
0.4
0.3
0.2
0.1
0.0
CON DM DR
Patient group
C
Fibrinogen outside / inside blood vessel
0.8
0.6
0.4
0.2
0.0
CON DM DR
Patient group
D
fibrinogen WGA DAPI
Brain
Control
Vascular leakage
E
Fibrinogen outside / inside blood vessel
0.20
0.15
0.10
0.05
0.00
CON DM AD DM+AD
Patient group
F
***
Fibrinogen outside / inside blood vessel
10
1
0.1
0.01
0.001
0.0001
CON DM AD DM + AD
Patient group

Figure 1. Assessment of vascular leakage via fibrinogen immunofluorescence in the human BRB and BBB in DM retina and DM and AD brain. (A) Fibrinogen (yellow) staining in the human retina under physiological control conditions, and pathological conditions showing fibrinogen extravasation (arrow heads). Vascular endothelial cells are stained with wheat germ agglutinin (WGA; magenta) and nuclei are stained with DAPI (blue). GCL = ganglion cell layer; INL = inner nuclear layer. Scale bar: 30 µm. **(B, C)** Quantification of the ratio of extravascular and intravascular fibrinogen fluorescence intensity in human retina samples (Control, DM, AD, DM+AD). **(B)** Individual donors (dots), with mean ± SD per group. **(C)** Individual vessels (dots, coloured by donor), with group median (grey line). **(D)** Immunofluorescence for fibrinogen (yellow) , endothelial WGA (magenta) and nuclei (DAPI, blue). White arrowheads n pathological samples indicate fibrinogen extravasation (vascular leakage). Scale bar: 50 µm. **(E, F)** Quantification of the ratio of extravascular and intravascular fibrinogen fluorescence intensity in the human frontal cortex (Control, DM, AD, DM+AD). **(E)** Individual donors (dots), mean ± SD. **(F)** Individual vessels (dots, colored by donor), group median (grey line). *** $p < 0.001$.

Taken together, these results demonstrate a clear tissue-specific pattern: higher fibrinogen permeability is a feature of the diabetic retina, especially in DR, but in the DM brain it occurs only when AD is also present.

Paracellular pathway

To assess the integrity of the paracellular pathway of vascular permeability, we performed immunostaining for the tight junction proteins occludin and claudin-5. In the retina, both proteins were readily detectable in the vasculature of all donor groups (Supplementary Fig. S3, Supplementary Fig. S4). In non-diabetic control retinas, occludin and claudin-5 predominantly appeared as sharp, continuous lines along endothelial cell borders, although a subset of vessels lacked detectable expression. In the diabetic retina without known DR, these staining patterns for claudin-5 and occludin were largely preserved. In contrast, retinas from DR donors showed a slight reduction in the expression of both proteins and altered junctional cell-border staining patterns. Grading of the tight junction organisation at cell borders and the formation of gaps (fragmentation) in tight junction complexes (Fig. 2) revealed sharply demarcated (Fig. 3A) and continuous (Fig. 3B) occludin staining in the control retina. In DR retinas, the proportion of the retinal vasculature lacking occludin staining was higher when compared to DM and control retinas. Quantitative analysis of the staining intensity per µm blood vessel confirmed a moderate reduction in occludin levels in both DM and DR groups compared to controls (Fig. 3C, D).

Analysis of claudin-5 staining morphology in controls revealed that most vessels showed a sharp, continuous pattern (Fig. 3E, F) or a fragmented pattern (Fig. 3F). DM and DR retinas showed a trend of more disorganisation of claudin-5 compared to controls. Claudin-5 staining intensity was similar in DM retinas and non-diabetic controls, but was reduced in the DR group ($p < 0.001$; Fig. 3G, H).

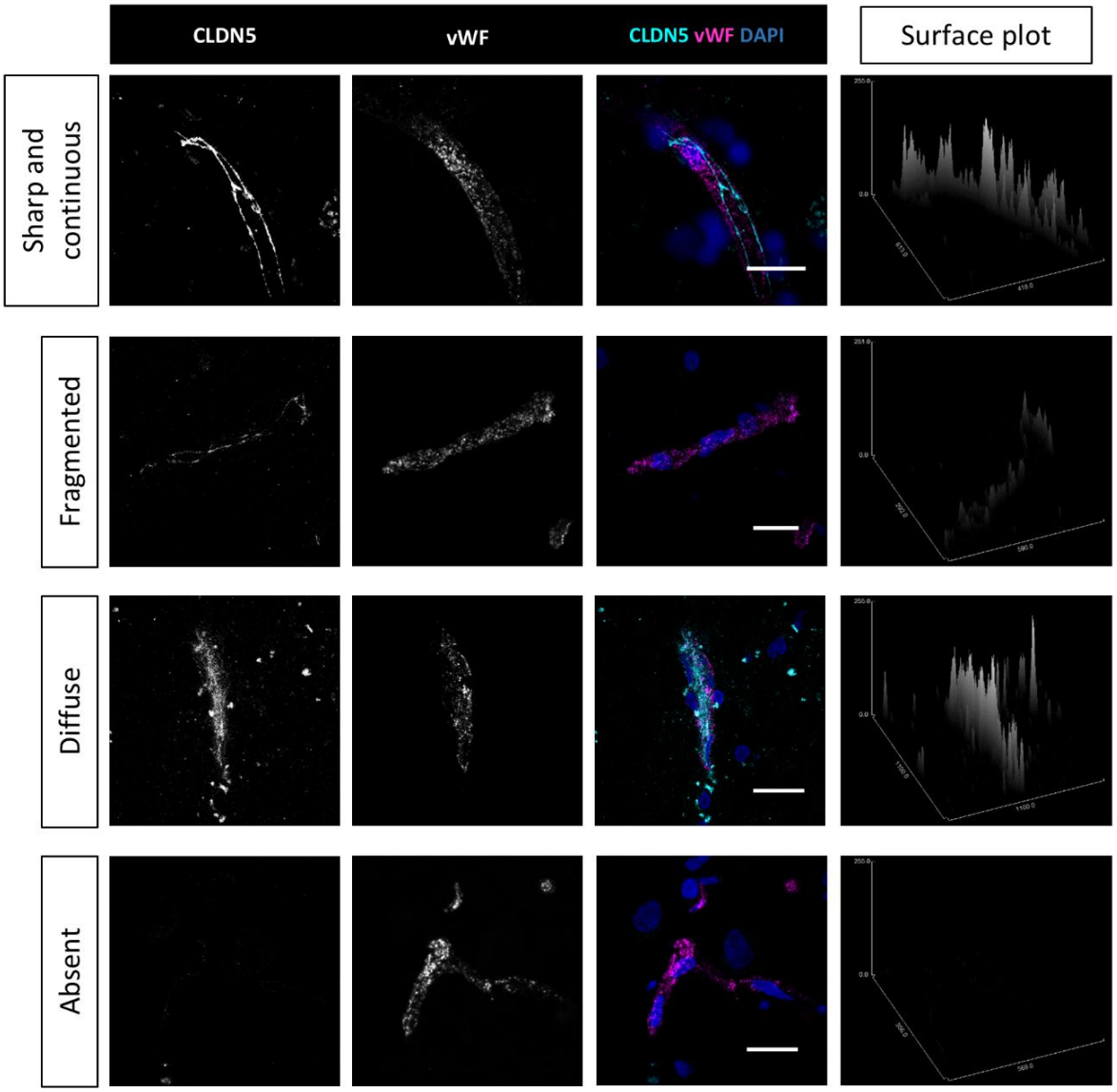

Figure 2. Immunofluorescence staining patterns of tight junction proteins of the barrier endothelium in human BRB and BBB. Tight junction protein claudin-5 (CLN5; cyan) staining in the human brain depicting staining pattern categories used for semi-quantification of tight junction proteins in the retina and brain. The staining pattern categories are 1) Sharp (located at the cell border forming a line), 2) Continuous (no major gaps in tight junction staining), 3) Diffuse (not at cell border, more intracellular expression), 4) Fragmented (large gaps/discontinuity in tight junction staining), 5) Absent (lack of expression). Vascular endothelial cells were stained for von Willebrand Factor (vWF; magenta) and nuclei are stained with DAPI (blue). Scale bar: 20 µm. The right panel depicts 3D histograms of the claudin-5 expression in each of the blood vessels in the immunofluorescence images.

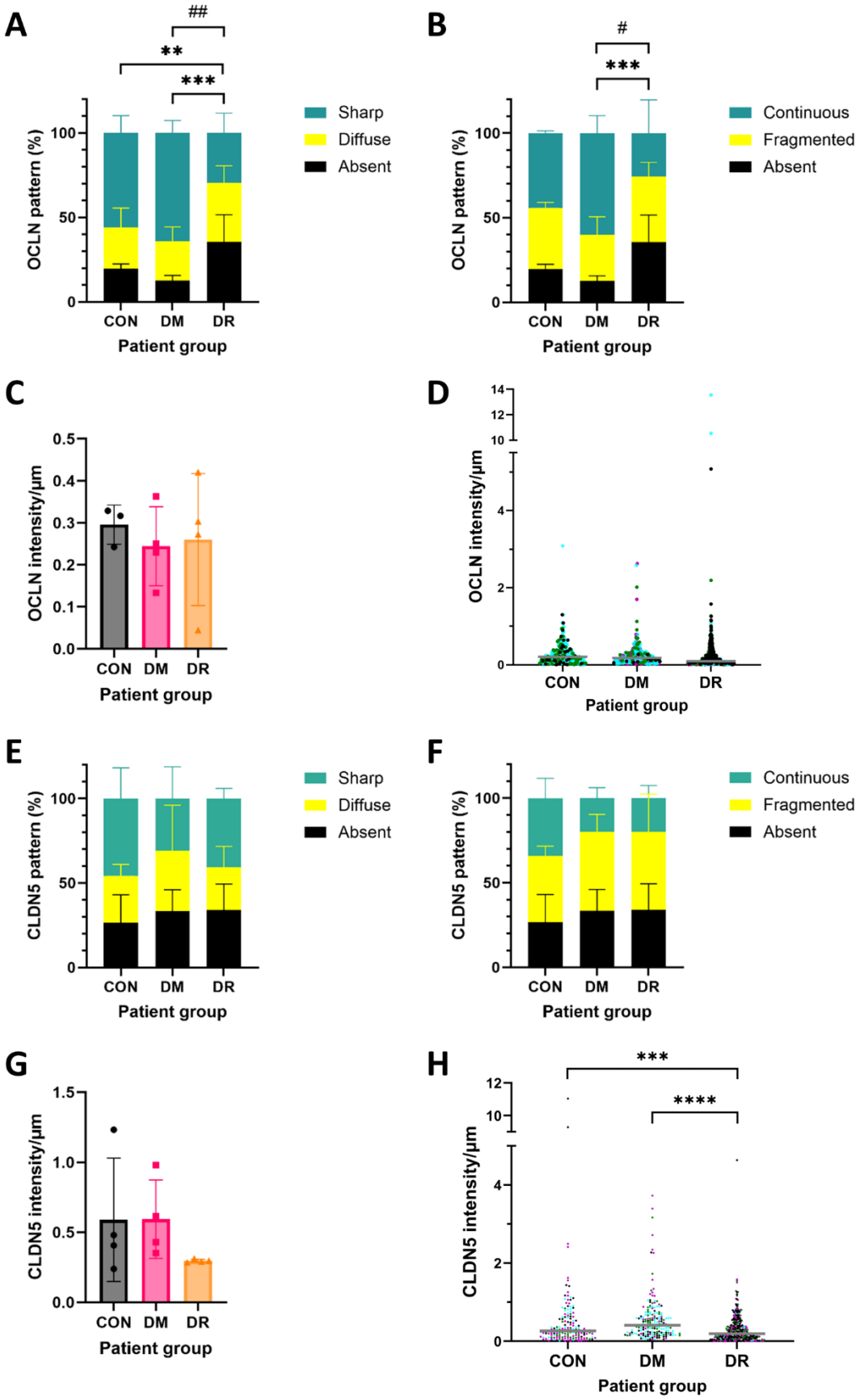

Figure 3. DR affects tight junction expression in the human BRB. Semi-quantification of staining patterns of tight junction proteins in retinal cryosections (CON, DM, DR) that are categorized into **(A,**

E) 1) Continuous, 2) Fragmented or 3) Absent and **(B, F)** 1) Sharp, 2) Diffuse or 3) Absent. Data are expressed as the mean ± SD. * for Sharp/Continuous and # for Absent. Quantification of **(C, D)** occludin (OCLN) and **(G, H)** claudin-5 (CLDN5) intensity per µm blood vessel in retinal cryosections. **(C, G)** Individual donors (dots), with mean ± SD per group. **(D, H)** Individual vessels (dots, coloured by donor), with group median (grey line). * $p < 0.05$, ** $p < 0.01$, *** $p < 0.001$, **** $p < 0.0001$.

We also confirmed the presence of occludin and claudin-5 in the cerebral vasculature (Supplementary Fig. S5). Qualitative analysis of the staining pattern in control brains showed that the majority of vessels exhibited a sharp (Fig. 4A) and continuous (Fig. 4B) occludin pattern. In contrast, a significant change towards a more diffuse and fragmented pattern was observed in the frontal cortex of donors with DM, AD, or both DM and AD compared to controls. The DM+AD group exhibited the highest percentage of diffuse occludin staining, suggesting a more cytoplasmic distribution, which may explain the higher intensity observed in the vasculature of this group ($p < 0.0001$; Fig. 4C, D). The intensity of the occludin staining in the cortex was similar in the control, DM and AD groups.

In control brain samples, claudin-5 staining showed a sharp pattern in most blood vessels, with a slightly smaller proportion displaying a diffuse pattern (Fig. 4E). The proportion of blood vessels exhibiting continuous and fragmented staining patterns was similar (Fig. 4F). Compared to controls, all disease groups (DM, AD, and DM+AD) exhibited a disorganised claudin-5 staining pattern in the brain (Fig. 4E, F). Claudin-5 staining intensity was the same in control, DM, and AD brains, but was on average 5-fold higher in the DM+AD group compared to controls ($p = 0.018$; Fig. 4G). When individual vessels were analysed, claudin-5 intensity in DM+AD brains was significantly higher than in controls, DM, or AD donors (all $p < 0.0001$; Fig. 4H).

In summary, disorganisation of tight junctions was found in both the retina of patients with DM and DR, and in the brain of patients with DM, AD and both DM and AD. In the DR retina, moderately lower levels of occludin and claudin-5 intensity were found compared to controls, reflecting in a higher percentage of absent tight junction markers. In the brain, disorganised tight junction proteins across all patients groups were reflected in a more diffuse and fragmented expression pattern.

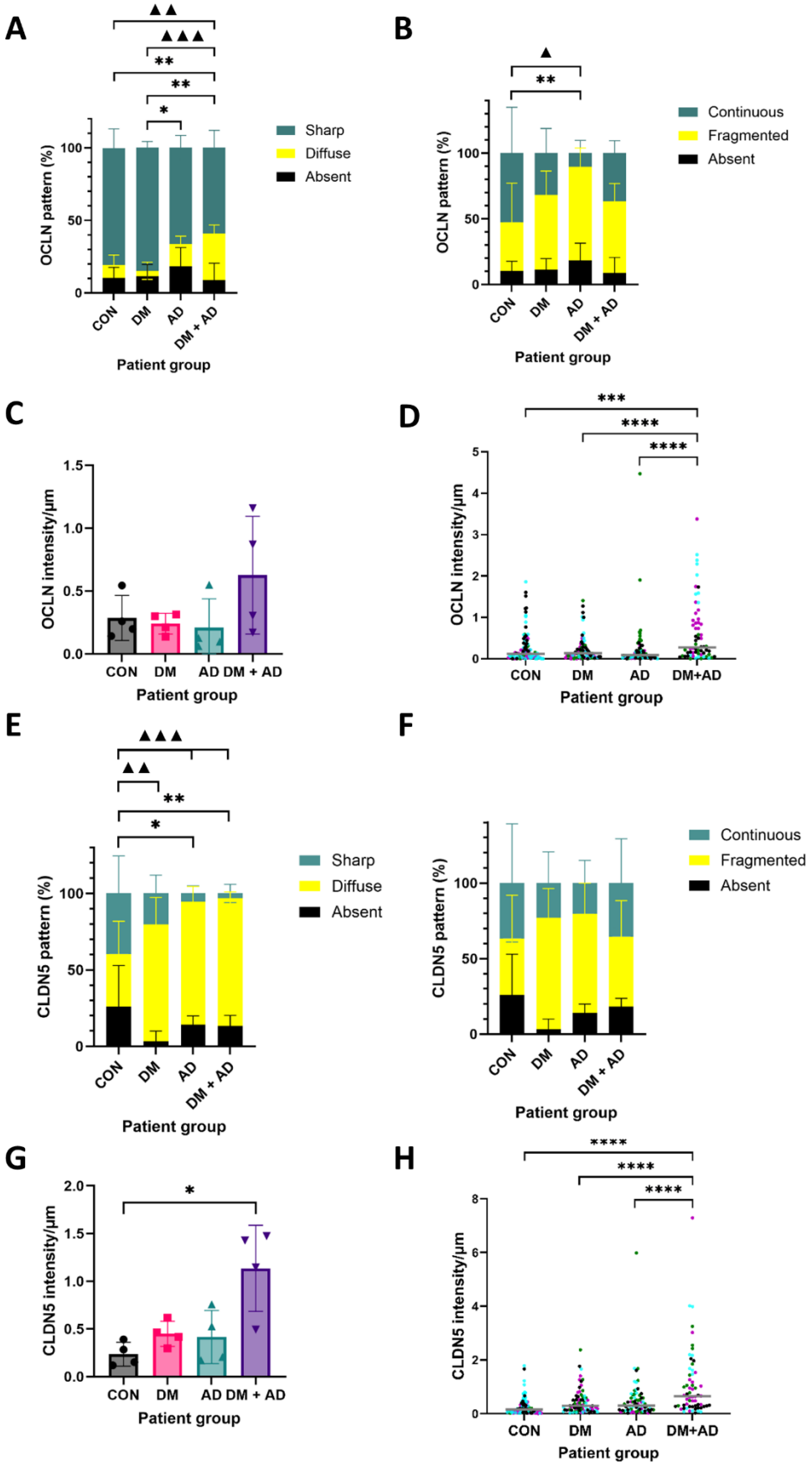

Figure 4. DM and AD affect tight junction expression in the human BBB. Semi-quantification of staining patterns of tight junction proteins in cryosections of frontal cortex (CON, DM, AD, DM+AD)

that are categorized into **(A, E)** 1) Continuous, 2) Fragmented or 3) Absent and **(B, F)** 1) Sharp, 2) Diffuse or 3) Absent. Data are expressed as the mean ± SD. * for Sharp/Continuous, ▲ for Diffuse/Fragmented and # for Absent. Quantification of **(C, D)** occludin (OCLN) and **(G, H)** claudin-5 (CLDN5) intensity per µm blood vessel in cortical cryosections. **(C, G)** Individual donors (dots), with mean ± SD per group. **(D, H)** Individual vessels (dots, coloured by donor), with group median (grey line). * $p < 0.05$, ** $p < 0.01$, *** $p < 0.001$, **** $p < 0.0001$.

Transcellular pathway

To assess alterations in the transcellular endothelial pathway of permeability (transcytosis) in the diabetic retina and in the diabetic and AD brain, we performed immunostaining of PLVAP and MFSD2A in the retina (Fig. 5, Supplementary Fig. S6) and in the brain (Fig. 6, Supplementary Fig. S7). PLVAP is a marker of increased transcytosis in immature and pathological barrier endothelium [130] and MFSD2A is an inhibitor of transcytosis essential for barrier integrity [131, 132]. In the case of positive staining, a granular pattern was observed within the vasculature for both proteins in all patient groups in the retina. In control retina, PLVAP was minimally or not expressed at all in capillaries as reported previously [61](Fig. 5, Supplementary Fig. S6). Retinas from DM individuals displayed higher expression of PLVAP compared to controls, with an average of 30% of blood vessels being positive for PLVAP, and the majority of these vessels exhibited high PLVAP expression (Fig. 5B). In DR retinas, the percentage of PLVAP-positive blood vessels was highest, averaging 50%, with most vessels showing strong PLVAP expression. Changes in PLVAP expression were not associated with alterations in MFSD2A expression. On average, 45% of blood vessels were positive for MFSD2A in non-diabetic controls, though this ranged from 0% to 82% across individual donors. In control retinas, the proportion of vessels with low and high MFSD2A expression was similar. DM retinas had the highest percentage of positive vessels (~65%), but the expression level was mostly low. DR retinas also showed an higher percentage of positive vessels (~60%) compared to controls, though expression levels remained predominantly low.

In the human frontal cortex, we did not observe any PLVAP staining for any of the groups using the same antibody that was applied to the retina samples. Consistent with our observations in retina samples, MFSD2A expression exhibited a granular staining pattern in the brain vasculature (Fig. 6, Supplementary Fig. S7). Semi-quantitative analysis demonstrated that on average 77% of cortical capillaries were MFSD2A-positive in control brain samples with high expression in 32% and low expression in 45% of the blood vessels (Fig. 6B). A significantly higher percentage of vessels showed high expression in brains of DM donors (63%) compared to controls ($p = 0.040$). MFSD2A expression was similar in AD brains compared to controls. In contrast, almost all blood vessels in brains of DM+AD donors showed a high MFSD2A expression (91%), which was higher than in controls ($p < 0.0001$) and AD brains ($p = 0.004$).

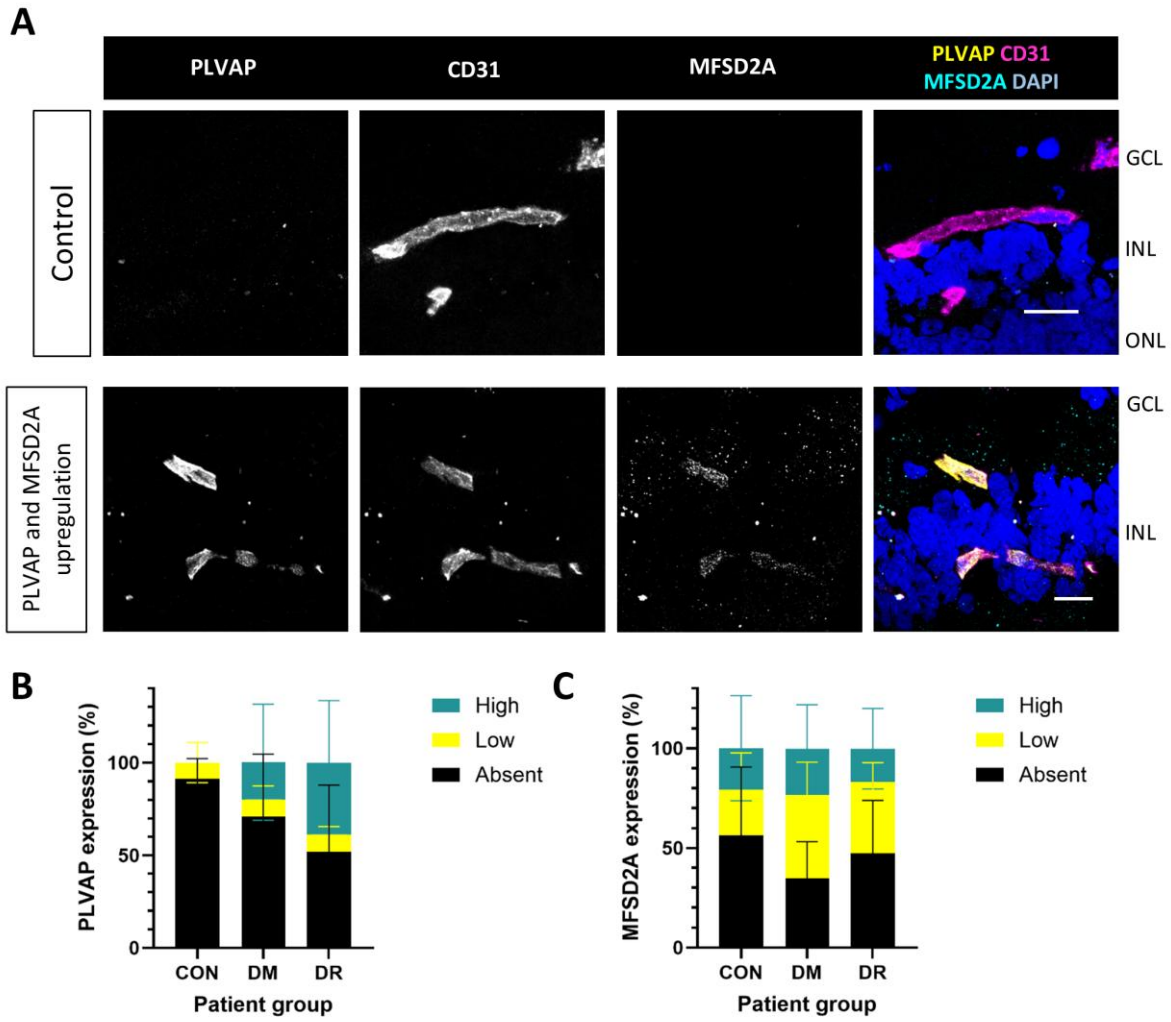

Figure 5. Affected transcellular transport pathway in the human BRB in DM. (A) Plasmalemma vesicle-associated protein (PLVAP; yellow) and MFSD2A (cyan) double staining in the human retina under physiological control conditions, and pathological conditions showing increased transcytosis. Vascular endothelial cells are stained with CD31 (magenta) and nuclei are stained with DAPI (blue). GCL = ganglion cell layer; INL = inner nuclear layer; ONL = outer nuclear layer. Scale bar: 20 µm. Semi-quantification of PLVAP **(B)** and MFSD2A **(C)** staining intensity in retinal cryosections (CON, DM, DR).

Taken together, the highest PLVAP expression is observed in DR retinas but completely absent in the brain. Conversely, MFSD2A expression was elevated in both retina and brain in DM compared to controls. Furthermore, DM+AD brains showed the highest percentage of MFSD2A positive vessels and the highest expression intensity.

Glial cell activation

In control and DM retinas, GFAP staining was confined to astrocytes in the inner retina (Fig. 7A, Supplementary Fig. S8). In contrast, DR retinas showed a marked upregulation of GFAP, characterized by intense focal staining in the inner retina and in the radial processes of

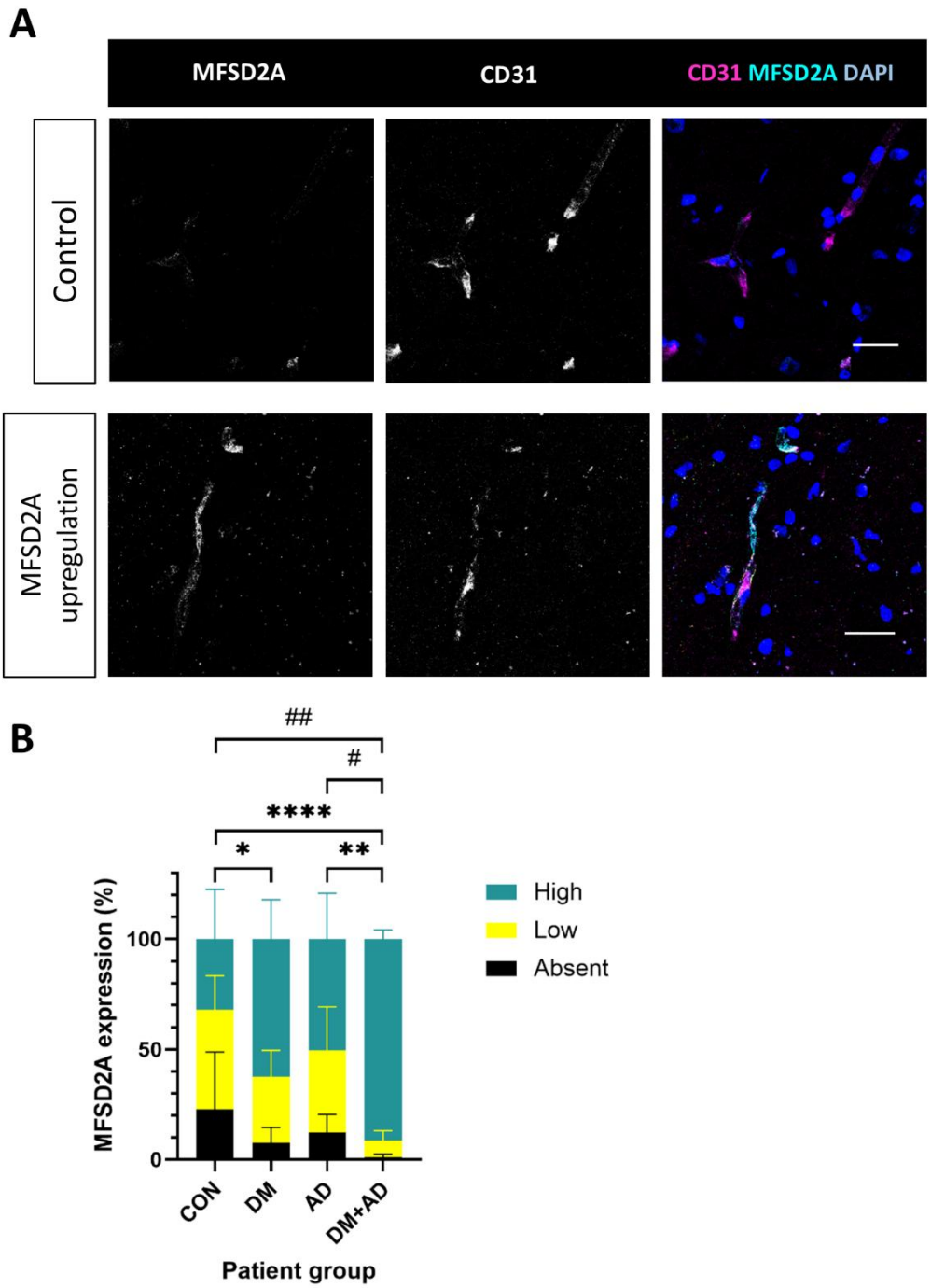

Figure 6. Altered transcellular transport pathway in DM and DM+AD in the human BBB. (A) MFSD2A (cyan) staining in the human brain under physiological control conditions, and pathological conditions showing vascular MFSD2A upregulation. Vascular endothelial cells are stained with CD31 (magenta) and nuclei are stained with DAPI (blue). Scale bar: 30 µm. **(B)** Semi-quantification of MFSD2A intensity in cortical cryosections (CON, DM, DR). * for High, and # for Low. * $p < 0.05$, ** $p < 0.01$, **** $p < 0.0001$.

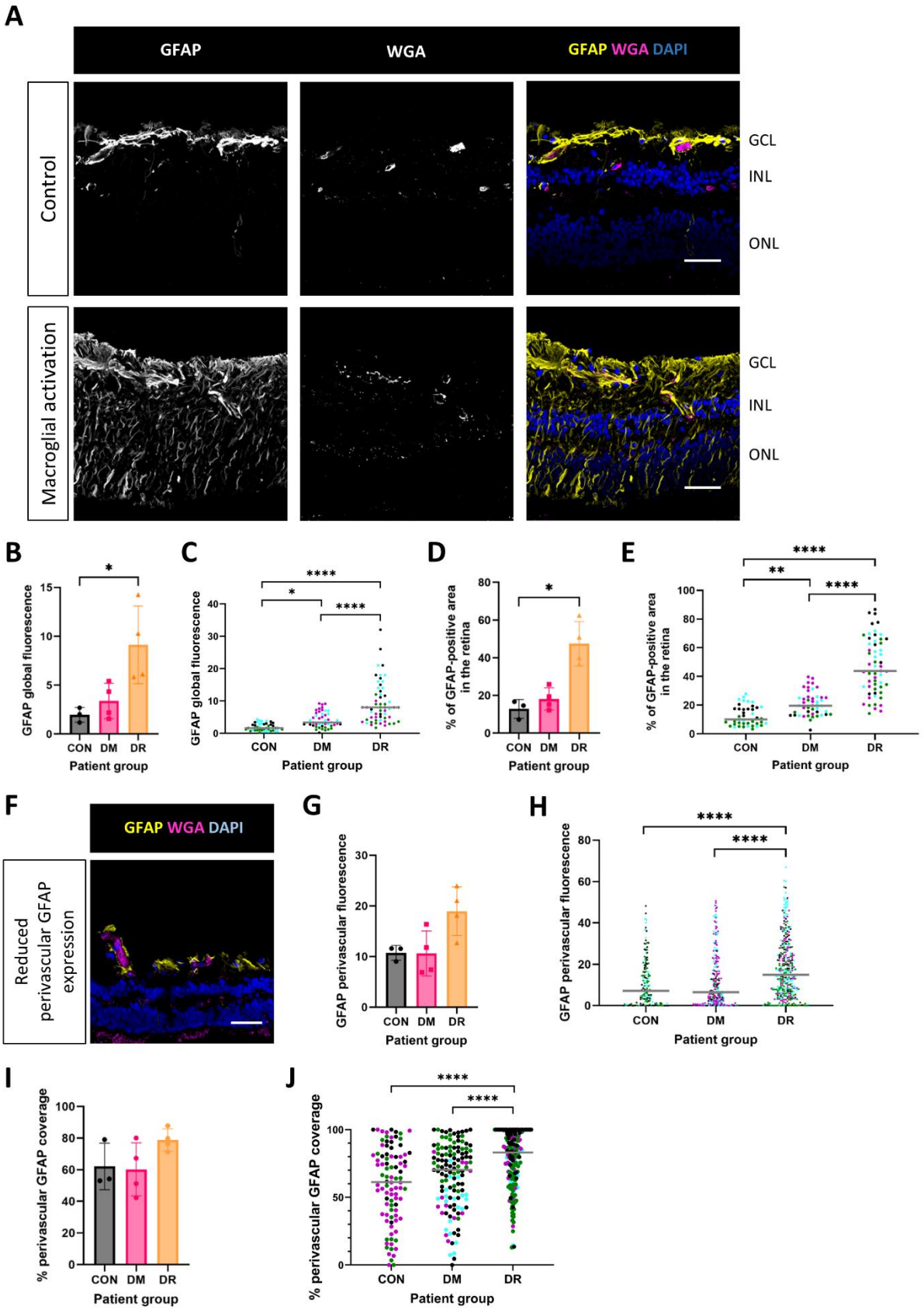

Figure 7. DR induces gliosis in the human BRB. (A) GFAP (yellow) staining in the human retina under physiological control conditions and in the case of macroglia activation. Vascular endothelial cells are stained with wheat germ agglutinin (WGA; magenta) and nuclei are stained with DAPI (blue).

GCL = ganglion cell layer; INL = inner nuclear layer; ONL = outer nuclear layer. Scale bar: 50 µm. Quantification of global **(B, C)** and perivascular **(G, H)** GFAP fluorescence staining intensity in retinal cryosections (CON, DM, DR). Quantification of the percentage of **(D, E)** total brain area and **(I, J)** perivascular area covered by macroglia expressing GFAP. **(F)** An example of a confocal image of a human retina with reduced perivascular GFAP expression. Scale bar: 50 µm. **(B, D, G, I)** Individual donors (dots), with mean ± SD per group. **(C, E, H, J)** Individual vessels (dots, coloured by donor), with group median (grey line). * $p < 0.05$, ** $p < 0.01$, **** $p < 0.0001$.

Müller cells in the inner and outer nuclear layers (INL and ONL) (Fig. 7A-C), indicating Müller cell activation (gliosis). Quantitative analysis showed a significantly higher retinal area covered by GFAP-positive macroglia in DR (48%) versus controls (13%; $p = 0.031$) or DM (18%; $p = 0.130$; Fig. 7D). At the single-vessel level, DM retinas had greater GFAP-positive coverage than controls ($p = 0.008$), with a further elevation in DR compared to both groups ($p < 0.0001$ for each; Fig. 7E). We additionally quantified perivascular GFAP expression, defined as the fluorescence intensity and area coverage of GFAP-positive macroglia immediately surrounding the blood-retinal barrier (Fig. 7F). Perivascular GFAP fluorescence intensity and area coverage (60%) in DM retinas were similar to controls (Fig. 7G-J). In contrast, when analysed at the level of individual vessels, DR retinas showed significantly higher perivascular intensity and a larger covered area (79%) than both control and DM retinas ($p < 0.0001$).

In the brain of control donors, GFAP staining was observed in both astrocytic cell bodies and processes, mainly in close proximity of blood vessels, independent of blood vessel size (Fig. 8, Supplementary Fig. S9). Global GFAP expression was moderately higher in DM, AD and DM+AD brains than in controls ($p > 0.050$; Fig. 8B, C). The cerebral area covered by GFAP-positive astrocytes was significantly higher in AD (58%; $p = 0.029$) compared to controls (19%; Fig. 8D). When analysed at the individual-vessel level, the percentage of cerebral area covered by GFAP-positive macroglia was significantly larger in DM (53%), AD (58%), and DM+AD (48%) compared to controls ($p < 0.0001$ for each; Fig. 8E). Cerebral perivascular GFAP fluorescence intensity was significantly elevated in all three disease groups versus controls ($p < 0.0001$; Fig. 8G). In controls, perivascular coverage by GFAP-positive astrocytes averaged 28% (Fig. 8H). This coverage was slightly higher in AD (33%) and DM+AD (34%) donors ($p < 0.0001$; Fig. 8I), and greatest in DM brains (41%; $p < 0.0001$ vs. controls).

In summary, these data indicate macroglial activation, also known as gliosis, in the retina of DR patients and in the brain of donors with DM, AD, and DM+AD.

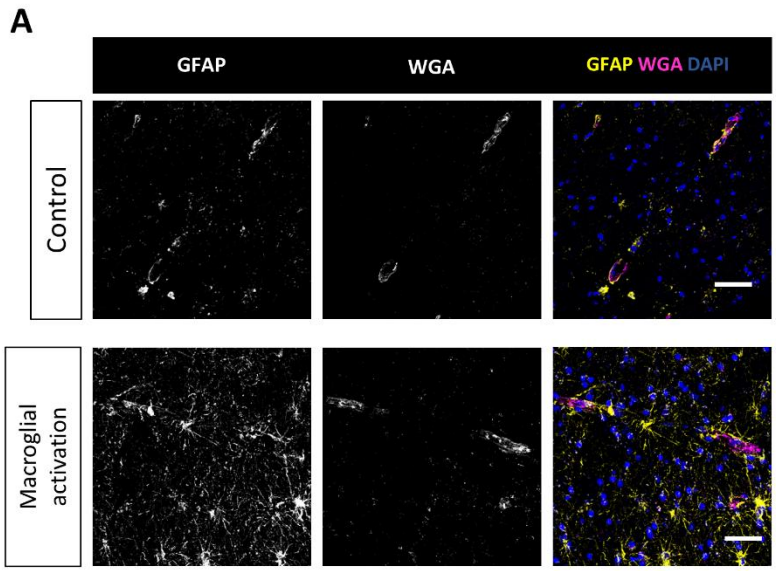
A
GFAP
WGA
GFAP WGA DAPI
Control
Macroglial activation

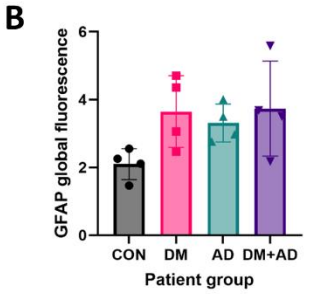
B
GFAP global fluorescence
CON
DM
AD
DM+AD
Patient group

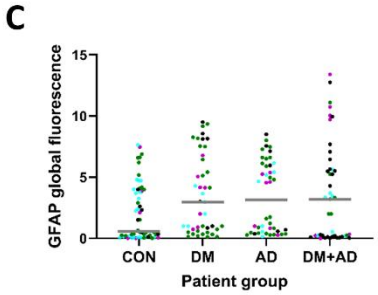
C
GFAP global fluorescence
CON
DM
AD
DM+AD
Patient group

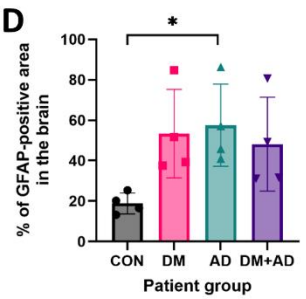
D
*
% of GFAP-positive area in the brain
CON
DM
AD
DM+AD
Patient group

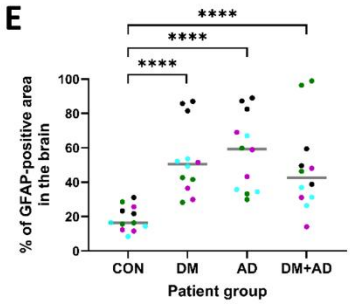
E
****
****
****
% of GFAP-positive area in the brain
CON
DM
AD
DM+AD
Patient group

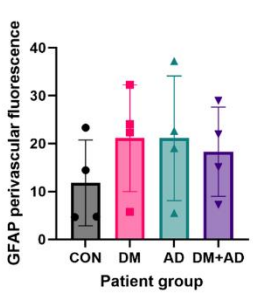
F
GFAP perivascular fluorescence
CON
DM
AD
DM+AD
Patient group

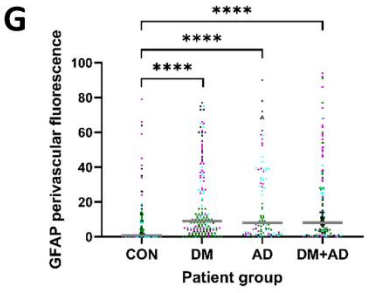
G
****
****
****
GFAP perivascular fluorescence
CON
DM
AD
DM+AD
Patient group

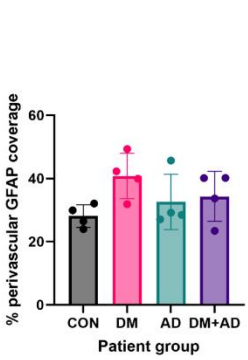
H
% perivascular GFAP coverage
CON
DM
AD
DM+AD
Patient group

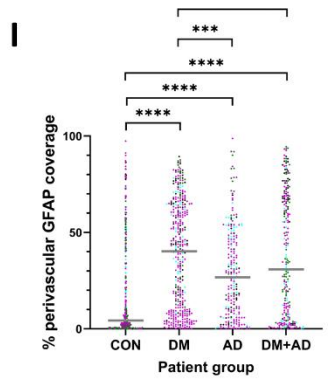
I
***
****
****
****
% perivascular GFAP coverage
CON
DM
AD
DM+AD
Patient group

Figure 8. DM and AD induce gliosis in the human BBB. (A) GFAP (yellow) staining in the human brain in physiological control conditions and in the case of macroglia activation. Vascular endothelial cells are stained with wheat germ agglutinin (WGA; magenta) and nuclei are stained with DAPI (blue). Scale bar: 50 µm. Quantification of global **(B, C)** and perivascular **(F, G)** GFAP fluorescence staining intensity in frontal cortex cryosections (CON, DM, AD, DM+AD). Quantification of the percentage of **(D, E)** total brain area and **(H, I)** perivascular area covered by macroglia expressing GFAP. **(B, D, F, H)** Individual donors (dots), with mean ± SD per group. **(C, E, G, I)** Individual vessels (dots, coloured by donor), with group median (grey line). * $p < 0.05$, ** $p < 0.01$, *** $p < 0.001$, **** $p < 0.0001$.

Water and potassium balance

Immunostaining for AQP4 and Kir4.1 revealed alterations in these water-regulating channels. In control retinas, AQP4 was enriched in perivascular regions compared to the neuronal tissue (Fig. 9, Supplementary Fig. S10). AQP4 expression in DM retinas, both global (Fig. 9B, E) and perivascular (Fig. 9C, F), was similar to that in the controls, showing only minimal global loss (Fig. 9A). Quantitative analysis revealed a modestly higher global fluorescence intensity in DR retinas compared to controls ($p = 0.005$), as well as a higher perivascular fluorescence intensity compared to controls ($p < 0.0001$) and DM retinas ($p = 0.003$; Fig. 9E, F). Additionally, a significant delocalisation of AQP4 from its perivascular localisation toward a more global neuronal tissue localisation was observed in DR retinas ($p = 0.045$; Fig. 9D) ($p < 0.0001$ compared to controls, $p < 0.001$ compared to DM; Fig. 9G).

Likewise, alterations in water-regulating channels were evaluated in the human frontal cortex via AQP4 immunostaining. AQP4 was predominantly localised around blood vessels, with additional expression in the neuronal tissue (Fig. 10, Supplementary Fig. S11). Figure 10A illustrates an example of cerebral AQP4 expression colocalised with GFAP-positive astrocyte processes, indicating reduced polarisation toward astrocytic endfeet. Although global AQP4 fluorescence was unchanged (Fig. 10B, E), the perivascular intensity was higher in AD brains than in controls and the DM+AD group ($p = 0.003$ and $p = 0.040$, respectively; Fig. 10F). In DM+AD brains, AQP4 was localised slightly more perivascular than global, compared to both controls ($p = 0.013$) and DM ($p = 0.013$), when analysed per vessel (Fig. 10G).

In the retina, Kir4.1 was typically localised in the ganglion cell layer independently of the condition (Fig. 11A, Supplementary Fig. S12). A less pronounced polarisation towards macroglial endfeet was observed for Kir4.1 compared to AQP4. An example of Kir4.1 expression in Müller cell processes in DR is shown in Fig. 11A. A significant reduction in global Kir4.1 fluorescence was observed in DR retinas compared to controls ($p = 0.026$) and DM retinas ($p = 0.005$; Fig. 11E) as well as a reduction in perivascular fluorescence in DR retinas compared to controls ($p < 0.0001$) and DM retinas ($p < 0.001$; Fig. 11F). Similar to AQP4, Kir4.1 staining in DR retinas demonstrated a significant reduction in polarisation compared to controls ($p = 0.031$; Fig. 11D, $p = 0.001$; Fig. 11G).

In the brain, Kir4.1 exhibited generally low expression, with a moderately higher perivascular expression (Fig. 12A, Supplementary Fig. S13). In DM, AD, and DM+AD, Kir4.1 expression was observed in cellular processes, yet it did not colocalise with GFAP immunostaining (Fig. 12A), suggesting that these processes originate from macroglial cells that do not express GFAP. A lower global Kir4.1 expression in the brain was found in DM compared to AD donors

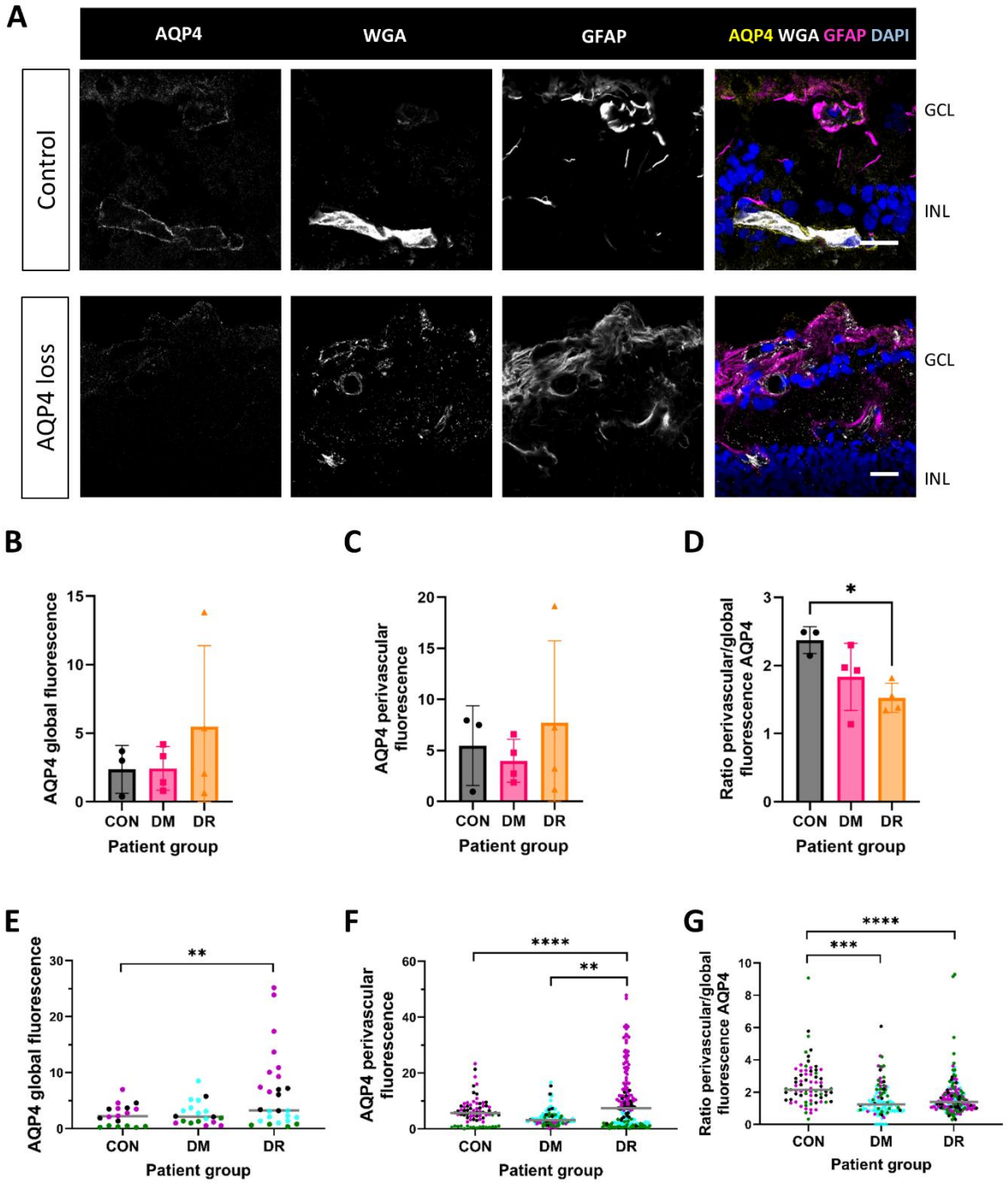

Figure 9. DR causes depolarization of AQP4 in the human BRB. (A) AQP4 (yellow) and GFAP (magenta) double staining in the human retina under physiological control conditions and in the case of AQP4 loss. Vascular endothelial cells are stained with wheat germ agglutinin (WGA; white) and nuclei are stained with DAPI (blue). GCL = ganglion cell layer; INL = inner nuclear layer. Scale bar: 20 µm. Quantification of global **(B, E)** and perivascular **(C, F)** AQP4 expression in the retina (CON, DM, DR). **(D, G)** Quantification of the ratio of perivascular and global AQP4 fluorescence intensity. **(B-D)** Individual donors (dots), with mean ± SD per group. **(E-G)** Individual vessels (dots, coloured by donor), with group median (grey line). * $p < 0.05$, ** $p < 0.01$, *** $p < 0.001$, **** $p < 0.0001$.

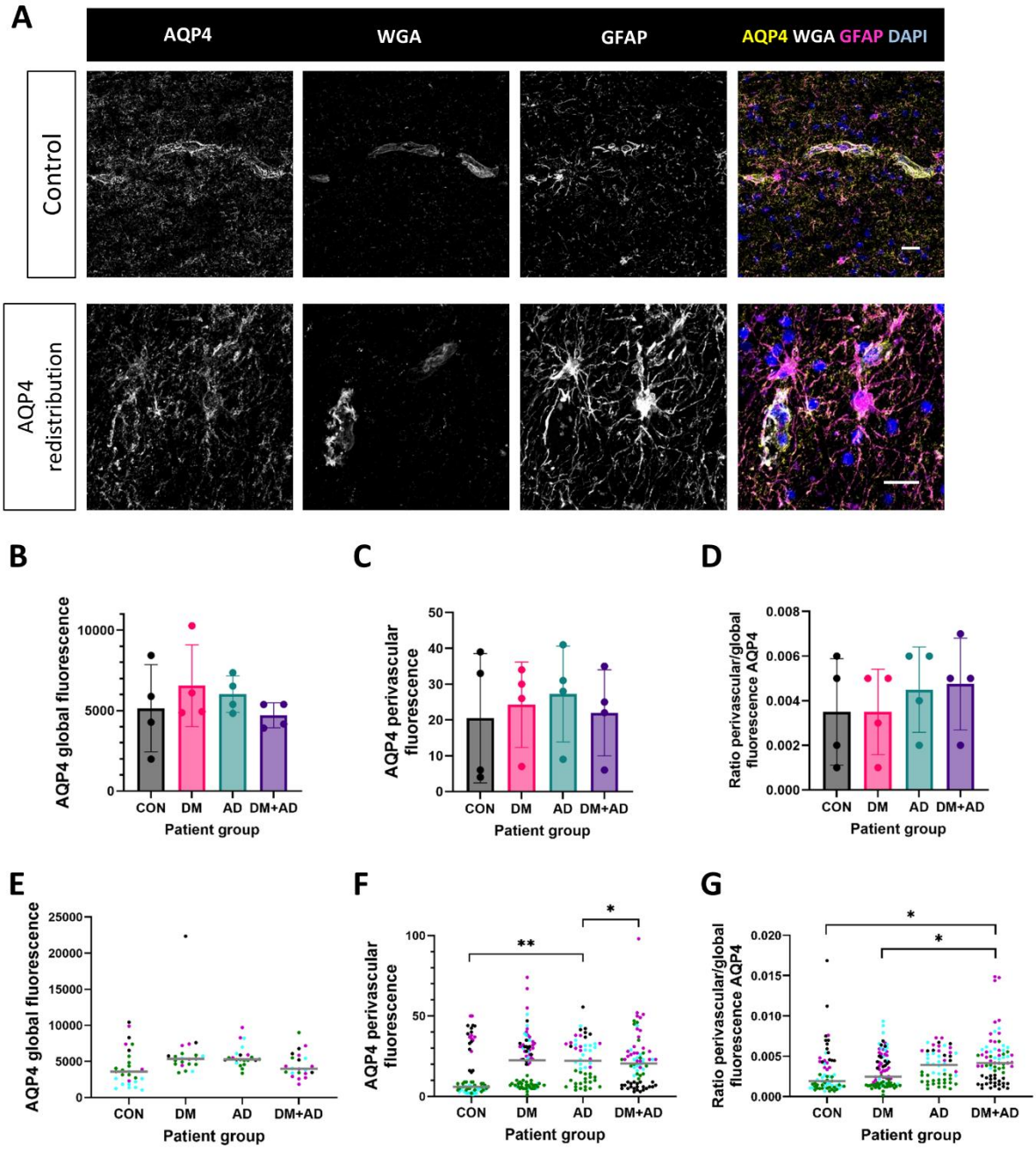

Figure 10. Increased perivascularAQP4 expression in the human BBB during AD with and without DM. (A) AQP4 (yellow) and GFAP (magenta) double staining in the human frontal cortex in physiological control conditions and in the case of AQP4 redistribution. Vascular endothelial cells are stained with wheat germ agglutinin (WGA; white) and nuclei are stained with DAPI (blue). Scale bar: 20 µm. Quantification of global **(B, E)** and perivascular **(C, F)** AQP4 expression in the frontal cortex of (CON, DM, AD, DM+AD). **(D, G)** Quantification of the ratio of perivascular and global AQP4 fluorescence intensity. **(B-D)** Individual donors (dots), with mean ± SD per group. **(E-G)** Individual vessels (dots, coloured by donor), with group median (grey line). * $p < 0.05$, ** $p < 0.01$.

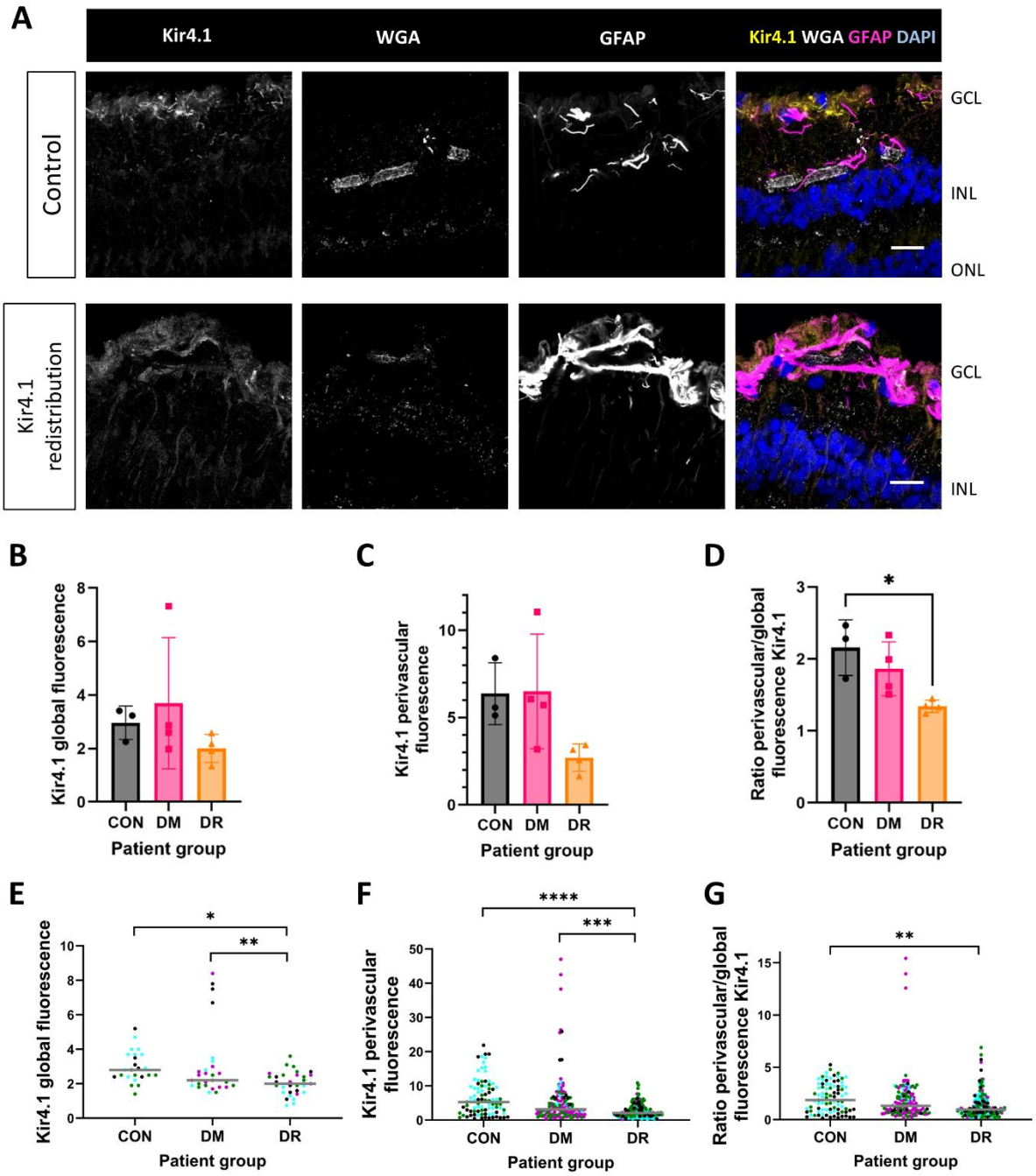

Figure 11. DR causes depolarization of Kir4.1 in the human BRB. (A) Kir4.1 (yellow) and GFAP (magenta) double staining in the human retina in physiological control conditions and in the case of Kir4.1 redistribution. Vascular endothelial cells are stained with wheat germ agglutinin (WGA; white) and nuclei are stained with DAPI (blue). GCL = ganglion cell layer; INL = inner nuclear layer; ONL = outer nuclear layer. Scale bar: 20 µm. Quantification of global **(B, E)** and perivascular **(C, F)** Kir4.1 expression in the retina (CON, DM, DR). **(D, G)** Quantification of the ratio of perivascular and global Kir4.1 fluorescence intensity. **(B-D)** Individual donors (dots), with mean ± SD per group. **(E-G)** Individual vessels (dots, coloured by donor), with group median (grey line). * $p < 0.05$, ** $p < 0.01$, *** $p < 0.001$, **** $p < 0.0001$.

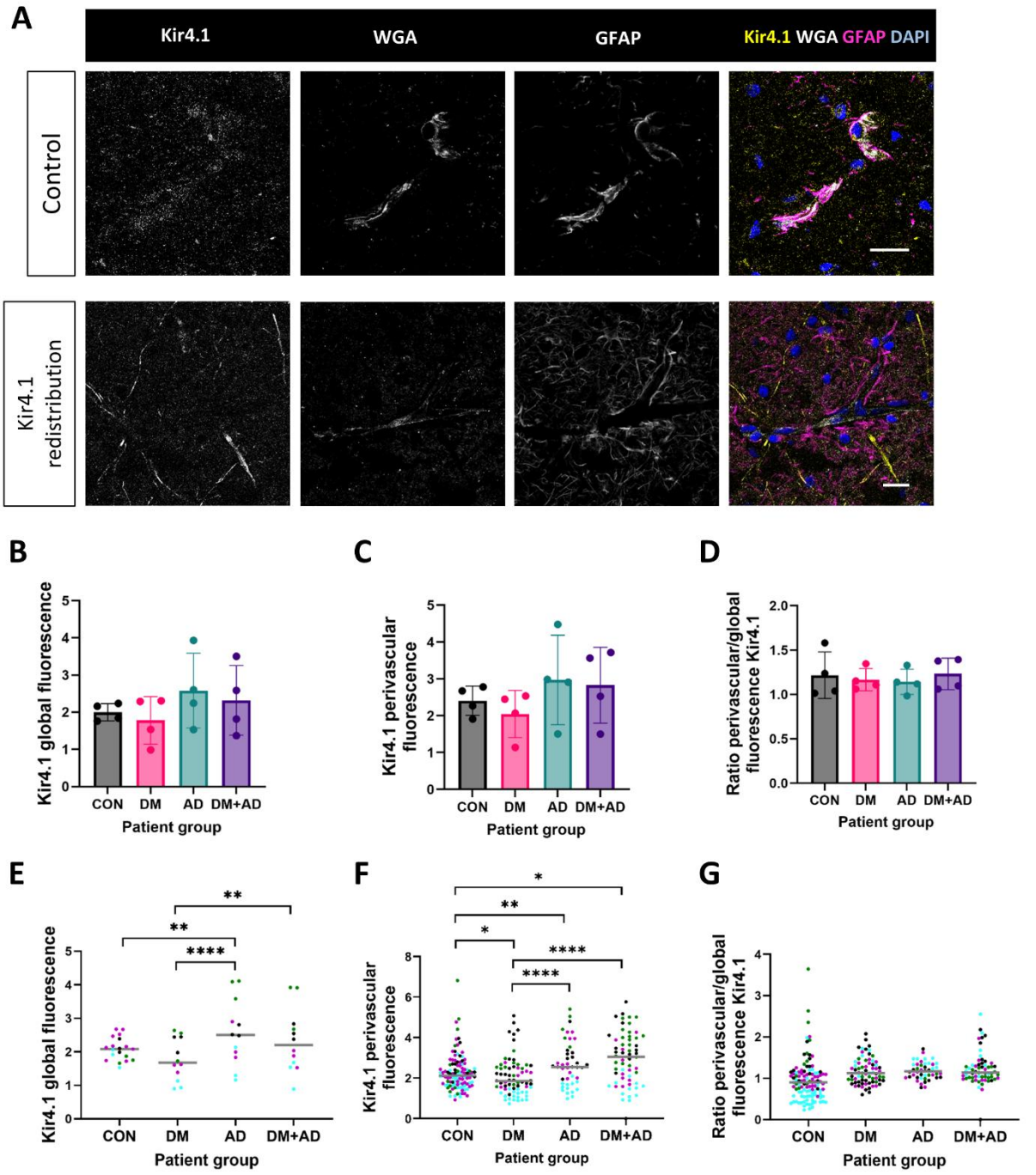

Figure 12. Moderate changes in Kir4.1 expression in human brains of patients with DM and AD. (A) Kir4.1 (yellow) and GFAP (magenta) double staining in the human frontal cortex in physiological control conditions and in the case of Kir4.1 redistribution. Vascular endothelial cells are stained with wheat germ agglutinin (WGA; white) and nuclei are stained with DAPI (blue). Scale bar: 20 µm. Quantification of global **(B, E)** and perivascular **(C, F)** Kir4.1 expression in the frontal cortex (CON, DM, AD, DM+AD). **(D, G)** Quantification of the ratio of perivascular and global Kir4.1 fluorescence intensity. **(B-D)** Individual donors (dots), with mean ± SD per group. **(E-G)** Individual vessels (dots, coloured by donor), with group median (grey line). * $p < 0.05$, ** $p < 0.01$, **** $p < 0.0001$.

($p < 0.0001$) and DM+AD donors ($p = 0.004$; Fig. 12E). In contrast, a higher global fluorescence was found for AD brain samples compared to controls ($p = 0.001$). Perivascular Kir4.1 fluorescence intensity was moderately lower in DM brains than in control ($p = 0.047$), AD ($p < 0.0001$), and DM+AD donors ($p < 0.0001$). In contrast, it was significantly higher in both AD ($p = 0.003$) and DM+AD donors ($p = 0.016$) compared to controls (Fig. 12F). The polarisation of Kir4.1 was similar in all disease groups compared to controls (Fig. 12D, G).

In summary, distinct patterns of AQP4 and Kir4.1 were observed across disease states. In the DR retina, both proteins showed a significant shift in polarisation from macroglial endfeet toward processes. In the brain, AD was characterised by modestly higher levels of perivascular AQP4 and higher Kir4.1 levels, while DM showed lower Kir4.1 expression. The DM+AD conditions exhibited a slightly more perivascular than global AQP4 localisation and higher Kir4.1 expression.

Pericyte coverage

To evaluate pericyte coverage of capillaries, we employed a dual-marker approach with the established pericyte markers NG2 and PDGFRβ [133-139]. In control retinas, only cells identifiable as pericytes due to their localisation in vessel walls were positive for NG2 (Fig. 13A, Supplementary Fig. S14) and PDGFRβ (Fig. 14A, Supplementary Fig. S15). Pericyte coverage based on NG2 expression in capillaries in DM and DR retinas was comparable to controls (~75%; Fig. 13B, C; Supplementary Fig. S14). Pericyte coverage based on PDGFRβ staining was comparable in control (87%) and DM (83%) retinas, but lower in DR retinas (75%) compared to both control ($p = 0.024$) and DM retinas ($p = 0.009$) (Fig. 14B, C).

In the human frontal cortex, pericyte coverage in controls was higher than in the control retina, averaging 88% for NG2 (Fig. 15; Supplementary Fig. S16) and 98% for PDGFRβ (Fig. 16; Supplementary Fig. S17). NG2 coverage was lowest in DM (80%) and AD (78%) brains compared to both controls ($p < 0.001$) and DM+AD (86%; $p < 0.001$). PDGFRβ coverage in DM brains was comparable to controls, but lower in AD (94%) and DM+AD (95%) donors compared to both controls ($p < 0.0001$) and DM donors (AD: $p < 0.001$; DM+AD: $p = 0.014$; Fig. 16C).

Taken together, vascular pericyte coverage based on NG2 staining was similar between the control, DM, and DR retinas, but was lower in DM and AD brains compared to controls and DM+AD. Coverage based on PDGFRβ staining was lower in DR retinas, and in AD and DM+AD brains. Additionally, the results indicate that the cerebral capillaries have a higher pericyte coverage than retinal capillaries.

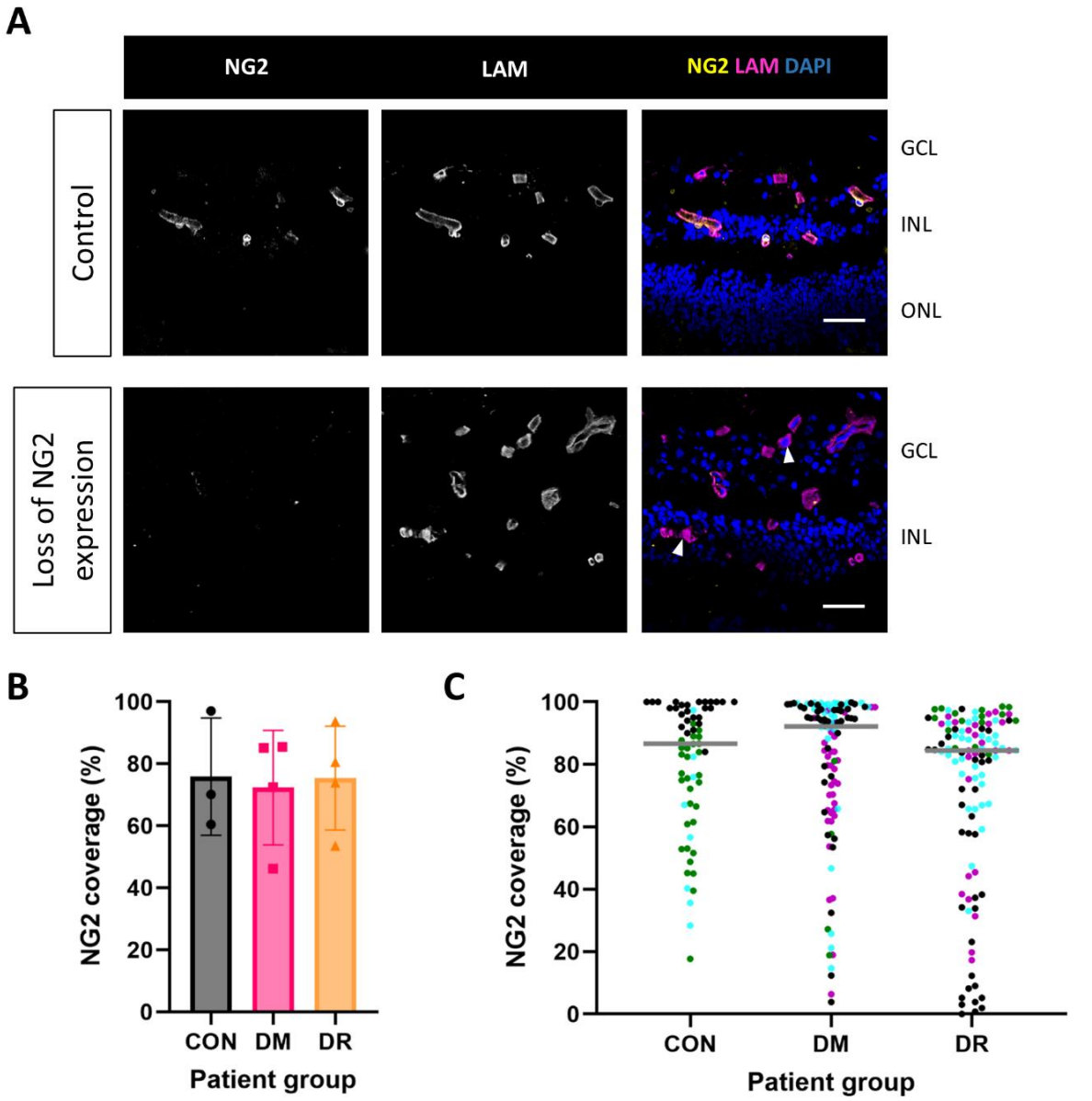

Figure 13. Vascular coverage by NG2-positive pericyte remain unchanged in the human BRB in DM. **(A)** NG2 (yellow) staining in the human retina in physiological control conditions, and an example of loss of NG2 expression under pathological conditions. White arrowheads indicate examples of NG2-negative blood vessels. The basal lamina of blood vessels is stained for laminin (LAM; magenta), and nuclei are stained with DAPI (blue). GCL = ganglion cell layer; INL = inner nuclear layer; ONL = outer nuclear layer. Scale bar: 50 µm. **(B, C)** Quantification of the percentage of total blood vessel surface covered by NG2-positive pericytes in the retina (CON, DM, DR). **(B)** Individual donors (dots), with mean ± SD per group. **(C)** Individual vessels (dots, coloured by donor), with group median (grey line).

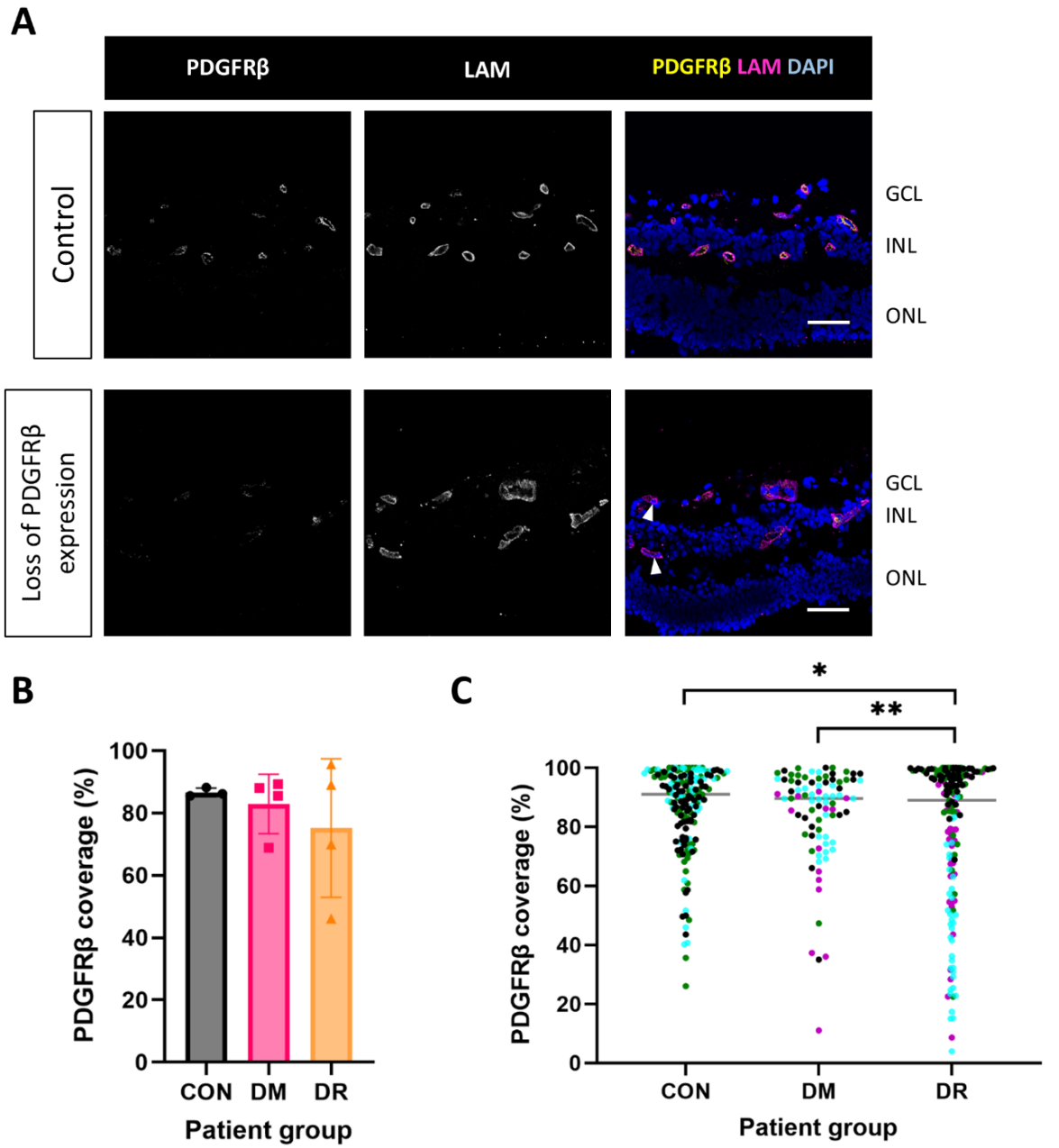

Figure 14. DR causes a moderately reduced PDGFRβ-positive pericyte coverage in the human BRB. **(A)** PDGFRβ (yellow) staining in the human retina in physiological control conditions, and an example showing the loss of PDGFRβ expression under pathological conditions. White arrowheads indicate examples of PDGFRβ-negative blood vessels. The basal lamina of blood vessels is stained for laminin (LAM; magenta), and nuclei are stained with DAPI (blue). GCL = ganglion cell layer; INL = inner nuclear layer; ONL = outer nuclear layer. Scale bar: 50 µm. **(B, C)** Quantification of the percentage of total blood vessel surface covered by PDGFRβ-positive pericytes in the retina (CON, DM, DR). **(B)** Individual donors (dots), with mean ± SD per group. **(C)** Individual vessels (dots, coloured by donor), with group median (grey line). * $p < 0.05$, ** $p < 0.01$.

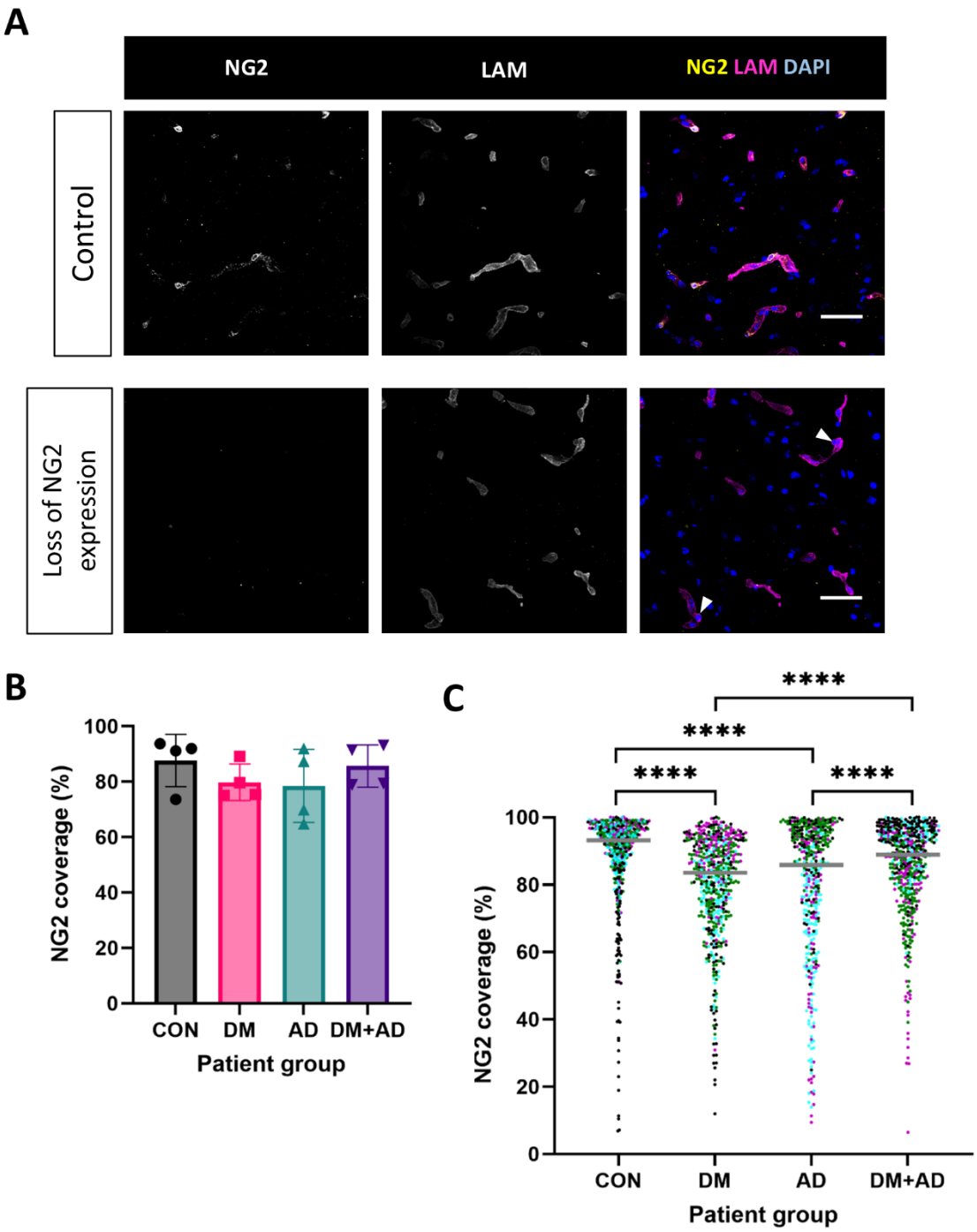

Figure 15. DM and AD cause a moderately reduced NG2-positive pericyte coverage in the BBB. (A) NG2 (yellow) staining in the human frontal cortex in physiological control conditions, and an example showing the loss of NG2 expression under pathological conditions. White arrowheads indicate examples NG2-negative blood vessels. The basal lamina of blood vessels is stained for laminin (LAM; magenta), and nuclei are stained with DAPI (blue). Scale bar: 50 µm. **(B, C)** Quantification of the percentage of total blood vessel surface covered by NG2-positive pericytes in the brain (CON, DM, AD, DM+AD). **(B)** Individual donors (dots), with mean ± SD per group. **(C)** Individual vessels (dots, coloured by donor), with group median (grey line). **** $p < 0.0001$.

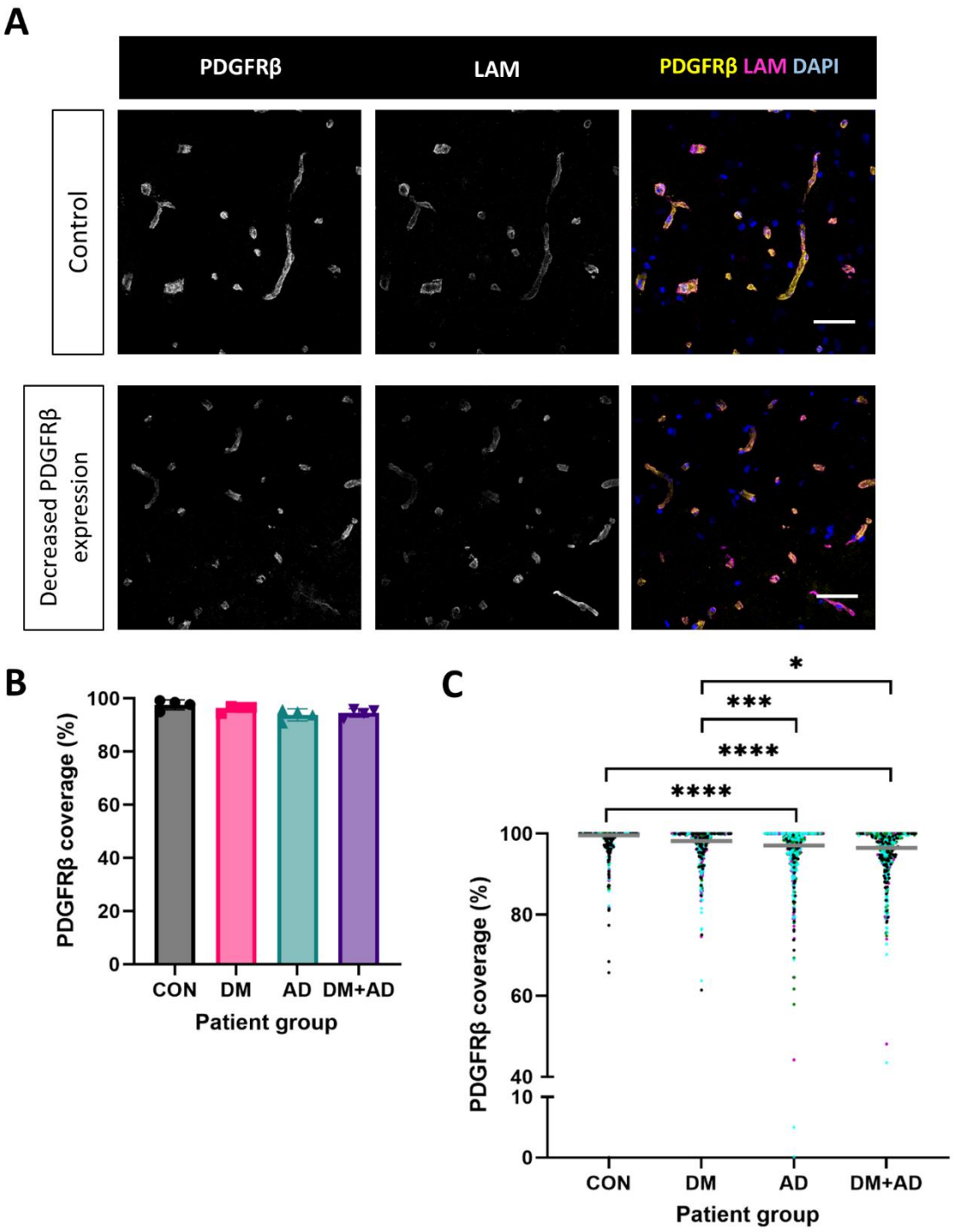

Figure 16. DM and AD cause a moderately reduced PDGFRβ -positive pericyte coverage in the BBB. **(A)** PDGFRβ (yellow) staining in the human frontal cortex in physiological control conditions and pathological conditions. The basal lamina of blood vessels is stained for laminin (LAM; magenta), and nuclei are stained with DAPI (blue). Scale bar: 50 µm. **(B, C)** Quantification of the percentage of total blood vessel surface covered by PDGFRβ-positive pericytes in the brain (CON, DM, AD, DM+AD). **(B)** Individual donors (dots), with mean ± SD per group. **(C)** Individual vessels (dots, coloured by donor), with group median (grey line). * $p < 0.05$, *** $p < 0.001$, **** $p < 0.0001$.

Correlations between NVU alterations

Based on our observations, we analysed correlations between the NVU components in the retina (Fig. 17) and brain (Fig. 18) The full analyses, including absolute Spearman correlation values and p-values, is available in Tables 5-8, with the strongest correlations summarized for each tissue (Supplementary Fig. S18 and S19). Several key relationships were unique to each tissue.

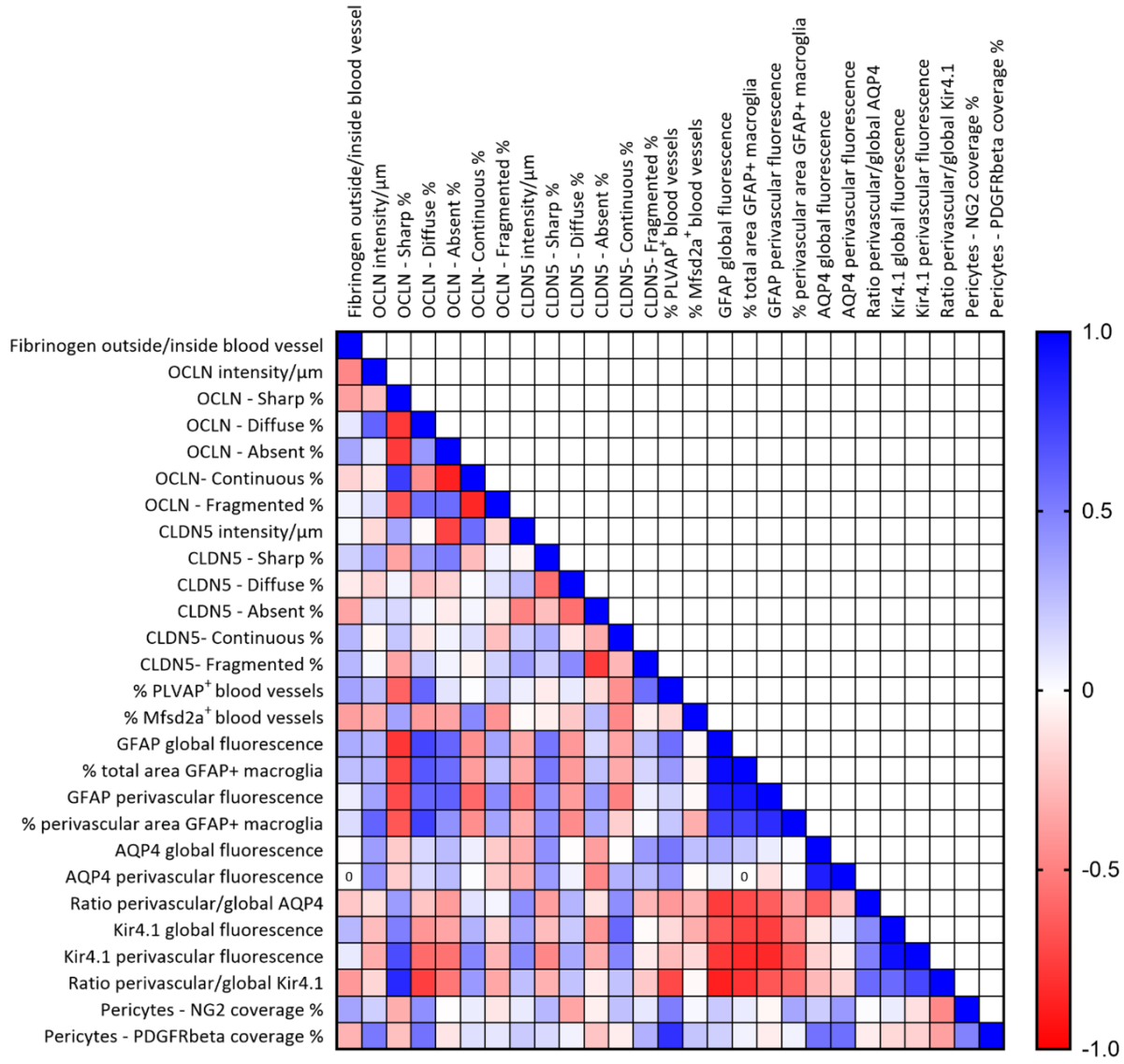

Figure 17. Correlations of NVU components in the human retina based on immunofluorescence staining assessments. Heatmap represents the Spearman correlation coefficient for each correlation between NVU-associated parameters in the retina (Control, DM, AD, DM+AD). Values for each marker are scaled from -1.0 to 1.0. High values are illustrated in blue, and low values in red.

Our analysis revealed a consistent, strong correlation between occludin and claudin-5 staining patterns in the brain, but not in the retina. In the retina, a sharply demarcated occludin staining pattern showed a positive correlation with Kir4.1 expression levels but a

negative correlation with higher GFAP expression and GFAP-positive macroglia coverage. On the other hand, diffuse and absent occludin staining was positively correlated with higher GFAP expression and GFAP-positive macroglia coverage. These correlations were lacking in the brain.

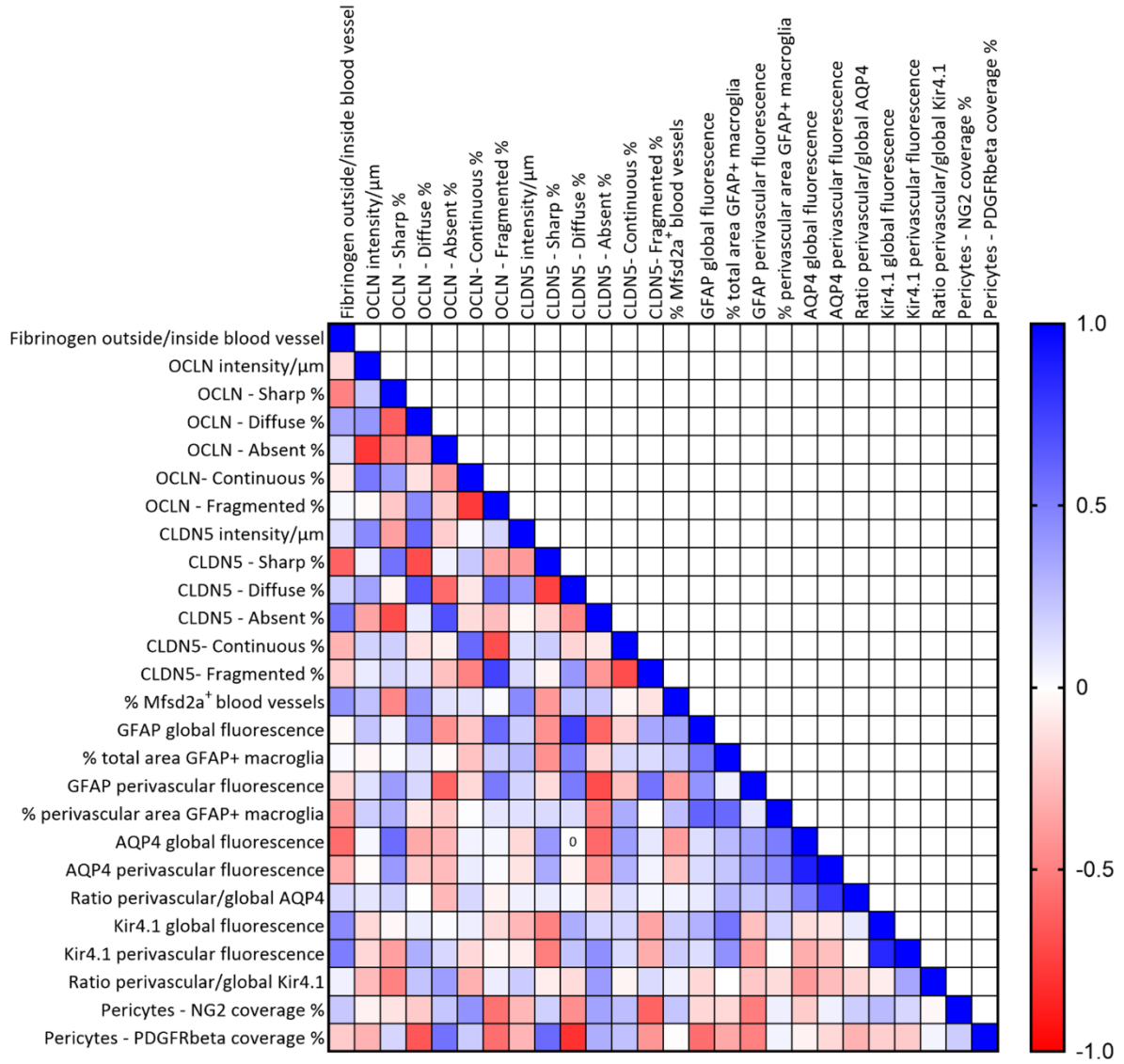

Figure 18. Correlations of NVU components in the human frontal cortex based on immunofluorescence staining assessments. Heatmap represents the Spearman correlation coefficient for each correlation between NVU-associated parameters in the retina (Control, DM, AD, DM+AD). Values for each marker are scaled from -1.0 to 1.0. High values are illustrated in blue, and low values in red.

In the brain, a strong negative correlation was identified between the vascular pericyte coverage based on PDGFRβ-positive pericytes and the percentage of capillaries with diffuse staining for both claudin-5 and occludin, a relation which was not found in the retina. Diffuse claudin-5 staining positively correlated with higher GFAP expression in the brain, whereas a weak negative correlation was demonstrated in the retina. The absence of claudin-5 in the

brain negatively correlated with the GFAP expression, a relation which was not observed in the retina.

Taken together, our initial analysis suggest correlations between several altered NVU characteristics in both the retina and the brain of DM and AD patients.

Table 5. The absolute values of the Spearman's rank correlation coefficients (r) for the human retina.

Spearman r values

	Fibrinogen outside/ inside blood vessel	OCLN intensity /µm	OCLN - Sharp %	OCLN - Diffuse %	OCLN - Absent %	OCLN- Continuous %	OCLN - Fragmented %	CLDN5 intensity /µm	CLDN5 - Sharp %	CLDN5 - Diffuse %	CLDN5 - Absent %	CLDN5- Continuous %	CLDN5- Fragmented %
OCLN intensity/µm	-0.473												
OCLN - Sharp %	-0.373	-0.255											
OCLN - Diffuse %	0.091	0.609	-0.782										
OCLN - Absent %	0.345	0.073	-0.773	0.400									
OCLN – Continuous %	-0.173	-0.091	0.764	-0.436	-0.873								
OCLN – Fragmented %	0.045	0.136	-0.673	0.564	0.573	-0.855							
CLDN5 intensity/µm	0.027	-0.155	0.346	-0.027	-0.743	0.574	-0.159						
CLDN5 - Sharp %	0.182	0.327	-0.364	0.391	0.509	-0.264	0.055	-0.042					
CLDN5 - Diffuse %	-0.082	-0.173	0.045	-0.245	-0.173	0.018	0.118	0.270	-0.566				
CLDN5 - Absent %	-0.355	0.118	0.155	0.036	-0.082	0.036	-0.091	-0.490	-0.259	-0.559			
CLDN5 – Continuous %	0.282	-0.036	0.227	-0.100	0.045	0.127	-0.255	0.203	0.329	-0.105	-0.329		
CLDN5 – Fragmented %	0.282	0.027	-0.355	0.200	0.045	-0.045	0.173	0.392	0.203	0.455	-0.769	-0.287	
% PLVAP$^+$ blood vessels	0.358	0.261	-0.612	0.600	0.103	0.006	0.188	0.064	-0.082	0.082	-0.145	-0.436	0.564
% MFSD2A$^+$ blood vessels	-0.382	-0.321	0.358	-0.394	-0.358	0.467	-0.430	-0.027	-0.064	-0.218	0.264	-0.464	-0.064
GFAP global fluorescence	0.327	0.291	-0.791	0.727	0.600	-0.436	0.355	-0.342	0.536	-0.400	0.155	-0.355	0.264
% total area GFAP$^+$ macroglia	0.251	0.296	-0.715	0.656	0.569	-0.387	0.255	-0.352	0.524	-0.396	0.241	-0.337	0.169
GFAP perivascular fluorescence	0.064	0.364	-0.709	0.600	0.618	-0.591	0.455	-0.510	0.436	-0.391	0.391	-0.491	0.064
% perivascular area GFAP$^+$ macroglia	0.136	0.609	-0.664	0.745	0.427	-0.445	0.355	-0.323	0.436	-0.455	0.336	-0.191	0.018
AQP4 global fluorescence	-0.009	0.382	-0.209	0.155	0.264	0.064	-0.209	-0.328	0.436	-0.009	-0.382	-0.009	0.400
AQP4 perivascular fluorescence	0.000	0.436	-0.200	0.155	0.264	0.009	-0.209	-0.319	0.391	0.055	-0.464	0.300	0.264
Ratio perivascular/global AQP4	-0.223	-0.132	0.387	-0.228	-0.387	0.109	0.036	0.443	-0.383	0.287	-0.114	0.442	-0.287
Kir4.1 global fluorescence	0.282	-0.264	0.500	-0.418	-0.355	0.300	-0.173	0.360	-0.264	0.209	-0.409	0.591	-0.018
Kir4.1 perivascular fluorescence	0.082	-0.327	0.700	-0.582	-0.555	0.473	-0.291	0.456	-0.473	0.336	-0.318	0.473	-0.082
Ratio perivascular/global Kir4.1	-0.400	-0.164	0.845	-0.755	-0.536	0.400	-0.345	0.251	-0.309	0.236	-0.082	0.236	-0.218
Pericytes - NG2 coverage %	0.355	0.191	-0.318	0.436	-0.009	0.073	-0.100	0.082	0.282	-0.355	-0.064	0.245	0.091
Pericytes - PDGFRβ coverage %	-0.301	0.524	-0.251	0.551	-0.105	0.123	0.096	0.205	0.146	0.050	-0.232	-0.077	0.305

Table 5. The absolute values of the Spearman's rank correlation coefficients (r) for the human retina (continued).

Spearman r values

	% PLVAP$^+$ blood vessels	% MFSD2A$^+$ blood vessels	GFAP global fluo-rescence	% total area GFAP$^+$ macroglia	GFAP peri-vascular fluo-rescence	% peri-vascular area GFAP$^+$ macroglia	AQP4 global fluo-rescence	AQP4 perivascular fluo-rescence	Ratio perivascular/ global AQP4	Kir4.1 global fluo-rescence	Kir4.1 peri-vascular fluo-rescence	Ratio peri-vascular/ global Kir4.1	Pericytes - NG2 coverage %
% MFSD2A$^+$ blood vessels	-0.154												
GFAP global fluorescence	0.564	-0.030											
% total area GFAP$^+$ macroglia	0.401	-0.067	0.961										
GFAP perivascular fluorescence	0.176	-0.030	0.873	0.902									
% perivascular area GFAP$^+$ macroglia	0.224	-0.321	0.736	0.743	0.827								
AQP4 global fluorescence	0.527	0.248	0.318	0.223	0.073	0.018							
AQP4 perivascular fluorescence	0.406	-0.018	0.082	0.000	-0.127	0.009	0.882						
Ratio perivascular/ global AQP4	-0.401	-0.304	-0.765	-0.708	-0.633	-0.378	-0.606	-0.237					
Kir4.1 global fluorescence	-0.152	-0.321	-0.645	-0.743	-0.755	-0.473	-0.109	0.064	0.456				
Kir4.1 perivascular fluorescence	-0.273	-0.152	-0.782	-0.838	-0.845	-0.645	-0.182	-0.064	0.497	0.945			
Ratio perivascular/ global Kir4.1	-0.721	-0.030	-0.882	-0.802	-0.664	-0.600	-0.282	-0.164	0.583	0.582	0.718		
Pericytes - NG2 coverage %	0.503	0.030	0.209	0.077	-0.036	0.345	0.200	0.400	0.009	0.073	-0.127	-0.464	
Pericytes - PDGFRβ coverage %	0.809	0.231	0.182	0.048	-0.077	0.050	0.551	0.565	-0.078	-0.155	-0.182	-0.369	0.487

Table 6. The p-values corresponding to the Spearman's rank correlation coefficients for the human retina.

p-value

	Fibrinogen outside/ inside blood vessel	OCLN intensity /µm	OCLN - Sharp %	OCLN - Diffuse %	OCLN - Absent %	OCLN- Continuous %	OCLN - Fragmented %	CLDN5 intensity /µm	CLDN5 - Sharp %	CLDN5 - Diffuse %	CLDN5 - Absent %	CLDN5- Continuous %	CLDN5- Fragmented %
OCLN intensity/µm	0.146												
OCLN - Sharp %	0.261	0.451											
OCLN - Diffuse %	0.796	0.052	0.006										
OCLN - Absent %	0.299	0.838	0.007	0.225									
OCLN – Continuous %	0.615	0.796	0.009	0.183	0.001								
OCLN – Fragmented %	0.903	0.694	0.028	0.076	0.071	0.001							
CLDN5 intensity/µm	0.940	0.647	0.295	0.940	0.011	0.069	0.638						
CLDN5 - Sharp %	0.595	0.327	0.273	0.237	0.114	0.435	0.881	0.899					
CLDN5 - Diffuse %	0.818	0.615	0.903	0.468	0.615	0.967	0.735	0.394	0.059				
CLDN5 - Absent %	0.286	0.735	0.654	0.924	0.818	0.924	0.796	0.107	0.417	0.063			
CLDN5 – Continuous %	0.402	0.924	0.503	0.776	0.903	0.714	0.451	0.523	0.297	0.749	0.297		
CLDN5 – Fragmented %	0.402	0.946	0.286	0.557	0.903	0.903	0.615	0.206	0.528	0.140	0.005	0.366	
% PLVAP$^+$ blood vessels	0.313	0.470	0.067	0.073	0.785	1.000	0.607	0.860	0.818	0.818	0.673	0.183	0.076
% MFSD2A$^+$ blood vessels	0.279	0.368	0.313	0.263	0.313	0.179	0.218	0.946	0.860	0.521	0.435	0.155	0.860
GFAP global fluorescence	0.327	0.386	0.005	0.014	0.056	0.183	0.286	0.302	0.094	0.225	0.654	0.286	0.435
% total area GFAP$^+$ macroglia	0.455	0.374	0.016	0.032	0.071	0.239	0.446	0.286	0.101	0.227	0.472	0.308	0.619
GFAP perivascular fluorescence	0.860	0.273	0.018	0.056	0.048	0.061	0.163	0.111	0.183	0.237	0.237	0.129	0.860
% perivascular area GFAP$^+$ macroglia	0.694	0.052	0.031	0.011	0.193	0.173	0.286	0.330	0.183	0.163	0.313	0.577	0.967
AQP4 global fluorescence	0.989	0.248	0.539	0.654	0.435	0.860	0.539	0.322	0.183	0.989	0.248	0.989	0.225
AQP4 perivascular fluorescence	1.000	0.183	0.557	0.654	0.435	0.989	0.539	0.336	0.237	0.881	0.155	0.371	0.435
Ratio perivascular/global AQP4	0.507	0.698	0.238	0.497	0.238	0.749	0.918	0.172	0.244	0.389	0.739	0.174	0.389
Kir4.1 global fluorescence	0.402	0.435	0.122	0.203	0.286	0.371	0.615	0.275	0.435	0.539	0.214	0.061	0.967
Kir4.1 perivascular fluorescence	0.818	0.327	0.020	0.066	0.082	0.146	0.386	0.160	0.146	0.313	0.342	0.146	0.818
Ratio perivascular/global Kir4.1	0.225	0.634	0.002	0.010	0.094	0.225	0.299	0.455	0.356	0.485	0.818	0.485	0.521
Pericytes - NG2 coverage %	0.286	0.577	0.342	0.183	0.989	0.838	0.776	0.811	0.402	0.286	0.860	0.468	0.796
Pericytes - PDGFRβ coverage %	0.366	0.101	0.455	0.083	0.760	0.719	0.781	0.541	0.667	0.887	0.489	0.823	0.359

Table 6. The p-values corresponding to the Spearman's rank correlation coefficients for the human retina (continued).

p-value

	% PLVAP$^+$ blood vessels	% MFSD2A$^+$ blood vessels	GFAP global fluo-rescence	% total area GFAP$^+$ macroglia	GFAP peri-vascular fluo-rescence	% peri-vascular area GFAP$^+$ macroglia	AQP4 global fluo-rescence	AQP4 perivascular fluo-rescence	Ratio perivascular/ global AQP4	Kir4.1 global fluo-rescence	Kir4.1 perivascular fluorescence	Ratio peri-vascular/ global Kir4.1	Pericytes - NG2 coverage %
% MFSD2A$^+$ blood vessels	0.635												
GFAP global fluorescence	0.096	0.946											
% total area GFAP$^+$ macroglia	0.250	0.857	0.000										
GFAP perivascular fluorescence	0.632	0.946	0.001	0.000									
% perivascular area GFAP$^+$ macroglia	0.537	0.368	0.013	0.011	0.003								
AQP4 global fluorescence	0.123	0.492	0.342	0.507	0.838	0.967							
AQP4 perivascular fluorescence	0.247	0.973	0.818	1.000	0.714	0.989	0.001						
Ratio perivascular/ global AQP4	0.250	0.390	0.008	0.018	0.041	0.250	0.053	0.480					
Kir4.1 global fluorescence	0.682	0.368	0.037	0.011	0.010	0.146	0.755	0.860	0.160				
Kir4.1 perivascular fluorescence	0.448	0.682	0.006	0.002	0.002	0.037	0.595	0.860	0.123	0.000			
Ratio perivascular/ global Kir4.1	0.023	0.946	0.001	0.004	0.031	0.056	0.402	0.634	0.064	0.066	0.016		
Pericytes - NG2 coverage %	0.144	0.946	0.539	0.823	0.924	0.299	0.557	0.225	0.983	0.838	0.714	0.155	
Pericytes - PDGFRβ coverage %	0.007	0.519	0.589	0.888	0.823	0.887	0.083	0.074	0.820	0.648	0.589	0.263	0.131

Table 7. The absolute values of the Spearman's rank correlation coefficients (r) for the human brain.

Spearman r values

	Fibrinogen outside/ inside blood vessel	OCLN intensity /µm	OCLN - Sharp %	OCLN - Diffuse %	OCLN - Absent %	OCLN- Continuous %	OCLN - Fragmented %	CLDN5 intensity /µm	CLDN5 - Sharp %	CLDN5 - Diffuse %	CLDN5 - Absent %	CLDN5- Continuous %	CLDN5- Fragmented %
OCLN intensity/µm	-0.143												
OCLN - Sharp %	-0.497	0.219											
OCLN - Diffuse %	0.349	0.411	-0.628										
OCLN - Absent %	0.145	-0.788	-0.472	-0.364									
OCLN – Continuous %	-0.078	0.524	0.385	-0.119	-0.385								
OCLN – Fragmented %	0.024	-0.019	-0.224	0.453	-0.202	-0.774							
CLDN5 intensity/µm	0.126	0.457	-0.374	0.588	-0.196	0.021	0.159						
CLDN5 - Sharp %	-0.618	0.044	0.551	-0.699	0.053	0.212	-0.347	-0.397					
CLDN5 - Diffuse %	0.185	0.362	-0.047	0.649	-0.583	-0.100	0.535	0.400	-0.747				
CLDN5 - Absent %	0.530	-0.358	-0.700	0.086	0.680	-0.137	-0.264	-0.037	-0.149	-0.471			
CLDN5 – Continuous %	-0.301	0.174	0.185	-0.120	-0.060	0.586	-0.698	0.128	0.196	-0.172	-0.091		
CLDN5 – Fragmented %	-0.192	0.077	0.150	0.110	-0.251	-0.488	0.738	0.144	-0.047	0.406	-0.410	-0.699	
% MFSD2A$^+$ blood vessels	0.419	0.242	-0.474	0.402	0.113	0.111	0.013	0.457	-0.403	0.222	0.215	-0.043	-0.111
GFAP global fluorescence	-0.028	0.228	0.059	0.390	-0.432	-0.224	0.579	0.197	-0.434	0.741	-0.601	-0.174	0.344
% total area GFAP$^+$ macroglia	0.021	-0.034	0.009	0.113	-0.025	-0.235	0.194	0.276	-0.433	0.485	-0.170	0.150	0.138
GFAP perivascular fluorescence	-0.158	0.119	0.385	0.159	-0.599	-0.156	0.518	0.171	-0.144	0.518	-0.706	-0.249	0.547
% perivascular area GFAP$^+$ macroglia	-0.413	0.186	0.306	-0.095	-0.205	0.006	0.097	0.118	0.142	0.135	-0.494	0.324	-0.006
AQP4 global fluorescence	-0.576	0.028	0.576	-0.333	-0.294	0.047	0.032	-0.156	0.401	0.000	-0.589	0.377	0.094
AQP4 perivascular fluorescence	-0.324	-0.019	0.400	-0.213	-0.269	0.074	0.015	-0.109	0.330	-0.053	-0.434	0.302	0.047
Ratio perivascular/ global AQP4	0.159	0.095	0.177	0.003	-0.284	0.153	-0.054	0.056	0.074	0.033	-0.146	0.130	0.036
Kir4.1 global fluorescence	0.452	-0.155	-0.032	0.074	0.019	0.065	-0.147	-0.282	-0.492	0.321	0.161	0.163	-0.359
Kir4.1 perivascular fluorescence	0.509	-0.159	-0.376	0.314	0.156	-0.150	-0.035	-0.076	-0.508	0.232	0.437	0.140	-0.326
Ratio perivascular/ global Kir4.1	0.059	-0.268	-0.492	0.232	0.384	-0.311	0.069	0.203	-0.073	-0.141	0.391	-0.044	0.144
Pericytes - NG2 coverage %	0.215	-0.057	-0.115	-0.209	0.226	0.421	-0.556	-0.285	0.181	-0.444	0.362	0.255	-0.615
Pericytes - PDGFRβ coverage %	-0.206	-0.305	0.162	-0.659	0.552	0.203	-0.571	-0.291	0.582	-0.809	0.316	0.241	-0.412

Table 7. The absolute values of the Spearman's rank correlation coefficients (r) for the human brain (continued)

Spearman r values

	% MFSD2A$^+$ blood vessels	GFAP global fluo-rescence	% total area GFAP$^+$ macroglia	GFAP peri-vascular fluo-rescence	% perivascular area GFAP$^+$ macroglia	AQP4 global fluorescence	AQP4 perivascular fluorescence	Ratio perivascular/ global AQP4	Kir4.1 global fluorescence	Kir4.1 perivascular fluorescence	Ratio perivascular/ global Kir4.1	Pericytes - NG2 coverage %
GFAP global fluorescence	0.370											
% total area GFAP$^+$ macroglia	0.234	0.524										
GFAP perivascular fluorescence	-0.392	0.421	0.056									
% perivascular area GFAP$^+$ macroglia	0.258	0.609	0.585	0.094								
AQP4 global fluorescence	-0.385	0.129	0.268	0.379	0.509							
AQP4 perivascular fluorescence	-0.232	0.141	0.229	0.379	0.468	0.882						
Ratio perivascular/ global AQP4	0.044	0.086	0.280	0.224	0.233	0.487	0.782					
Kir4.1 global fluorescence	0.197	0.306	0.541	-0.247	0.165	-0.132	-0.094	0.081				
Kir4.1 perivascular fluorescence	0.198	0.132	0.435	-0.376	-0.006	-0.321	-0.253	-0.039	0.844			
Ratio perivascular/ global Kir4.1	0.056	-0.160	-0.001	-0.222	-0.140	-0.397	-0.263	-0.164	-0.075	0.347		
Pericytes - NG2 coverage %	0.227	-0.159	-0.153	-0.512	0.062	-0.203	0.059	0.195	0.268	0.159	-0.032	
Pericytes - PDGFRβ coverage %	-0.012	-0.571	-0.341	-0.497	0.047	-0.053	-0.153	-0.302	-0.191	-0.209	0.043	0.200

Table 8. The p-values corresponding to the Spearman's rank correlation coefficients for the human brain.

p-value

	Fibrinogen outside/ inside blood vessel	OCLN intensity /µm	OCLN - Sharp %	OCLN - Diffuse %	OCLN - Absent %	OCLN- Continuous %	OCLN - Fragmented %	CLDN5 intensity/µm	CLDN5 - Sharp %	CLDN5 - Diffuse %	CLDN5 - Absent %	CLDN5- Continuous %	CLDN5- Fragmented %
OCLN intensity/µm	0.593												
OCLN - Sharp %	0.052	0.411											
OCLN - Diffuse %	0.184	0.114	0.011										
OCLN - Absent %	0.589	0.000	0.066	0.165									
OCLN – Continuous %	0.772	0.039	0.141	0.660	0.141								
OCLN – Fragmented %	0.932	0.945	0.404	0.079	0.450	0.001							
CLDN5 intensity/µm	0.640	0.077	0.155	0.019	0.463	0.943	0.556						
CLDN5 - Sharp %	0.012	0.871	0.029	0.004	0.845	0.427	0.187	0.128					
CLDN5 - Diffuse %	0.489	0.167	0.865	0.008	0.020	0.713	0.035	0.126	0.001				
CLDN5 - Absent %	0.037	0.173	0.003	0.750	0.005	0.610	0.320	0.893	0.576	0.067			
CLDN5 – Continuous %	0.255	0.516	0.489	0.654	0.824	0.019	0.003	0.634	0.461	0.521	0.735		
CLDN5 – Fragmented %	0.472	0.777	0.579	0.684	0.346	0.057	0.002	0.594	0.862	0.120	0.115	0.003	
% MFSD2A$^+$ blood vessels	0.107	0.364	0.065	0.123	0.675	0.681	0.963	0.076	0.122	0.405	0.419	0.874	0.681
GFAP global fluorescence	0.919	0.392	0.831	0.136	0.095	0.404	0.021	0.463	0.094	0.001	0.016	0.517	0.192
% total area GFAP$^+$ macroglia	0.941	0.902	0.978	0.676	0.928	0.379	0.470	0.299	0.095	0.059	0.527	0.576	0.609
GFAP perivascular fluorescence	0.555	0.658	0.141	0.554	0.016	0.563	0.042	0.527	0.593	0.042	0.003	0.350	0.031
% perivascular area GFAP$^+$ macroglia	0.112	0.489	0.249	0.725	0.443	0.987	0.721	0.664	0.596	0.617	0.053	0.220	0.987
AQP4 global fluorescence	0.022	0.919	0.022	0.206	0.267	0.865	0.908	0.563	0.124	1.000	0.018	0.150	0.730
AQP4 perivascular fluorescence	0.219	0.945	0.126	0.424	0.312	0.788	0.961	0.689	0.210	0.848	0.094	0.254	0.865
Ratio perivascular/global AQP4	0.553	0.725	0.508	0.992	0.285	0.568	0.842	0.838	0.783	0.904	0.586	0.627	0.895
Kir4.1 global fluorescence	0.081	0.565	0.908	0.784	0.945	0.814	0.586	0.288	0.055	0.226	0.549	0.543	0.173
Kir4.1 perivascular fluorescence	0.046	0.554	0.151	0.234	0.560	0.579	0.900	0.780	0.047	0.385	0.092	0.603	0.217
Ratio perivascular/global Kir4.1	0.828	0.313	0.055	0.383	0.142	0.240	0.799	0.448	0.785	0.599	0.134	0.871	0.592
Pericytes - NG2 coverage %	0.421	0.833	0.672	0.434	0.397	0.106	0.028	0.283	0.500	0.087	0.168	0.339	0.013
Pericytes - PDGFRβ coverage %	0.441	0.249	0.549	0.007	0.029	0.450	0.023	0.273	0.020	0.000	0.232	0.365	0.114

Table 8 The p-values corresponding to the Spearman's rank correlation coefficients for the human brain (continued)

p-value

	% MFSD2A$^+$ blood vessels	GFAP global fluo-rescence	% total area GFAP$^+$ macroglia	GFAP peri-vascular fluo-rescence	% peri-vascular area GFAP$^+$ macroglia	AQP4 global fluorescence	AQP4 perivascular fluorescence	Ratio perivascular/ global AQP4	Kir4.1 global fluorescence	Kir4.1 peri-vascular fluo-rescence	Ratio peri-vascular/ global Kir4.1	Pericytes - NG2 coverage %
GFAP global fluorescence	0.158											
% total area GFAP$^+$ macroglia	0.380	0.040										
GFAP perivascular fluorescence	0.133	0.106	0.839									
% perivascular area GFAP$^+$ macroglia	0.333	0.014	0.019	0.730								
AQP4 global fluorescence	0.141	0.633	0.315	0.148	0.046							
AQP4 perivascular fluorescence	0.383	0.602	0.391	0.148	0.070	0.000						
Ratio perivascular/ global AQP4	0.872	0.752	0.292	0.402	0.383	0.057	0.001					
Kir4.1 global fluorescence	0.462	0.249	0.033	0.355	0.541	0.625	0.730	0.764				
Kir4.1 perivascular fluorescence	0.458	0.625	0.094	0.151	0.987	0.226	0.343	0.886	0.000			
Ratio perivascular/ global Kir4.1	0.835	0.550	0.998	0.405	0.603	0.128	0.322	0.541	0.782	0.187		
Pericytes – NG2 coverage %	0.396	0.556	0.571	0.045	0.822	0.450	0.831	0.465	0.315	0.556	0.906	
Pericytes – PDGFRβ coverage %	0.967	0.023	0.196	0.052	0.865	0.848	0.571	0.254	0.477	0.436	0.876	0.456

Discussion

The aim of this study was to comprehensively characterize and compare pathological alterations in the NVU between the retina in type 2 DM and DR and in the brain in DM and AD, using a unique series of human tissue samples. Our explorative semi-quantitative and qualitative analyses indicate that DM does not exert identical effects on relevant vascular parameters such as vascular permeability, tight junction integrity, transcytosis and vascular coverage of pericytes in the human brain, compared to the retina. This finding indicates tissue-specific and biologically fundamental differences in the pathophysiology of diabetic microvascular pathology, in line with the fact that no microvascular complication equivalent to DR is known in the brain.

In addition, our data indicate that in AD, NVU alterations in the brain are similar to those in DM for most of the NVU markers studied here. The observed trends regarding differences in vascular and tight junction pathology in the brain between DM, AD and DM+AD may suggest that in patients with both DM and AD, the NVU and BBB are more impaired than in DM or AD alone.

There are multiple causes for the development of AD [140], and for individual patients with DM it remains unclear whether the development of AD is induced by DM or occurs independently of DM. Individuals with DM carrying AD risk alleles, such as those in the APOE region, may experience earlier onset or faster progression of AD pathology when exposed to the metabolic and vascular disturbances of DM [141-144]. The presence of DM may exacerbate subclinical AD through an effect on the microvasculature, potentially facilitating its progression to clinical AD, but this hypothesis warrants further investigation. It has been suggested that diabetes may contribute to AD development via increased occurrence of ischemic lesions, although other mechanisms, such as alterations in cerebral glucose and insulin metabolism, or direct effects of DM on neurons, may also play a role [145]. However, the genetic risk factors identified for AD [146], with the APOE ε4 allele being one of the most well-established risk genes, differ from those associated with DR, such as erythropoietin (EPO) and tumour necrosis factor-alpha (TNF-α) [147, 148].

While higher vascular permeability, based on fibrinogen staining, is observed in retinas of diabetic patients with and without DR, we did not find similar alterations in the brain in patients with DM alone. However, we found higher vascular permeability in the brains of patients with both AD and DM. In these circumstances, higher vascular leakage may be due to enhanced paracellular transport, as indicated by the changes in tight junction protein expression observed in both the retina of DR patients and in the brains of patients with both AD and DM. The highest expression levels of both occludin and claudin-5 were observed in DM+AD brain. However, protein expression levels alone do not reflect tight junction integrity. A more critical indicator is proper localisation at endothelial cell borders. The elevated expression in DM+AD brains likely indicates a more diffuse vascular distribution, leading to increased overall signal intensity. Although signalling of inflammatory reactive astrocytes is mostly barrier-disruptive in response to chronic hyperglycaemia, neuroinflammation, and Aβ accumulation, astrocytes can also upregulate signals that drive endothelial expression of tight junction proteins [21].

We observed conformational changes in tight junction proteins in retinas of donors with DM and DR and in brains of donors with DM, AD, and DM+AD. Relocation of tight junction proteins from the cell membrane to an intracellular compartment occurs via endocytosis, a process regulated by phosphorylation, primarily at serine and threonine residues [149, 150]. Studies have reported both reduced and unchanged tight junction protein expression in the human AD brain [103-105, 151], as well as both reduced and elevated levels in the brains of DM patients [152]. A potential explanation is a biphasic response: early stress triggers a compensatory upregulation and remodeling of tight junctions at the BBB to counteract dysfunction. This ultimately fails under sustained pathology, leading to junction loss and BBB breakdown, explaining the observed discrepancies across studies. Additionally, increased transcytosis probably contributes to the higher vascular permeability in retinas in DR retinas, as indicated by the highest PLVAP expression found in DR compared to DM without DR and controls. While previous studies have established PLVAP expression in the retinal vasculature of DR patients [153, 154], our study confirms that its expression is upregulated in DR and further identifies high expression in a subset of blood vessels in DM patients without DR. However, limited clinical data on patient comorbidities restricts a fuller analysis of potential contributing factors to this higher PLVAP expression. Vascular endothelial growth factor (VEGF) induces PLVAP via VEGF receptor 2 (VEGFR2), leading to increased caveolae formation and transcytosis in barrier endothelium [130, 155, 156]. VEGF also induces changes in endothelial junction integrity [155, 157-160], aligning with the present results. In the brain, PLVAP expression was absent, pointing at a biologically fundamental difference between the BRB and BBB.

To our knowledge, this is the first study to examine MFSD2A expression in the human diabetic retina and brain. Since MFSD2A suppresses transcytosis [161], and as PLVAP (a marker of increased transcytosis) is elevated in diabetes, we anticipated lower MFSD2A expression in diabetic retinas. Studies using the oxygen-induced retinopathy and streptozotocin diabetes mouse models have reported a significant decrease in MFSD2A expression [162]. However, contrary to expectations, we observed higher MFSD2A expression in DM and DR retinas compared to controls. Activation of the Wnt/β-catenin pathway has been previously reported in both diabetes and DR [163, 164] and can upregulate MFSD2A transcription [161]. However, activation of this pathway downregulates PLVAP expression [165, 166], which contradicts our findings. Alternatively, a higher presence of astrocytes may contribute to MFSD2A upregulation [167, 168], although their effects on PLVAP expression are currently unknown. These higher MFSD2A levels remain therefore unexplained, but may represent a protective response to counterbalance the higher transcytosis in these conditions. This could also be related to maintaining the lipid composition of the cell membrane or sustaining the uptake of docosahexaenoic acid (DHA), which is an anti-inflammatory an neuroprotective mediator [169].

MFSD2A was the only measurable marker in the brain indicative of alterations in the transcytosis pathway. Higher MFSD2A expression was observed in brains of DM and in particular in the brain of DM+AD donors compared to controls, whereas expression in AD was similar. In accordance with the present results, a previous study in human AD brain has demonstrated similar upregulation of MFSD2A expression compared to controls [170].

Although overall vascular permeability, assessed through fibrinogen extravasation, remained minimal across pathological groups, a statistically significant increase was detected only in the most severe condition, DM+AD brains. This elevated leakage may reflect cumulative disruptions in both transcellular and paracellular transport mechanisms, exceeding the effects observed in either DM or AD alone. Fibrinogen extravasation due to barrier loss may lead to neuroinflammation and neuronal degeneration [171-173]. Our GFAP staining confirmed neuroinflammation, as astrocyte activation was observed in the retina in DR and in the brains of patients with both DM and AD. Astrocyte activation has repeatedly been reported in the human AD brain [91-94, 110, 174-177], which is in agreement with our findings. However, in AD, we did not find higher vascular permeability, indicating this cannot explain the observed macroglial activation. Instead, exposure to Aβ, resulting from an imbalance between cerebral production and clearance of Aβ, may directly upregulate GFAP in astrocytes and induce morphological changes [178-181]. Exposure to Aβ also activates microglia, which can lead to neuroinflammation [182]. Macroglial activation can be interpreted as a protective mechanism aimed at restoring neuronal homeostasis [176], a response often associated with the acute phase of a disease [183]. In contrast, prolonged upregulation of GFAP may contribute to neurodegeneration by damaging synapses and neurons [176, 183]. The upregulation of GFAP, similar as the upregulation of tight junction proteins that we observed in the DM+AD brain may initially serve as compensatory responses to vascular stress and , aiming to counteract barrier dysfunction. However, these adaptions are ultimately unsustainable. This paradoxical progression, wherein early protective mechanisms fail and eventually lead to further pathology, highlights a critical aspect in disease progression.

Consistent with previous studies in diabetic rats [184-186] and mice [187], the present results indicate dysregulation of water channels and potassium channels in the retina during DR. In addition, in the aqueous humour of DR patients, AQP4 was found to be significantly elevated, whereas Kir4.1 expression was reported as both higher and lower compared to controls [188-190]. In the present study, we observed higher Kir4.1 expression in the brain in AD and DM+AD, whereas Kir4.1 polarisation at the macroglial endfeet remained stable across all conditions. AQP4 expression remained generally stable in the brain, except for the higher perivascular expression observed in brains of AD donors compared to controls. The higher expression of both Kir4.1 and AQP4 in the AD brain may be due to activation of astrocytes induced by pathological stimuli, aimed at enhancing the clearance of accumulating Aβ and restoring water and ion homeostasis [177, 191-193]. Although dysfunction and depolarisation of AQP4 and Kir4.1 have been associated with retinal and brain oedema and impaired Aβ clearance, the available evidence remains limited [191, 193, 194].

Loss of pericytes in the retina is an early event in DM [195-200], which we could not confirm in this study using cryosections. In contrast, we have previously confirmed loss of pericytes in retinas of DM patients using retinal flatmounts instead of cryosections for 3D imaging and by counting the nuclei based on NG2 staining [201], which underscores the superior visualisation and sensitivity of the flatmount technique. A lower pericyte coverage was observed in retinas of DR donors compared to DM donors and controls, based on PDGFRβ staining, but not on NG2 staining. Studies on pericyte coverage in brains of DM patients are lacking. Studies on DM type 1 and type 2 rodent mostly report decreased cerebral pericyte

coverage in diabetes [152, 202-204], similar to the observed reduction in pericyte coverage in DM brains based on NG2 staining. In AD, we found a moderately lower vascular coverage of both NG2 and PDGFRβ staining. This observed reduction in pericyte marker coverage aligns with previous findings in post-mortem human AD brain tissue [94, 95, 99]. Loss of pericytes may result from retraction of pericyte processes, apoptosis, transdifferentiation or migration [11, 205]. These events are potentially driven by inflammation, oxidative stress, elevated levels of advanced glycation end-products, increased levels of angiopoietin-2, and the basal lamina thickening [2, 102, 206]. In addition, we found a higher vascular pericyte coverage in the brain (NG2: 88%; PDGFRβ: 98%) than in the retina (NG2: 76%; PDGFRβ: 87%), which contrasts with prior morphometric analyses using electron microscopy [207]. These discrepancies in coverage may arise from limitations in the markers used, which could fail to identify all retinal pericytes, from post-mortem effects or from regional variations in pericyte distribution within the brain.

In addition to the evidence for tissue-specific differential NVU alterations listed above, we also observed similarities in DM-induced NVU pathology between the retina and brain. A key parallel was the effect on macroglia. We observed macroglial activation in diabetic retinas, consistent with previously reported macroglial activation in the human diabetic eye [43, 208, 209]. Similar to the retina, we also observed macroglial activation in the DM brain. However, the currently observed elevated GFAP expression in the frontal cortex contrasts the only other human study, which found reduced GFAP in the diabetic (n=28) hypothalamus [210]. This discrepancy may relate to differences in brain region, tissue preservation (paraffin vs. frozen), fixation methods, species or antibodies used. Another similarity is the disorganisation of tight junctions observed in both the retina of patients with DM and DR and in the brain of patients with DM, AD, and DM+AD. Additionally, higher MFSD2A expression and vascular permeability based on fibrinogen staining was observed in the worst pathology group of the retina (DR) and the brain (DM+AD). We also found that PDGFRβ expression was lower in retinas of patients with DR and in brains of patients with AD and DM+AD.

Our present comprehensive study on multiple components of the NVU in human tissues in DM and AD is unique and allowed us to correlate changes across its components. The associations found here were largely tissue-specific. In the retina, we identified associations between macroglial activation and the delocalisation of water and potassium channels within these cells, which also correlated with tight junction protein disorganisation. Activation of astrocytic AQP4 indirectly regulates the expression and distribution of tight junction proteins via intracellular Ca^{2+} signalling [21]. Additionally, inflammatory factors, including IL-1β, IL-6, IFN-γ, TNF-α, VEGF-A, MCP-1 and CXCL-1 and matrix metalloproteinase-9 (MMP-9), expressed by astrocytes, are known to redistribute tight junctions [21, 211]. Cerebral macroglial activation and potassium channel delocalisation was negatively associated with the extent of vascular coverage by pericytes. The literature on pericyte-astrocyte crosstalk is limited and contradictory [21, 212-214]. Whereas previous studies have suggested that pericytes regulate the polarisation of astrocyte endfeet [14, 215], we did not find a correlation between pericyte loss and AQP4 redistribution. A key common finding was the positive correlation between the vascular coverage of PDGFRβ-positive pericytes and occludin localisation at cell borders in both the retina and brain. These results may suggest that pericyte loss in the human NVU disrupts the structural integrity of tight junction proteins. In accordance with the present results, previous reports link both pericyte

dysfunction and pericyte loss with the degradation of endothelial junctional proteins in mouse models [95, 99]. In Pdgfrb−/− mice, structural abnormalities in tight junctions have been reported, including disorganization and misorientation at various angles in the cerebral vasculature [165]. These *in vivo* findings are supported by *in vitro* evidence that pericytes induce occludin expression and strengthen BBB barrier function during development [216, 217].

Vascular leakage, a phenomenon observed in clinical settings [218, 219], may serve as a biomarker for NVU status. In our analysis, however, fibrinogen extravasation did not correlate significantly with NVU markers in the retina. The single timepoint analysis in post-mortem tissue makes it challenging to compare with real-time *in vivo* fluorescent angiography. In the brain, by contrast, vascular leakage positively correlated with Kir4.1 expression and negatively with global AQP4 expression caused by delocalisation. Overall, our findings suggest that the brain has more compensatory capacity than the retina, as the NVU appears less affected under the pathologies studied. Consistent with this phenomenon, it has been hypothesized that microglia and macroglia may contribute to minimizing tissue damage, inflammation, and neurodegeneration, whereas retinal microglia, due to their proximity to the external environment, may prioritize inflammatory regulation [176, 220]. Additionally, the high demand for oxygen and glucose by photoreceptors can contribute to a more inflammatory environment, particularly in conditions like diabetes [221].

Our study is subject to multiple limitations. The scarcity of human brain and retina samples from donors with DM and/or AD resulted in small sample sizes. Furthermore, substantial inter-individual variability was observed, likely influenced by unrecorded donor comorbidities and the spectrum of DM and AD severity. Collectively, these factors reduce the statistical power of the study and may limit the generalizability of our findings to the broader patient population. A further limitation is the lack of matched retinal and brain tissue from the same donors, which prevents direct correlation of pathologies, and the longer post-mortem intervals for retinal samples, which may affect protein integrity patterns [222-224]. The study also does not account for the influence of circadian rhythms, which are known to regulate key NVU components such as tight junction protein expression, pericyte function, and glial cell activation [225-230]. Furthermore, while we sampled patients across DM stages (no DR vs DR), the cross-sectional design captures the NVU at a single time point. This makes it impossible to determine the temporal sequence of dysfunction in DM and AD progression. Additionally, the analysis was restricted to the frontal cortex, and the findings may not be generalizable to other brain regions. Future studies should therefore include a larger, well-characterized cohort with matched retinal and multi-region brain samples from the same donors.

Despite these limitations, this study offers valuable insights into cellular alterations within the NVU of the retina and brain under pathology. The panel of markers used is also applicable to other neuropathological disorders affecting the BRB or BBB, such as stroke, multiple sclerosis, and epilepsy [231]. Taken together, our findings in a unique human tissue collection, provide a preliminary indication that the pathogenic mechanisms affecting the NVU in the brain in DM and AD are distinct from those in the DM retina. Given the global rise in the prevalence of both DM and AD [232, 233], further research is crucial to determine the exact role of NVU alterations in AD and to explain the increased risk of AD in DM patients.

Acknowledgements
The authors acknowledge the Microscopy and Cytometry Core Facility - location AMC (MCCF-AMC) for their technical assistance. We wish to thank Gabrielle Krebbers of the Electron Microscopy Center Amsterdam, Amsterdam, The Netherlands, for training in cryostat sectioning.

Funding
This work is supported by the RECOGNISED consortium grant (EU GA 847749), and The Encouraging European Research (EER) regulation of The Dutch Research Council (NWO, grant 200629). The study funders were not involved in the study design; the data collection, analysis, or interpretation; or the writing of the report; nor did they impose any restrictions regarding the publication of the report.

Author information
Authors and Affiliations
Ocular Angiogenesis Group, Department of Ophthalmology, Amsterdam UMC location University of Amsterdam, Amsterdam, The Netherlands.
Noëlle Bakker-van Bugnum, Amber Teppema, Aïcha A. Croes, Eva Prevaes, Gwen van de Brug, Alexander M. Emeis Escalante, Hinke Groeneveld, Cornelis J.F. van Noorden, Reinier O. Schlingemann & Ingeborg Klaassen

Amsterdam Neuroscience, Cellular & Molecular Mechanisms, Amsterdam, The Netherlands.
Noëlle Bakker-van Bugnum, Reinier O. Schlingemann & Ingeborg Klaassen

Contributions
The authors have contributed to this article as follows: IK, NBVB, CJFVN, ROS contributed to the conception and design, AAC, EP, GVDB, AMEE, HG, NBVB performed immunofluorescence staining experiments, microscopical fluorescence imaging and quantification, all authors contributed to scientific discussions, IK, NBVB, CJFVN, ROS contributed to manuscript writing, and IK, CJFVN, ROS, NB supervised the entire study. All authors have approved the final manuscript.

Data availability
The data that support the findings of this study are available on request from the corresponding author.

References

[1] Biessels GJ, Staekenborg S, Brunner E, Brayne C, Scheltens P (2006) Risk of dementia in diabetes mellitus: a systematic review. Lancet Neurol 5(1): 64–74. doi: 10.1016/S1474-4422(05)70284-2

[2] Little K, Llorian-Salvador M, Scullion S, Hernandez C, Simo-Servat O, Del Marco A, et al. (2022) Common pathways in dementia and diabetic retinopathy: understanding the mechanisms of diabetes-related cognitive decline. Trends Endocrinol Metab 33(1): 50–71. doi: 10.1016/j.tem.2021.10.008

[3] Erener S (2020) Diabetes, infection risk and COVID-19. Mol Metab 39: 101044. doi: 10.1016/j.molmet.2020.101044

[4] Pedersen FN, Stokholm L, Pouwer F, Hass Rubin K, Peto T, Frydkjaer-Olsen U, et al. (2022) Diabetic Retinopathy Predicts Risk of Alzheimer's Disease: A Danish Registry-Based Nationwide Cohort Study. J Alzheimers Dis 86(1): 451–460. doi: 10.3233/JAD-215313

[5] Nian S, Lo ACY, Mi Y, Ren K, Yang D (2021) Neurovascular unit in diabetic retinopathy: pathophysiological roles and potential therapeutical targets. Eye Vis (Lond) 8(1): 15. doi: 10.1186/s40662-021-00239-1

[6] Little K, Llorián-Salvador M, Scullion S, Hernández C, Simó-Servat O, del Marco A, et al. (2022) Common pathways in dementia and diabetic retinopathy: understanding the mechanisms of diabetes-related cognitive decline. Trends Endocrin Met 33(1): 50–71. doi: 10.1016/j.tem.2021.10.008

[7] Li TT, Li DY, Wei QY, Shi MH, Xiang JK, Gao RW, et al. (2023) Dissecting the neurovascular unit in physiology and Alzheimer’s disease: Functions, imaging tools and genetic mouse models. Neurobiology of Disease 181. doi: 10.1016/j.nbd.2023.106114

[8] Soto-Rojas LO, Pacheco-Herrero M, Martinez-Gomez PA, Campa-Cordoba BB, Apatiga-Perez R, Villegas-Rojas MM, et al. (2021) The Neurovascular Unit Dysfunction in Alzheimer's Disease. Int J Mol Sci 22(4). doi: 10.3390/ijms22042022

[9] McConnell HL, Mishra A (2022) Cells of the Blood-Brain Barrier: An Overview of the Neurovascular Unit in Health and Disease. Methods Mol Biol 2492: 3–24. doi: 10.1007/978-1-0716-2289-6_1

[10] Manu DR, Slevin M, Barcutean L, Forro T, Boghitoiu T, Balasa R (2023) Astrocyte Involvement in Blood-Brain Barrier Function: A Critical Update Highlighting Novel, Complex, Neurovascular Interactions. Int J Mol Sci 24(24). doi: 10.3390/ijms242417146

[11] Klaassen I, Van Noorden CJ, Schlingemann RO (2013) Molecular basis of the inner blood-retinal barrier and its breakdown in diabetic macular edema and other pathological conditions. Prog Retin Eye Res 34: 19–48. doi: 10.1016/j.preteyeres.2013.02.001

[12] Hofman P, Blaauwgeers HG, Tolentino MJ, Adamis AP, Nunes Cardozo BJ, Vrensen GF, et al. (2000) VEGF-A induced hyperpermeability of blood-retinal barrier endothelium in vivo is predominantly associated with pinocytotic vesicular transport and not with formation of fenestrations. Vascular endothelial growth factor-A. Curr Eye Res 21(2): 637–645.

[13] Galea I (2021) The blood-brain barrier in systemic infection and inflammation. Cell Mol Immunol 18(11): 2489–2501. doi: 10.1038/s41423-021-00757-x

[14] Armulik A, Genove G, Mae M, Nisancioglu MH, Wallgard E, Niaudet C, et al. (2010) Pericytes regulate the blood-brain barrier. Nature 468(7323): 557–561. doi: 10.1038/nature09522

[15] Bhowmick S, D'Mello V, Caruso D, Wallerstein A, Abdul-Muneer PM (2019) Impairment of pericyte-endothelium crosstalk leads to blood-brain barrier dysfunction following traumatic brain injury. Exp Neurol 317: 260–270. doi: 10.1016/j.expneurol.2019.03.014

[16] Faal T, Phan DTT, Davtyan H, Scarfone VM, Varady E, Blurton-Jones M, et al. (2019) Induction of Mesoderm and Neural Crest-Derived Pericytes from Human Pluripotent Stem Cells to Study Blood-Brain Barrier Interactions. Stem Cell Reports 12(3): 451–460. doi: 10.1016/j.stemcr.2019.01.005

[17] Fernandez-Klett F, Potas JR, Hilpert D, Blazej K, Radke J, Huck J, et al. (2013) Early loss of pericytes and perivascular stromal cell-induced scar formation after stroke. J Cereb Blood Flow Metab 33(3): 428–439. doi: 10.1038/jcbfm.2012.187
[18] van Noorden CJF, Yetkin-Arik B, Martinez PS, Bakker N, Smallenburg MEV, Schlingemann RO, et al. (2024) New Insights in ATP Synthesis as Therapeutic Target in Cancer and Angiogenic Ocular Diseases. J Histochem Cytochem 72(5): 329–352. doi: 10.1369/00221554241249515
[19] Newman E, Reichenbach A (1996) The Muller cell: a functional element of the retina. Trends Neurosci 19(8): 307–312. doi: 10.1016/0166-2236(96)10040-0
[20] Bojarskaite L, Nafari S, Ravnanger AK, Frey MM, Skauli N, Abjorsbraten KS, et al. (2024) Role of aquaporin-4 polarization in extracellular solute clearance. Fluids Barriers CNS 21(1): 28. doi: 10.1186/s12987-024-00527-7
[21] Sun J, He Z (2025) Interactions between astrocytes and cerebral endothelial cells in central nervous system diseases. Biomed Pharmacother 191: 118516. doi: 10.1016/j.biopha.2025.118516
[22] Nagelhus EA, Mathiisen TM, Ottersen OP (2004) Aquaporin-4 in the central nervous system: cellular and subcellular distribution and coexpression with KIR4.1. Neuroscience 129(4): 905–913. doi: 10.1016/j.neuroscience.2004.08.053
[23] Masaki H, Wakayama Y, Hara H, Jimi T, Unaki A, Iijima S, et al. (2010) Immunocytochemical studies of aquaporin 4, Kir4.1, and alpha1-syntrophin in the astrocyte endfeet of mouse brain capillaries. Acta Histochem Cytochem 43(4): 99–105. doi: 10.1267/ahc.10016
[24] Nagelhus EA, Ottersen OP (2013) Physiological roles of aquaporin-4 in brain. Physiol Rev 93(4): 1543–1562. doi: 10.1152/physrev.00011.2013
[25] Ohno Y, Kunisawa N, Shimizu S (2021) Emerging Roles of Astrocyte Kir4.1 Channels in the Pathogenesis and Treatment of Brain Diseases. Int J Mol Sci 22(19). doi: 10.3390/ijms221910236
[26] Le YZ (2017) VEGF production and signaling in Muller glia are critical to modulating vascular function and neuronal integrity in diabetic retinopathy and hypoxic retinal vascular diseases. Vision Res 139: 108–114. doi: 10.1016/j.visres.2017.05.005
[27] Yoo HS, Shanmugalingam U, Smith PD (2021) Harnessing Astrocytes and Muller Glial Cells in the Retina for Survival and Regeneration of Retinal Ganglion Cells. Cells 10(6). doi: 10.3390/cells10061339
[28] Huang W, Xia Q, Zheng F, Zhao X, Ge F, Xiao J, et al. (2023) Microglia-Mediated Neurovascular Unit Dysfunction in Alzheimer's Disease. J Alzheimers Dis 94(s1): S335–S354. doi: 10.3233/JAD-221064
[29] Fu X, Feng S, Qin H, Yan L, Zheng C, Yao K (2023) Microglia: The breakthrough to treat neovascularization and repair blood-retinal barrier in retinopathy. Front Mol Neurosci 16: 1100254. doi: 10.3389/fnmol.2023.1100254
[30] Ding Z, Guo S, Luo L, Zheng Y, Gan S, Kang X, et al. (2021) Emerging Roles of Microglia in Neuro-vascular Unit: Implications of Microglia-Neurons Interactions. Front Cell Neurosci 15: 706025. doi: 10.3389/fncel.2021.706025
[31] Gao C, Jiang J, Tan Y, Chen S (2023) Microglia in neurodegenerative diseases: mechanism and potential therapeutic targets. Signal Transduct Target Ther 8(1): 359. doi: 10.1038/s41392-023-01588-0
[32] Cheung N, Mitchell P, Wong TY (2010) Diabetic retinopathy. Lancet 376(9735): 124–136. doi: 10.1016/S0140-6736(09)62124-3
[33] Barber AJ, Gardner TW, Abcouwer SF (2011) The significance of vascular and neural apoptosis to the pathology of diabetic retinopathy. Invest Ophthalmol Vis Sci 52(2): 1156–1163. doi: 10.1167/iovs.10-6293
[34] Simo R, Stitt AW, Gardner TW (2018) Neurodegeneration in diabetic retinopathy: does it really matter? Diabetologia 61(9): 1902–1912. doi: 10.1007/s00125-018-4692-1
[35] Barot M, Gokulgandhi MR, Patel S, Mitra AK (2013) Microvascular complications and diabetic retinopathy: recent advances and future implications. Future Med Chem 5(3): 301–314. doi: 10.4155/fmc.12.206

[36] Lynch SK, Abramoff MD (2017) Diabetic retinopathy is a neurodegenerative disorder. Vision Res 139: 101–107. doi: 10.1016/j.visres.2017.03.003
[37] Peng RP, Zhu ZQ, Shen HY, Lin HM, Zhong L, Song SQ, et al. (2022) Retinal Nerve and Vascular Changes in Prediabetes. Front Med (Lausanne) 9: 777646. doi: 10.3389/fmed.2022.777646
[38] Vujosevic S, Midena E (2013) Retinal layers changes in human preclinical and early clinical diabetic retinopathy support early retinal neuronal and Muller cells alterations. J Diabetes Res 2013: 905058. doi: 10.1155/2013/905058
[39] van Dijk HW, Verbraak FD, Kok PH, Stehouwer M, Garvin MK, Sonka M, et al. (2012) Early neurodegeneration in the retina of type 2 diabetic patients. Invest Ophthalmol Vis Sci 53(6): 2715–2719. doi: 10.1167/iovs.11-8997
[40] De Clerck EEB, Schouten J, Berendschot T, Goezinne F, Dagnelie PC, Schaper NC, et al. (2018) Macular thinning in prediabetes or type 2 diabetes without diabetic retinopathy: the Maastricht Study. Acta Ophthalmol 96(2): 174–182. doi: 10.1111/aos.13570
[41] van Dijk HW, Verbraak FD, Stehouwer M, Kok PH, Garvin MK, Sonka M, et al. (2011) Association of visual function and ganglion cell layer thickness in patients with diabetes mellitus type 1 and no or minimal diabetic retinopathy. Vision Res 51(2): 224–228. doi: 10.1016/j.visres.2010.08.024
[42] Abu El-Asrar AM, Dralands L, Missotten L, Geboes K (2007) Expression of antiapoptotic and proapoptotic molecules in diabetic retinas. Eye (Lond) 21(2): 238–245. doi: 10.1038/sj.eye.6702225
[43] Mizutani M, Gerhardinger C, Lorenzi M (1998) Muller cell changes in human diabetic retinopathy. Diabetes 47(3): 445–449. doi: 10.2337/diabetes.47.3.445
[44] Villarroel M, Ciudin A, Hernandez C, Simo R (2010) Neurodegeneration: An early event of diabetic retinopathy. World J Diabetes 1(2): 57–64. doi: 10.4239/wjd.v1.i2.57
[45] Simo R, Hernandez C, European Consortium for the Early Treatment of Diabetic R (2012) Neurodegeneration is an early event in diabetic retinopathy: therapeutic implications. Br J Ophthalmol 96(10): 1285–1290. doi: 10.1136/bjophthalmol-2012-302005
[46] Chihara E, Matsuoka T, Ogura Y, Matsumura M (1993) Retinal nerve fiber layer defect as an early manifestation of diabetic retinopathy. Ophthalmology 100(8): 1147–1151. doi: 10.1016/s0161-6420(93)31513-7
[47] van Dijk HW, Kok PH, Garvin M, Sonka M, Devries JH, Michels RP, et al. (2009) Selective loss of inner retinal layer thickness in type 1 diabetic patients with minimal diabetic retinopathy. Invest Ophthalmol Vis Sci 50(7): 3404–3409. doi: 10.1167/iovs.08-3143
[48] Lim HB, Shin YI, Lee MW, Park GS, Kim JY (2019) Longitudinal Changes in the Peripapillary Retinal Nerve Fiber Layer Thickness of Patients With Type 2 Diabetes. JAMA Ophthalmol 137(10): 1125–1132. doi: 10.1001/jamaophthalmol.2019.2537
[49] Hietala K, Forsblom C, Summanen P, Groop PH, FinnDiane Study G (2008) Heritability of proliferative diabetic retinopathy. Diabetes 57(8): 2176–2180. doi: 10.2337/db07-1495
[50] Kim J, Jensen A, Ko S, Raghavan S, Phillips LS, Hung A, et al. (2022) Systematic Heritability and Heritability Enrichment Analysis for Diabetes Complications in UK Biobank and ACCORD Studies. Diabetes 71(5): 1137–1148. doi: 10.2337/db21-0839
[51] Simo-Servat O, Hernandez C, Simo R (2013) Genetics in diabetic retinopathy: current concepts and new insights. Curr Genomics 14(5): 289–299. doi: 10.2174/13892029113149990008
[52] Kern TS, Engerman RL (1996) Capillary lesions develop in retina rather than cerebral cortex in diabetes and experimental galactosemia. Arch Ophthalmol-Chic 114(3): 306–310. doi: DOI 10.1001/archopht.1996.01100130302013
[53] Mukai N, Hori S, Pomeroy M (1980) Cerebral-Lesions in Rats with Streptozotocin-Induced Diabetes. Acta Neuropathologica 51(1): 79–84. doi: Doi 10.1007/Bf00688853
[54] Frank RN, Dutta S, Frank SE (1987) Cerebral cortical capillary basement membrane thickening in galactosaemic rats. Diabetologia 30(9): 739–744. doi: 10.1007/BF00296999
[55] Johnson PC, Brendel K, Meezan E (1982) Thickened cerebral cortical capillary basement membranes in diabetics. Arch Pathol Lab Med 106(5): 214–217.

[56] Jakobsen J, Sidenius P, Gundersen HJ, Osterby R (1987) Quantitative changes of cerebral neocortical structure in insulin-treated long-term streptozocin-induced diabetes in rats. Diabetes 36(5): 597–601. doi: 10.2337/diab.36.5.597
[57] Woerdeman J, van Duinkerken E, Wattjes MP, Barkhof F, Snoek FJ, Moll AC, et al. (2014) Proliferative retinopathy in type 1 diabetes is associated with cerebral microbleeds, which is part of generalized microangiopathy. Diabetes Care 37(4): 1165–1168. doi: 10.2337/dc13-1586
[58] Sanahuja J, Alonso N, Diez J, Ortega E, Rubinat E, Traveset A, et al. (2016) Increased Burden of Cerebral Small Vessel Disease in Patients With Type 2 Diabetes and Retinopathy. Diabetes Care 39(9): 1614–1620. doi: 10.2337/dc15-2671
[59] de Oliveira F (1966) Pericytes in diabetic retinopathy. Br J Ophthalmol 50(3): 134–143. doi: 10.1136/bjo.50.3.134
[60] Addison DJ, Garner A, Ashton N (1970) Degeneration of intramural pericytes in diabetic retinopathy. Br Med J 1(5691): 264–266. doi: 10.1136/bmj.1.5691.264
[61] Dai J, Vrensen GF, Schlingemann RO (2002) Blood-brain barrier integrity is unaltered in human brain cortex with diabetes mellitus. Brain Res 954(2): 311–316. doi: 10.1016/s0006-8993(02)03294-8
[62] Mahmood S, Dkhar W, Kadavigere R, Sukumar S, Nayak K, Pradhan A, et al. (2025) An analysis of brain structural changes in type 2 diabetes using advanced MRI techniques. Magn Reson Imaging 121: 110419. doi: 10.1016/j.mri.2025.110419
[63] Hussain S, Mansouri S, Sjoholm A, Patrone C, Darsalia V (2014) Evidence for cortical neuronal loss in male type 2 diabetic Goto-Kakizaki rats. J Alzheimers Dis 41(2): 551–560. doi: 10.3233/JAD-131958
[64] Kodl CT, Franc DT, Rao JP, Anderson FS, Thomas W, Mueller BA, et al. (2008) Diffusion tensor imaging identifies deficits in white matter microstructure in subjects with type 1 diabetes that correlate with reduced neurocognitive function. Diabetes 57(11): 3083–3089. doi: 10.2337/db08-0724
[65] Musen G, Lyoo IK, Sparks CR, Weinger K, Hwang J, Ryan CM, et al. (2006) Effects of type 1 diabetes on gray matter density as measured by voxel-based morphometry. Diabetes 55(2): 326–333. doi: 10.2337/diabetes.55.02.06.db05-0520
[66] Hughes TM, Ryan CM, Aizenstein HJ, Nunley K, Gianaros PJ, Miller R, et al. (2013) Frontal gray matter atrophy in middle aged adults with type 1 diabetes is independent of cardiovascular risk factors and diabetes complications. J Diabetes Complications 27(6): 558–564. doi: 10.1016/j.jdiacomp.2013.07.001
[67] van Duinkerken E, Schoonheim MM, Steenwijk MD, Klein M, RG IJ, Moll AC, et al. (2014) Ventral striatum, but not cortical volume loss, is related to cognitive dysfunction in type 1 diabetic patients with and without microangiopathy. Diabetes Care 37(9): 2483–2490. doi: 10.2337/dc14-0016
[68] Klein JP, Waxman SG (2003) The brain in diabetes: molecular changes in neurons and their implications for end-organ damage. Lancet Neurol 2(9): 548–554. doi: 10.1016/s1474-4422(03)00503-9
[69] Luna R, Talanki Manjunatha R, Bollu B, Jhaveri S, Avanthika C, Reddy N, et al. (2021) A Comprehensive Review of Neuronal Changes in Diabetics. Cureus 13(10): e19142. doi: 10.7759/cureus.19142
[70] van Duinkerken E, Ijzerman RG, Klein M, Moll AC, Snoek FJ, Scheltens P, et al. (2016) Disrupted subject-specific gray matter network properties and cognitive dysfunction in type 1 diabetes patients with and without proliferative retinopathy. Hum Brain Mapp 37(3): 1194–1208. doi: 10.1002/hbm.23096
[71] McCrimmon RJ, Ryan CM, Frier BM (2012) Diabetes and cognitive dysfunction. Lancet 379(9833): 2291–2299. doi: 10.1016/S0140-6736(12)60360-2
[72] Umegaki H (2010) Pathophysiology of cognitive dysfunction in older people with type 2 diabetes: vascular changes or neurodegeneration? Age Ageing 39(1): 8–10. doi: 10.1093/ageing/afp211
[73] van Duinkerken E, Schoonheim MM, Sanz-Arigita EJ, RG IJ, Moll AC, Snoek FJ, et al. (2012) Resting-state brain networks in type 1 diabetic patients with and without microangiopathy and their

relation to cognitive functions and disease variables. Diabetes 61(7): 1814–1821. doi: 10.2337/db11-1358
[74] Akhtar A, Sah SP (2020) Insulin signaling pathway and related molecules: Role in neurodegeneration and Alzheimer's disease. Neurochem Int 135: 104707. doi: 10.1016/j.neuint.2020.104707
[75] van Sloten TT, Sedaghat S, Carnethon MR, Launer LJ, Stehouwer CDA (2020) Cerebral microvascular complications of type 2 diabetes: stroke, cognitive dysfunction, and depression. Lancet Diabetes Endocrinol 8(4): 325–336. doi: 10.1016/S2213-8587(19)30405-X
[76] Kodl CT, Seaquist ER (2008) Cognitive dysfunction and diabetes mellitus. Endocr Rev 29(4): 494–511. doi: 10.1210/er.2007-0034
[77] Zhang S, Zhang Y, Wen Z, Yang Y, Bu T, Bu X, et al. (2023) Cognitive dysfunction in diabetes: abnormal glucose metabolic regulation in the brain. Front Endocrinol (Lausanne) 14: 1192602. doi: 10.3389/fendo.2023.1192602
[78] Rizzo MR, Marfella R, Barbieri M, Boccardi V, Vestini F, Lettieri B, et al. (2010) Relationships between daily acute glucose fluctuations and cognitive performance among aged type 2 diabetic patients. Diabetes Care 33(10): 2169–2174. doi: 10.2337/dc10-0389
[79] Mekala A, Qiu H (2025) Interplay Between Vascular Dysfunction and Neurodegenerative Pathology: New Insights into Molecular Mechanisms and Management. Biomolecules 15(5). doi: 10.3390/biom15050712
[80] Vickers JC, Dickson TC, Adlard PA, Saunders HL, King CE, McCormack G (2000) The cause of neuronal degeneration in Alzheimer's disease. Prog Neurobiol 60(2): 139–165. doi: 10.1016/s0301-0082(99)00023-4
[81] Krumm S, Kivisaari SL, Probst A, Monsch AU, Reinhardt J, Ulmer S, et al. (2016) Cortical thinning of parahippocampal subregions in very early Alzheimer's disease. Neurobiol Aging 38: 188–196. doi: 10.1016/j.neurobiolaging.2015.11.001
[82] Xiao Y, Hu Y, Huang K, Alzheimer's Disease Neuroimaging I (2023) Atrophy of hippocampal subfields relates to memory decline during the pathological progression of Alzheimer's disease. Front Aging Neurosci 15: 1287122. doi: 10.3389/fnagi.2023.1287122
[83] Punzi M, Sestieri C, Picerni E, Chiarelli AM, Padulo C, Delli Pizzi A, et al. (2024) Atrophy of hippocampal subfields and amygdala nuclei in subjects with mild cognitive impairment progressing to Alzheimer's disease. Heliyon 10(6): e27429. doi: 10.1016/j.heliyon.2024.e27429
[84] Grande G, Qiu C, Fratiglioni L (2020) Prevention of dementia in an ageing world: Evidence and biological rationale. Ageing Res Rev 64: 101045. doi: 10.1016/j.arr.2020.101045
[85] Jack CR, Jr., Therneau TM, Weigand SD, Wiste HJ, Knopman DS, Vemuri P, et al. (2019) Prevalence of Biologically vs Clinically Defined Alzheimer Spectrum Entities Using the National Institute on Aging-Alzheimer's Association Research Framework. JAMA Neurol 76(10): 1174–1183. doi: 10.1001/jamaneurol.2019.1971
[86] Almohmadi NH, Al-Kuraishy HM, Albuhadily AK, Al-Gareeb AI, Abdelaziz AM, Alexiou A, et al. (2025) Alzheimer disease: Amyloid peptide controversies and challenges of anti-Abeta immunotherapy. J Pharmacol Exp Ther 392(8): 103639. doi: 10.1016/j.jpet.2025.103639
[87] Andrews SJ, Renton AE, Fulton-Howard B, Podlesny-Drabiniok A, Marcora E, Goate AM (2023) The complex genetic architecture of Alzheimer's disease: novel insights and future directions. Ebiomedicine 90: 104511. doi: 10.1016/j.ebiom.2023.104511
[88] Gatz M, Reynolds CA, Fratiglioni L, Johansson B, Mortimer JA, Berg S, et al. (2006) Role of genes and environments for explaining Alzheimer disease. Arch Gen Psychiatry 63(2): 168–174. doi: 10.1001/archpsyc.63.2.168
[89] Fisher RA, Miners JS, Love S (2022) Pathological changes within the cerebral vasculature in Alzheimer's disease: New perspectives. Brain Pathol 32(6): e13061. doi: 10.1111/bpa.13061
[90] Iadecola C, Gottesman RF (2018) Cerebrovascular Alterations in Alzheimer Disease. Circ Res 123(4): 406–408. doi: 10.1161/CIRCRESAHA.118.313400

[91] Hoozemans JJ, Rozemuller AJ, van Haastert ES, Eikelenboom P, van Gool WA (2011) Neuroinflammation in Alzheimer's disease wanes with age. J Neuroinflammation 8: 171. doi: 10.1186/1742-2094-8-171
[92] Kamphuis W, Middeldorp J, Kooijman L, Sluijs JA, Kooi EJ, Moeton M, et al. (2014) Glial fibrillary acidic protein isoform expression in plaque related astrogliosis in Alzheimer's disease. Neurobiol Aging 35(3): 492–510. doi: 10.1016/j.neurobiolaging.2013.09.035
[93] Vehmas AK, Kawas CH, Stewart WF, Troncoso JC (2003) Immune reactive cells in senile plaques and cognitive decline in Alzheimer's disease. Neurobiol Aging 24(2): 321–331. doi: 10.1016/s0197-4580(02)00090-8
[94] Kirabali T, Rust R, Rigotti S, Siccoli A, Nitsch RM, Kulic L (2020) Distinct changes in all major components of the neurovascular unit across different neuropathological stages of Alzheimer's disease. Brain Pathol 30(6): 1056–1070. doi: 10.1111/bpa.12895
[95] Sengillo JD, Winkler EA, Walker CT, Sullivan JS, Johnson M, Zlokovic BV (2013) Deficiency in mural vascular cells coincides with blood-brain barrier disruption in Alzheimer's disease. Brain Pathol 23(3): 303–310. doi: 10.1111/bpa.12004
[96] Ding R, Hase Y, Ameen-Ali KE, Ndung'u M, Stevenson W, Barsby J, et al. (2020) Loss of capillary pericytes and the blood-brain barrier in white matter in poststroke and vascular dementias and Alzheimer's disease. Brain Pathol 30(6): 1087–1101. doi: 10.1111/bpa.12888
[97] Hase Y, Jobson D, Cheong J, Gotama K, Maffei L, Hase M, et al. (2024) Hippocampal capillary pericytes in post-stroke and vascular dementias and Alzheimer's disease and experimental chronic cerebral hypoperfusion. Acta Neuropathol Commun 12(1): 29. doi: 10.1186/s40478-024-01737-8
[98] Nielsen HM, Ek D, Avdic U, Orbjorn C, Hansson O, Netherlands Brain B, et al. (2013) NG2 cells, a new trail for Alzheimer's disease mechanisms? Acta Neuropathol Commun 1(1): 7. doi: 10.1186/2051-5960-1-7
[99] Halliday MR, Rege SV, Ma Q, Zhao Z, Miller CA, Winkler EA, et al. (2016) Accelerated pericyte degeneration and blood-brain barrier breakdown in apolipoprotein E4 carriers with Alzheimer's disease. J Cereb Blood Flow Metab 36(1): 216–227. doi: 10.1038/jcbfm.2015.44
[100] Baloyannis SJ, Baloyannis IS (2012) The vascular factor in Alzheimer's disease: a study in Golgi technique and electron microscopy. J Neurol Sci 322(1-2): 117–121. doi: 10.1016/j.jns.2012.07.010
[101] Shi H, Koronyo Y, Rentsendorj A, Regis GC, Sheyn J, Fuchs DT, et al. (2020) Identification of early pericyte loss and vascular amyloidosis in Alzheimer's disease retina. Acta Neuropathol 139(5): 813–836. doi: 10.1007/s00401-020-02134-w
[102] Li P, Fan H (2023) Pericyte Loss in Diseases. Cells 12(15). doi: 10.3390/cells12151931
[103] Wang Q, Huang X, Su Y, Yin G, Wang S, Yu B, et al. (2022) Activation of Wnt/beta-catenin pathway mitigates blood-brain barrier dysfunction in Alzheimer's disease. Brain 145(12): 4474–4488. doi: 10.1093/brain/awac236
[104] Yamazaki Y, Shinohara M, Shinohara M, Yamazaki A, Murray ME, Liesinger AM, et al. (2019) Selective loss of cortical endothelial tight junction proteins during Alzheimer's disease progression. Brain 142(4): 1077–1092. doi: 10.1093/brain/awz011
[105] Keaney J, Walsh DM, O'Malley T, Hudson N, Crosbie DE, Loftus T, et al. (2015) Autoregulated paracellular clearance of amyloid-beta across the blood-brain barrier. Sci Adv 1(8): e1500472. doi: 10.1126/sciadv.1500472
[106] Frisoni GB, Hansson O, Nichols E, Garibotto V, Schindler SE, van der Flier WM, et al. (2025) New landscape of the diagnosis of Alzheimer's disease. Lancet 406(10510): 1389–1407. doi: 10.1016/S0140-6736(25)01294-2
[107] Koronyo-Hamaoui M, Koronyo Y, Ljubimov AV, Miller CA, Ko MK, Black KL, et al. (2011) Identification of amyloid plaques in retinas from Alzheimer's patients and noninvasive in vivo optical imaging of retinal plaques in a mouse model. Neuroimage 54 Suppl 1: S204–217. doi: 10.1016/j.neuroimage.2010.06.020
[108] den Haan J, Morrema THJ, Verbraak FD, de Boer JF, Scheltens P, Rozemuller AJ, et al. (2018) Amyloid-beta and phosphorylated tau in post-mortem Alzheimer's disease retinas. Acta Neuropathol Commun 6(1): 147. doi: 10.1186/s40478-018-0650-x

[109] Koronyo Y, Biggs D, Barron E, Boyer DS, Pearlman JA, Au WJ, et al. (2017) Retinal amyloid pathology and proof-of-concept imaging trial in Alzheimer's disease. JCI Insight 2(16). doi: 10.1172/jci.insight.93621
[110] Blanks JC, Schmidt SY, Torigoe Y, Porrello KV, Hinton DR, Blanks RH (1996) Retinal pathology in Alzheimer's disease. II. Regional neuron loss and glial changes in GCL. Neurobiol Aging 17(3): 385–395. doi: 10.1016/0197-4580(96)00009-7
[111] Kim JI, Kang BH (2019) Decreased retinal thickness in patients with Alzheimer's disease is correlated with disease severity. PLoS One 14(11): e0224180. doi: 10.1371/journal.pone.0224180
[112] Coppola G, Di Renzo A, Ziccardi L, Martelli F, Fadda A, Manni G, et al. (2015) Optical Coherence Tomography in Alzheimer's Disease: A Meta-Analysis. PLoS One 10(8): e0134750. doi: 10.1371/journal.pone.0134750
[113] Trebbastoni A, D'Antonio F, Bruscolini A, Marcelli M, Cecere M, Campanelli A, et al. (2016) Retinal nerve fibre layer thickness changes in Alzheimer's disease: Results from a 12-month prospective case series. Neurosci Lett 629: 165–170. doi: 10.1016/j.neulet.2016.07.006
[114] Parisi V, Restuccia R, Fattapposta F, Mina C, Bucci MG, Pierelli F (2001) Morphological and functional retinal impairment in Alzheimer's disease patients. Clin Neurophysiol 112(10): 1860–1867. doi: 10.1016/s1388-2457(01)00620-4
[115] Hedges TR, 3rd, Perez Galves R, Speigelman D, Barbas NR, Peli E, Yardley CJ (1996) Retinal nerve fiber layer abnormalities in Alzheimer's disease. Acta Ophthalmol Scand 74(3): 271–275. doi: 10.1111/j.1600-0420.1996.tb00090.x
[116] Kesler A, Vakhapova V, Korczyn AD, Naftaliev E, Neudorfer M (2011) Retinal thickness in patients with mild cognitive impairment and Alzheimer's disease. Clin Neurol Neurosurg 113(7): 523–526. doi: 10.1016/j.clineuro.2011.02.014
[117] Berisha F, Feke GT, Trempe CL, McMeel JW, Schepens CL (2007) Retinal abnormalities in early Alzheimer's disease. Invest Ophthalmol Vis Sci 48(5): 2285–2289. doi: 10.1167/iovs.06-1029
[118] Feke GT, Hyman BT, Stern RA, Pasquale LR (2015) Retinal blood flow in mild cognitive impairment and Alzheimer's disease. Alzheimers Dement (Amst) 1(2): 144–151. doi: 10.1016/j.dadm.2015.01.004
[119] Frost S, Kanagasingam Y, Sohrabi H, Vignarajan J, Bourgeat P, Salvado O, et al. (2013) Retinal vascular biomarkers for early detection and monitoring of Alzheimer's disease. Transl Psychiatry 3(2): e233. doi: 10.1038/tp.2012.150
[120] Cheung CY, Ong YT, Ikram MK, Ong SY, Li X, Hilal S, et al. (2014) Microvascular network alterations in the retina of patients with Alzheimer's disease. Alzheimers Dement 10(2): 135–142. doi: 10.1016/j.jalz.2013.06.009
[121] Williams MA, McGowan AJ, Cardwell CR, Cheung CY, Craig D, Passmore P, et al. (2015) Retinal microvascular network attenuation in Alzheimer's disease. Alzheimers Dement (Amst) 1(2): 229–235. doi: 10.1016/j.dadm.2015.04.001
[122] Beason-Held LL, Goh JO, An Y, Kraut MA, O'Brien RJ, Ferrucci L, et al. (2013) Changes in brain function occur years before the onset of cognitive impairment. J Neurosci 33(46): 18008–18014. doi: 10.1523/JNEUROSCI.1402-13.2013
[123] DeTure MA, Dickson DW (2019) The neuropathological diagnosis of Alzheimer's disease. Mol Neurodegener 14(1): 32. doi: 10.1186/s13024-019-0333-5
[124] Metaxas A, Thygesen C, Briting SRR, Landau AM, Darvesh S, Finsen B (2019) Increased Inflammation and Unchanged Density of Synaptic Vesicle Glycoprotein 2A (SV2A) in the Postmortem Frontal Cortex of Alzheimer's Disease Patients. Front Cell Neurosci 13: 538. doi: 10.3389/fncel.2019.00538
[125] Thomas T, Miners S, Love S (2015) Post-mortem assessment of hypoperfusion of cerebral cortex in Alzheimer's disease and vascular dementia. Brain 138(Pt 4): 1059–1069. doi: 10.1093/brain/awv025
[126] Govindpani K, McNamara LG, Smith NR, Vinnakota C, Waldvogel HJ, Faull RL, et al. (2019) Vascular Dysfunction in Alzheimer's Disease: A Prelude to the Pathological Process or a Consequence of It? J Clin Med 8(5). doi: 10.3390/jcm8050651

[127] Stillman JM, Lopes F, Lin JP, Hu K, Reich DS, Schafer DP (2023) Lipofuscin-like autofluorescence within microglia and its impact on studying microglial engulfment. Nature Communications 14(1). doi: 10.1038/s41467-023-42809-y
[128] Zhang H, Tan C, Shi X, Xu J (2022) Impacts of autofluorescence on fluorescence based techniques to study microglia. BMC Neurosci 23(1): 21. doi: 10.1186/s12868-022-00703-1
[129] Schneider CA, Rasband WS, Eliceiri KW (2012) NIH Image to ImageJ: 25 years of image analysis. Nat Methods 9(7): 671–675. doi: 10.1038/nmeth.2089
[130] Bosma EK, van Noorden CJF, Schlingemann RO, Klaassen I (2018) The role of plasmalemma vesicle-associated protein in pathological breakdown of blood-brain and blood-retinal barriers: potential novel therapeutic target for cerebral edema and diabetic macular edema. Fluids Barriers CNS 15(1): 24. doi: 10.1186/s12987-018-0109-2
[131] Wood CAP, Zhang JR, Aydin D, Xu Y, Andreone BJ, Langen UH, et al. (2021) Structure and mechanism of blood-brain-barrier lipid transporter MFSD2A. Nature 596(7872): 444–+. doi: 10.1038/s41586-021-03782-y
[132] Ben-Zvi A, Lacoste B, Kur E, Andreone BJ, Mayshar Y, Yan H, et al. (2014) Mfsd2a is critical for the formation and function of the blood-brain barrier. Nature 509(7501): 507–+. doi: 10.1038/nature13324
[133] Armulik A, Genove G, Betsholtz C (2011) Pericytes: developmental, physiological, and pathological perspectives, problems, and promises. Dev Cell 21(2): 193–215. doi: 10.1016/j.devcel.2011.07.001
[134] Craggs LJL, Fenwick R, Oakley AE, Ihara M, Kalaria RN (2015) Immunolocalization of platelet-derived growth factor receptor- (PDGFR-) and pericytes in cerebral autosomal dominant arteriopathy with subcortical infarcts and leukoencephalopathy (CADASIL). Neuropath Appl Neuro 41(4): 557–570. doi: 10.1111/nan.12188
[135] Ding R, Hase Y, Ameen-Ali KE, Ndung'u M, Stevenson W, Barsby J, et al. (2020) Loss of capillary pericytes and the blood-brain barrier in white matter in poststroke and vascular dementias and Alzheimer's disease. Brain Pathology 30(6): 1087–1101. doi: 10.1111/bpa.12888
[136] Stallcup WB (2018) The NG2 Proteoglycan in Pericyte Biology. Pericyte Biology - Novel Concepts 1109: 5–19. doi: 10.1007/978-3-030-02601-1_2
[137] Dominguez E, Raoul W, Calippe B, Sahel JA, Guillonneau X, Paques M, et al. (2015) Experimental Branch Retinal Vein Occlusion Induces Upstream Pericyte Loss and Vascular Destabilization. Plos One 10(7). doi: 10.1371/journal.pone.0132644
[138] Girolamo F, de Trizio I, Errede M, Longo G, D'Amati A, Virgintino D (2021) Neural crest cell-derived pericytes act as pro-angiogenic cells in human neocortex development and gliomas. Fluids and Barriers of the Cns 18(1). doi: 10.1186/s12987-021-00242-7
[139] Bakker N, Croes AA, Prevaes E, van Noorden CJF, Schlingemann RO, Klaassen I (2025) Development of Immunostaining Protocols for 3D Visualization of Pericytes in Human Retinal Flatmounts. J Histochem Cytochem: 221554251323655. doi: 10.1369/00221554251323655
[140] Breijyeh Z, Karaman R (2020) Comprehensive Review on Alzheimer's Disease: Causes and Treatment. Molecules 25(24). doi: 10.3390/molecules25245789
[141] Litkowski EM, Logue MW, Zhang R, Charest BR, Lange EM, Hokanson JE, et al. (2022) A Diabetes Genetic Risk Score Is Associated With All-Cause Dementia and Clinically Diagnosed Vascular Dementia in the Million Veteran Program. Diabetes Care 45(11): 2544–2552. doi: 10.2337/dc22-0105
[142] Hardy J, de Strooper B, Escott-Price V (2022) Diabetes and Alzheimer's disease: shared genetic susceptibility? Lancet Neurol 21(11): 962–964. doi: 10.1016/S1474-4422(22)00395-7
[143] Yuan X, Wang H, Zhang F, Zhang M, Wang Q, Wang J (2023) The common genes involved in the pathogenesis of Alzheimer's disease and type 2 diabetes and their implication for drug repositioning. Neuropharmacology 223: 109327. doi: 10.1016/j.neuropharm.2022.109327
[144] Boukhalfa W, Jmel H, Kheriji N, Gouiza I, Dallali H, Hechmi M, et al. (2023) Decoding the genetic relationship between Alzheimer's disease and type 2 diabetes: potential risk variants and future direction for North Africa. Front Aging Neurosci 15: 1114810. doi: 10.3389/fnagi.2023.1114810

[145] Biessels GJ, De Leeuw FE, Lindeboom J, Barkhof F, Scheltens P (2006) Increased cortical atrophy in patients with Alzheimer's disease and type 2 diabetes mellitus. J Neurol Neurosurg Psychiatry 77(3): 304–307. doi: 10.1136/jnnp.2005.069583
[146] Karagas N, Young JE, Blue EE, Jayadev S (2025) The Spectrum of Genetic Risk in Alzheimer Disease. Neurol Genet 11(1): e200224. doi: 10.1212/NXG.0000000000200224
[147] Cho H, Sobrin L (2014) Genetics of diabetic retinopathy. Curr Diab Rep 14(8): 515. doi: 10.1007/s11892-014-0515-z
[148] Pei X, Huang D, Li Z (2024) Genetic insights and emerging therapeutics in diabetic retinopathy: from molecular pathways to personalized medicine. Front Genet 15: 1416924. doi: 10.3389/fgene.2024.1416924
[149] Rudraraju M, Narayanan SP, Somanath PR (2020) Regulation of blood-retinal barrier cell-junctions in diabetic retinopathy. Pharmacol Res 161: 105115. doi: 10.1016/j.phrs.2020.105115
[150] Kanwal A, Kanwar N, Shetty MP, Rana K, Alisi A, Bhatia A, et al. (2025) Impact of diabetes on cellular connections: Pathological insights and emerging therapeutic targets. Diabetes Metab Syndr 19(8): 103300. doi: 10.1016/j.dsx.2025.103300
[151] Viggars AP, Wharton SB, Simpson JE, Matthews FE, Brayne C, Savva GM, et al. (2011) Alterations in the blood brain barrier in ageing cerebral cortex in relationship to Alzheimer-type pathology: a study in the MRC-CFAS population neuropathology cohort. Neurosci Lett 505(1): 25–30. doi: 10.1016/j.neulet.2011.09.049
[152] Little K, Singh A, Del Marco A, Llorian-Salvador M, Vargas-Soria M, Turch-Anguera M, et al. (2023) Disruption of cortical cell type composition and function underlies diabetes-associated cognitive decline. Diabetologia 66(8): 1557–1575. doi: 10.1007/s00125-023-05935-2
[153] Hofman P, Blaauwgeers HG, Vrensen GF, Schlingemann RO (2001) Role of VEGF-A in endothelial phenotypic shift in human diabetic retinopathy and VEGF-A-induced retinopathy in monkeys. Ophthalmic Res 33(3): 156–162. doi: 10.1159/000055663
[154] Schlingemann RO, Hofman P, Vrensen GF, Blaauwgeers HG (1999) Increased expression of endothelial antigen PAL-E in human diabetic retinopathy correlates with microvascular leakage. Diabetologia 42(5): 596–602. doi: 10.1007/s001250051200
[155] Klaassen I, Hughes JM, Vogels IM, Schalkwijk CG, Van Noorden CJ, Schlingemann RO (2009) Altered expression of genes related to blood-retina barrier disruption in streptozotocin-induced diabetes. Exp Eye Res 89(1): 4–15. doi: 10.1016/j.exer.2009.01.006
[156] Wisniewska-Kruk J, van der Wijk AE, van Veen HA, Gorgels TGMF, Vogels IMC, Versteeg D, et al. (2016) Plasmalemma Vesicle-Associated Protein Has a Key Role in Blood-Retinal Barrier Loss. American Journal of Pathology 186(4): 1044–1054. doi: 10.1016/j.ajpath.2015.11.019
[157] Wang W, Dentler WL, Borchardt RT (2001) VEGF increases BMEC monolayer permeability by affecting occludin expression and tight junction assembly. Am J Physiol Heart Circ Physiol 280(1): H434–440. doi: 10.1152/ajpheart.2001.280.1.H434
[158] Antonetti DA, Barber AJ, Hollinger LA, Wolpert EB, Gardner TW (1999) Vascular endothelial growth factor induces rapid phosphorylation of tight junction proteins occludin and zonula occluden 1. A potential mechanism for vascular permeability in diabetic retinopathy and tumors. J Biol Chem 274(33): 23463–23467. doi: 10.1074/jbc.274.33.23463
[159] Murakami T, Frey T, Lin C, Antonetti DA (2012) Protein kinase cbeta phosphorylates occludin regulating tight junction trafficking in vascular endothelial growth factor-induced permeability in vivo. Diabetes 61(6): 1573–1583. doi: 10.2337/db11-1367
[160] Argaw AT, Gurfein BT, Zhang Y, Zameer A, John GR (2009) VEGF-mediated disruption of endothelial CLN-5 promotes blood-brain barrier breakdown. Proc Natl Acad Sci U S A 106(6): 1977–1982. doi: 10.1073/pnas.0808698106
[161] Wang Z, Liu CH, Huang S, Fu Z, Tomita Y, Britton WR, et al. (2020) Wnt signaling activates MFSD2A to suppress vascular endothelial transcytosis and maintain blood-retinal barrier. Sci Adv 6(35): eaba7457. doi: 10.1126/sciadv.aba7457

[162] Zhang CL, Wang HL, Li PC, Hong CD, Chen AQ, Qiu YM, et al. (2021) Mfsd2a overexpression alleviates vascular dysfunction in diabetic retinopathy. Pharmacol Res 171: 105755. doi: 10.1016/j.phrs.2021.105755
[163] Chen Q, Ma JX (2017) Canonical Wnt signaling in diabetic retinopathy. Vision Res 139: 47–58. doi: 10.1016/j.visres.2017.02.007
[164] Chen Y, Hu Y, Zhou T, Zhou KK, Mott R, Wu M, et al. (2009) Activation of the Wnt pathway plays a pathogenic role in diabetic retinopathy in humans and animal models. Am J Pathol 175(6): 2676–2685. doi: 10.2353/ajpath.2009.080945
[165] Daneman R, Zhou L, Kebede AA, Barres BA (2010) Pericytes are required for blood-brain barrier integrity during embryogenesis. Nature 468(7323): 562–566. doi: 10.1038/nature09513
[166] Liebner S, Corada M, Bangsow T, Babbage J, Taddei A, Czupalla CJ, et al. (2008) Wnt/beta-catenin signaling controls development of the blood-brain barrier. J Cell Biol 183(3): 409–417. doi: 10.1083/jcb.200806024
[167] Alashmali SM, Lin L, Trepanier MO, Cisbani G, Bazinet RP (2019) The effects of n-6 polyunsaturated fatty acid deprivation on the inflammatory gene response to lipopolysaccharide in the mouse hippocampus. J Neuroinflammation 16(1): 237. doi: 10.1186/s12974-019-1615-0
[168] Tiwary S, Morales JE, Kwiatkowski SC, Lang FF, Rao G, McCarty JH (2018) Metastatic Brain Tumors Disrupt the Blood-Brain Barrier and Alter Lipid Metabolism by Inhibiting Expression of the Endothelial Cell Fatty Acid Transporter Mfsd2a. Sci Rep 8(1): 8267. doi: 10.1038/s41598-018-26636-6
[169] Nguyen C, Lei HT, Lai LTF, Gallenito MJ, Mu X, Matthies D, et al. (2023) Lipid flipping in the omega-3 fatty-acid transporter. Nat Commun 14(1): 2571. doi: 10.1038/s41467-023-37702-7
[170] Sanchez-Campillo M, Ruiz-Pastor MJ, Gazquez A, Marin-Munoz J, Noguera-Perea F, Ruiz-Alcaraz AJ, et al. (2019) Decreased Blood Level of MFSD2a as a Potential Biomarker of Alzheimer's Disease. Int J Mol Sci 21(1). doi: 10.3390/ijms21010070
[171] Ryu JK, McLarnon JG (2009) A leaky blood-brain barrier, fibrinogen infiltration and microglial reactivity in inflamed Alzheimer's disease brain. J Cell Mol Med 13(9A): 2911–2925. doi: 10.1111/j.1582-4934.2008.00434.x
[172] Cortes-Canteli M, Zamolodchikov D, Ahn HJ, Strickland S, Norris EH (2012) Fibrinogen and altered hemostasis in Alzheimer's disease. J Alzheimers Dis 32(3): 599–608. doi: 10.3233/JAD-2012-120820
[173] Cortes-Canteli M, Mattei L, Richards AT, Norris EH, Strickland S (2015) Fibrin deposited in the Alzheimer's disease brain promotes neuronal degeneration. Neurobiol Aging 36(2): 608–617. doi: 10.1016/j.neurobiolaging.2014.10.030
[174] Miller SJ, Dhodapkar RM, Sutova HE, Xue Y, Lee S, Logan R, et al. (2025) SARS-CoV-2 induces Alzheimer's disease-related amyloid-beta pathology in ex vivo human retinal explants and retinal organoids. Sci Adv 11(27): eads5006. doi: 10.1126/sciadv.ads5006
[175] Koronyo Y, Rentsendorj A, Mirzaei N, Regis GC, Sheyn J, Shi H, et al. (2023) Retinal pathological features and proteome signatures of Alzheimer's disease. Acta Neuropathol 145(4): 409–438. doi: 10.1007/s00401-023-02548-2
[176] Serrano-Pozo A, Gomez-Isla T, Growdon JH, Frosch MP, Hyman BT (2013) A phenotypic change but not proliferation underlies glial responses in Alzheimer disease. Am J Pathol 182(6): 2332–2344. doi: 10.1016/j.ajpath.2013.02.031
[177] Liu H, Tan AYS, Mehrabi NF, Turner CP, Curtis MA, Faull RLM, et al. (2025) Astrocytic proteins involved in regulation of the extracellular environment are increased in the Alzheimer's disease middle temporal gyrus. Neurobiol Dis 204: 106749. doi: 10.1016/j.nbd.2024.106749
[178] Datki Z, Papp R, Zadori D, Soos K, Fulop L, Juhasz A, et al. (2004) In vitro model of neurotoxicity of Abeta 1-42 and neuroprotection by a pentapeptide: irreversible events during the first hour. Neurobiol Dis 17(3): 507–515. doi: 10.1016/j.nbd.2004.08.007
[179] Hu J, Akama KT, Krafft GA, Chromy BA, Van Eldik LJ (1998) Amyloid-beta peptide activates cultured astrocytes: morphological alterations, cytokine induction and nitric oxide release. Brain Res 785(2): 195–206. doi: 10.1016/s0006-8993(97)01318-8

[180] Nielsen HM, Veerhuis R, Holmqvist B, Janciauskiene S (2009) Binding and uptake of A beta1-42 by primary human astrocytes in vitro. Glia 57(9): 978–988. doi: 10.1002/glia.20822
[181] Salinero O, Moreno-Flores MT, Ceballos ML, Wandosell F (1997) beta-Amyloid peptide induced cytoskeletal reorganization in cultured astrocytes. J Neurosci Res 47(2): 216–223.
[182] Wang WY, Tan MS, Yu JT, Tan L (2015) Role of pro-inflammatory cytokines released from microglia in Alzheimer's disease. Ann Transl Med 3(10): 136. doi: 10.3978/j.issn.2305-5839.2015.03.49
[183] Hippert C, Graca AB, Barber AC, West EL, Smith AJ, Ali RR, et al. (2015) Muller glia activation in response to inherited retinal degeneration is highly varied and disease-specific. PLoS One 10(3): e0120415. doi: 10.1371/journal.pone.0120415
[184] Zhang Y, Xu G, Ling Q, Da C (2011) Expression of Aquaporin 4 and Kir4.1 in Diabetic Rat Retina: Treatment with Minocycline. J Int Med Res 39(2): 464–479. doi: Doi 10.1177/147323001103900214
[185] Pannicke T, Iandiev I, Wurm A, Uckermann O, vom Hagen F, Reichenbach A, et al. (2006) Diabetes alters osmotic swelling characteristics and membrane conductance of glial cells in rat retina. Diabetes 55(3): 633–639. doi: 10.2337/diabetes.55.03.06.db05-1349
[186] Kida T, Oku H, Horie T, Fukumoto M, Okuda Y, Morishita S, et al. (2017) Implication of VEGF and aquaporin 4 mediating Muller cell swelling to diabetic retinal edema. Graefes Arch Clin Exp Ophthalmol 255(6): 1149–1157. doi: 10.1007/s00417-017-3631-z
[187] Alex A, Luo Q, Mathew D, Di R, Bhatwadekar AD (2020) Metformin Corrects Abnormal Circadian Rhythm and Kir4.1 Channels in Diabetes. Invest Ophthalmol Vis Sci 61(6): 46. doi: 10.1167/iovs.61.6.46
[188] Vujosevic S, Micera A, Bini S, Berton M, Esposito G, Midena E (2015) Aqueous Humor Biomarkers of Muller Cell Activation in Diabetic Eyes. Invest Ophthalmol Vis Sci 56(6): 3913–3918. doi: 10.1167/iovs.15-16554
[189] Zhao M, Zhao S, Tang M, Sun T, Zheng Z, Ma M (2022) Aqueous Humor Biomarkers of Retinal Glial Cell Activation in Patients With or Without Age-Related Cataracts and With Different Stages of Diabetic Retinopathy. Invest Ophthalmol Vis Sci 63(3): 8. doi: 10.1167/iovs.63.3.8
[190] Midena E, Bini S, Martini F, Enrica C, Pilotto E, Micera A, et al. (2020) Changes of Aqueous Humor Muller Cells' Biomarkers in Human Patients Affected by Diabetic Macular Edema after Subthreshold Micropulse Laser Treatment. Retina 40(1): 126–134. doi: 10.1097/IAE.0000000000002356
[191] Manescu MD, Catalin B, Baldea I, Mateescu VO, Rosu GC, Boboc IKS, et al. (2025) Aquaporin 4 modulation drives amyloid burden and cognitive abilities in an APPPS1 mouse model of Alzheimer's disease. Alzheimers Dement 21(5): e70164. doi: 10.1002/alz.70164
[192] Valenza M, Facchinetti R, Steardo L, Scuderi C (2019) Altered Waste Disposal System in Aging and Alzheimer's Disease: Focus on Astrocytic Aquaporin-4. Front Pharmacol 10: 1656. doi: 10.3389/fphar.2019.01656
[193] Wang S, Wang B, Shang D, Zhang K, Yan X, Zhang X (2022) Ion Channel Dysfunction in Astrocytes in Neurodegenerative Diseases. Front Physiol 13: 814285. doi: 10.3389/fphys.2022.814285
[194] Nwaobi SE, Cuddapah VA, Patterson KC, Randolph AC, Olsen ML (2016) The role of glial-specific Kir4.1 in normal and pathological states of the CNS. Acta Neuropathol 132(1): 1–21. doi: 10.1007/s00401-016-1553-1
[195] Wisniewska-Kruk J, Klaassen I, Vogels IM, Magno AL, Lai CM, Van Noorden CJ, et al. (2014) Molecular analysis of blood-retinal barrier loss in the Akimba mouse, a model of advanced diabetic retinopathy. Exp Eye Res 122: 123–131. doi: 10.1016/j.exer.2014.03.005
[196] Price TO, Eranki V, Banks WA, Ercal N, Shah GN (2012) Topiramate treatment protects blood-brain barrier pericytes from hyperglycemia-induced oxidative damage in diabetic mice. Endocrinology 153(1): 362–372. doi: 10.1210/en.2011-1638
[197] Hammes HP, Lin J, Wagner P, Feng Y, Vom Hagen F, Krzizok T, et al. (2004) Angiopoietin-2 causes pericyte dropout in the normal retina: evidence for involvement in diabetic retinopathy. Diabetes 53(4): 1104–1110. doi: 10.2337/diabetes.53.4.1104

[198] Pfister F, Feng Y, vom Hagen F, Hoffmann S, Molema G, Hillebrands JL, et al. (2008) Pericyte migration: a novel mechanism of pericyte loss in experimental diabetic retinopathy. Diabetes 57(9): 2495–2502. doi: 10.2337/db08-0325
[199] Mizutani M, Kern TS, Lorenzi M (1996) Accelerated death of retinal microvascular cells in human and experimental diabetic retinopathy. J Clin Invest 97(12): 2883–2890. doi: 10.1172/JCI118746
[200] Li G, Tang J, Du Y, Lee CA, Kern TS (2011) Beneficial effects of a novel RAGE inhibitor on early diabetic retinopathy and tactile allodynia. Mol Vis 17: 3156–3165.
[201] Bakker-van Bugnum N, Croes AA, Prevaes E, van Noorden CJF, Schlingemann RO and Klaassen I (2026) Differential pericyte pathology in the human retina and brain in diabetes mellitus and Alzheimer's disease. Front. Neurosci. 20:1749112. doi: 10.3389/fnins.2026.1749112
[202] Liu Y, Chen D, Smith A, Ye Q, Gao Y, Zhang W (2021) Three-dimensional remodeling of functional cerebrovascular architecture and gliovascular unit in leptin receptor-deficient mice. J Cereb Blood Flow Metab 41(7): 1547–1562. doi: 10.1177/0271678X211006596
[203] Liu Y, Zhang H, Wang S, Guo Y, Fang X, Zheng B, et al. (2021) Reduced pericyte and tight junction coverage in old diabetic rats are associated with hyperglycemia-induced cerebrovascular pericyte dysfunction. Am J Physiol Heart Circ Physiol 320(2): H549–H562. doi: 10.1152/ajpheart.00726.2020
[204] Rom S, Zuluaga-Ramirez V, Gajghate S, Seliga A, Winfield M, Heldt NA, et al. (2019) Hyperglycemia-Driven Neuroinflammation Compromises BBB Leading to Memory Loss in Both Diabetes Mellitus (DM) Type 1 and Type 2 Mouse Models. Mol Neurobiol 56(3): 1883–1896. doi: 10.1007/s12035-018-1195-5
[205] Kuiper EJ, Witmer AN, Klaassen I, Oliver N, Goldschmeding R, Schlingemann RO (2004) Differential expression of connective tissue growth factor in microglia and pericytes in the human diabetic retina. Br J Ophthalmol 88(8): 1082–1087. doi: 10.1136/bjo.2003.032045
[206] Bosma EK, van Noorden CJF, Klaassen I, Schlingemann RO (2019) Microvascular Complications in the Eye: Diabetic Retinopathy. In: Roelofs JJ, Vogt L (eds) Diabetic Nephropathy. Springer International Publishing AG, Switzerland, pp 305–321
[207] Frank RN, Turczyn TJ, Das A (1990) Pericyte coverage of retinal and cerebral capillaries. Invest Ophthalmol Vis Sci 31(6): 999–1007.
[208] Carrasco E, Hernandez C, de Torres I, Farres J, Simo R (2008) Lowered cortistatin expression is an early event in the human diabetic retina and is associated with apoptosis and glial activation. Mol Vis 14: 1496–1502.
[209] Sundstrom JM, Hernandez C, Weber SR, Zhao Y, Dunklebarger M, Tiberti N, et al. (2018) Proteomic Analysis of Early Diabetic Retinopathy Reveals Mediators of Neurodegenerative Brain Diseases. Invest Ophthalmol Vis Sci 59(6): 2264–2274. doi: 10.1167/iovs.17-23678
[210] Hogenboom R, Kalsbeek MJ, Korpel NL, de Goede P, Koenen M, Buijs RM, et al. (2019) Loss of arginine vasopressin- and vasoactive intestinal polypeptide-containing neurons and glial cells in the suprachiasmatic nucleus of individuals with type 2 diabetes. Diabetologia 62(11): 2088–2093. doi: 10.1007/s00125-019-4953-7
[211] Takeshita Y, Obermeier B, Cotleur AC, Spampinato SF, Shimizu F, Yamamoto E, et al. (2017) Effects of neuromyelitis optica-IgG at the blood-brain barrier in vitro. Neurol Neuroimmunol Neuroinflamm 4(1): e311. doi: 10.1212/NXI.0000000000000311
[212] Bonkowski D, Katyshev V, Balabanov RD, Borisov A, Dore-Duffy P (2011) The CNS microvascular pericyte: pericyte-astrocyte crosstalk in the regulation of tissue survival. Fluids Barriers CNS 8(1): 8. doi: 10.1186/2045-8118-8-8
[213] Al Ahmad A, Taboada CB, Gassmann M, Ogunshola OO (2011) Astrocytes and pericytes differentially modulate blood-brain barrier characteristics during development and hypoxic insult. J Cereb Blood Flow Metab 31(2): 693–705. doi: 10.1038/jcbfm.2010.148
[214] Liao K, Niu F, Hu G, Buch S (2022) Morphine-mediated release of astrocyte-derived extracellular vesicle miR-23a induces loss of pericyte coverage at the blood-brain barrier: Implications for neuroinflammation. Front Cell Dev Biol 10: 984375. doi: 10.3389/fcell.2022.984375

[215] Zheng Z, Chopp M, Chen J (2020) Multifaceted roles of pericytes in central nervous system homeostasis and disease. J Cereb Blood Flow Metab 40(7): 1381–1401. doi: 10.1177/0271678X20911331
[216] Hori S, Ohtsuki S, Hosoya K, Nakashima E, Terasaki T (2004) A pericyte-derived angiopoietin-1 multimeric complex induces occludin gene expression in brain capillary endothelial cells through Tie-2 activation in vitro. J Neurochem 89(2): 503–513. doi: 10.1111/j.1471-4159.2004.02343.x
[217] Nakagawa S, Deli MA, Nakao S, Honda M, Hayashi K, Nakaoke R, et al. (2007) Pericytes from brain microvessels strengthen the barrier integrity in primary cultures of rat brain endothelial cells. Cell Mol Neurobiol 27(6): 687–694. doi: 10.1007/s10571-007-9195-4
[218] Comin CH, Tsirukis DI, Sun Y, Xu X (2021) Quantification of retinal blood leakage in fundus fluorescein angiography in a retinal angiogenesis model. Sci Rep 11(1): 19903. doi: 10.1038/s41598-021-99434-2
[219] Joseph CR (2020) Novel MRI Techniques Identifying Vascular Leak and Paravascular Flow Reduction in Early Alzheimer Disease. Biomedicines 8(7). doi: 10.3390/biomedicines8070228
[220] Bloomfield CL, Gong J, Droho S, Makinde HM, Gurra MG, Stumpf CH, et al. (2024) Retinal microglia express more MHC class I and promote greater T-cell-driven inflammation than brain microglia. Front Immunol 15: 1399989. doi: 10.3389/fimmu.2024.1399989
[221] Majidi SP, Rajagopal R (2020) Photoreceptor responses to light in the pathogenesis of diabetic retinopathy. Vis Neurosci 37: E007. doi: 10.1017/S0952523820000061
[222] Pittner S, Merold V, Anders S, Lohner L, Amendt J, Klinger M, et al. (2022) A standard protocol for the analysis of postmortem muscle protein degradation: process optimization and considerations for the application in forensic PMI estimation. Int J Legal Med 136(6): 1913–1923. doi: 10.1007/s00414-022-02849-3
[223] Kocsmar E, Schmid M, Cosenza-Contreras M, Kocsmar I, Foll M, Krey L, et al. (2023) Proteome alterations in human autopsy tissues in relation to time after death. Cell Mol Life Sci 80(5): 117. doi: 10.1007/s00018-023-04754-3
[224] Crecelius A, Gotz A, Arzberger T, Frohlich T, Arnold GJ, Ferrer I, et al. (2008) Assessing quantitative post-mortem changes in the gray matter of the human frontal cortex proteome by 2-D DIGE. Proteomics 8(6): 1276–1291. doi: 10.1002/pmic.200700728
[225] Skapetze L, Owino S, Lo EH, Arai K, Merrow M, Harrington M (2023) Rhythms in barriers and fluids: Circadian clock regulation in the aging neurovascular unit. Neurobiol Dis 181: 106120. doi: 10.1016/j.nbd.2023.106120
[226] Hudson N, Celkova L, Hopkins A, Greene C, Storti F, Ozaki E, et al. (2019) Dysregulated claudin-5 cycling in the inner retina causes retinal pigment epithelial cell atrophy. JCI Insight 4(15). doi: 10.1172/jci.insight.130273
[227] Hastings MH, Brancaccio M, Gonzalez-Aponte MF, Herzog ED (2023) Circadian Rhythms and Astrocytes: The Good, the Bad, and the Ugly. Annu Rev Neurosci 46: 123–143. doi: 10.1146/annurev-neuro-100322-112249
[228] Li W, Tiedt S, Lawrence JH, Harrington ME, Musiek ES, Lo EH (2024) Circadian Biology and the Neurovascular Unit. Circ Res 134(6): 748–769. doi: 10.1161/CIRCRESAHA.124.323514
[229] Mitchell JW, Gillette MU (2023) Development of circadian neurovascular function and its implications. Front Neurosci 17: 1196606. doi: 10.3389/fnins.2023.1196606
[230] Elliott BD, Kisamore CO, Nelson RJ, DeVries AC, Walker WH, 2nd (2025) Circadian influences on central nervous system barriers and the glymphatic system. Front Physiol 16: 1622236. doi: 10.3389/fphys.2025.1622236
[231] Archie SR, Al Shoyaib A, Cucullo L (2021) Blood-Brain Barrier Dysfunction in CNS Disorders and Putative Therapeutic Targets: An Overview. Pharmaceutics 13(11). doi: 10.3390/pharmaceutics13111779
[232] (2025) 2025 Alzheimer's disease facts and figures. Alzheimers & Dementia 21(4). doi: 10.1002/alz.70235

[233] Zhang XX, Tian Y, Wang ZT, Ma YH, Tan L, Yu JT (2021) The Epidemiology of Alzheimer's Disease Modifiable Risk Factors and Prevention. J Prev Alzheimers Dis 8(3): 313–321. doi: 10.14283/jpad.2021.15

Supplementary materials

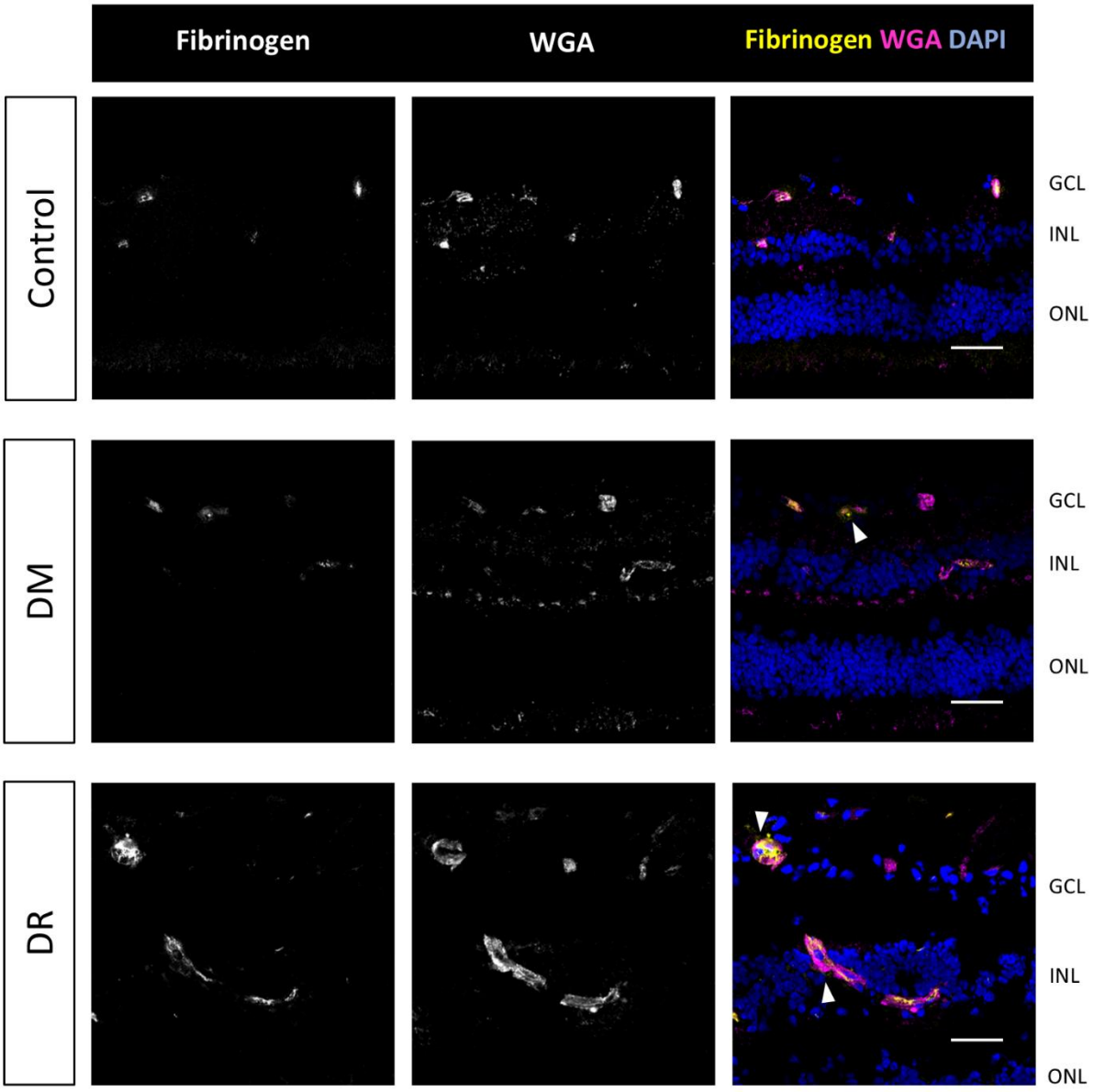

Supplementary Figure S1. **Immunofluorescence staining of fibrinogen in the human retina.** Representative confocal microscopy images of fibrinogen (yellow) immunofluorescence staining in human retinal cryosections (10 µm) (Control, DM, DR). Vascular endothelial cells are stained with wheat germ agglutinin (WGA; magenta) and nuclei are stained with DAPI (blue). White arrowheads indicate examples of vascular leakage. GCL = ganglion cell layer; INL = inner nuclear layer; ONL = outer nuclear layer. Scale bar: 50 µm.

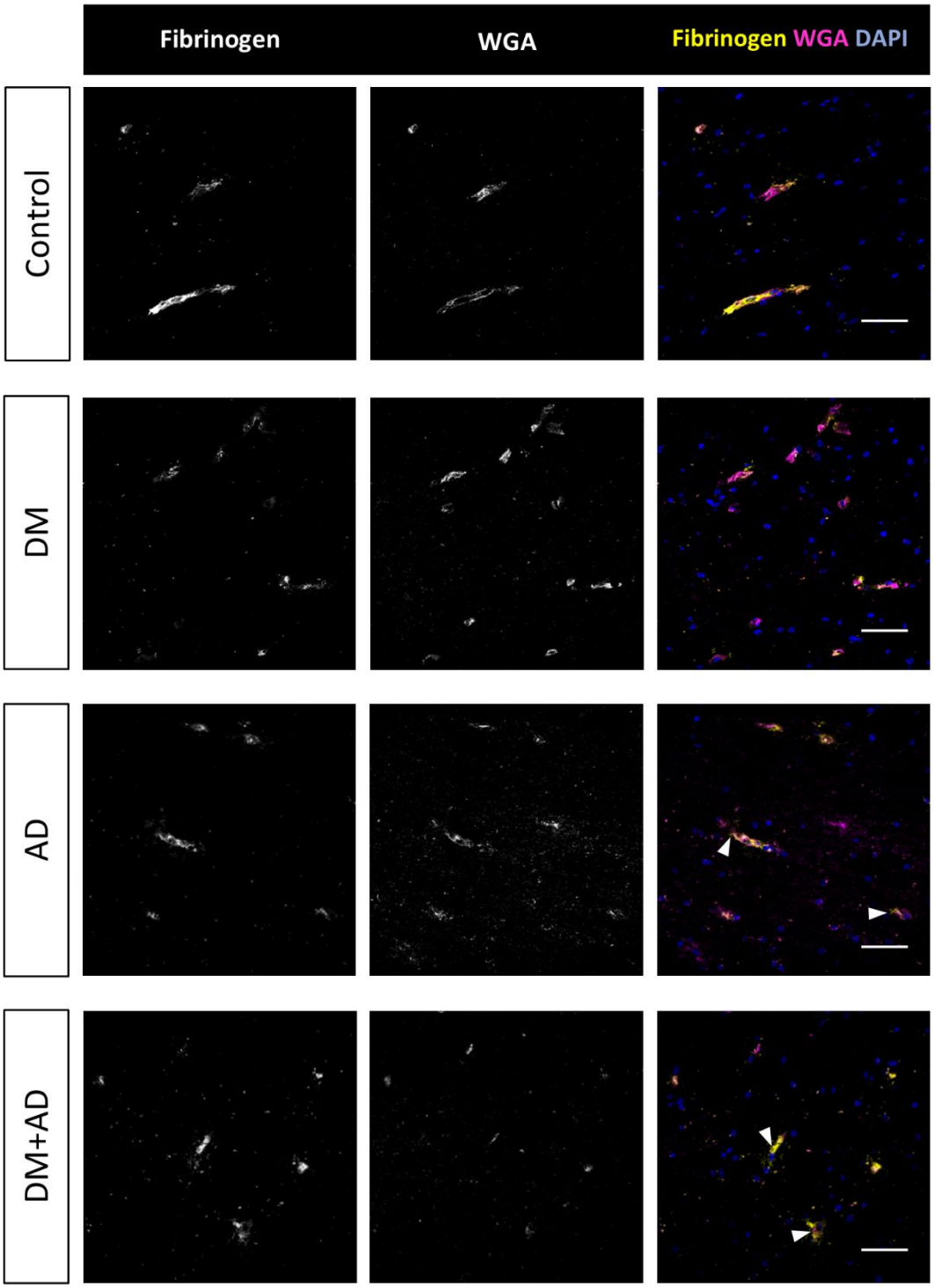

Supplementary Figure S2. Immunofluorescence staining of fibrinogen in the human frontal cortex. Representative confocal microscopy images of fibrinogen (yellow) immunofluorescence staining in human cortical cryosections (10 µm) (Control, DM, AD, DM+AD). Vascular endothelial cells are stained with wheat germ agglutinin (WGA; magenta) and nuclei are stained with DAPI (blue). White arrowheads indicate examples of vascular leakage. Scale bar: 50 µm.

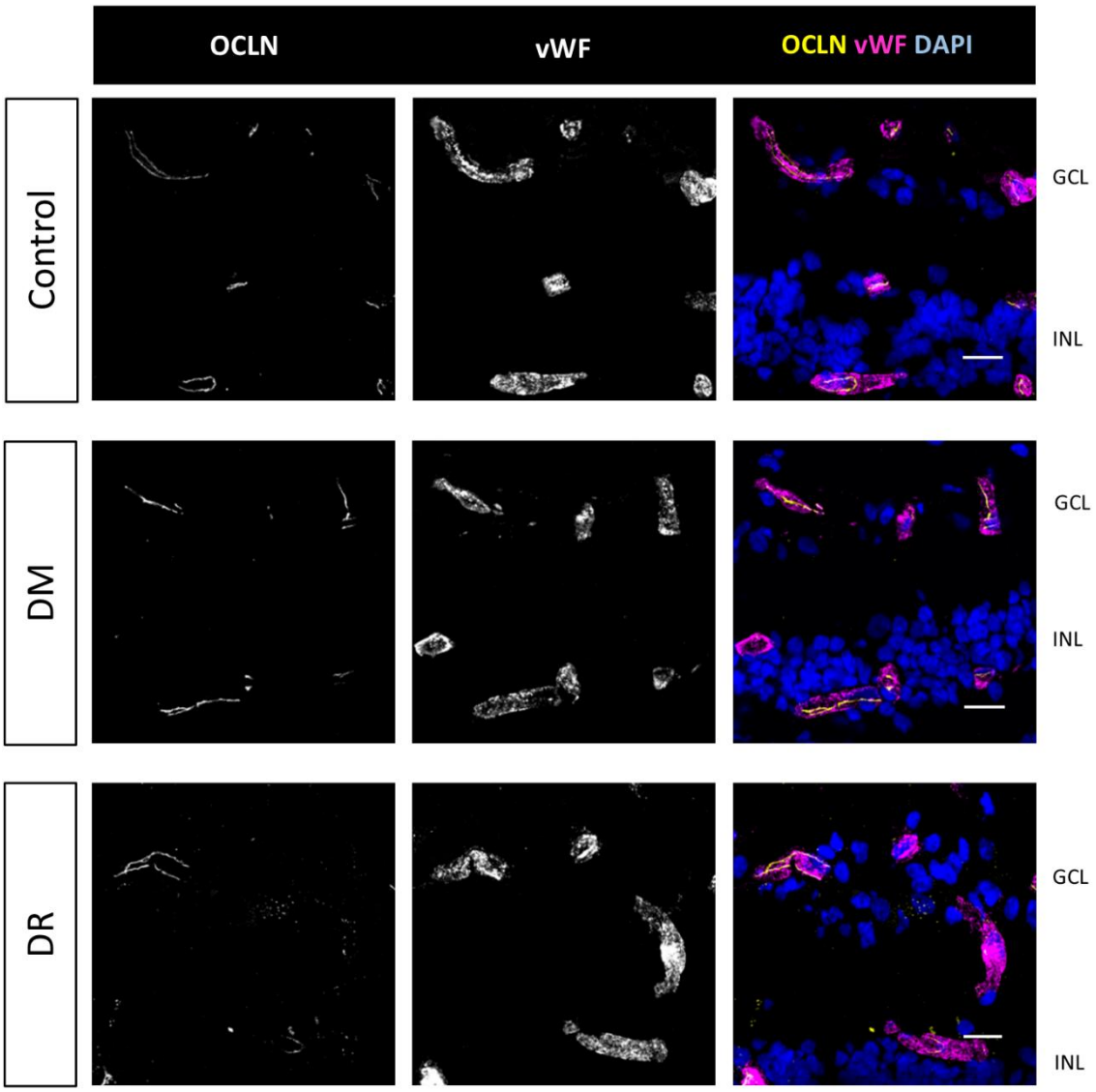

Supplementary Figure S3. Immunofluorescence staining of occludin in the human retina. Representative confocal microscopy images of tight junction protein occludin (OCLN; yellow) immunofluorescence staining in human retinal cryosections (10 µm) (Control, DM, DR). Vascular endothelial cells are stained for von Willebrand Factor (vWF; magenta) and nuclei are stained with DAPI (blue). GCL = ganglion cell layer; INL = inner nuclear layer. Scale bar: 20 µm.

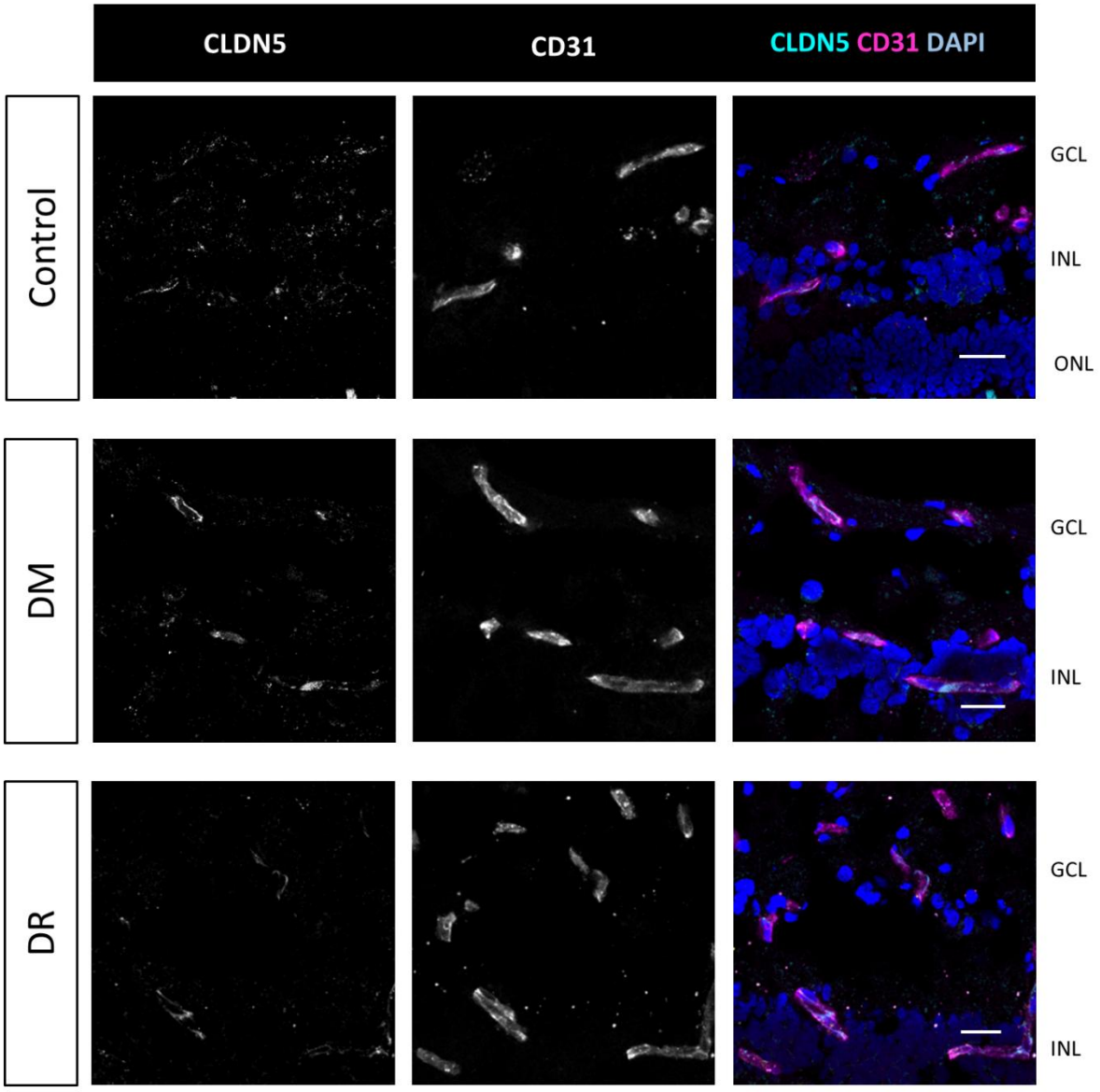

Supplementary Figure S4. Immunofluorescence staining of claudin-5 in the human retina.
Representative confocal microscopy images of tight junction protein claudin-5 (CLDN5; cyan) immunofluorescence staining in human retinal cryosections (10 µm) (Control, DM, DR). Vascular endothelial cells are stained for CD31 (magenta) and nuclei are stained with DAPI (blue).
GCL = ganglion cell layer; INL = inner nuclear layer; ONL = outer nuclear layer. Scale bar: 25 µm.

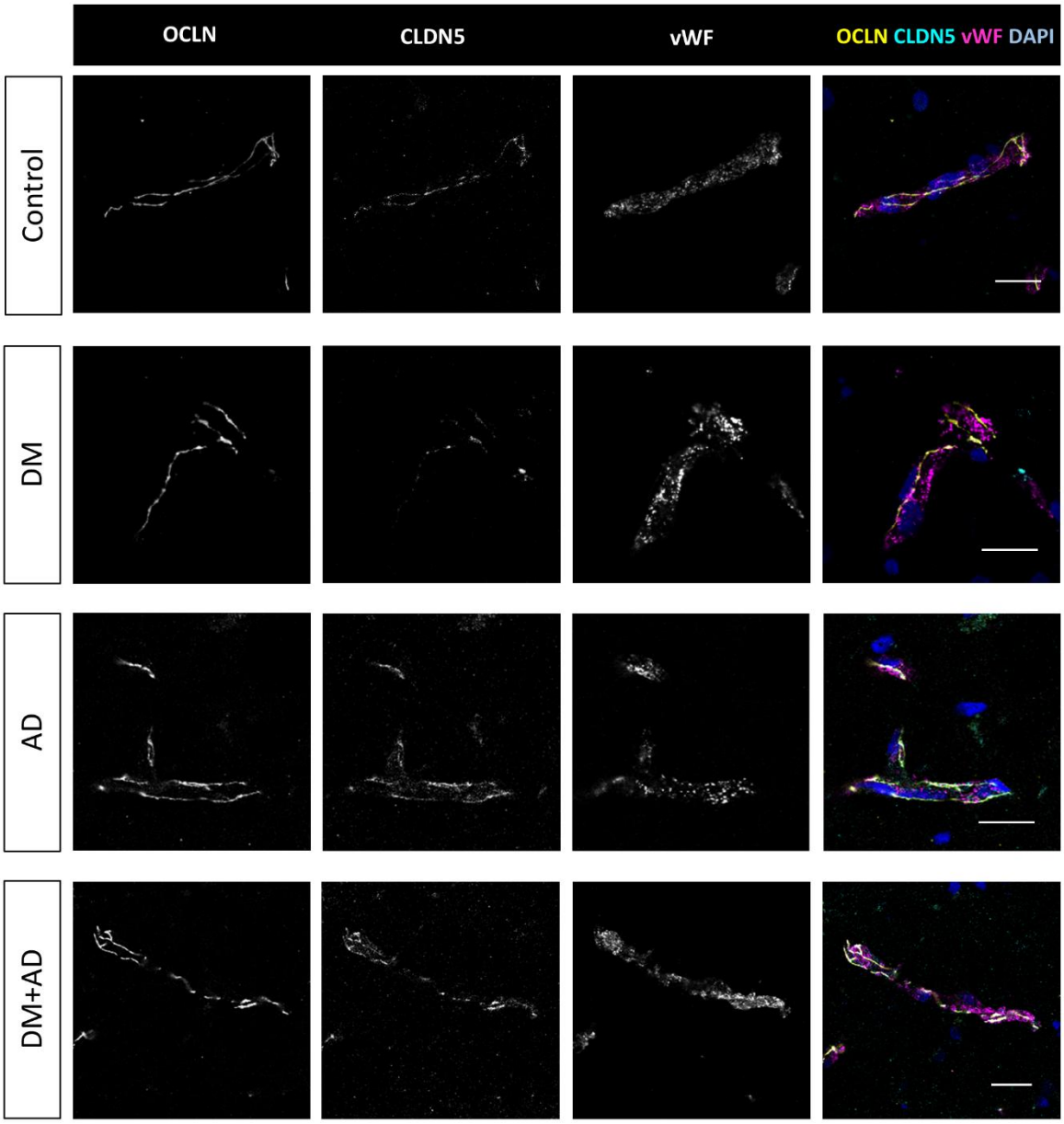

Supplementary Figure S5. Immunofluorescence double staining of occludin and claudin-5 in the human frontal cortex. Representative confocal microscopy images of tight junction proteins occludin (OCLN; yellow) and claudin-5 (CLDN5; cyan) immunofluorescence double staining in human cortical cryosections (10 µm) (Control, DM, AD, DM+AD). Vascular endothelial cells are stained for von Willebrand Factor (vWF; magenta) and nuclei are stained with DAPI (blue). Scale bar: 20 µm.

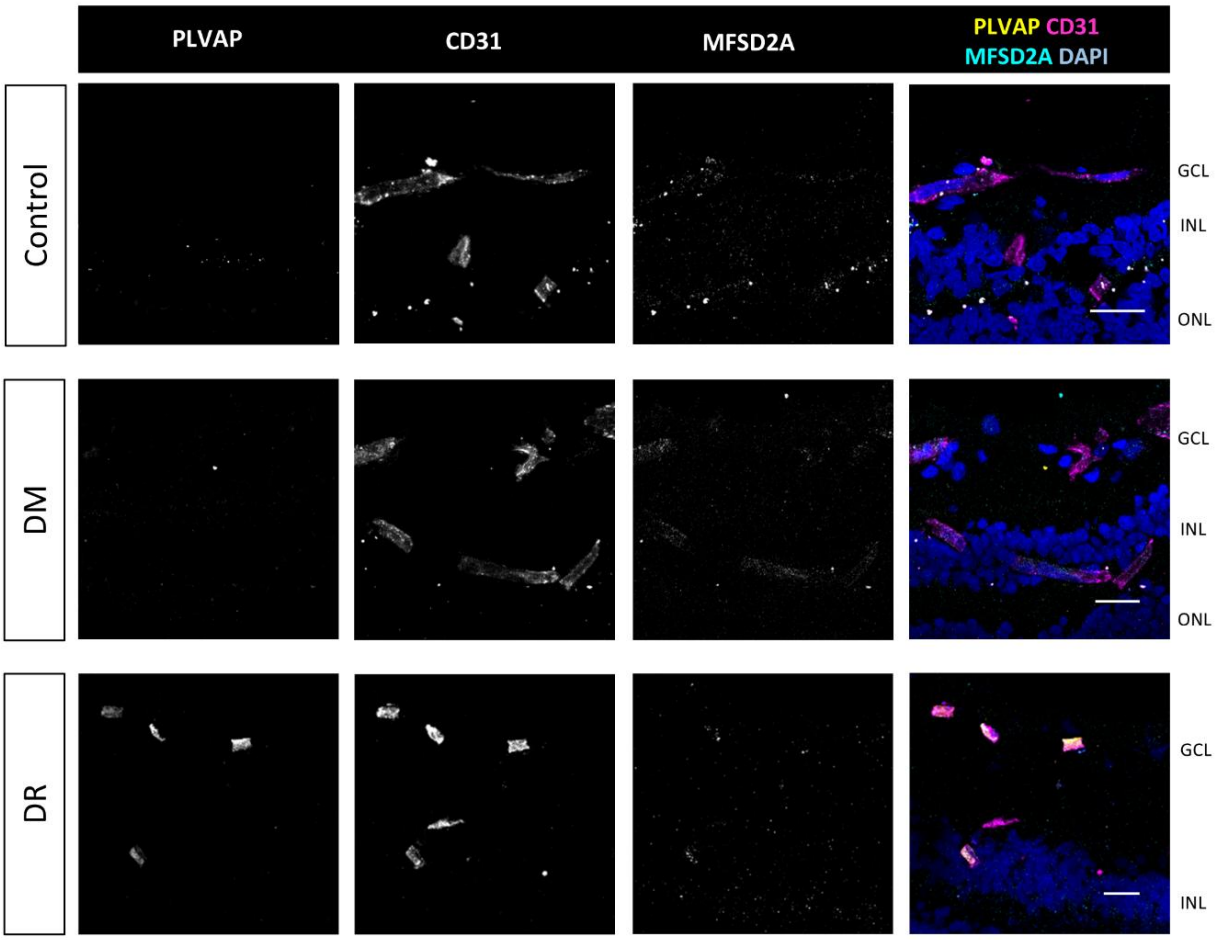

Supplementary Figure S6. Immunofluorescence double staining of plasmalemma vesicle-associated protein (PLVAP) and MFSD2A in the human retina. Representative confocal microscopy images of PLVAP (yellow) and MFSD2A (cyan) immunofluorescence double staining in human retinal cryosections (10 µm) (Control, DM, DR). Vascular endothelial cells are stained for CD31 (magenta) and nuclei are stained with DAPI (blue). GCL = ganglion cell layer; INL = inner nuclear layer; ONL = outer nuclear layer. Scale bar: 50 µm.

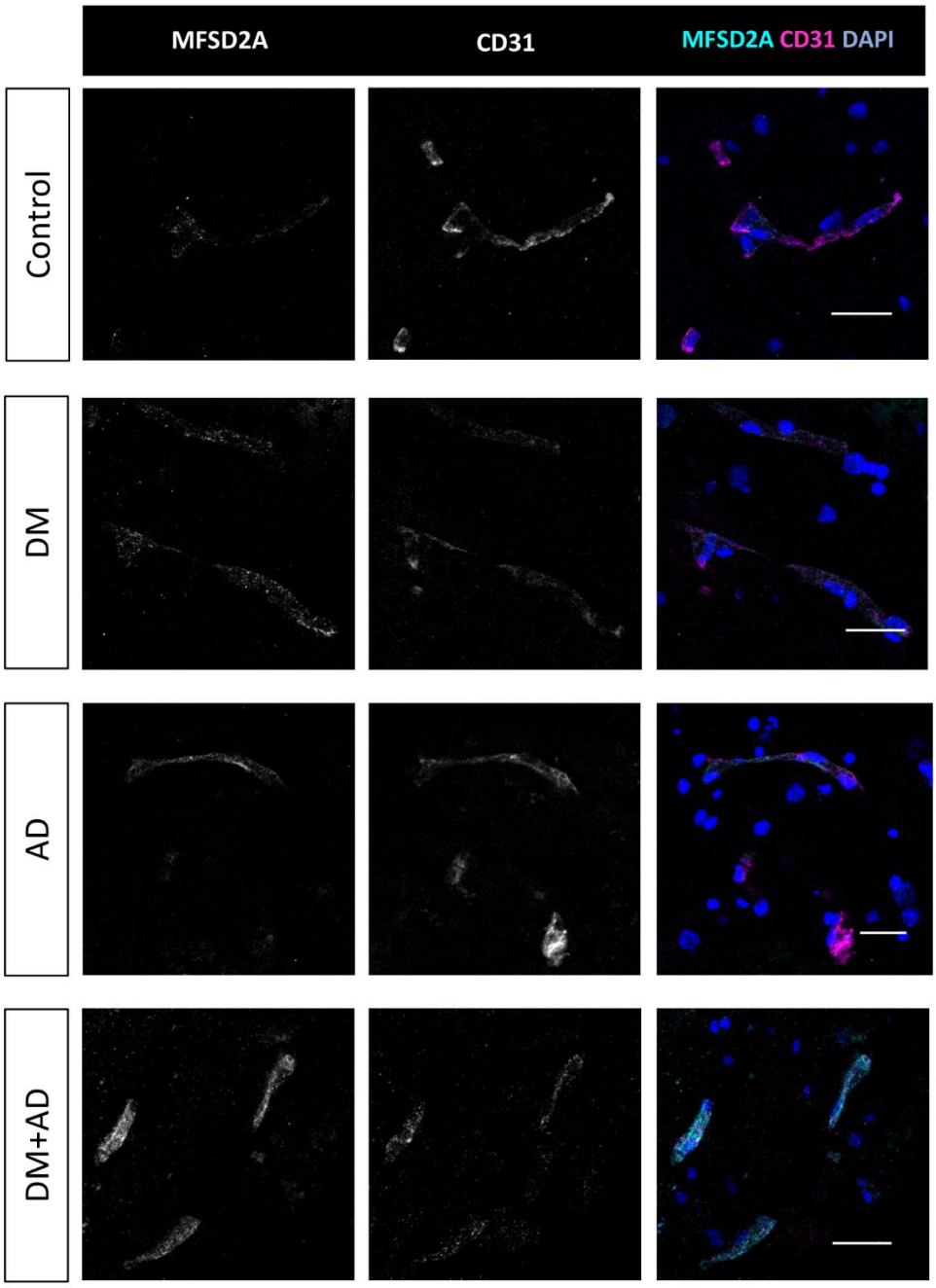

Supplementary Figure S7. Immunofluorescence staining of MFSD2A in the human frontal cortex. Representative confocal microscopy images of MFSD2A (cyan) immunofluorescence staining in human cortical cryosections (10 µm) (Control, DM, AD, DM+AD). Vascular endothelial cells are stained for CD31 (magenta) and nuclei are stained with DAPI (blue). Scale bar: 30 µm.

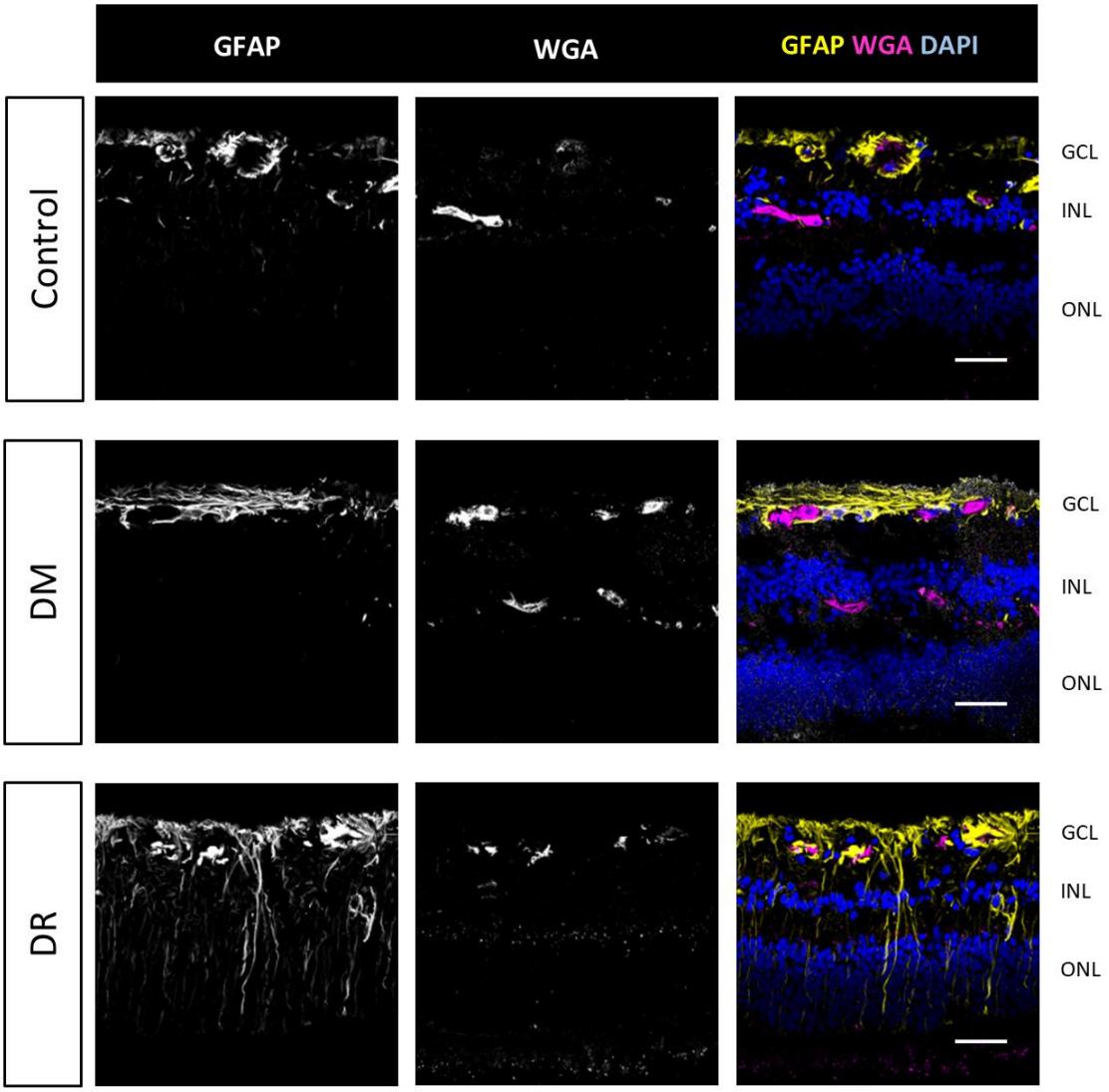

Supplementary Figure S8. Immunofluorescence staining of glial fibrillary acidic protein (GFAP) in the human retina. Representative confocal microscopy images of immunofluorescence staining of GFAP-positive (yellow) macroglia in human retinal cryosections (10 µm) (Control, DM, DR). Vascular endothelial cells are stained with wheat germ agglutinin (WGA; magenta) and nuclei are stained with DAPI (blue). GCL = ganglion cell layer; INL = inner nuclear layer; ONL = outer nuclear layer. Scale bar: 50 µm.

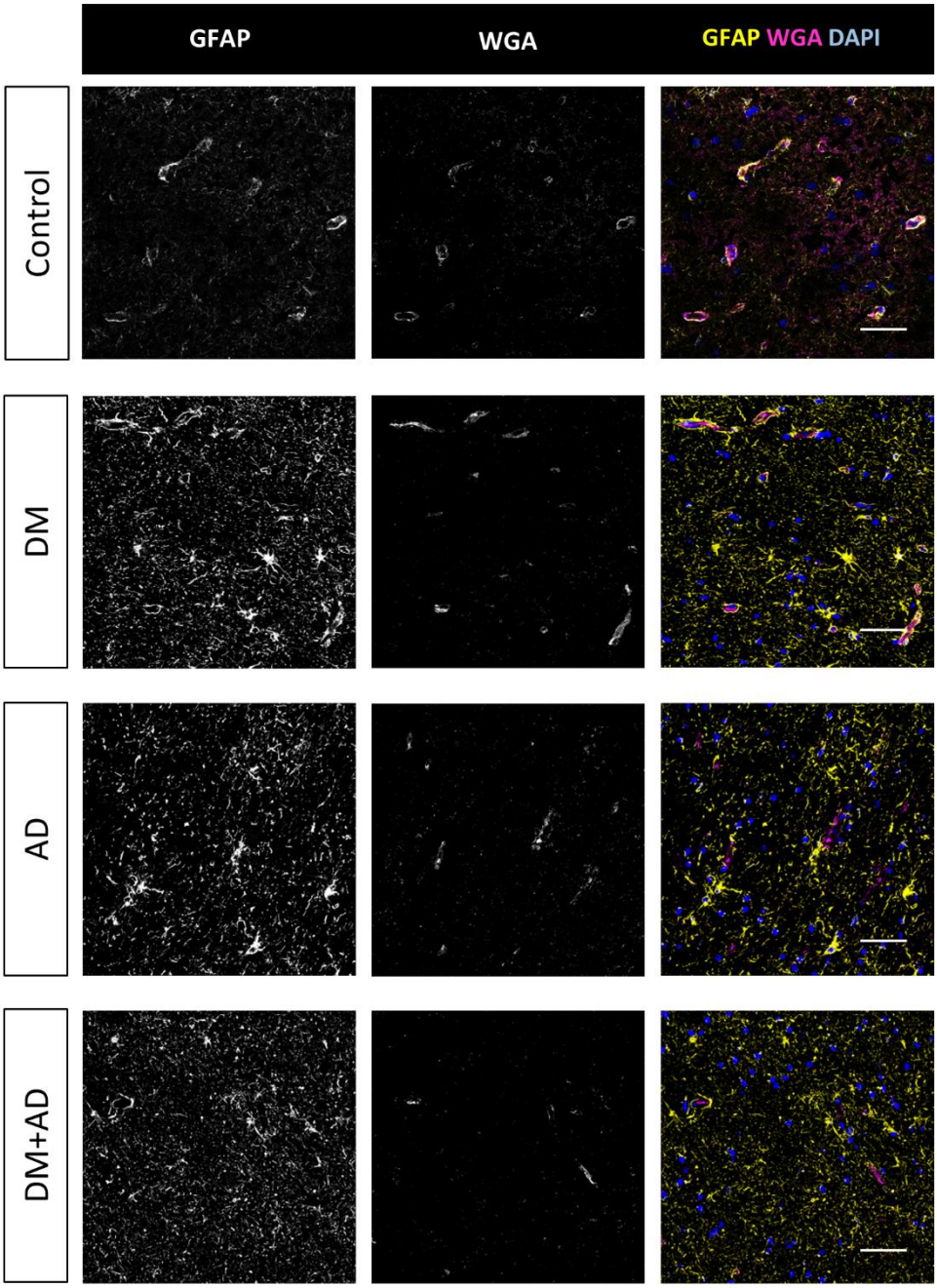

Supplementary Figure S9. Immunofluorescence staining of glial fibrillary acidic protein (GFAP) in the human frontal cortex. Representative confocal microscopy images of immunofluorescence staining of GFAP-positive (yellow) astrocytes in human cortical cryosections (10 µm) (Control, DM, AD, DM+AD). Vascular endothelial cells are stained with wheat germ agglutinin (WGA; magenta) and nuclei are stained with DAPI (blue). Scale bar: 50 µm.

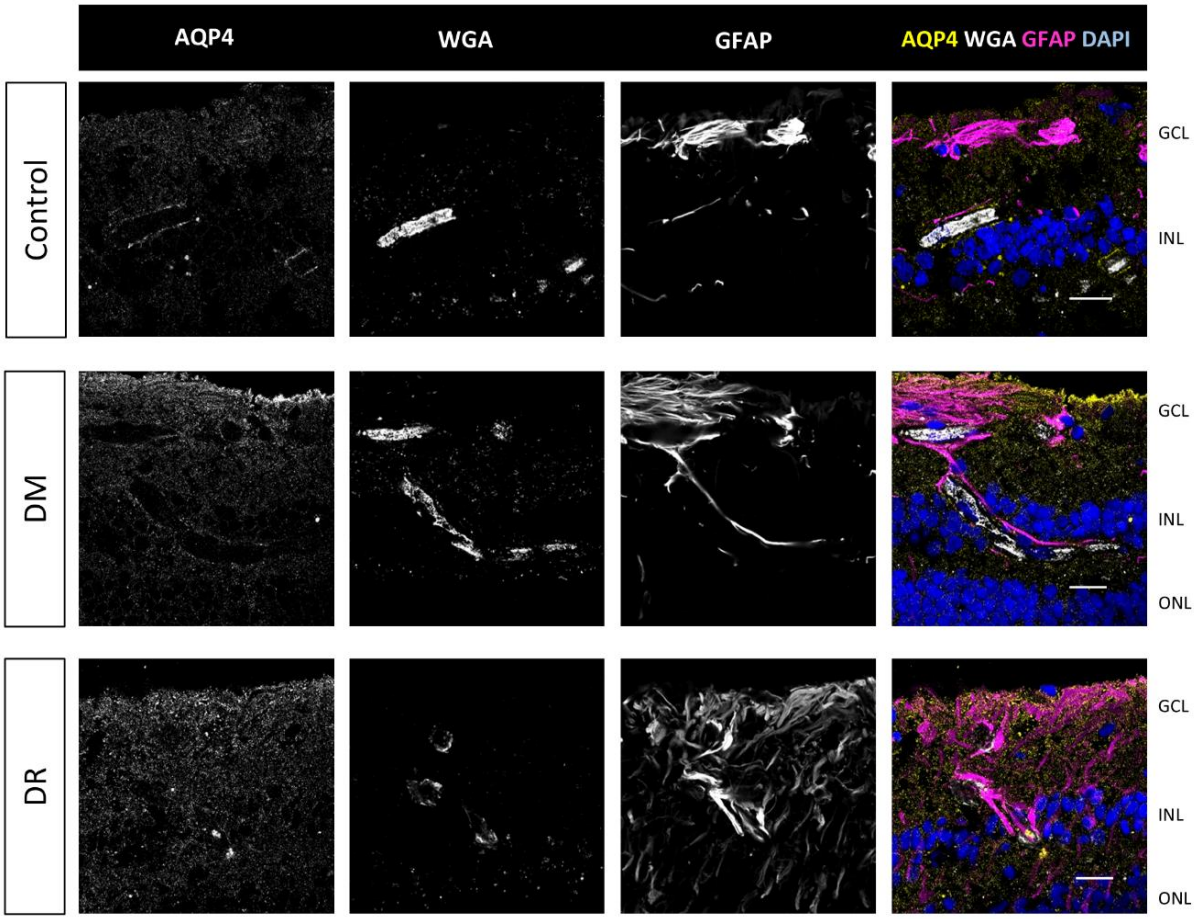

Supplementary Figure S10. Immunofluorescence staining of aquaporin-4 (AQP4) in the human retina. Representative confocal microscopy images of immunofluorescence double staining for the water channel AQP4 (yellow) and GFAP-positive (magenta) macroglia in human retinal cryosections (10 µm) (Control, DM, DR). Vascular endothelial cells are stained with wheat germ agglutinin (WGA; white) and nuclei are stained with DAPI (blue). GCL = ganglion cell layer; INL = inner nuclear layer; ONL = outer nuclear layer. Scale bar: 20 µm.

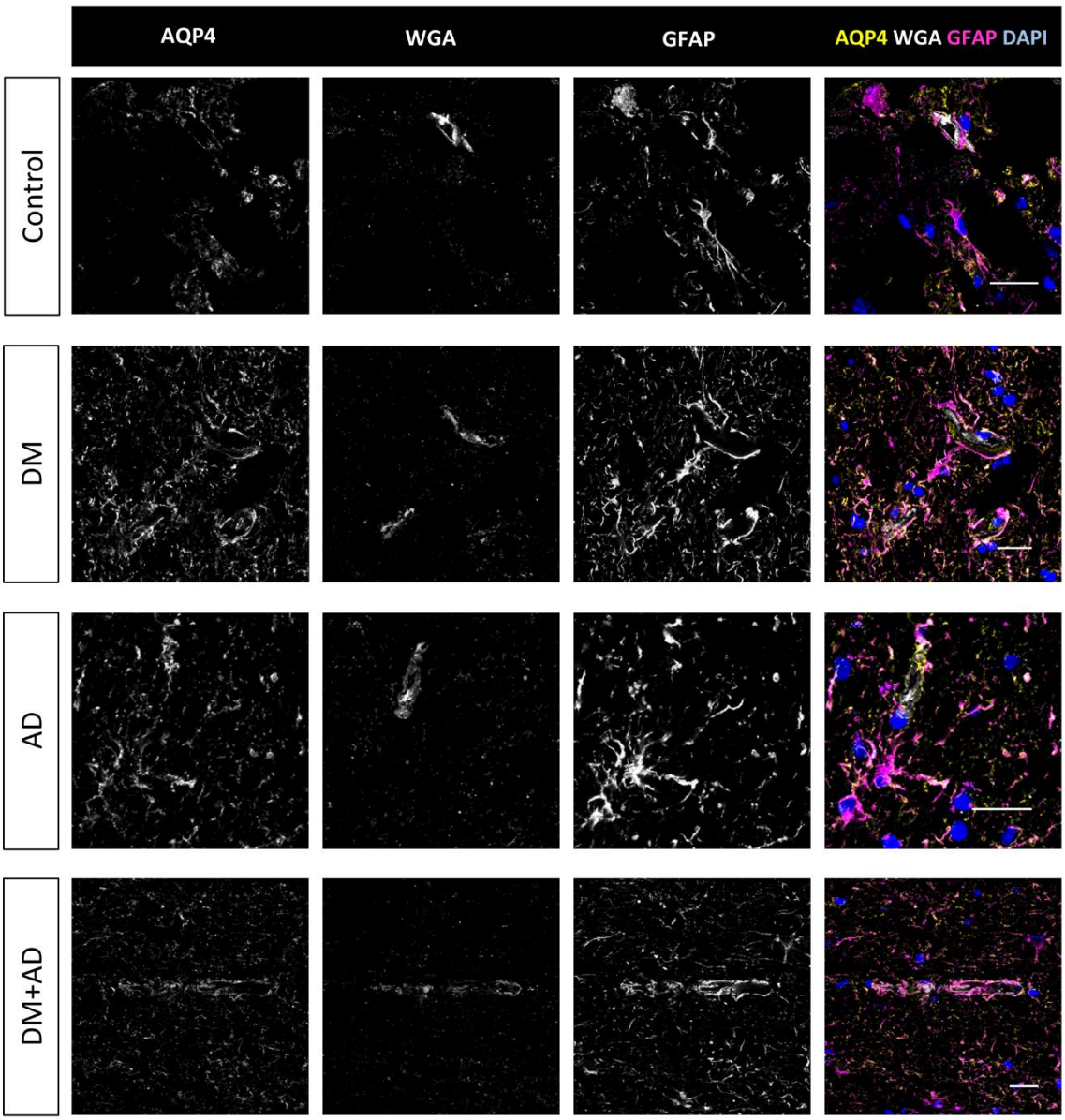

Supplementary Figure S11. Immunofluorescence staining of aquaporin-4 (AQP4) in the human frontal cortex. Representative confocal microscopy images of immunofluorescence double staining of the water channel AQP4 (yellow) and GFAP-positive (magenta) astrocytes in human cortical cryosections (10 µm) (Control, DM, AD, DM+AD).Vascular endothelial cells are stained with wheat germ agglutinin (WGA; white) and nuclei are stained with DAPI (blue). Scale bar: 20 µm.

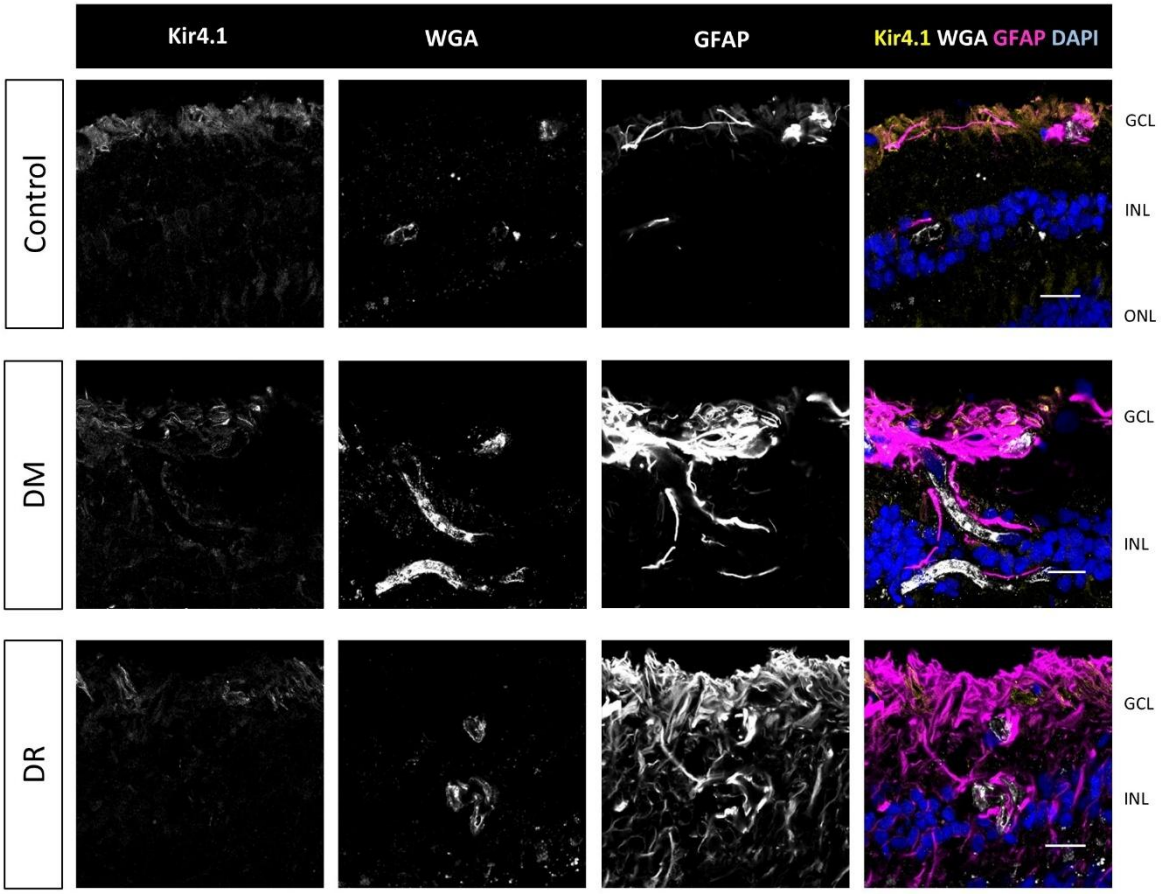

Supplementary Figure S12. Immunofluorescence staining of Kir4.1 in the human retina.
Representative confocal microscopy images of immunofluorescence double staining for the inwardly rectifying potassium channel Kir4.1 (yellow) and GFAP-positive (magenta) macroglia in human retinal cryosections (10 µm) (Control, DM, DR). Vascular endothelial cells are stained with wheat germ agglutinin (WGA; white) and nuclei are stained with DAPI (blue). GCL = ganglion cell layer; INL = inner nuclear layer; ONL = outer nuclear layer. Scale bar: 20 µm.

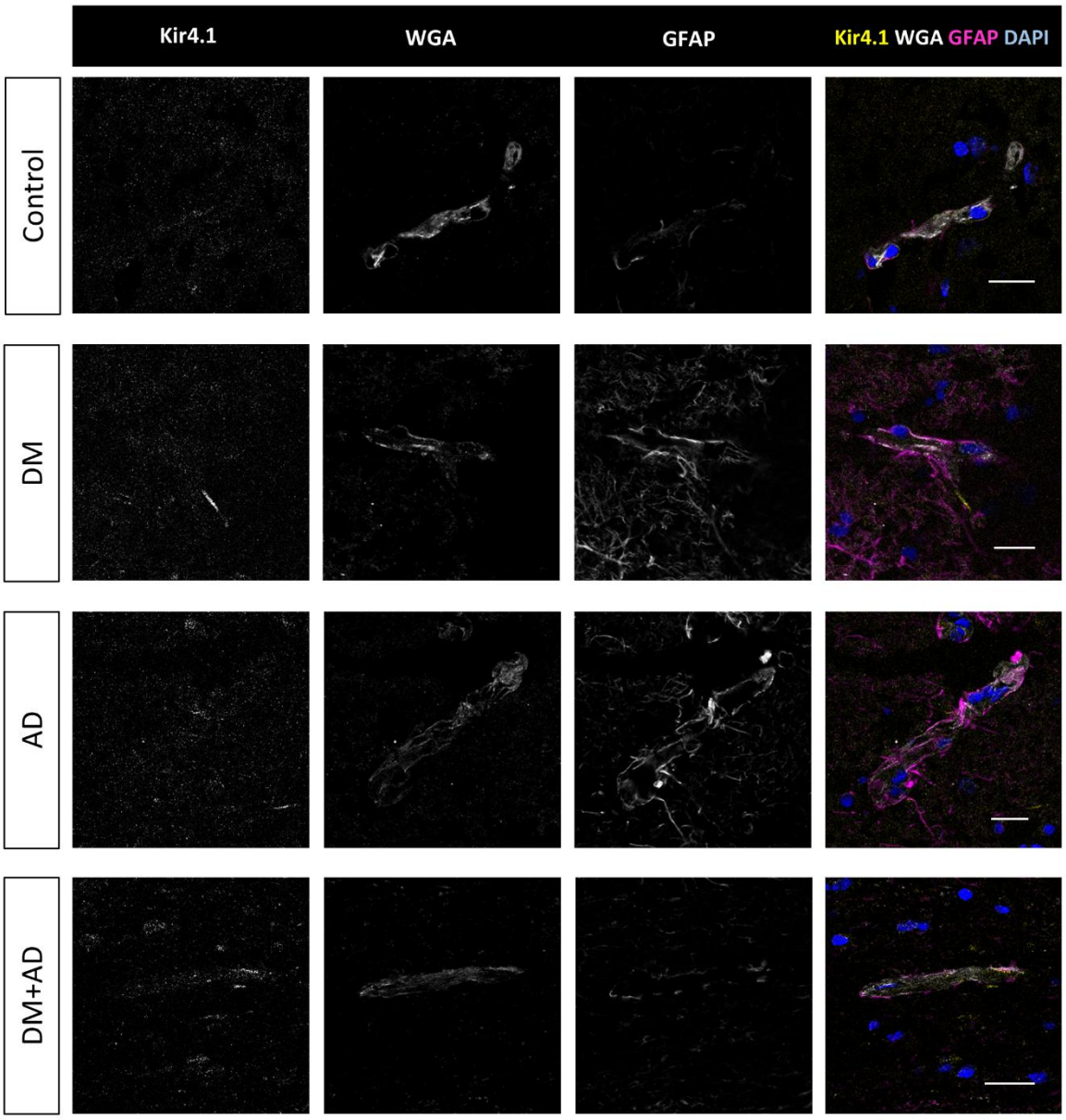

Supplementary Figure S13. Immunofluorescence staining of Kir4.1 in the human frontal cortex. Representative confocal microscopy images of immunofluorescence double staining for the inwardly rectifying potassium channel Kir4.1 (yellow) and GFAP-positive (magenta) astrocytes in human cortical cryosections (10 µm) (Control, DM, AD, DM+AD).Vascular endothelial cells are stained with wheat germ agglutinin (WGA; white) and nuclei are stained with DAPI (blue). Scale bar: 20 µm.

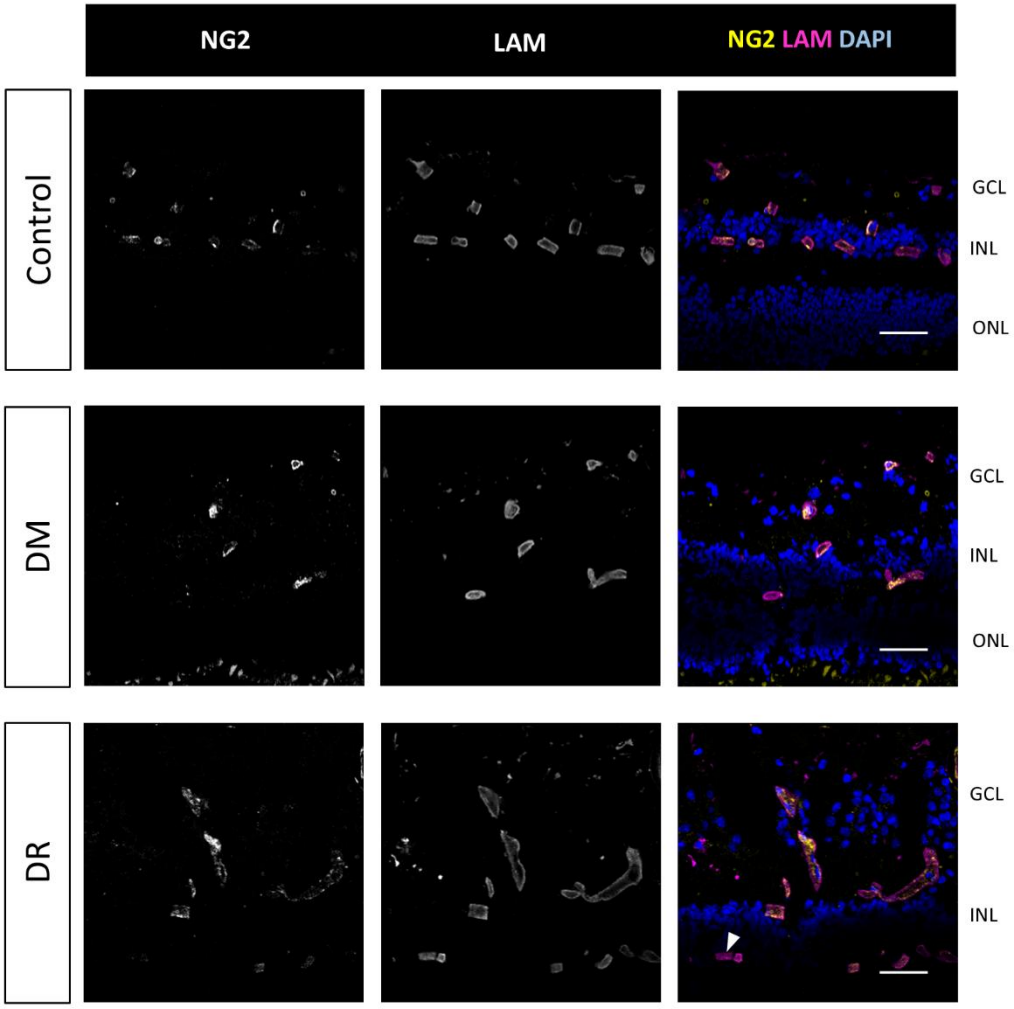

Supplementary Figure S14. Immunofluorescence staining of NG2 in the human retina.
Representative confocal microscopy images of immunofluorescence staining of NG2-positive (yellow) pericytes on the vasculature in human retinal cryosections (10 µm) (Control, DM, DR). The basal lamina of blood vessels is stained for laminin (LAM; magenta), and nuclei are stained with DAPI (blue). The white arrowhead indicates an example of pericyte loss. GCL = ganglion cell layer; INL = inner nuclear layer; ONL = outer nuclear layer. Scale bar: 50 µm.

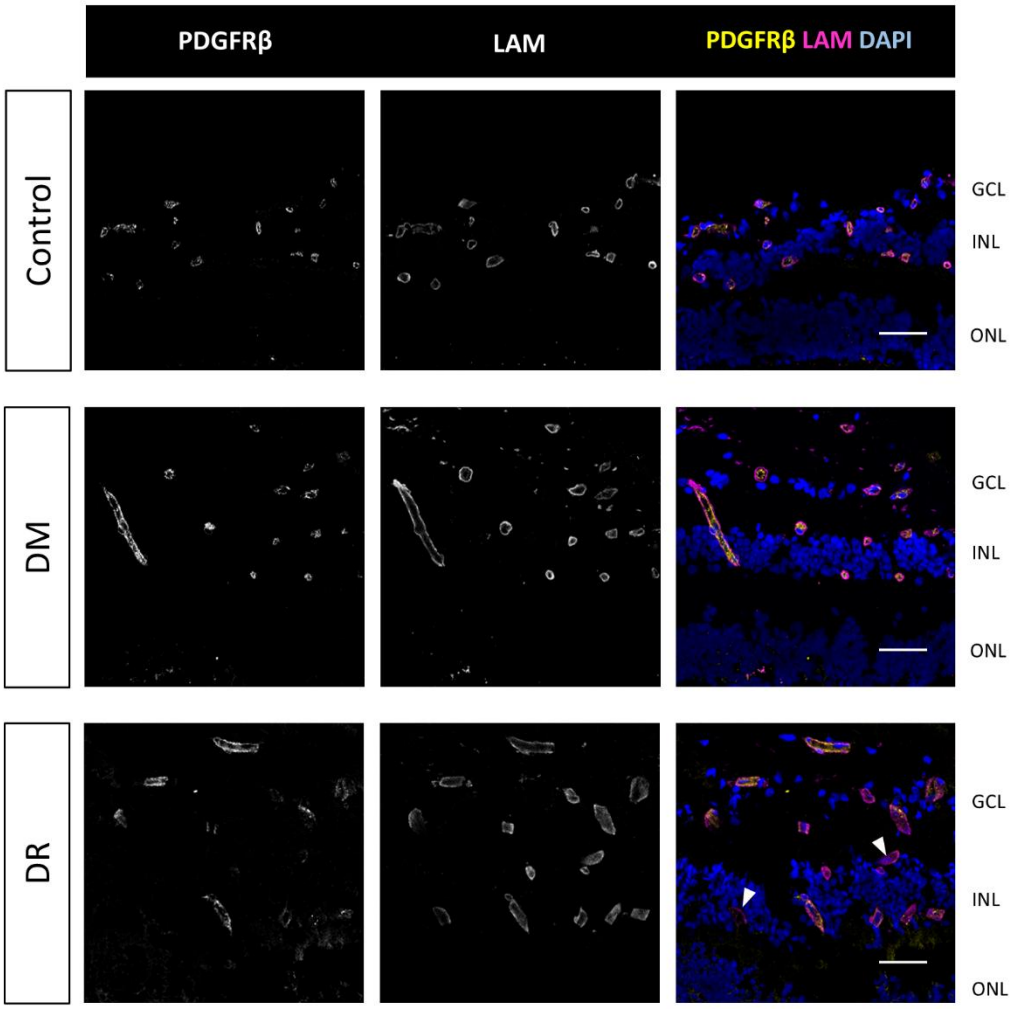

Supplementary Figure S15. Immunofluorescence staining of PDGFRβ in the human retina. Representative confocal microscopy images of immunofluorescence staining of PDGFRβ-positive (yellow) pericytes on the vasculature in human retinal cryosections (10 µm) (Control, DM, DR). The basal lamina of blood vessels is stained for laminin (LAM; magenta), and nuclei are stained with DAPI (blue). White arrowheads indicate examples of pericyte loss. GCL = ganglion cell layer; INL = inner nuclear layer; ONL = outer nuclear layer. Scale bar: 50 µm.

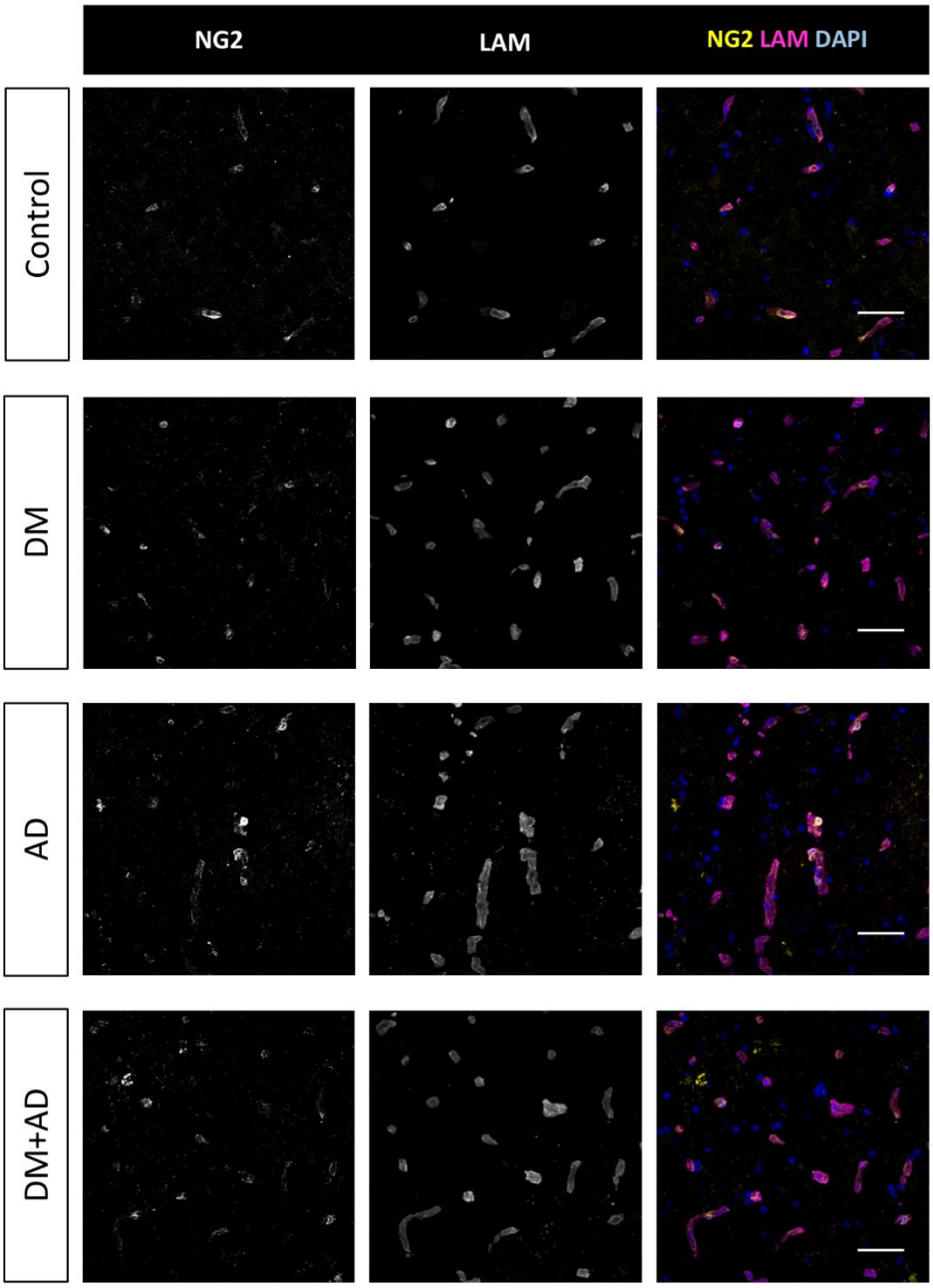

Supplementary Figure S16. Immunofluorescence staining of NG2 in the human frontal cortex. Representative confocal microscopy images of immunofluorescence staining of NG2-positive (yellow) pericytes on the vasculature in human cortical cryosections (10 µm) (Control, DM, AD, DM+AD). The basal lamina of blood vessels is stained for laminin (LAM; magenta), and nuclei are stained with DAPI (blue). Scale bar: 50 µm.

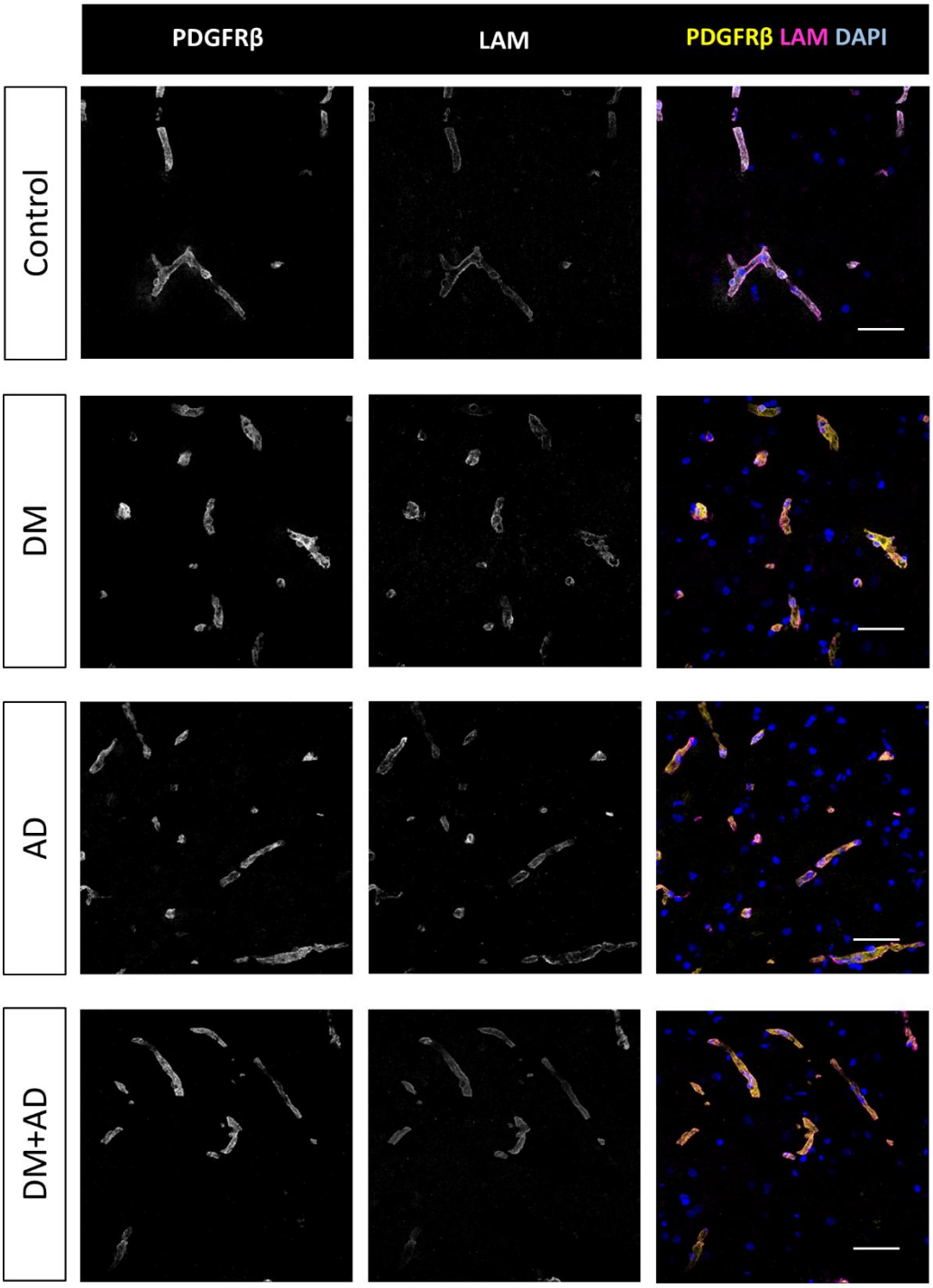

Supplementary Figure S17. Immunofluorescence staining of PDGFRβ in the human frontal cortex. Representative confocal microscopy images of immunofluorescence staining of PDGFRβ-positive (yellow) pericytes on the vasculature in human cortical cryosections (10 µm) (Control, DM, AD, DM+AD). The basal lamina of blood vessels is stained for laminin (LAM; magenta), and nuclei are stained with DAPI (blue). Scale bar: 50 µm.

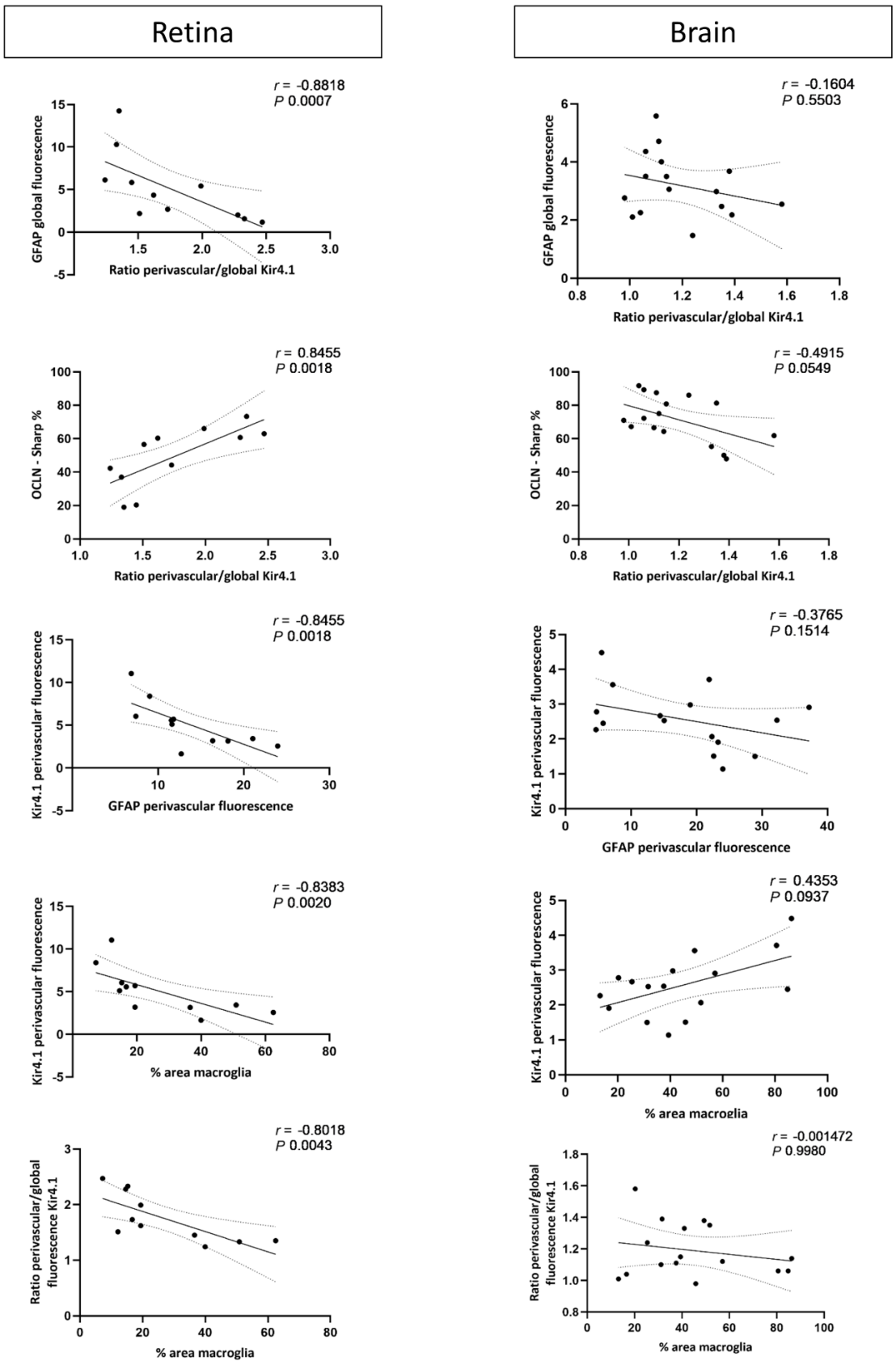

Supplementary Figure S18. Highest correlation found for NVU parameters in the retina as compared with correlations in the brain.

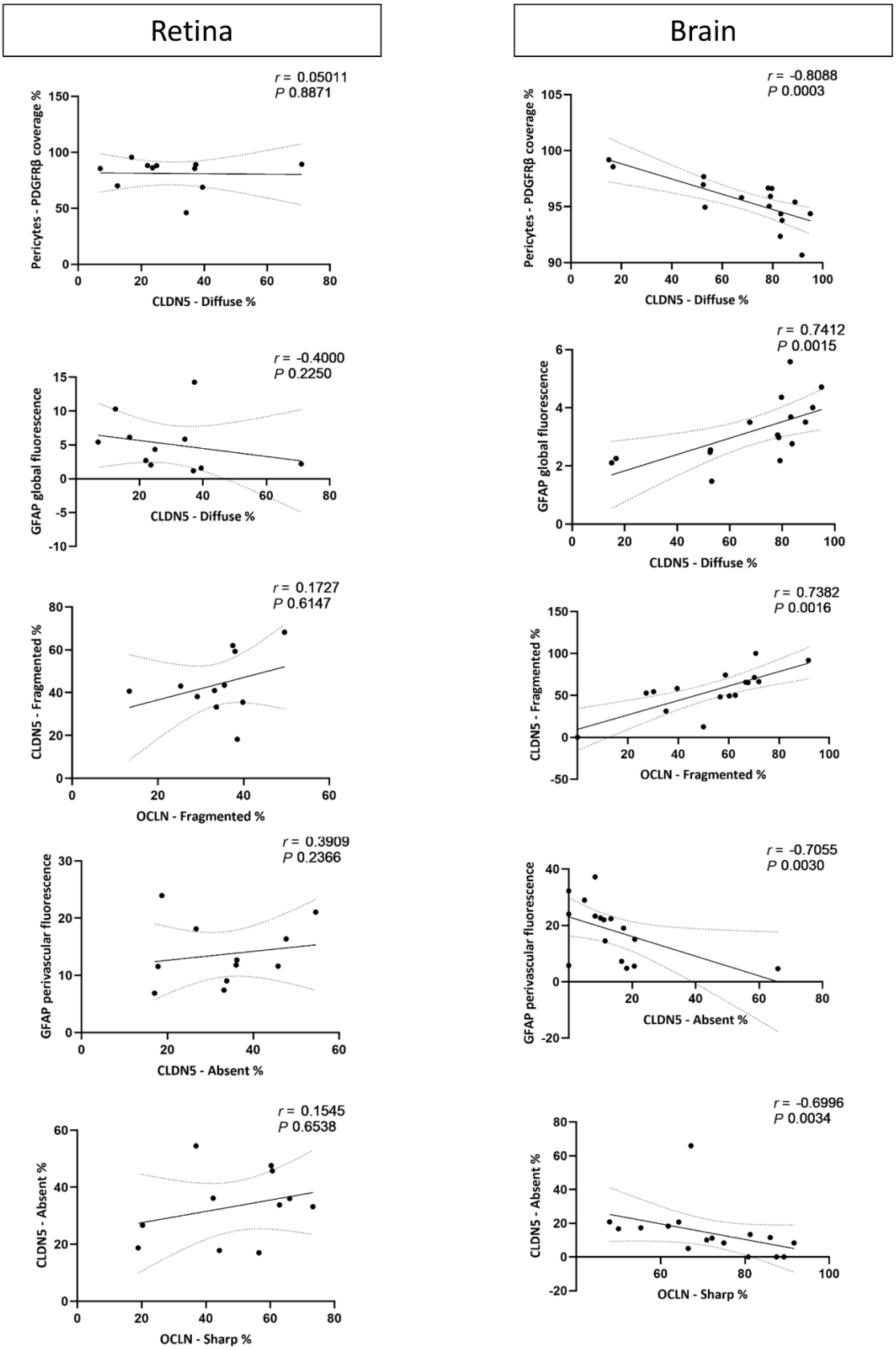

Supplementary Figure S19. Highest correlation found for NVU parameters in the brain as compared with correlations in the retina.

Chapter 5

Development of Immunostaining Protocols for 3D Visualization of Pericytes in Human Retinal Flatmounts

Noëlle Bakker[1,2,3], Aïcha A. Croes[1], Eva Prevaes[1], Cornelis J. F. van Noorden[1], Reinier O. Schlingemann[1,2,3,4], and Ingeborg Klaassen[1,2,3], on behalf of the RECOGNISED Consortium

[1] Ocular Angiogenesis Group, Department of Ophthalmology, Amsterdam UMC location University of Amsterdam, Amsterdam, The Netherlands.
[2] Amsterdam Cardiovascular Sciences, Microcirculation, Amsterdam, The Netherlands.
[3] Amsterdam Neuroscience, Cellular & Molecular Mechanisms, Amsterdam, The Netherlands.
[4] Department of Ophthalmology, Jules-Gonin Eye Hospital, Fondation Asile des Aveugles, University of Lausanne, Lausanne, Switzerland

Journal of Histochemistry & Cytochemistry (2025) 73(3-4):147-170

Abstract

Vascular pericytes are widely present across the human body and crucial in regulating vascular flow, permeability, and homeostasis. In the human retina, pericytes are important for forming and maintaining the blood–retinal barrier, as well as for autoregulation of blood flow. Pericyte loss has been implicated in various pathological conditions. Visualization of pericytes by immunofluorescence (IF) staining provides valuable information on pericyte number, morphology, location, and on expression of anatomic and functional markers. However, species-specific differences in pericyte marker expression exist. In this study, we aimed to develop a novel IF co-staining protocol to detect the pericyte markers NG2, PDGFRβ, αSMA, CD13, and RFC1 in human retinal flatmounts. Unlike retinal sections, retinal flatmounts enable 3D visualization of pericyte distribution across the entire vascular network. Key optimizations included tailoring the fixation method, blocking buffer composition and antibody solvent, as well as using jasplakinolide to enhance αSMA detection. Our protocol successfully enabled double staining of NG2 and PDGFRβ, as well as αSMA and PDGFRβ, whereas CD13 and RFC1 expression was not detectable in human retinal flatmounts. This novel 3D IF protocol enhances in situ visualization of human retinal pericytes, enabling accurate studies of their role in vascular health and disease to aid targeted therapy development.

Introduction

Pericytes play a crucial role in the formation and maintenance of the inner blood-retinal barrier (iBRB) and blood-brain barrier (BBB). Pericyte dysfunction or loss is a hallmark of a wide range of diseases including Alzheimer's disease, diabetes-induced microvascular diseases throughout the body, such as diabetic retinopathy (DR), macular oedema and various infectious diseases [1-4]. Changes in pericyte functions during pathological conditions are reflected in altered marker profiles [5]. Therefore, we aimed to identify reliable pericyte markers. Pericyte markers identified in this study will ultimately be used in immunofluorescence (IF) staining to study pericytes under pathological conditions. Important to highlight is that most previous studies have been performed in animal models and knowledge about pericyte marker expression in the human retina is limited.

Pericytes are mural cells embedded in the microvascular wall and are important in vascular development and homeostasis [5]. In retinal capillaries, this is also reflected by the high prevalence of pericytes in the BRB in comparison with other organs, as the ratio of pericyte to endothelial cell is 1:1–1:3 [4-9]. Pericytes of the iBRB and BBB are part of the neurovascular unit, together with endothelial cells, glial cells, microglia, neurons and a basal lamina (Figure 1) [10-12]. These cell types are in constant to regulate the permeability and function of the barrier in the brain and retina [13], thereby tightly controlling the transport of molecules and cells in and out of surrounding tissues. This highly specialized environment ensures proper functioning of neuronal tissue in the retina and brain [14, 15].

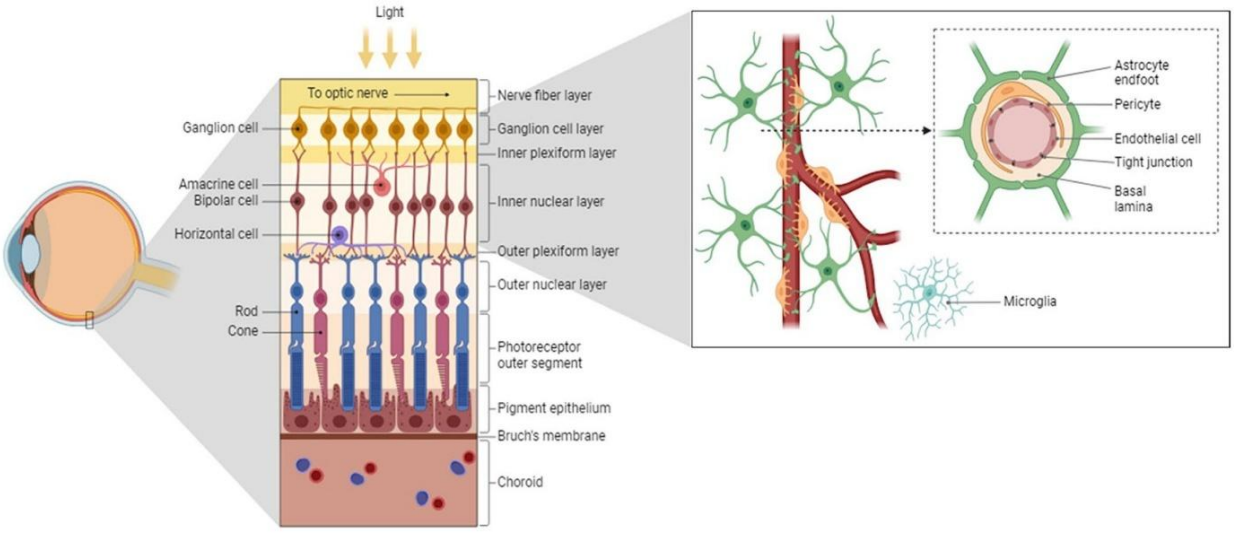

Figure 1. Retinal morphology and structure of the neurovascular unit of the inner blood-retinal barrier. The left panel shows the retinal layers. The microvasculature in the inner retina forms the inner blood retinal barrier (iBRB) (right panel). The iBRB protects the neuronal layers in the retina and consists of endothelial cells forming capillaries in the retina as part of the neurovascular unit. This unit also includes pericytes sharing the basal lamina with endothelial cells, microglia, astrocytes projecting their end feet onto the capillaries, and surrounding neurons. Created with BioRender.com.

Under physiological conditions, pericytes maintain the barrier physically by regulating the polarization of astrocyte endfeet [16], by inhibiting transcytosis, and by inducing expression of tight junction proteins by endothelial cells [14]. Pericytes locally regulate blood flow, clear

harmful metabolites such as lactate released in the extracellular matrix by endothelial cells [6, 17], control endothelial cell proliferation, and contribute to the basal lamina by secreting extracellular matrix proteins [18, 19]. In this way, pericytes stabilize existing and newly-formed blood vessels.

To date, there is no single universal marker exclusively specific for pericytes in the iBRB and BBB. Pericytes are a heterogeneous cell population, and their identification often relies on a combination of markers. Markers that are often used in such a combination are platelet-derived growth factor receptor β (PDGFRβ), nerve/glial antigen 2 (NG2), CD13 (also known as aminopeptidase N), alpha smooth muscle actin (αSMA), and desmin [5, 20, 21]. A more recently identified pericyte marker is reduced folate carrier 1 (RFC1), also named solute carrier family 19 member 1 (SLC19A1) [22, 23]. However, all these markers identify either a subset of pericytes in the tissue or are not uniquely expressed by pericytes, but by other cell types as well. Pericytes can be best identified on the basis of a combination of their location in capillary walls, morphological characteristics and expression of molecular markers. Notably, there are differences in the ontogeny of pericytes in the central nervous system as compared to pericytes elsewhere in the body [5]. Therefore, the marker expression of pericytes differs between organs, and there are also differences between species [24-26].

To investigate the expression of various molecular markers in human retinal pericytes, we performed IF staining using antibodies against NG2, PDGFRβ, αSMA, CD13 and RFC1 in human retinal flatmounts. The NG2 proteoglycan, also known as chondroitin sulfate proteoglycan-4, melanoma proteoglycan or high-molecular weight melanoma-associated antigen [27], is a transmembrane receptor that interacts extracellularly with more than 40 presumed ligands and can interact intracellularly with the cytoskeleton [28, 29]. NG2 is important in pericyte proliferation, motility and formation and maturation of endothelial junctions through the integrin signaling pathway [27, 28, 30]. It has been reported to have higher expression in activated pericytes in tumor stroma and wound healing tissues [27]. PDGFRβ is a membrane-bound receptor, of which one of its major ligands, PDGF-B, is expressed by endothelial cells [31, 32]. Pericyte proliferation and recruitment to vascular endothelial cells is promoted by the PDGF-B/PDGFRβ signaling pathway [33-36]. αSMA is a contractile protein found in smooth muscle cells and a subset of pericytes [37, 38]. Pericytes expressing αSMA were found at the branching points of retinal capillaries in mice, suggesting their role in vessel contraction [38]. CD13 is a membrane-bound metalloprotease that proteolytically activates or inactivates regulatory peptides, such as enkephalins, neurotensin and somatostatin [18, 19, 39, 40]. In addition, CD13 is involved in the nociception pathway and in inflammation through inactivation of the cytokine interleukin-8 [40]. CD13 promotes pericyte proliferation and migration in response to stimulation with angiogenic growth factors [41, 42]. In a previous *in vitro* study, increased expression of CD13 in migratory pericytes was observed, suggesting that the motility of pericytes may be increased, at least partly, via CD13 proteolysis [42]. The novel pericyte marker RFC1, identified by single-cell expression profiling of retinal microvessels in adult mice [22, 23], is a membrane transport protein. RFC1 is responsible for transport of the B9 family of vitamins, known as folates, or a subset of cyclic dinucleotides, driven by the export of organic anions across the BRB [22, 23]. The presence of RFC1 highlights the importance of pericytes in vitamin metabolism, which is crucial for DNA replication and repair.

The expression of these markers in pericytes may change in pathological conditions. While pericytes in healthy tissue exhibit αSMA expression to a limited extent, αSMA expression alters in pericytes in DR, tumor angiogenesis, fibrosis and inflammation [5, 43, 44]. In DR, signaling through PDGFRβ is impaired, which may play a role in pericyte apoptosis [5]. A reduction in NG2 expression in retinal pericytes was found in previous studies in streptozotocin-induced diabetic mice [45-47].

IF staining provides spatiotemporal information about pericyte markers at a quantitative level [48]. IF methodology optimization is key for each pericyte marker before studying the changes in marker expression in pericytes in pathological conditions. The current study includes retinal flatmounts instead of retinal sections to enhance spatial information. In this way, pericytes can be reconstructed in 3D after IF staining, and flatmounts provide insights in the pericyte location in relation to arteries, microvascular branching and veins. To our knowledge, IF staining has not been performed on human retinal flatmounts for any pericyte marker apart from one study that investigated PDGFRβ in Alzheimer's disease [49]. Therefore, we have developed an IF protocol for detecting various pericyte markers in human retinal flatmounts. This IF methodology can be applied to study how various diseases affect pericytes in the human retina.

Material and methods

Human retina

Human post-mortem eyes were provided by the Corneabank, Beverwijk, the Netherlands. The current research was performed in accordance with all requirements stated in the Dutch law "Wet op orgaandonatie" that describes the use of donor material for research purposes. According to this law, donors provide written informed consent for donation with an opt out of left-over material for related scientific research purposes. Specific requirements for the use for scientific research of left-over material originating from corneal grafting have been described in an additional document formulated by the Ministry of Health, Welfare, and Sport and the BIS foundation (Eurotransplant; Leiden, July 21, 1995; 6714.ht). The eyes were stored anonymously and therefore, approval of their use by the Ethics Committee was not required by Dutch law. The use of human material was also in accordance with the Declaration of Helsinki on the use of human material for scientific research. Several hours post mortem, eyes were enucleated and the anterior parts of the eye, including the cornea and lens, were dissected. Fundoscopy images of the retina were taken before storage in the freezer and were evaluated by two independent ophthalmologists to determine the ophthalmologic status. The eyecup was filled with Tissue-tek (cat# 4583, Sakura, Finetek Europe, Alphen aan de Rijn, The Netherlands) and eyes were snap frozen before being stored at −80 °C. Information on the type and duration of diabetes, when available, was kindly provided by Bio Implant Services Foundation (Leiden, The Netherlands). A summary of donor characteristics is listed in Table 1. Radial cuts of the eyecup were made to facilitate staining and microscopical imaging of the staining.

Table 1. Donor information for retinal tissues.

Case	Ophthal-mological status	Sex (F/M)	Age at death (y)	Post-mortem delay (h)	Diagnosis	Cause of death
1	Normal	M	49	15	Melanoma	Heart dysfunction
2	Normal	F	54	20	Tendinitis wrist	Circulatory system complication
3	Normal	F	68	14	Stomach cancer	Cancer
4	Normal	F	67	5	Atherosclerosis, chronic kidney failure, percutaneous transluminal coronary angioplasty	Circulatory system complication

Fixation of retinal tissue

The eyecup pieces were fixed with 4% formaldehyde (28908, Thermo Fisher Scientific, Bleiswijk, The Netherlands) at 4°C and were washed twice in phosphate buffered saline (PBS) for 10 min, after which the retina was detached from the eyecup and cut into sections to compare various experimental conditions. The sectioned retinas were collected in a PCR tube. Various additional fixation methods of human retinal flatmounts were tested: (1) methanol gradient fixation, which exists of a gradient of methanol in PBS with 0.1% Tween20 (PBST) for 10 min (25% >50%>75%>100%), followed by rehydration with a reversed gradient (0.2 M hydrogen chloride in 100% methanol for 30 min>75% (in PBST for 10 min)>50%>25%) at room temperature (RT); (2) cold methanol fixation with 100% methanol pre-chilled at -20°C and incubated at -20°C; or (3) no methanol fixation. After methanol treatment, flatmounts were washed twice in PBS for 10 min. To minimize the use of human tissue, 10 µm retinal cryosections were included for double staining with antibodies against PDGFRβ and RFC1, instead of flatmounts. Cryosections were air-dried for 20 min and fixed with 4% formaldehyde for 20 min. Sections were washed 3 times in PBS for 10 min. For all fixation conditions, the washing step was directly followed by incubation of blocking buffer.

Permeabilization and blocking of retinal tissue

Flatmounts and cryosections were subsequently incubated in blocking buffers for 1 h at RT unless stated otherwise. Different blocking buffers, with varying quantities of Triton X-100 (TX; T8787, Merck Life Science, Amsterdam, The Netherlands), fetal bovine serum (FBS; F7524, Merck Life Science), normal goat serum (0060-01, Southern Biotech, Birmingham, AL), normal donkey serum (0030-01, Southern Biotech), Tween20 (P1379, Merck Life Science), bovine serum albumin (BSA; 10735094001, Roche Diagnostics GmbH, Mannheim, Germany), or sodium azide (1.06688.0100, Merck Life Science) in PBS or Tris-buffered saline, were tested. Details on blocking buffer content are shown in Table 2. Blocking buffer 2 was previously described in the IF staining protocol for murine retinal wholemounts by Van der

Wijk et al. [50]. Immediately after the blocking procedure, flatmounts and cryosections were incubated with primary antibodies.

Table 2. Blocking buffers used in this study.

Blocking buffer number	Blocking buffer content
1	PBS-0.3%TX + 0.2% BSA + 5% normal goat/donkey serum
2	PBS-3%TX + 1% FBS + 0.5% Tween20 + 0.1% sodium azide
3	PBS-0.1%TX + 10% normal donkey serum
4	PBS-0.1%TX + 5% BSA
5	PBS-0.1%TX + 2% BSA
6	PBS + 5% BSA
7	PBS-0.5%TX + 2% BSA + 0.2 M glycine
8	PBS-0.5%TX + 10% normal donkey serum
9	Tris-buffered saline-0.3%TX
10	PBS + 10% normal donkey serum

BSA = bovine serum albumin, FBS = fetal bovine serum, PBS = phosphate buffered saline, PBS-0.3%TX = PBS supplemented with 0.3% Triton X-100

Jasplakinolide treatment for actin stabilization

For double staining of PDGFRβ and αSMA, fixation and blocking were adapted from the methods described in Mai-Morente et al [51]. Jasplakinolide was included as a F-actin stabilizing reagent to enhance αSMA detection. Flatmounts were first incubated with a blocking buffer. Immediately after blocking, flatmounts were incubated with jasplakinolide (20 µM) (ab141409, Abcam, Amsterdam, The Netherlands) for 40 min at 4°C, followed by fixation. Subsequently, flatmounts were washed 3 times for 10 min with PBS-0.05%TX. Alternatively, flatmounts were incubated with jasplakinolide followed by fixation and incubation with a blocking buffer. Then, flatmounts were washed 3 times for 10 min with PBS-0.05%TX. Additionally, a condition without jasplakinolide was included.

IF staining of pericyte markers in human retinal flatmounts

Flatmounts and cryosections were incubated overnight with primary antibodies against NG2, PDGFRβ, αSMA, CD13 and RFC1 at 4°C (Table 3). Antibody solvents with varying quantities of TX, FBS, NGS, NDS, Tween20, BSA or sodium azide in PBS or Tris-buffered saline were tested and are described in Table 4. Antibody solvent 4 was previously described in the IF staining protocol for hippocampal slices by Mai-Morente et al. [47]. Additionally, commercially available (phosphate buffered) normal antibody diluent (ABB999, ScyTek Laboratories, Logan, UT) was tested as antibody solvent as well as antibody solvents identical to the blocking buffer (NG2; CD13).

Table 3. Primary antibodies used in this study.

Antigen	Host species	Source	Working dilution	Working concentration
Collagen type IV	Mouse	Invitrogen, MA1-22148	1:1000	7.9 µg/ml
Laminin	Rabbit	Abcam, Ab11575	1:1000	0.72 µg/ml
NG2	Mouse	Merck Life Science, MAB2029	1:100	10 µg/ml
PDGFRβ	Goat	R&D Systems, AF385	1:100	2 µg/ml
αSMA	Mouse	DAKO, M0851	1:250-1000	71-284 µg/l
CD13	Mouse	R&D Systems, MAB3815	1:200	2.5 µg/ml
RFC1	Rabbit	Merck Life Science, AV44167	1:100-500	1-10 µg/ml

NG2 = neural/glial antigen 2, PDGFRβ = platelet-derived growth factor receptor beta, RFC = reduced folate carrier, αSMA = alpha smooth muscle actin. Invitrogen (Waltcam, MA); R&D systems (Minneapolis, MI); DAKO (Santa Clara, CA).

Table 4. Solvents used for antibody dilution in this study.

Solvent number	Solvent content
1	(phosphate buffered) normal antibody diluent
2	PBS-0.01%TX + 1% BSA
3	PBS-0.01%TX + 0.2% BSA
4	PBS-0.5%TX + 2% BSA

BSA = bovine serum albumin, PBS = phosphate buffered saline, PBS-0.01%TX = PBS supplemented with 0.01% Triton X-100.

Different antibody concentrations were tested for RFC1 and αSMA (Table 3). As a negative control, primary antibodies were omitted. After primary antibody incubation, flatmounts or sections were washed 3 times with PBS-0.3%TX for 20 min (NG2; PDGFRβ), or 3 times with PBS for 20 min (PDGFRB) or 10 min (PDGFRβ and RFC1), or 6 times with PBS for 10 min (PDGFRβ; PDGFRβ and NG2; PDGFRβ and CD13), or 2 times with PBS-0.05%TX for 10 min (PDGFRβ and αSMA). Flatmounts or sections were incubated with secondary antibodies (Table 5) for 2 h at RT in the dark in the same antibody solvent as was used for primary antibodies. Following secondary antibody incubation, flatmounts were washed in the same manner as after primary antibody incubation, apart from double staining of PDGFRβ and αSMA, that was washed 3 times with PBS-0.05%TX for 10 min. Retinal sections were washed 3 times with Tris-buffered saline for 5 min or 3 times with PBS for 10 min.

Table 5. Secondary antibodies used in this study.

Antibody	Conjugate	Source	Working dilution	Working concentration
Donkey anti-rabbit IgG	Alexa Fluor 488	Invitrogen, A-21206	1:400	5 µg/ml
Donkey anti-mouse IgG	Alexa Fluor Plus 488	Invitrogen, A32766	1:1000	2 µg/ml
Goat anti-mouse IgG	Cy3	Jackson, 115-165-166	1:100	15 µg/ml
Goat anti-rabbit IgG	Cy3	Jackson, 111-165-144	1:400	3.75 µg/ml
Donkey anti-goat IgG	Cy3	Jackson, 705-165-147	1:200	7.5 µg/ml
Goat anti-mouse IgG	Alexa Fluor 633	Invitrogen, A-21052	1:500	4 µg/ml
Goat anti-rabbit IgG	Alexa Fluor 633	Invitrogen, A-21071	1:200	10 µg/ml
Donkey anti-rabbit IgG	Alexa Fluor Plus 647	Invitrogen, A32795	1:1000	2 µg/ml
Donkey anti-mouse IgG	Alexa Fluor 647	Invitrogen, A31571	1:200	10 µg/ml

Jackson ImmunoResearch Laboratories (West Grove, PA)

Mounting of retinal tissue

After the final washing step, flatmounts were positioned on a microscope slide with the inside of the eye facing upwards. Flatmounts or cryosections were mounted with Vectashield antifading mounting medium containing DAPI (H-1200-10, Vector Laboratories, Newark, CA, USA), covered with a cover glass and sealed with transparent nail varnish.

Microscopical analysis of pericyte staining

Flatmounts and sections were imaged using a Leica STELLARIS confocal microscope (Leica Microsystems, Wetzlar, Germany) with a HC APO CS2 40x/1.30 oil-immersion objective. The confocal images were made with bidirectional sequential scanning at 1024x1024 resolution with a scanning speed of 600 Hz and line average of 8. Acquired images were processed and exported from Leica Application Suite X.

Expression analysis of CD13 and RFC1

The mRNA expression of ANPEP (CD13) and SLC19A1 (RFC1) in pericytes of the mature human eye, specifically in the retina, was explored using the following resources: The Human Protein Atlas (http://www.proteinatlas.org/, accessed on 16 December 2024), the Human Eye Transcriptome Atlas v3.0 (https://www.eye-transcriptome.com/index.php, accessed on 17 December 2024) and the Eye Integration database of the National Eye Institute (https://eyeintegration.nei.nih.gov/, v2.12accessed on 17 December 2024). This analysis utilized RNA-sequencing data generated by the Genotype-Tissue Expression project accessed from Tissue data in the Human Protein Atlas, selecting “Retina” as tissue. In the Human Eye Transcriptome Atlas, mRNA data of ANPEP and SLC19A1 in the “Retina periphery” and “Retina centre” were selected. mRNA expression of ANPEP and SLC19A1 reported by eyeIntegration was accessed by the Single Cell Plots function, selecting “Mature” and

"Pericyte" for each gene. mRNA data from the Human Protein Atlas were analysed using GraphPad Prism 10 (GraphPad Software, Inc., La Jolla, CA). A Mann-Whitney U test was performed to compare the expression of each gene between human and mouse data. Statistical significance was determined as $P < 0.05$.

Results

Human retinal flatmounts were immunofluorescently stained to localize pericytes using antibodies against NG2, PDGFRβ, αSMA, CD13 and RFC1.

NG2 staining

IF staining with anti-NG2 was developed to detect $NG2^+$ pericytes in the human retina. Various fixation methods were tested to compare staining results using anti-NG2 antibodies, including fixation with formaldehyde followed by (1) fixation with a methanol gradient; (2) cold 100% methanol (-20°C) for 5, 15 or 30 min; or (3) no methanol fixation. Methanol can improve tissue penetration and may help unmask epitopes that are masked by formaldehyde crosslinking, but on the other hand, it may disrupt established crosslinks. NG2-antibody signal was not detectable after fixation conditions 1 and 2, which both included methanol (Figure 2A-D). Only condition 3, without the use of methanol, resulted in staining of pericytes (Figure 2E).

Next, the impact of formaldehyde fixation time on NG2 staining was studied. Retinal flatmounts fixed for 1 h exhibited stronger and more specific NG2 staining of pericytes as compared to 2 h fixation (Figure 3), indicating that shorter fixation time better preserves the epitopes necessary for optimal antibody binding.
The composition of the blocking buffer was also optimized to enhance specific NG2 staining. Of the two blocking buffers used, blocking buffer 1 (Table 2) (Figure 4A) and blocking buffer 2 (Figure 4B), blocking buffer 1 provided the best NG2 staining. This buffer minimized non-specific staining and allowed for clearer visualization of both the pericyte cell bodies and their processes in the human retina. Optimal staining conditions for NG2 staining are listed in Table 6.

PDGFRβ staining

Our study aimed to perform a double staining with antibodies for PDGFRβ and NG2 to assess simultaneous marker expression in pericytes and potentially identify pericyte subsets. In the initial trials for optimizing PDGFRβ staining, NG2 antibodies were excluded to minimize antibody usage.

PDGFRβ staining on human retinal flatmounts was initially tested using the same protocol established for NG2 staining. However, these conditions did not result in positive staining of PDGFRβ (Figure 5A). Altering blocking buffer 1 to blocking buffer 3, thereby reducing the percentage of TX and replacing BSA by an increased percentage of normal serum (Table 2), also failed to improve PDGFRβ staining (Figure 5B). Specific staining of PDGFRβ was successfully achieved after applying blocking buffers 4, 5 or 6 (Figure 5C-E), that all contained low amounts of TX or no TX and in which normal serum was replaced by BSA. Optimal results were obtained after blocking with blocking buffer 5 (Figure 5D). Apparently, the omission of

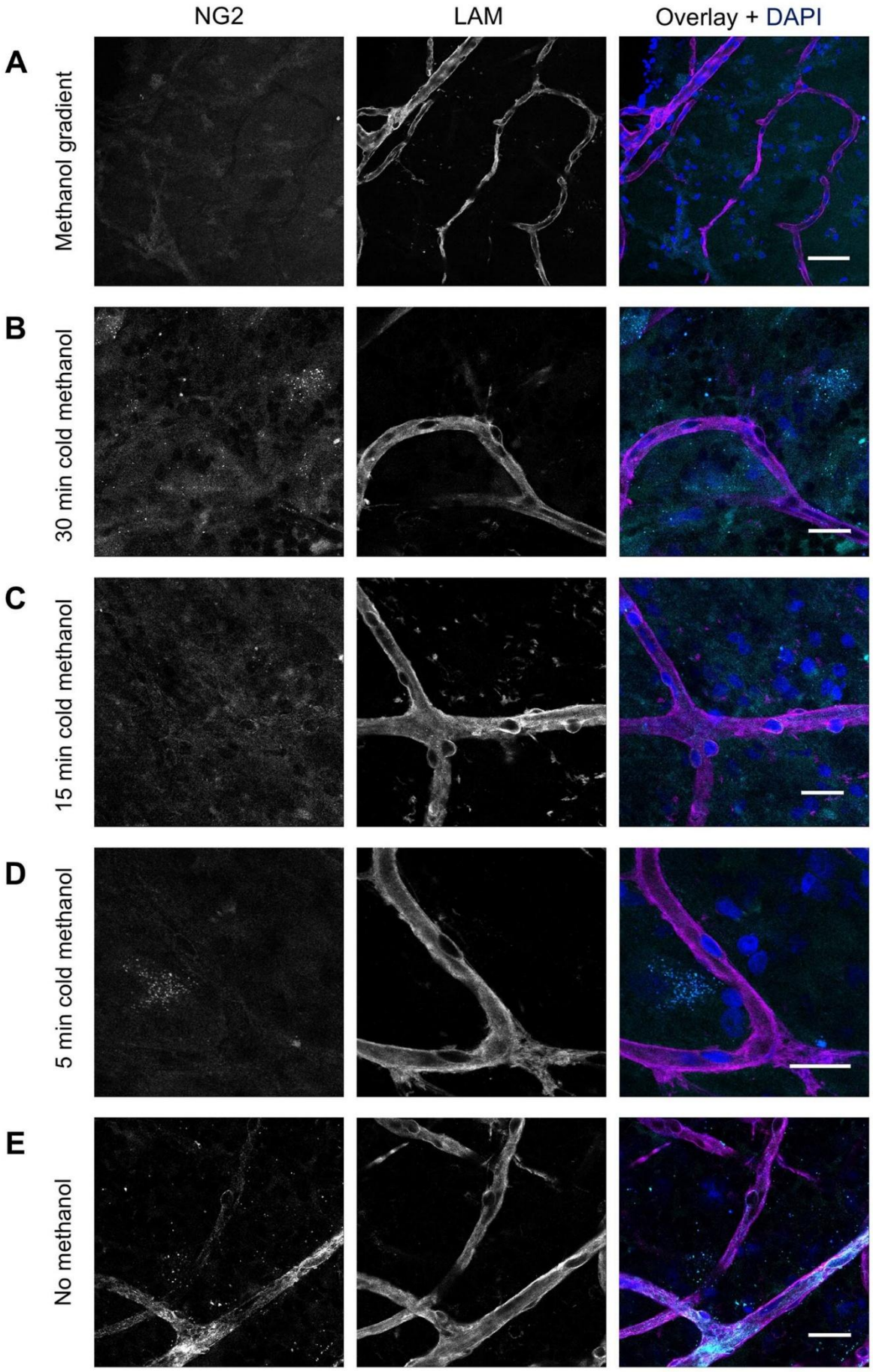
NG2
LAM
Overlay + DAPI
A
Methanol gradient
B
30 min cold methanol
C
15 min cold methanol
D
5 min cold methanol
E
No methanol

Figure 2. Effect of different fixation methods on immunofluorescence staining of NG2 in human retinal flatmounts. Flatmounts were stained for laminin (LAM) for basal lamina (magenta), NG2 for pericytes (cyan) and DAPI for nuclei (blue) after different fixation methods. After initial fixation with 4% formaldehyde, additional fixation was performed with (A) a methanol gradient, (B) cold 100% methanol for 30 min, (C) cold 100% methanol for 15 min, (D) cold 100% methanol for 5 min or (E) no methanol. Nuclei were stained with DAPI (blue). Scale bar = 25 µm.

normal serum from the blocking buffer improved the specificity of PDGFRβ staining, suggesting that the absence of normal serum may reduce non-specific binding and enhance the immunodetection of PDGFRβ^{+} pericytes.

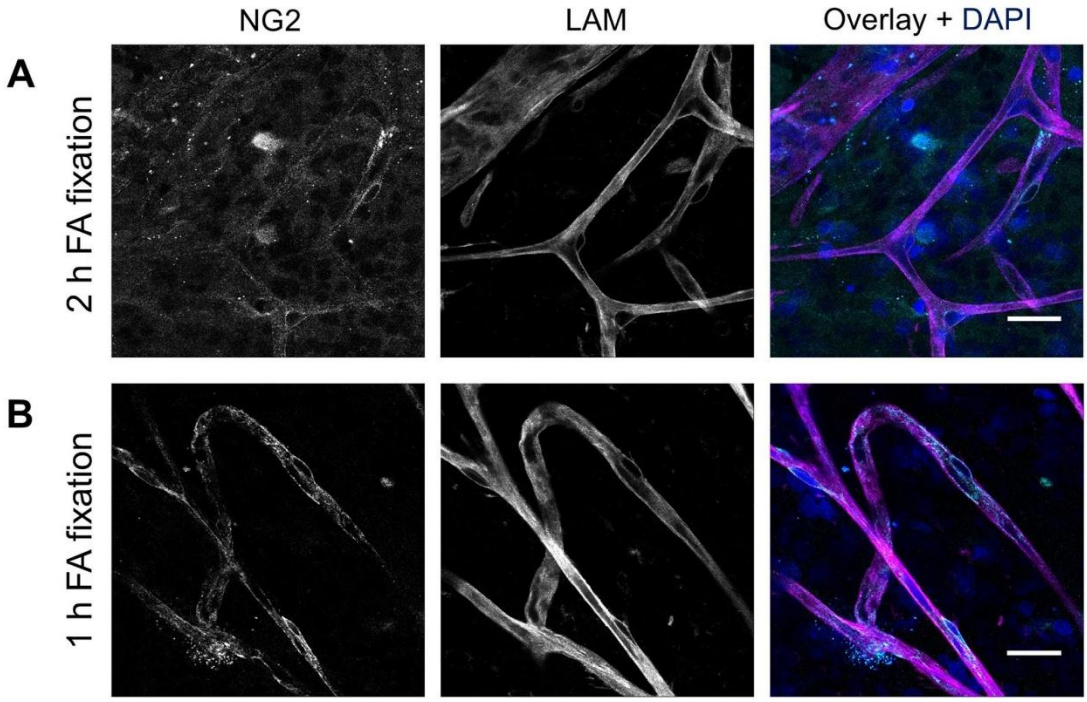

Figure 3. Effect of fixation time on immunofluorescence staining of NG2 in human retinal flatmounts. NG2 staining (cyan) after formaldehyde fixation for 2 h (A), or 1 h (B). Basal lamina was stained with anti-laminin (LAM) antibodies (magenta) and nuclei with DAPI (blue). Scale bar = 25 µm.

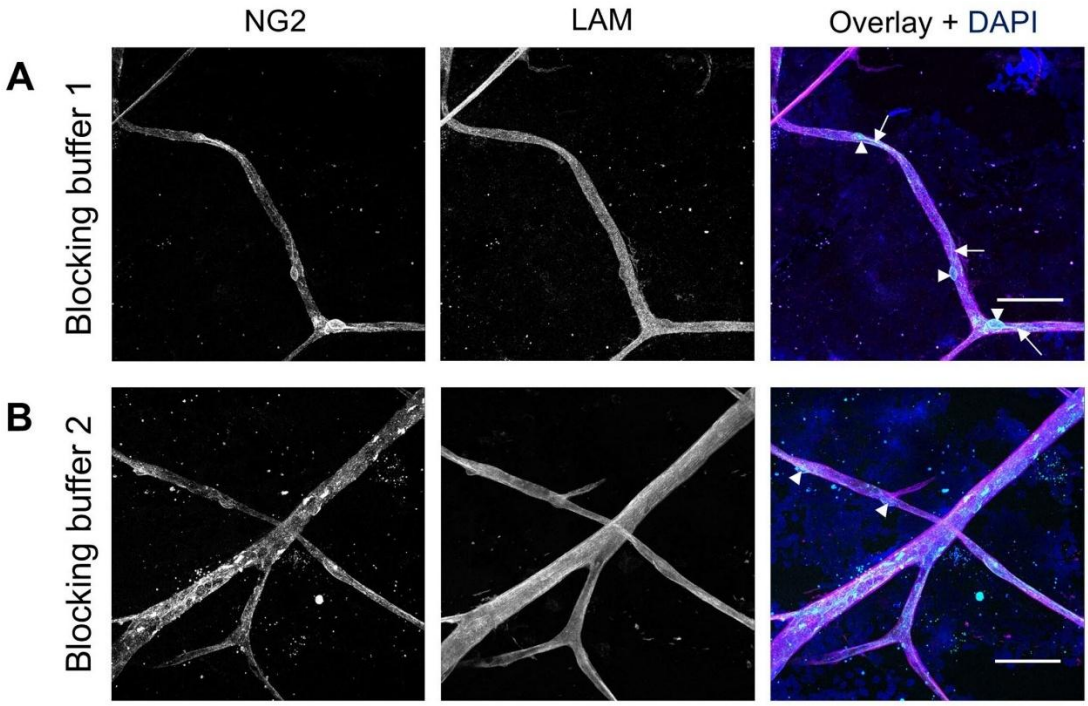

Figure 4. Effect of different blocking buffers on immunofluorescence staining of NG2 in human retinal flatmounts. Specific NG2 staining (cyan) was observed for incubation with blocking buffer 1 (A) and blocking buffer 2 (B). Basal lamina was stained with anti-laminin (LAM) antibodies (magenta) and nuclei with DAPI (blue). Arrowheads indicate pericyte cell bodies and arrows indicate pericyte processes. Scale bar = 50 µm.

Table 6. Optimal conditions for IF staining of pericytes in human retinal flatmounts.

Markers	Fixation	Blocking buffer	Antibody solvent	Optimal concentration primary antibody	Wash solution
NG2	4% FA for 1 h	PBS-0.3%TX + 0.2% BSA + 5% normal serum	PBS-0.3%TX + 0.2% BSA + 5% normal serum	NG2 1:100	PBS-0.3%TX
NG2+ PDGFRβ	4% FA for 1 h	(1) PBS-0.3%TX + 0.2% BSA + 5% normal serum; (2) PBS-0.1%TX + 2% BSA	PBS-0.01%TX + 0.2% BSA	NG2 1:100, PDGFRβ 1:100	PBS
αSMA + PDGFRβ	100% methanol for 20 min	PBS-0.5%TX + 2% BSA + 0.2M glycine	PBS-0.01%TX + 2% BSA	αSMA 1:500, PDGFRβ 1:100	PBS-0.05%TX

In addition to varying blocking buffers, different antibody solvents (Table 4) were compared: solvent 1 (Figure 6A), solvent 2 (Figure 6B); and solvent 3 (Figure 6C). All experimental conditions incorporated the application of blocking buffer 5. While all three conditions resulted in specific PDGFRβ staining, the use of solvent 1 produced the lowest background signal, providing the clearest and most specific staining (Figure 6A). This suggests that the

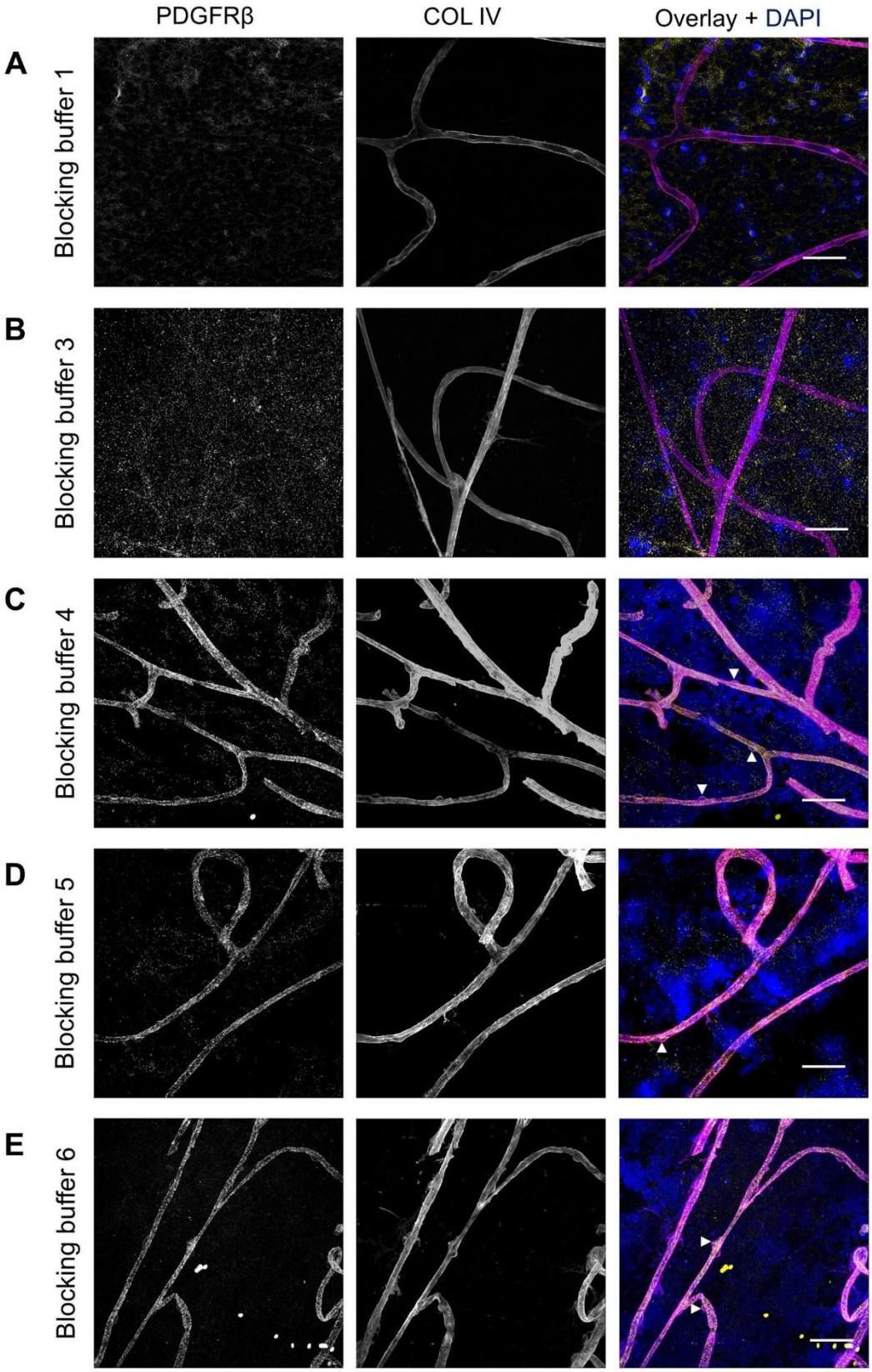

Figure 5. Effect of different blocking buffers on immunofluorescence staining of PDGFRβ in human retinal flatmounts. The pericyte marker PDGFRβ (yellow) was immunostained using antibodies in conditions optimized for NG2 staining, performed with blocking buffer 1 (A) or buffer 3-6 (B-E). Basal lamina was stained with anti-collagen type IV (COL IV) antibodies (magenta) and nuclei with DAPI (blue). Examples of pericytes are indicated with arrowheads. Scale bar = 50 µm.

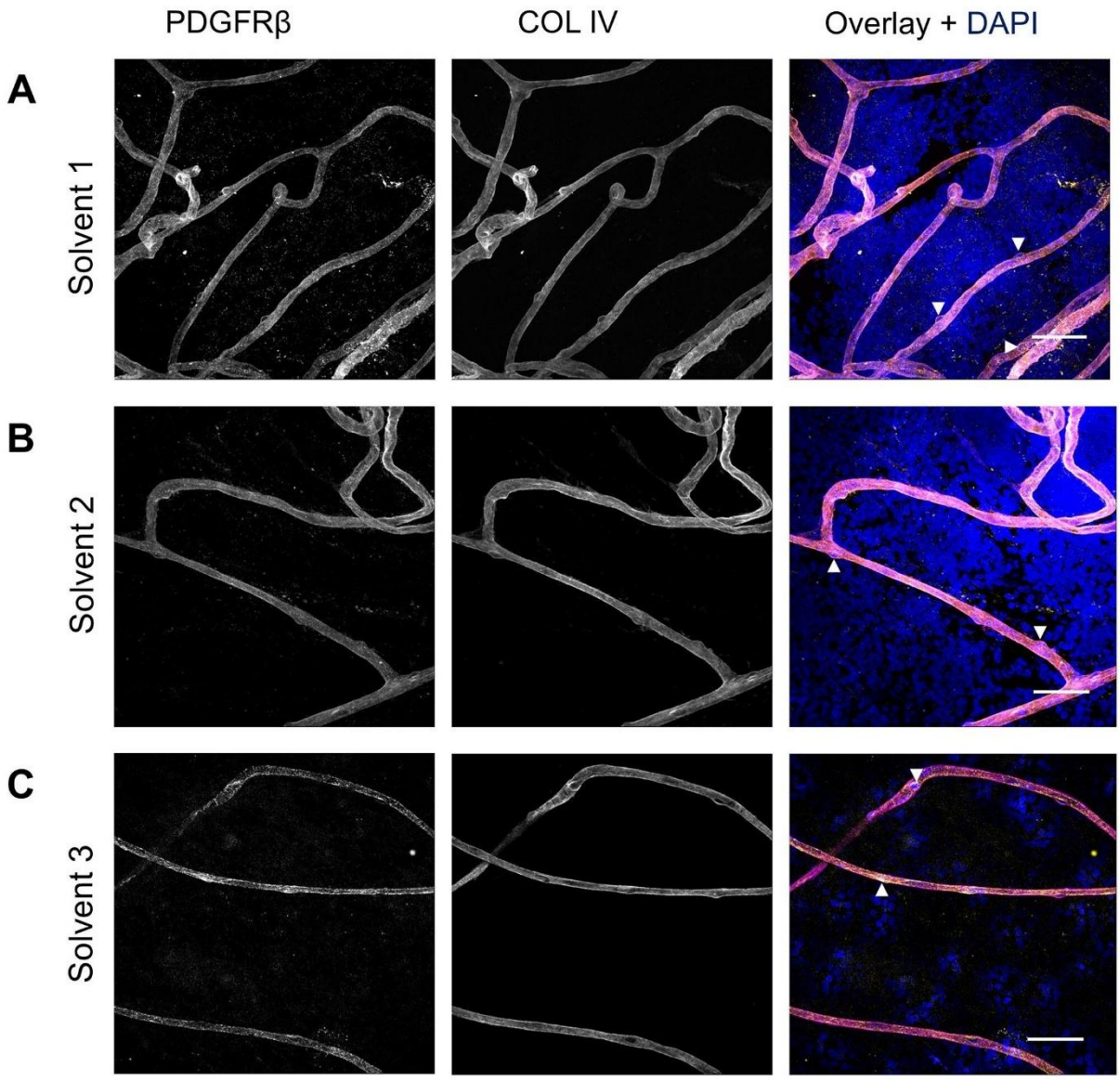

Figure 6. Effect of different antibody solvents on immunofluorescence staining of PDGFRβ in human retinal flatmounts. Specific PDGFRβ staining (yellow) was obtained when using antibody solvent 1 (A), solvent 2 (B) or solvent 3 (C). Basal lamina was stained with anti-collagen type IV (COL IV) antibodies (magenta) and nuclei with DAPI (blue). Examples of pericytes are indicated with arrowheads. Scale bar = 50 µm.

normal antibody diluent was the most effective for minimizing non-specific binding and improving the overall signal-to-noise ratio for PDGFRβ detection.

NG2 and PDGFRβ double staining

After separately optimizing the staining of NG2 and PDGFRβ, the protocol for double staining of these markers was optimized. As shown in Figure 7A, the optimized condition for NG2

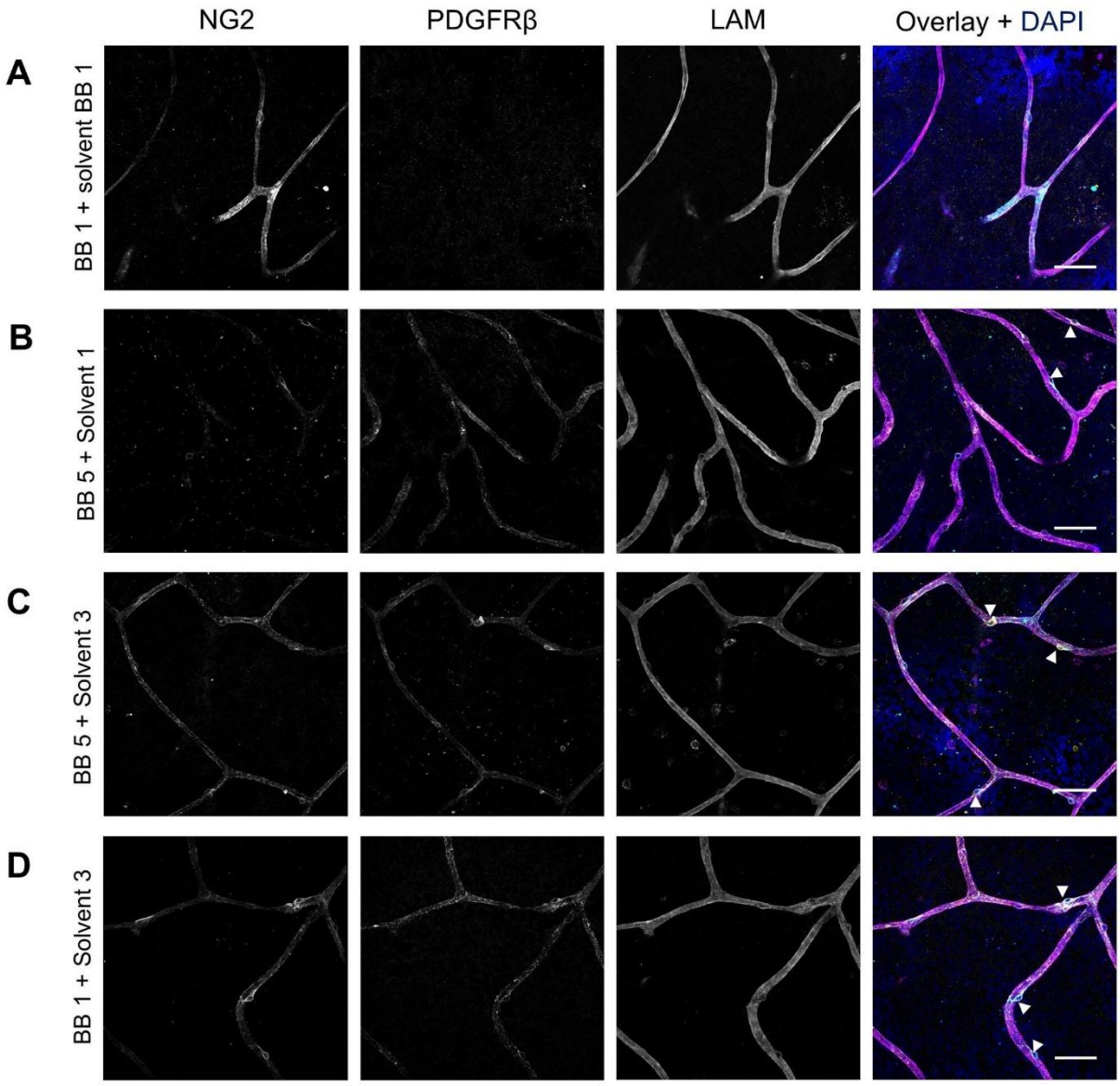

Figure 7. Effect of different blocking buffers and antibody solvents on immunofluorescence double staining of NG2 and PDGFRβ in human retinal flatmounts. The immunofluorescence conditions optimized for NG2 (A) or PDGFRβ (B) did not result in specific double staining of NG2 (cyan) and PDGFRβ (yellow). Optimized immunofluorescence conditions for PDGFRβ were tested with solvent 3 as antibody solvent instead of solvent 1 (C) and optimized immunofluorescence conditions for NG2 were tested with solvent 3 as antibody solvent instead of blocking buffer 1 as antibody solvent (D). Basal lamina was stained with anti-laminin (LAM) antibodies (magenta) and nuclei with DAPI (blue). Examples of pericytes are indicated with arrowheads. BB = blocking buffer. Scale bar = 50 µm.

staining did not result in positive PDGFRβ staining, and similarly, Figure 7B demonstrates that the optimized PDGFRβ conditions did not yield positive NG2 staining. However, when the optimized IF conditions for PDGFRβ were applied with solvent 3 (10x diluted blocking buffer 5) as antibody solvent, instead of solvent 1, the retinal flatmounts showed specific expression of both NG2 and PDGFRβ (Figure 7C). Likewise, when the optimized IF staining condition for NG2 was applied with solvent 3 instead of blocking buffer 1 as antibody solvent, strong expression of both NG2 and PDGFRβ was observed in retinal flatmounts (Figure 7D).

Negative control flatmounts revealed no unspecific staining caused by the application of the secondary antibodies (Supplementary Figure 1). These results suggest that optimizing the antibody solvent composition is crucial for achieving specific and robust double staining of NG2 and PDGFRβ, enabling the detection of both markers simultaneously in retinal tissue. Optimal staining conditions for NG2 and PDGFRβ double staining are listed in Table 6 and the result is shown at higher magnification in Figure 9A.

αSMA and PDGFRβ double staining

For double staining with αSMA and PDGFRβ antibodies, we adapted the IF staining protocol for hippocampal slices of Mai-Morente et al. [51]. The protocol includes the use of jasplakinolide, a reagent that stabilizes F-actin by promoting actin filament polymerization, which is essential to detect αSMA in pericytes using IF staining. To achieve this, flatmounts were incubated with jasplakinolide prior to fixation.

When fixation of retinal flatmounts with 4% formaldehyde for 20 min (Figure 8A) or 100% methanol for 20 min (Figure 8B) was performed after incubation with blocking buffer 7 for 2 h at RT, the tissue morphology was severely damaged. To preserve tissue integrity, the fixation step with methanol was performed before incubation with blocking buffer rather than afterwards (Figure 8C). As a result, αSMA^{+} $PDGFR\beta^{+}$ pericytes were clearly visible in the human retinal flatmounts. When incubation with jasplakinolide was omitted, specific αSMA was still detected (Figure 8D). However, there was an increase in non-specific signal, and the integrity of the flatmounts was compromised. Negative control flatmounts revealed no unspecific staining caused by the application of the secondary antibodies (Supplementary Figure 1).

These results suggest that the use of jasplakinolide is crucial for achieving specific staining of αSMA. The order of incubation with jasplakinolide, followed by fixation and blocking enables the detection of both αSMA and PDGFRβ simultaneously in retinal tissue. Optimal staining conditions for αSMA and PDGFRβ double staining are listed in Table 6 and the result is shown at higher magnification in Figure 9B.

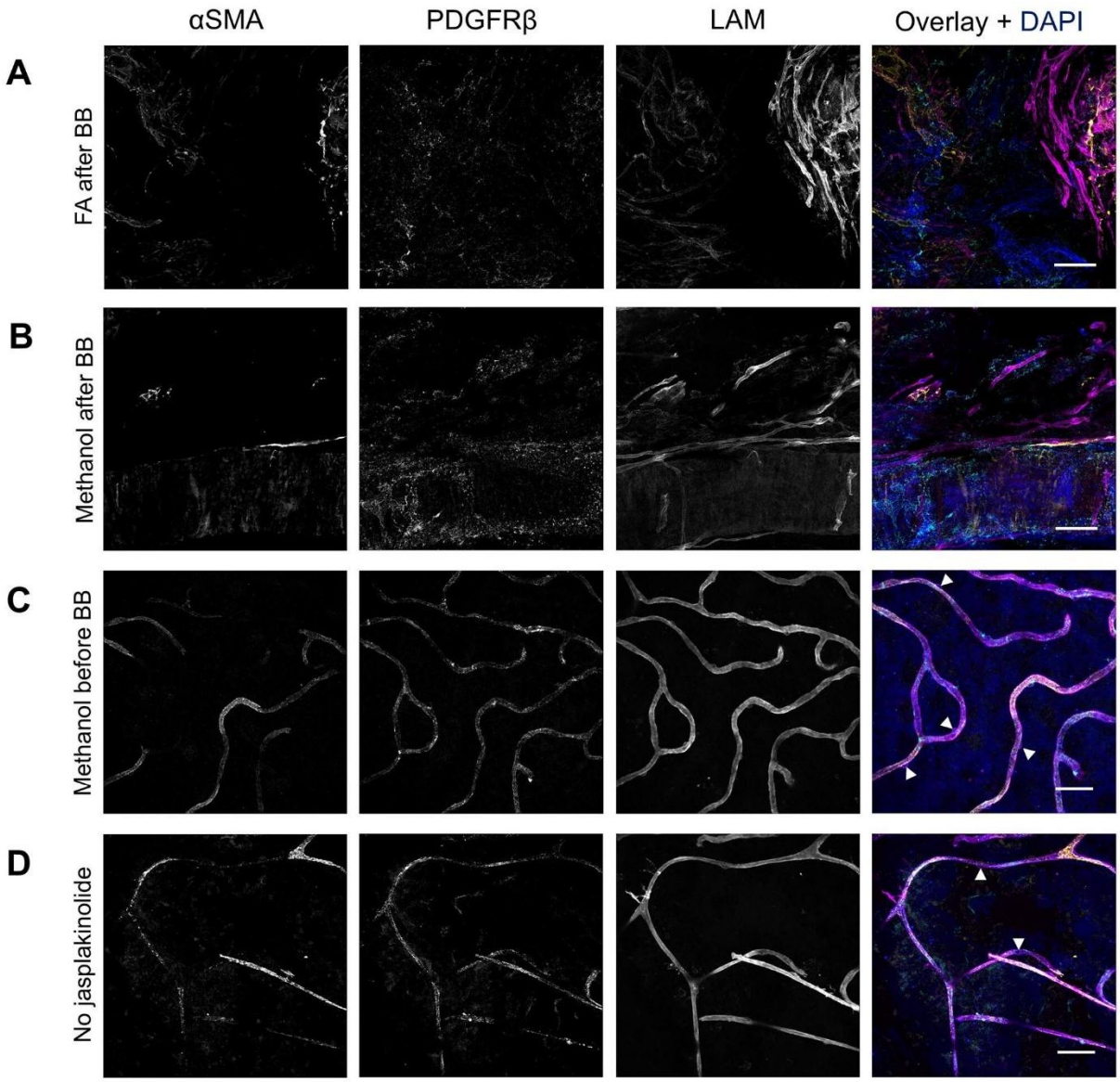

Figure 8. Effect of different fixatives and jasplakinolide on immunofluorescence double staining of αSMA and PDGFRβ in human retinal flatmounts.
Immunofluorescence staining of αSMA (yellow) and PDGFRβ (cyan) after fixation with 4% formaldehyde (A) or methanol (B and C). Tissue integrity was compromised after fixation with formaldehyde (A) and fixation with methanol (B) after blocking buffer incubation. αSMA and PDGFRβ staining was best after fixation with methanol before application of the blocking buffer in combination with the use of jasplakinolide (C). αSMA and PDGFRβ staining without the use of jasplakinolide (D). Basal lamina was stained with anti-laminin (LAM) antibodies (magenta) and nuclei with DAPI (blue). Examples of pericytes are indicated with arrowheads. BB = blocking buffer. Scale bar = 50 µm.

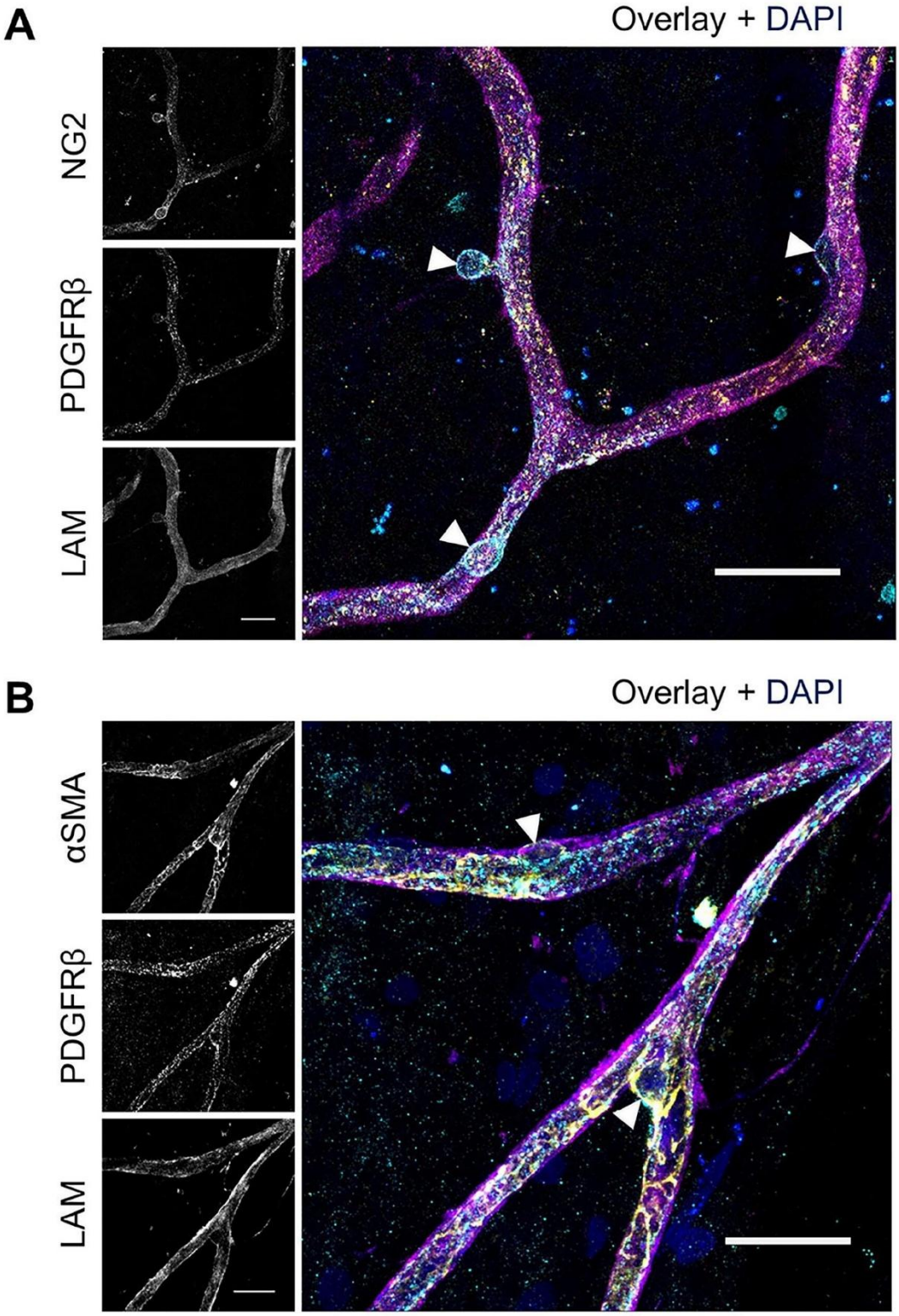

Figure 9. Immunofluorescence double staining of NG2 and PDGFRβ and of αSMA and PDGFRβ in human retinal flatmounts. Higher magnification images of pericytes detected with immunofluorescence double staining of (A) NG2 (cyan) with PDGFRβ (yellow) and (B) αSMA (yellow) with PDGFRβ (cyan). Pericyte bodies are indicated with arrowheads. Basal lamina was stained with anti-laminin (LAM) antibodies (magenta) and nuclei with DAPI (blue). Scale bar = 25 µm.

CD13 and PDGFRβ double staining

Our study aimed to perform a double staining with antibodies for CD13 and PDGFRβ. As shown in Supplementary Figure 2A and B, the conditions optimized for NG2 and PDGFRβ were tested for this purpose, but did not result in positive CD13 staining. Altering the blocking buffer to blocking buffer 8 also failed to improve CD13 staining (Supplementary Figure 2C). Furthermore, no specific signal for CD13 was detected when varying the antibody solvents (Supplementary Figure 3). Since no optimal staining condition could be identified for CD13 staining in human retinal flatmounts, and CD13 staining has only been reported in mouse retinas, we considered the possibility that CD13 expression may differ between species. According to RNA sequencing data from the Human Protein Atlas, CD13 expression is reported in the mouse retina (3.2 normalized transcripts per million), whereas CD13 expression in human retina is completely absent (Figure 10). Similarly, the Human Eye Transcriptome atlas and the Eye Integration database from the National Eye Institute found a low number of reads for CD13 in pericytes in the mature human eye. The absence of mRNA expression may well be an explanation for the failure to detect CD13 protein in the human retina.

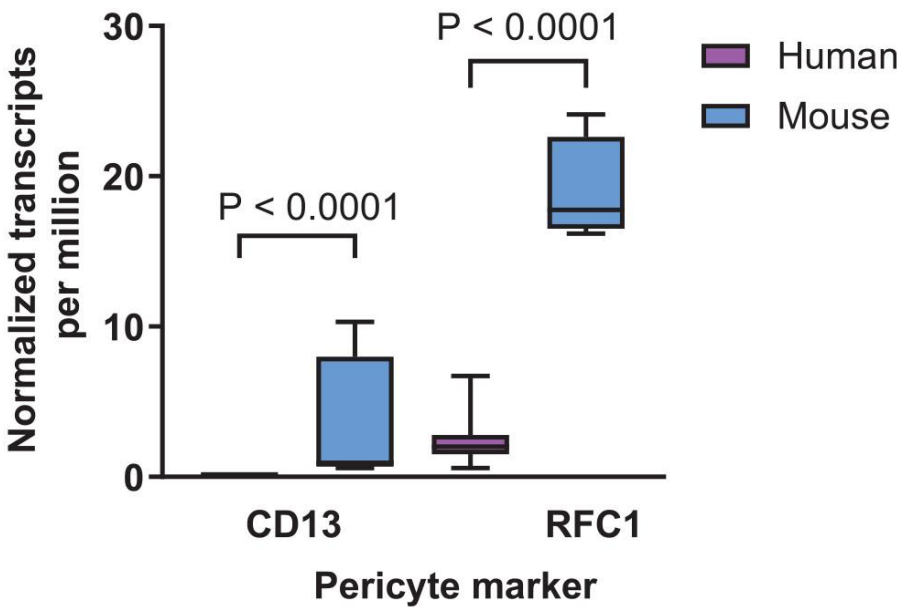

Figure 10. CD13 and RFC1 mRNA expression levels in the human and mouse retina. RNA sequencing data for CD13 and RFC1 are shown in boxplots as normalized transcripts per million for human retina (magenta bars) and mouse retina (blue bars). Box plots indicate median, min and max and 1st and 3rd quartile. Based on GTEx RNA-seq data from the Human Protein Atlas.

RFC1 and PDGFRβ double staining

For double staining of RFC1 and PDGFRβ, we first tested the conditions optimized previously for double staining of NG2 and PDGFRβ in retinal cryosections. Supplementary Figure 4A shows that these conditions resulted in positive staining of PDGFRβ, but not of RFC1. We also adapted and tested the IF staining protocol of Gurler et al. [22], performing permeabilization with blocking buffer 9 for 30 min at RT followed by incubation with blocking buffer 10 for 1 h at RT. These staining conditions did not improve detection of RFC1 in the retinal vasculature

(Supplementary Figure 4B). No optimal staining condition could be found for RFC1 staining in human retinal tissue. This was in line with the Human Protein Atlas for RNA sequencing data, which showed that RFC1 mRNA expression (2.2 normalized transcripts per million) in human retina is considerable lower than that in the mouse retina (Figure 10). Similarly, the Human Eye Transcriptome atlas and the Eye Integration database from the National Eye Institute found a low number of reads for RFC1 in pericytes in the mature human eye. The low mRNA expression may be an explanation for the lack of RFC1 protein detection in the human retina.

Discussion

In this study, we developed IF staining protocols to detect NG2, αSMA, and PDGFRβ as pericyte markers in human retinal flatmounts. Based on IF staining of these pericyte markers, we were able to identify pericytes with typical morphological characteristics: pericytes that have a cell body with a prominent nucleus and large processes covering blood vessels. CD13 and RFC1 could not be detected in the human retina in contrast to their reported expression in mouse retina. We have identified variations in the IF staining protocol that led to the most significant improvement in staining for each marker. Appropriate fixation is essential for frozen tissues to improve tissue morphology and proper detection of the protein of interest [52, 53]. The importance of fixation solution and timing of fixation is illustrated by this study. For NG2 staining, fixation with methanol did not result in a positive staining signal. On the contrary, fixation with formaldehyde resulted in specific NG2 signal. This outcome is in contrast to earlier findings which have suggested that methanol is suitable to fix retinal wholemounts for immunostaining [54], also specifically for NG2 staining [10, 38, 55]. This discrepancy could be attributed to the difference in species as murine retinas were used in previous studies. Also, the importance of timing of fixation was demonstrated here for the double staining with PDGFRβ and αSMA antibodies. Fixation enhances specific IF signal by preventing autolytic activity of enzymes in the tissue and conserves tissue morphology by crosslinking macromolecules [56, 57]. Delaying fixation leads to protein degradation in the retina, and thus reduces the IF signal as well as tissue morphology.

Selecting the appropriate detergents and blocking reagents is crucial to optimize IF staining. Detergents such as Tween20 or TX allow antibodies to access intracellular epitopes, but using too much of these agents may lead to loss of pericyte marker detection for proteins that are sensitive to detergents [58]. Detergents in washing buffers help to remove non-specifically bound antibodies, resulting in more specific staining. Excessive presence of detergents may also wash off specifically bound antibodies, resulting in less specific staining. Blocking reagents reduce non-specific antibody binding and background noise by covering reactive sites on the antigens in the tissue and can additionally stabilize cellular morphology [59].

We recommend to optimize the IF staining protocols for each tissue type and protein of interest. Parameters that can be adjusted to optimize specific staining, and that were not shown in this study, include: antibody concentration, antibody clonality, isotype and host species, temperature and duration of each incubation step, composition of washing solvent, number of washing steps, type of mounting medium, and the use of fresh tissue instead of frozen tissue [60, 61]. When using frozen tissue for IF staining, limiting post-mortem time improves protein signal detection in immunostaining [62]. Antibody clonality affects IF staining because monoclonal antibodies are more specific, whereas polyclonal antibodies

provide higher sensitivity. Matching antibody isotype and host species ensures compatibility between epitope, primary and secondary antibodies and preventing species-on-species non-specific staining. Optimization of washing further improves specific staining, because the washing step allows for removal of antibodies that are bound non-specifically. In addition, appropriate microscope settings and software settings for image acquisition and image analysis are essential to obtain high-quality and accurate images and help achieve a high signal-to-noise ratio while limiting photobleaching [63].

After optimization of the IF staining, all markers were detected and localized in pericytes in both the cell body and the processes covering the blood vessel. We are the first to report a staining protocol for multiple pericyte markers in human retinal flatmounts. Using retinal flatmounts instead of retinal tissue sections has several advantages. First, flatmounts allow for visualization of the entire vascular network, which is not possible in tissue sections. This provides information on the location of the pericyte, for example regarding the proximity to an arteriole or venule or regarding the branch order of capillaries. Furthermore, pericytes that are migrating away from blood vessels can be visualized. In addition, visualization of pericytes in a 3D reconstruction image is easier in flatmounts compared to serial tissue sections.

Using our protocol, we observed that the expression of NG2 was evenly distributed throughout pericytes in the human retina. These results are consistent with the staining pattern previously found in human retina [64]. In addition, the staining pattern found in humans was similar to that in retinas of mice [10, 55, 65, 66] and rats [67]. In the current study, PDGFRβ was detected as granulated staining in pericytes. The granulated staining pattern found here matches with the staining pattern previously found in human retina [49] and murine retina [68]. PDGFRβ is primarily localized at the pericyte membrane and internalization of PDGFRβ upon ligand binding relocates PDGFRβ to endosomes that can attribute to the granulated appearance of PDGFRβ staining [31, 69]. Staining patterns in other studies that reported staining of PDGFRβ in murine retina could not be assessed properly due to the low magnifications used in these studies [66, 70]. For αSMA, we found a patchy appearance localizing at blood vessels of the human retina. This finding corresponds to the staining pattern found in human retina [43] and mouse retina [38, 51, 71]. The expression of each pericyte marker did not fully colocalize with that of the other pericyte markers. The observed differences in expression location and expression pattern of the included pericytes markers may be attributed to the distinct function of pericytes or state of maturity, suggesting the presence of pericyte subpopulations [20, 21, 44, 72-74]. For example, arteriolar pericytes express NG2 and αSMA, while capillary pericytes lack these markers in some tissues. This distinction suggests that arteriolar pericytes may play role in blood flow regulation, linked to their contractile function. Postcapillary pericytes that lack NG2 have been shown to regulate neutrophil movement across the basal lamina in muscles [75]. However, little is known about pericyte heterogeneity and the function of pericyte subpopulations [20, 73]. Therefore, double staining of pericyte markers is crucial to identify pericyte subpopulations.

Other reported pericyte markers include CD13 [76, 77], also known as aminopeptidase N, and SLC19A1 [22, 23], also known as RFC1. However, immunostaining of CD13 and RFC1 was only reported in the mouse retina and not yet in the human retina. IF staining of these

markers was tested in the current study. The antibodies detecting human CD13 and RFC1 did not show any immunoreactivity in pericytes in the human retina. For CD13, our results are in line with RNA sequencing data from the Human Protein Atlas. Although for RFC1 mRNA expression was found in the human retina, its expression was significantly lower than that in mouse retina. The Human Eye Transcriptome atlas and the Eye Integration database from the National Eye Institute reported a low number of reads for both CD13 and RFC1 in pericytes in the mature human eye. The presence of mRNA in the human retina may be due to expression in other cell types in the retina than pericytes, for example RFC1 is also expressed in retinal microglia [78]. The difference in pericyte marker expression between mice and humans highlight the importance of established IF protocols specifically tailored for human tissues.

IF staining allows multiple pericyte markers and supporting markers to be simultaneously stained in flatmounts [59]. In addition, visualization of pericytes by immunostaining provides information on pericyte number, morphology and location, and permits quantitative microscopy [59, 67, 68]. The limitation of using fluorophores to detect proteins of interest is the possibility of photobleaching of fluorophores and autofluorescence of the tissue of interest [59, 79]. To circumvent the issues related to fluorophores, chromogenic immunohistochemistry offers a staining alternative that also provides additional information on the tissue morphology [59, 80]. However, IF staining offers increased sensitivity, 3D visualization, quantification possibilities related to abundance of protein and multiplexing opportunities compared to chromogenic immunohistochemistry [59, 81]. An alternative technique to visualize pericytes in human retina includes electron microscopy [82, 83]. Electron microscopy studies provide information on pericyte number and morphology, but functional information based on pericyte markers and numbers is lacking. Another drawback is that the thin sections used in electron microscopy offer limited spatial information in relation to the vasculature. Another limitation of IF staining and electron microscopy is the use of fixed, non-living cells, while seeking information regarding the state in living organisms, tissues and cells. Visualization of pericytes in the living human retina is possible by combining adaptive optics scanning laser ophthalmoscopy with a modified dark-field detection scheme [84-86]. This technique provides information on pericyte number and location, and visualization in living retina allows for studying of pericytes during disease progression or during treatment. However, this technique cannot identify pericyte subsets based on pericyte markers.

Pericytes are widely spread throughout the human body and play an important role in vascular flow and homeostasis [7, 20, 87]. Pericytes also have roles not related to the vasculature, depending on the location in different organs. The prevalence of pericytes in the retina is, together with the brain, significantly higher compared to other organs to enable proper functioning of the neuronal tissue [4, 5, 7-9, 88]. In the retina, pericytes share the basal lamina with endothelial cells and provide structural support by covering most of the microvascular area [4, 9, 87, 89, 90]. During angiogenesis, pericytes regulate endothelial cell proliferation and sprouting and stabilize the newly formed blood vessels. Endothelial cells directly communicate with pericytes through direct gap junctions and peg-sockets and via paracrine signaling factors to facilitate formation, maturation, and stabilization of the microvasculature [6]. Pericytes also regulate blood flow by contracting or relaxing to facilitate the high metabolic demand of the retina, especially neuronal tissue. Some studies show a

role of pericytes in immune cell trafficking by remodeling of the basal lamina or expression of cytokine receptors and toll-like receptors and release of cytokines and chemokines [91]. The high ratio of pericytes allows for precise control of these functions. Pericyte dysfunction or loss has been reported in various pathologies, for example diabetic retinopathy, ischemia, glaucoma and tumor formation [4, 7, 8, 20, 87, 89]. Therefore, restoring pericyte function as a future therapy may well ameliorate the pathological developments.

Further research is required to establish the underlying mechanisms related to pericyte dysfunction and loss and whether manipulating pericytes can be used to treat retinal disorders. With this study, we have visualized pericytes in human retinal flatmounts using IF staining. Using a combination of pericyte markers can shed more light on heterogeneity in the pericyte population. Pericytes are heterogeneous in a tissue- and context-dependent way [9, 73]. Understanding pericyte heterogeneity can provide insights into regional population differences, for example in specific parts of the retina with vascular leakage or angiogenesis. The developed IF staining can be applied to study changes in pericytes in conditions affecting the human retina, such as ischemia in retinal vein occlusions or diabetic retinopathy. Staining pericytes in the human retina can provide valuable insight into the pathogenesis of these retinal conditions and can lead to development of new, more effective therapeutic approaches. In the near future, we will apply this newly developed staining protocols to retinas from patients with diabetic retinopathy to investigate the changes in pericytes associated with the disease.

Funding Statement

This work is supported by the RECOGNISED consortium grant (EU GA 847749), and The Encouraging European Research (EER) regulation of The Dutch Research Council (NWO, grant 200629). The study funders were not involved in the design of the study; the collection, analysis, or interpretation of data; the writing of the report; nor did they impose any restrictions regarding the publication of the report.

Author contributions

The authors have contributed to this article as follows: conception and design (IK, NB, CJFVN, ROS), immunofluorescence staining experiments and microscopical fluorescence imaging (AAC, EP, NB), scientific discussions (all authors), manuscript writing (IK, NB, CJFVN), final approval of the manuscript (all authors) and supervision of the entire study (IK, CJFVN, ROS, NB).

References

[1] Hammes HP, Lin J, Wagner P, Feng Y, Vom Hagen F, Krzizok T, et al. (2004) Angiopoietin-2 causes pericyte dropout in the normal retina: evidence for involvement in diabetic retinopathy. Diabetes 53(4): 1104–1110. doi: 10.2337/diabetes.53.4.1104

[2] Joussen AM, Doehmen S, Le ML, Koizumi K, Radetzky S, Krohne TU, et al. (2009) TNF-alpha mediated apoptosis plays an important role in the development of early diabetic retinopathy and long-term histopathological alterations. Mol Vis 15: 1418–1428.

[3] Klaassen I, van Geest RJ, Kuiper EJ, van Noorden CJ, Schlingemann RO (2015) The role of CTGF in diabetic retinopathy. Exp Eye Res 133: 37–48. doi: 10.1016/j.exer.2014.10.016

[4] Li P, Fan H (2023) Pericyte Loss in Diseases. Cells 12(15). doi: 10.3390/cells12151931

[5] Armulik A, Genove G, Betsholtz C (2011) Pericytes: developmental, physiological, and pathological perspectives, problems, and promises. Dev Cell 21(2): 193–215. doi: 10.1016/j.devcel.2011.07.001

[6] van Noorden CJF, Yetkin-Arik B, Martinez PS, Bakker N, Smallenburg MEV, Schlingemann RO, et al. (2024) New Insights in ATP Synthesis as Therapeutic Target in Cancer and Angiogenic Ocular Diseases. J Histochem Cytochem 72(5): 329–352. doi: 10.1369/00221554241249515

[7] Ferland-McCollough D, Slater S, Richard J, Reni C, Mangialardi G (2017) Pericytes, an overlooked player in vascular pathobiology. Pharmacol Ther 171: 30–42. doi: 10.1016/j.pharmthera.2016.11.008

[8] Caporarello N, D'Angeli F, Cambria MT, Candido S, Giallongo C, Salmeri M, et al. (2019) Pericytes in Microvessels: From "Mural" Function to Brain and Retina Regeneration. Int J Mol Sci 20(24). doi: 10.3390/ijms20246351

[9] Huang H (2020) Pericyte-Endothelial Interactions in the Retinal Microvasculature. Int J Mol Sci 21(19). doi: 10.3390/ijms21197413

[10] van der Wijk AE, Vogels IMC, van Veen HA, van Noorden CJF, Schlingemann RO, Klaassen I (2018) Spatial and temporal recruitment of the neurovascular unit during development of the mouse blood-retinal barrier. Tissue Cell 52: 42–50. doi: 10.1016/j.tice.2018.03.010

[11] Nian S, Lo ACY, Mi Y, Ren K, Yang D (2021) Neurovascular unit in diabetic retinopathy: pathophysiological roles and potential therapeutical targets. Eye Vis (Lond) 8(1): 15. doi: 10.1186/s40662-021-00239-1

[12] Rezzani R, Favero G, Giano M, Pinto D, Labanca M, van Noorden CJF, et al. (2024) Transient Receptor Potential Channels in the Healthy and Diseased Blood-Brain Barrier. J Histochem Cytochem 72(4): 199–231. doi: 10.1369/00221554241246032

[13] Wisniewska-Kruk J, Klaassen I, Vogels IM, Magno AL, Lai CM, Van Noorden CJ, et al. (2014) Molecular analysis of blood-retinal barrier loss in the Akimba mouse, a model of advanced diabetic retinopathy. Exp Eye Res 122: 123–131. doi: 10.1016/j.exer.2014.03.005

[14] Galea I (2021) The blood-brain barrier in systemic infection and inflammation. Cell Mol Immunol 18(11): 2489–2501. doi: 10.1038/s41423-021-00757-x

[15] Diaz-Coranguez M, Ramos C, Antonetti DA (2017) The inner blood-retinal barrier: Cellular basis and development. Vision Res 139: 123–137. doi: 10.1016/j.visres.2017.05.009

[16] Armulik A, Genove G, Mae M, Nisancioglu MH, Wallgard E, Niaudet C, et al. (2010) Pericytes regulate the blood-brain barrier. Nature 468(7323): 557–561. doi: 10.1038/nature09522

[17] Bhowmick S, D'Mello V, Caruso D, Wallerstein A, Abdul-Muneer PM (2019) Impairment of pericyte-endothelium crosstalk leads to blood-brain barrier dysfunction following traumatic brain injury. Exp Neurol 317: 260–270. doi: 10.1016/j.expneurol.2019.03.014

[18] Fernandez-Klett F, Potas JR, Hilpert D, Blazej K, Radke J, Huck J, et al. (2013) Early loss of pericytes and perivascular stromal cell-induced scar formation after stroke. J Cereb Blood Flow Metab 33(3): 428–439. doi: 10.1038/jcbfm.2012.187

[19] Faal T, Phan DTT, Davtyan H, Scarfone VM, Varady E, Blurton-Jones M, et al. (2019) Induction of Mesoderm and Neural Crest-Derived Pericytes from Human Pluripotent Stem Cells to Study Blood-Brain Barrier Interactions. Stem Cell Reports 12(3): 451–460. doi: 10.1016/j.stemcr.2019.01.005

[20] Santos GSP, Prazeres P, Mintz A, Birbrair A (2018) Role of pericytes in the retina. Eye (Lond) 32(3): 483–486. doi: 10.1038/eye.2017.220
[21] Pfister F, Feng Y, vom Hagen F, Hoffmann S, Molema G, Hillebrands JL, et al. (2008) Pericyte migration: a novel mechanism of pericyte loss in experimental diabetic retinopathy. Diabetes 57(9): 2495–2502. doi: 10.2337/db08-0325
[22] Gurler G, Belder N, Beker MC, Sever-Bahcekapili M, Uruk G, Kilic E, et al. (2023) Reduced folate carrier 1 is present in retinal microvessels and crucial for the inner blood retinal barrier integrity. Fluids and Barriers of the Cns 20(1). doi: ARTN 47
10.1186/s12987-023-00442-3
[23] Sziraki A, Zhong Y, Neltner AM, Niedowicz DM, Rogers CB, Wilcock DM, et al. (2023) A high-throughput single-cell RNA expression profiling method identifies human pericyte markers. Neuropathol Appl Neurobiol 49(6): e12942. doi: 10.1111/nan.12942
[24] Song HW, Foreman KL, Gastfriend BD, Kuo JS, Palecek SP, Shusta EV (2020) Transcriptomic comparison of human and mouse brain microvessels. Sci Rep 10(1): 12358. doi: 10.1038/s41598-020-69096-7
[25] Picoli CC, Birbrair A, Li Z (2024) Pericytes as the Orchestrators of Vasculature and Adipogenesis. Genes (Basel) 15(1). doi: 10.3390/genes15010126
[26] Gastfriend BD, Foreman KL, Katt ME, Palecek SP, Shusta EV (2021) Integrative analysis of the human brain mural cell transcriptome. J Cereb Blood Flow Metab 41(11): 3052–3068. doi: 10.1177/0271678X211013700
[27] Schlingemann RO, Rietveld FJ, de Waal RM, Ferrone S, Ruiter DJ (1990) Expression of the high molecular weight melanoma-associated antigen by pericytes during angiogenesis in tumors and in healing wounds. Am J Pathol 136(6): 1393–1405.
[28] Birbrair A (2018) Pericyte Biology - Novel Concepts Preface. Pericyte Biology - Novel Concepts 1109: V–Vi. doi: Book_Doi 10.1007/978-3-030-02601-1
[29] Tamburini E, Dallatomasina A, Quartararo J, Cortelazzi B, Mangieri D, Lazzaretti M, et al. (2019) Structural deciphering of the NG2/CSPG4 proteoglycan multifunctionality. FASEB J 33(3): 3112–3128. doi: 10.1096/fj.201801670R
[30] Stallcup WB (2018) The NG2 Proteoglycan in Pericyte Biology. Adv Exp Med Biol 1109: 5–19. doi: 10.1007/978-3-030-02601-1_2
[31] Hosaka K, Yang Y, Nakamura M, Andersson P, Yang X, Zhang Y, et al. (2018) Dual roles of endothelial FGF-2-FGFR1-PDGF-BB and perivascular FGF-2-FGFR2-PDGFRbeta signaling pathways in tumor vascular remodeling. Cell Discov 4: 3. doi: 10.1038/s41421-017-0002-1
[32] Bannykh KS, Fuentes-Fayos AC, Linesch PW, Breunig JJ, Bannykh SI (2024) Laminin Beta 2 Is Localized at the Sites of Blood-Brain Barrier and Its Disruption Is Associated With Increased Vascular Permeability, Histochemical, and Transcriptomic Study. J Histochem Cytochem 72(10): 641–667. doi: 10.1369/00221554241281896
[33] Enge M, Bjarnegard M, Gerhardt H, Gustafsson E, Kalen M, Asker N, et al. (2002) Endothelium-specific platelet-derived growth factor-B ablation mimics diabetic retinopathy. EMBO J 21(16): 4307–4316. doi: 10.1093/emboj/cdf418
[34] Lindahl P, Johansson BR, Leveen P, Betsholtz C (1997) Pericyte loss and microaneurysm formation in PDGF-B-deficient mice. Science 277(5323): 242–245. doi: 10.1126/science.277.5323.242
[35] Tallquist MD, Soriano P (2003) Cell autonomous requirement for PDGFRalpha in populations of cranial and cardiac neural crest cells. Development 130(3): 507–518. doi: 10.1242/dev.00241
[36] Tallquist MD, French WJ, Soriano P (2003) Additive effects of PDGF receptor beta signaling pathways in vascular smooth muscle cell development. PLoS Biol 1(2): E52. doi: 10.1371/journal.pbio.0000052
[37] Alarcon-Martinez L, Yilmaz-Ozcan S, Yemisci M, Schallek J, Kilic K, Villafranca-Baughman D, et al. (2019) Retinal ischemia induces alpha-SMA-mediated capillary pericyte contraction coincident with perivascular glycogen depletion. Acta Neuropathol Commun 7(1): 134. doi: 10.1186/s40478-019-0761-z

[38] Alarcon-Martinez L, Yilmaz-Ozcan S, Yemisci M, Schallek J, Kiliç K, Can A, et al. (2018) Capillary pericytes express α-smooth muscle actin, which requires prevention of filamentous-actin depolymerization for detection. Elife 7. doi: ARTN e34861 10.7554/eLife.34861
[39] Dondossola E, Rangel R, Guzman-Rojas L, Barbu EM, Hosoya H, St John LS, et al. (2013) CD13-positive bone marrow-derived myeloid cells promote angiogenesis, tumor growth, and metastasis. Proc Natl Acad Sci U S A 110(51): 20717–20722. doi: 10.1073/pnas.1321139110
[40] Alliot F, Rutin J, Leenen PJM, Pessac B (1999) Pericytes and periendothelial cells of brain parenchyma vessels Co-express aminopeptidase N, aminopeptidase A, and nestin. J Neurosci Res 58(3): 367–378.
[41] Quan WQ, Luo QH, Tang QQ, Furihata T, Li D, Fassbender K, et al. (2020) NLRP3 Is Involved in the Maintenance of Cerebral Pericytes. Front Cell Neurosci 14. doi: ARTN 276 10.3389/fncel.2020.00276
[42] Cai J, Kehoe O, Smith GM, Hykin P, Boulton ME (2008) The angiopoietin/Tie-2 system regulates pericyte survival and recruitment in diabetic retinopathy. Invest Ophthalmol Vis Sci 49(5): 2163–2171. doi: 10.1167/iovs.07-1206
[43] An D, Chung-Wah-Cheong J, Yu DY, Balaratnasingam C (2022) Alpha-Smooth Muscle Actin Expression and Parafoveal Blood Flow Pathways Are Altered in Preclinical Diabetic Retinopathy. Invest Ophthalmol Vis Sci 63(5): 8. doi: 10.1167/iovs.63.5.8
[44] Schlingemann RO, Rietveld FJ, Kwaspen F, van de Kerkhof PC, de Waal RM, Ruiter DJ (1991) Differential expression of markers for endothelial cells, pericytes, and basal lamina in the microvasculature of tumors and granulation tissue. Am J Pathol 138(6): 1335–1347.
[45] Liu C, Ge HM, Liu BH, Dong R, Shan K, Chen X, et al. (2019) Targeting pericyte-endothelial cell crosstalk by circular RNA-cPWWP2A inhibition aggravates diabetes-induced microvascular dysfunction. Proc Natl Acad Sci U S A 116(15): 7455–7464. doi: 10.1073/pnas.1814874116
[46] Ivanova E, Kovacs-Oller T, Sagdullaev BT (2017) Vascular Pericyte Impairment and Connexin43 Gap Junction Deficit Contribute to Vasomotor Decline in Diabetic Retinopathy. J Neurosci 37(32): 7580–7594. doi: 10.1523/JNEUROSCI.0187-17.2017
[47] Ding L, Cheng R, Hu Y, Takahashi Y, Jenkins AJ, Keech AC, et al. (2014) Peroxisome proliferator-activated receptor alpha protects capillary pericytes in the retina. Am J Pathol 184(10): 2709–2720. doi: 10.1016/j.ajpath.2014.06.021
[48] Pina R, Santos-Diaz AI, Orta-Salazar E, Aguilar-Vazquez AR, Mantellero CA, Acosta-Galeana I, et al. (2022) Ten Approaches That Improve Immunostaining: A Review of the Latest Advances for the Optimization of Immunofluorescence. Int J Mol Sci 23(3). doi: 10.3390/ijms23031426
[49] Shi H, Koronyo Y, Rentsendorj A, Regis GC, Sheyn J, Fuchs DT, et al. (2020) Identification of early pericyte loss and vascular amyloidosis in Alzheimer's disease retina. Acta Neuropathol 139(5): 813–836. doi: 10.1007/s00401-020-02134-w
[50] van der Wijk AE, Wisniewska-Kruk J, Vogels IMC, van Veen HA, Ip WF, van der Wel NN, et al. (2019) Expression patterns of endothelial permeability pathways in the development of the blood-retinal barrier in mice. FASEB J 33(4): 5320–5333. doi: 10.1096/fj.201801499RRR
[51] Mai-Morente SP, Marset VM, Blanco F, Isasi EE, Abudara V (2021) A nuclear fluorescent dye identifies pericytes at the neurovascular unit. J Neurochem 157(4): 1377–1391. doi: 10.1111/jnc.15193
[52] Baykal B, Korkmaz C, Kocabiyik N, Ceylan OM (2018) The influence of post-fixation on visualising vimentin in the retina using immunofluorescence method. Folia Morphol (Warsz) 77(2): 246–252. doi: 10.5603/FM.a2017.0082
[53] Fra-Bido S, Walker SA, Innocentin S, Linterman MA (2021) Optimized immunofluorescence staining protocol for imaging germinal centers in secondary lymphoid tissues of vaccinated mice. STAR Protoc 2(3): 100499. doi: 10.1016/j.xpro.2021.100499
[54] Zhang N, Cao W, He X, Xing Y, Yang N (2022) Using methanol to preserve retinas for immunostaining. Clin Exp Ophthalmol 50(3): 325–333. doi: 10.1111/ceo.14042

[55] Tual-Chalot S, Allinson KR, Fruttiger M, Arthur HM (2013) Whole mount immunofluorescent staining of the neonatal mouse retina to investigate angiogenesis in vivo. J Vis Exp(77): e50546. doi: 10.3791/50546
[56] van Seijen M, Brcic L, Gonzales AN, Sansano I, Bendek M, Brcic I, et al. (2019) Impact of delayed and prolonged fixation on the evaluation of immunohistochemical staining on lung carcinoma resection specimen. Virchows Arch 475(2): 191–199. doi: 10.1007/s00428-019-02595-9
[57] Stumptner C, Pabst D, Loibner M, Viertler C, Zatloukal K (2019) The impact of crosslinking and non-crosslinking fixatives on antigen retrieval and immunohistochemistry. N Biotechnol 52: 69–83. doi: 10.1016/j.nbt.2019.05.003
[58] Goldenthal KL, Hedman K, Chen JW, August JT, Willingham MC (1985) Postfixation detergent treatment for immunofluorescence suppresses localization of some integral membrane proteins. J Histochem Cytochem 33(8): 813–820. doi: 10.1177/33.8.3894499
[59] Im K, Mareninov S, Diaz MFP, Yong WH (2019) An Introduction to Performing Immunofluorescence Staining. Methods Mol Biol 1897: 299–311. doi: 10.1007/978-1-4939-8935-5_26
[60] Meyerholz DK, Beck AP (2018) Principles and approaches for reproducible scoring of tissue stains in research. Lab Invest 98(7): 844–855. doi: 10.1038/s41374-018-0057-0
[61] North AJ (2006) Seeing is believing? A beginners' guide to practical pitfalls in image acquisition. J Cell Biol 172(1): 9–18. doi: 10.1083/jcb.200507103
[62] Pittner S, Merold V, Anders S, Lohner L, Amendt J, Klinger M, et al. (2022) A standard protocol for the analysis of postmortem muscle protein degradation: process optimization and considerations for the application in forensic PMI estimation. Int J Legal Med 136(6): 1913–1923. doi: 10.1007/s00414-022-02849-3
[63] Shihan MH, Novo SG, Le Marchand SJ, Wang Y, Duncan MK (2021) A simple method for quantitating confocal fluorescent images. Biochem Biophys Rep 25: 100916. doi: 10.1016/j.bbrep.2021.100916
[64] Chan-Ling T, Koina ME, McColm JR, Dahlstrom JE, Bean E, Adamson S, et al. (2011) Role of CD44+ stem cells in mural cell formation in the human choroid: evidence of vascular instability due to limited pericyte ensheathment. Invest Ophth Vis Sci 52(1): 399–410. doi: 10.1167/iovs.10-5403
[65] Dominguez E, Raoul W, Calippe B, Sahel JA, Guillonneau X, Paques M, et al. (2015) Experimental Branch Retinal Vein Occlusion Induces Upstream Pericyte Loss and Vascular Destabilization. PLoS One 10(7): e0132644. doi: 10.1371/journal.pone.0132644
[66] Gu X, Fliesler SJ, Zhao YY, Stallcup WB, Cohen AW, Elliott MH (2014) Loss of caveolin-1 causes blood-retinal barrier breakdown, venous enlargement, and mural cell alteration. Am J Pathol 184(2): 541–555. doi: 10.1016/j.ajpath.2013.10.022
[67] Trost A, Motloch K, Bruckner D, Schroedl F, Bogner B, Kaser-Eichberger A, et al. (2015) Time-dependent retinal ganglion cell loss, microglial activation and blood-retina-barrier tightness in an acute model of ocular hypertension. Exp Eye Res 136: 59–71. doi: 10.1016/j.exer.2015.05.010
[68] Kovacs-Oller T, Ivanova E, Szarka G, Tengolics AJ, Volgyi B, Sagdullaev BT (2020) Imatinib Sets Pericyte Mosaic in the Retina. Int J Mol Sci 21(7). doi: 10.3390/ijms21072522
[69] Smyth LCD, Highet B, Jansson D, Wu J, Rustenhoven J, Aalderink M, et al. (2022) Characterisation of PDGF-BB:PDGFRbeta signalling pathways in human brain pericytes: evidence of disruption in Alzheimer's disease. Commun Biol 5(1): 235. doi: 10.1038/s42003-022-03180-8
[70] Lee SJ, Kim S, Jo DH, Cho CS, Kim SR, Kang D, et al. (2021) Specific ablation of PDGFRbeta-overexpressing pericytes with antibody-drug conjugate potently inhibits pathologic ocular neovascularization in mouse models. Commun Med (Lond) 1: 58. doi: 10.1038/s43856-021-00059-3
[71] Reagan AM, Gu XW, Paudel S, Ashpole NM, Zalles M, Sonntag WE, et al. (2018) Age-related focal loss of contractile vascular smooth muscle cells in retinal arterioles is accelerated by caveolin-1 deficiency. Neurobiol Aging 71: 1–12. doi: 10.1016/j.neurobiolaging.2018.06.039
[72] Crisan M, Corselli M, Chen WC, Peault B (2012) Perivascular cells for regenerative medicine. J Cell Mol Med 16(12): 2851–2860. doi: 10.1111/j.1582-4934.2012.01617.x

[73] Yamazaki T, Mukouyama YS (2018) Tissue Specific Origin, Development, and Pathological Perspectives of Pericytes. Front Cardiovasc Med 5: 78. doi: 10.3389/fcvm.2018.00078
[74] Zhang ZS, Zhou HN, He SS, Xue MY, Li T, Liu LM (2020) Research advances in pericyte function and their roles in diseases. Chin J Traumatol 23(2): 89–95. doi: 10.1016/j.cjtee.2020.02.006
[75] Stark K, Eckart A, Haidari S, Tirniceriu A, Lorenz M, von Bruhl ML, et al. (2013) Capillary and arteriolar pericytes attract innate leukocytes exiting through venules and 'instruct' them with pattern-recognition and motility programs. Nat Immunol 14(1): 41–51. doi: 10.1038/ni.2477
[76] Kitahara H, Kajikawa S, Ishii Y, Yamamoto S, Hamashima T, Azuma E, et al. (2018) The Novel Pathogenesis of Retinopathy Mediated by Multiple RTK Signals is Uncovered in Newly Developed Mouse Model. Ebiomedicine 31: 190–201. doi: 10.1016/j.ebiom.2018.04.021
[77] Paul G, Ozen I, Christophersen NS, Reinbothe T, Bengzon J, Visse E, et al. (2012) The adult human brain harbors multipotent perivascular mesenchymal stem cells. PLoS One 7(4): e35577. doi: 10.1371/journal.pone.0035577
[78] Wolf J, Boneva S, Schlecht A, Lapp T, Auw-Haedrich C, Lagreze W, et al. (2022) The Human Eye Transcriptome Atlas: A searchable comparative transcriptome database for healthy and diseased human eye tissue. Genomics 114(2): 110286. doi: 10.1016/j.ygeno.2022.110286
[79] Piña R, Santos-Díaz AI, Orta-Salazar E, Aguilar-Vazquez AR, Mantellero CA, Acosta-Galeana I, et al. (2022) Ten Approaches That Improve Immunostaining: A Review of the Latest Advances for the Optimization of Immunofluorescence. International Journal of Molecular Sciences 23(3). doi: 10.3390/ijms23031426
[80] Kim SW, Roh J, Park CS (2016) Immunohistochemistry for Pathologists: Protocols, Pitfalls, and Tips. J Pathol Transl Med 50(6): 411–418. doi: 10.4132/jptm.2016.08.08
[81] Peck AR, Girondo MA, Liu C, Kovatich AJ, Hooke JA, Shriver CD, et al. (2016) Validation of tumor protein marker quantification by two independent automated immunofluorescence image analysis platforms. Mod Pathol 29(10): 1143–1154. doi: 10.1038/modpathol.2016.112
[82] Bianchi E, Ripandelli G, Feher J, Plateroti AM, Plateroti R, Kovacs I, et al. (2015) Occlusion of retinal capillaries caused by glial cell proliferation in chronic ocular inflammation. Folia Morphol (Warsz) 74(1): 33–41. doi: 10.5603/FM.2015.0006
[83] Kur J, Newman EA, Chan-Ling T (2012) Cellular and physiological mechanisms underlying blood flow regulation in the retina and choroid in health and disease. Prog Retin Eye Res 31(5): 377–406. doi: 10.1016/j.preteyeres.2012.04.004
[84] Huang BB, Fukuyama H, Burns SA, Fawzi AA (2024) Imaging the Retinal Vascular Mural Cells In Vivo: Elucidating the Timeline of Their Loss in Diabetic Retinopathy. Arterioscl Throm Vas 44(2): 465–476. doi: 10.1161/Atvbaha.123.320169
[85] Burns SA, Elsner AE, Sapoznik KA, Warner RL, Gast TJ (2019) Adaptive optics imaging of the human retina. Prog Retin Eye Res 68: 1–30. doi: 10.1016/j.preteyeres.2018.08.002
[86] Chui TY, Gast TJ, Burns SA (2013) Imaging of vascular wall fine structure in the human retina using adaptive optics scanning laser ophthalmoscopy. Invest Ophthalmol Vis Sci 54(10): 7115–7124. doi: 10.1167/iovs.13-13027
[87] Trost A, Lange S, Schroedl F, Bruckner D, Motloch KA, Bogner B, et al. (2016) Brain and Retinal Pericytes: Origin, Function and Role. Front Cell Neurosci 10: 20. doi: 10.3389/fncel.2016.00020
[88] Goncalves LM, Barboza CA, Almaça J (2024) Diabetes as a Pancreatic Microvascular Disease-A Pericytic Perspective. J Histochem Cytochem 72(3): 131–148. doi: 10.1369/00221554241236535
[89] Park DY, Lee J, Kim J, Kim K, Hong S, Han S, et al. (2017) Plastic roles of pericytes in the blood-retinal barrier. Nat Commun 8: 15296. doi: 10.1038/ncomms15296
[90] Benarroch E (2023) What Are the Roles of Pericytes in the Neurovascular Unit and Its Disorders? Neurology 100(20): 970–977. doi: 10.1212/WNL.0000000000207379
[91] Eltanahy AM, Koluib YA, Gonzales A (2021) Pericytes: Intrinsic Transportation Engineers of the CNS Microcirculation. Front Physiol 12: 719701. doi: 10.3389/fphys.2021.719701

Supplementary figures

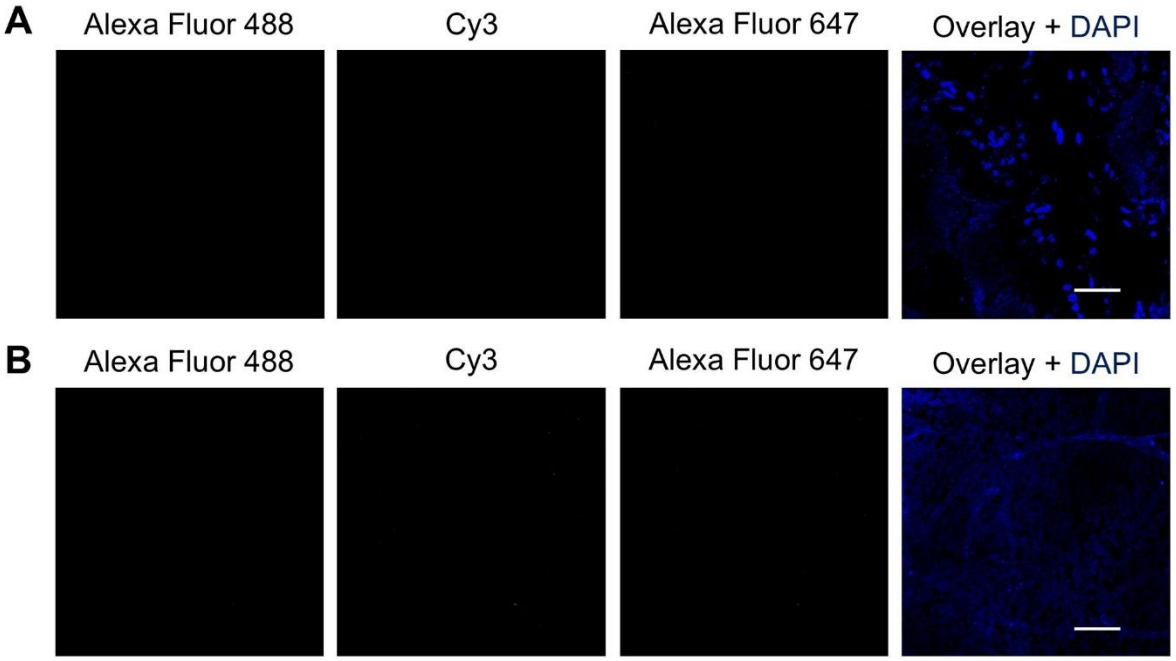

Supplementary Figure 1. Representative immunofluorescence staining images of negative controls of human retinal flatmounts. Immunostaining with secondary antibody only as a negative control under identical conditions for staining of (A) NG2, PDGFRβ and laminin, and (B) αSMA, PDGFRβ and laminin. Nuclei were stained with DAPI (blue). Scale bar = 50 µm.

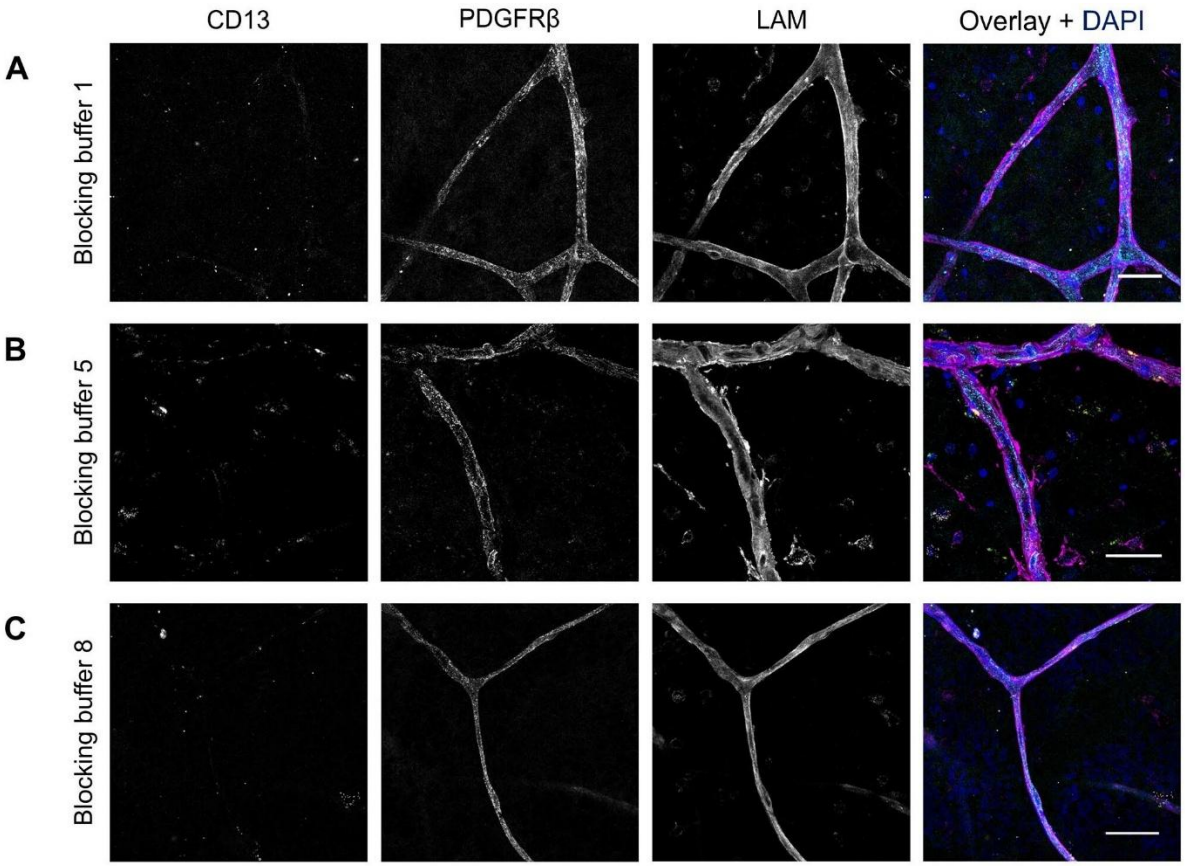

Supplementary Figure 2. Effect of different blocking buffers on immunofluorescence double staining of CD13 and PDGFRβ in human retinal flatmounts. The pericyte markers CD13 (yellow) and PDGFRβ (cyan) were immunostained using antibodies in conditions optimized for double staining of NG2 and PDGFRβ, performed with blocking buffer 1 (A), blocking buffer 5 (B) or blocking buffer 8 (C). Basal lamina was stained with anti-laminin (LAM) antibodies (magenta) and nuclei with DAPI (blue). Scale bar = 50 µm.

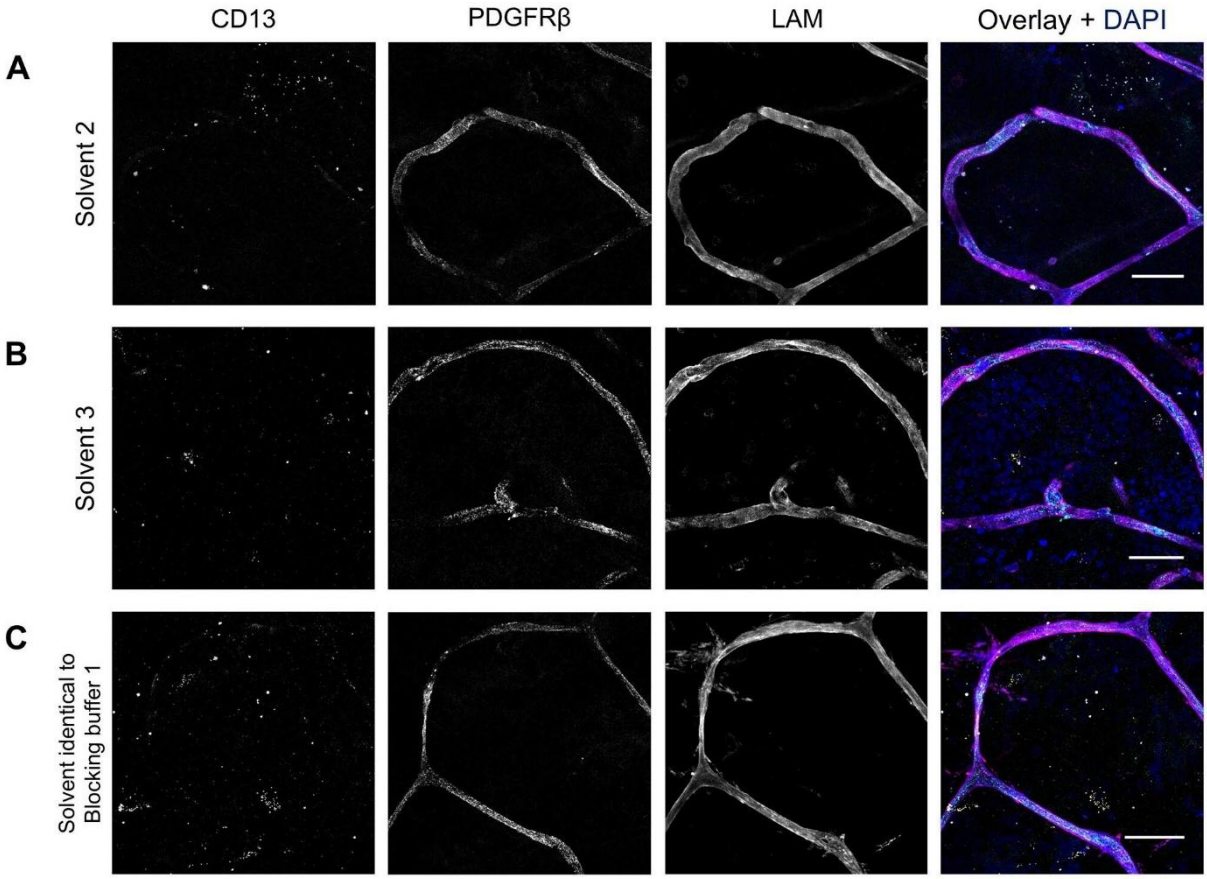

Supplementary Figure 3. Effect of different antibody solvents on immunofluorescence double staining of CD13 and PDGFRβ in human retinal flatmounts. Immunofluorescence double staining of CD13 (yellow) and PDGFRβ (cyan) after testing antibody solvent 2 (A), solvent 3 (B) or a solvent identical to blocking buffer 1 (C). Basal lamina was stained with anti-laminin antibodies (magenta) and nuclei with DAPI (blue). Scale bar = 50 µm.

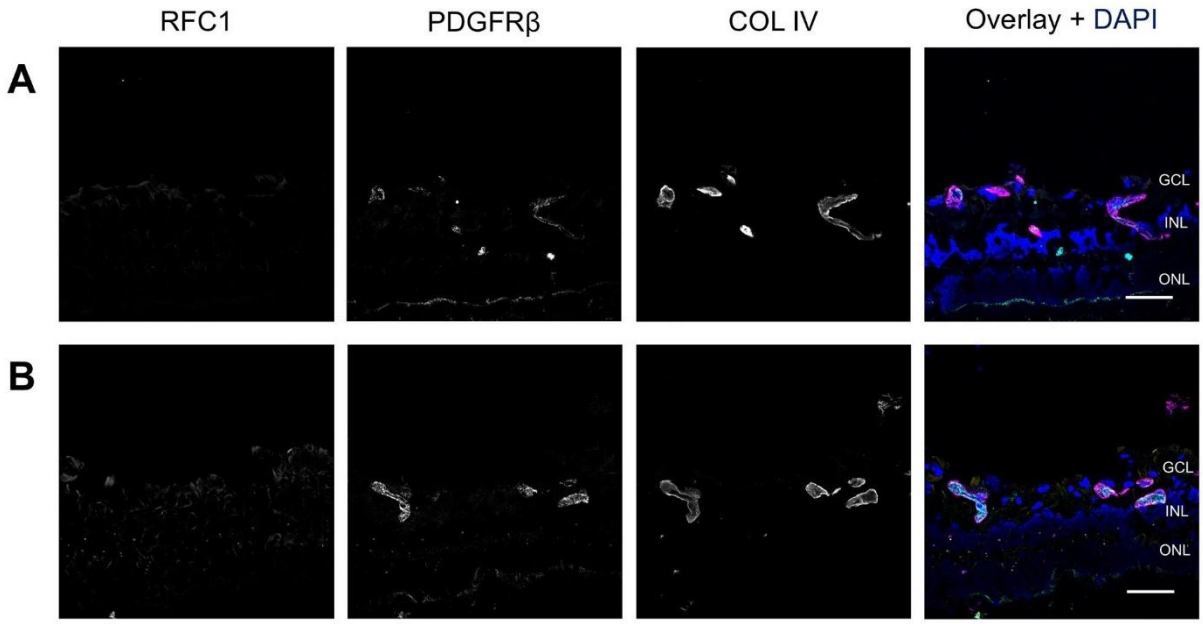

Supplementary Figure 4. Comparing optimized immunofluorescence protocols for immunofluorescence double staining of RFC1 and PDGFRβ in human retinal cryosections. Immunofluorescence double staining of RFC1 (yellow) and PDGFRβ (cyan) using the optimized double staining protocol for PDGFRβ and NG2 (A) or using an adapted protocol from Gurler at al. (B). Basal lamina was stained with anti-collagen type IV (COL IV) antibodies (magenta) and nuclei with DAPI (blue). Scale bar = 50 µm. Abbreviations: GCL = ganglion cell layer, INL = inner nuclear layer, ONL = outer nuclear layer.

Chapter 6

Differential pericyte pathology in the human retina and brain in diabetes mellitus and Alzheimer's disease

Noëlle Bakker-van Bugnum[1,2,3], Aïcha A. Croes[1], Eva Prevaes[1], Cornelis J. F. van Noorden[1], Reinier O. Schlingemann[1,2,3,4], and Ingeborg Klaassen[1,2,3], on behalf of the RECOGNISED Consortium

[1] Ocular Angiogenesis Group, Department of Ophthalmology, Amsterdam UMC location University of Amsterdam, Amsterdam, The Netherlands.
[2] Amsterdam Cardiovascular Sciences, Microcirculation, Amsterdam, The Netherlands.
[3] Amsterdam Neuroscience, Cellular & Molecular Mechanisms, Amsterdam, The Netherlands.
[4] Department of Ophthalmology, Jules-Gonin Eye Hospital, Fondation Asile des Aveugles, University of Lausanne, Lausanne, Switzerland

Frontiers in Neuroscience (2026) 20:1749112

Abstract

In diabetic retinopathy, pericyte dysfunction, pericyte loss, and inner blood–retinal barrier (iBRB) dysfunction contribute to neurovascular unit (NVU) impairment. Diabetes mellitus (DM) is also associated with increased risk of Alzheimer's disease (AD), and it has been hypothesized that DM-induced NVU impairment in brain capillaries, including pericyte dysfunction, may contribute to AD pathogenesis In the present hypothesis-generating explorative study, we investigated pericyte characteristics in the iBRB in patients with type 2 DM with or without diabetic retinopathy (DR), and in the blood–brain barrier (BBB) in type 2 DM and AD. We analysed human retina and brain samples from controls and donors with DM and/or AD. Immunofluorescence staining for NG2, PDGFRβ, and αSMA was performed to analyse pericyte marker expression, vascular staining coverage, and pericyte cellular density on capillaries. In control retina and brain, the average pericyte staining coverage of capillaries was 70–80% based on NG2 and PDGFRβ expression, but only 25% when based on αSMA expression. Pericyte densities were 7 and 9 pericytes/mm capillary length in the control retina and brain, respectively. DM and DR retinas showed marked density reductions to 4 pericytes/mm capillary length. In DM without DR, retinal vascular staining coverage of NG2 and PDGFRβ decreased to 50–56%. In DR retinas, vascular coverage based on NG2 staining was comparable to controls, whereas coverage based on PDGFRβ staining was significantly reduced to 45%. Such reductions were not observed in brain samples from donors with DM or AD; however, NG2 staining was reduced. Both NG2 and PDGFRβ staining were markedly reduced in brain samples from donors with both DM and AD. These trends suggest a specific pericyte pathology in the brain in cases of DM and AD, particularly in patients with both conditions, which differs from the well-characterized pericyte loss observed in the diabetic retina.

Introduction

Individuals with diabetes mellitus (DM) carry a higher risk of developing dementia, but the mechanisms underlying this association remain unclear [1]. Diabetes impairs the retinal neurovascular unit (NVU) through various molecular and cellular alterations, driving diabetic retinopathy (DR) progression [2]. Patients with diabetes may exhibit thickening of the basal lamina, decreased junctional protein levels, pericyte dysfunction and loss, neurodegeneration, increased endothelial transcellular transport, microglia activation, glial cell dysfunction and loss, and endothelial cell damage or death. It is presently unknown whether similar NVU changes occur in the brain in cases of DM or DM-associated Alzheimer's disease (AD). Studies in experimental animal models of diabetes, and incidental reports on human DM brain tissue, have yielded conflicting results regarding diabetes-induced NVU impairment [3-11].

Pericytes play crucial roles in the formation and maintenance of the inner blood–retinal barrier (iBRB) and blood–brain barrier (BBB) [1, 8, 12-14]. Retinal pericyte loss is an early event in diabetic retinopathy [1, 2, 12], which has also been reported to occur in the brain during experimental diabetes [3, 15], although human studies are lacking. Pericyte loss occurs via migration away from capillaries or cell death [12], and may be caused by inflammatory mechanisms, oxidative stress, increased levels of advanced glycation end-products, high levels of angiopoietin-2, and thickening of the basal lamina [1, 2, 16]. Pericyte loss can result in changes in blood flow, microaneurysm formation, abnormal capillary remodelling and nonperfusion, and increased capillary permeability resulting in oedema [1, 17, 18].

No clinical biomarkers are currently available to identify DM patients at higher risk of cognitive decline or dementia [1, 19]. Given the shared embryonic origin of the retina and brain [8], it is possible that retinal biomarkers reflecting NVU degeneration could serve as early indicators of cognitive impairment in DM patients. However, this assumes that common vascular pathological mechanisms underlie both brain and retinal changes in DM and AD. To further explore this possibility, in the present study, we investigated the brain and retinal vasculature in DM and AD, with particular focus on the pericytes of the NVU in the human retina and brain.

In this explorative hypothesis-generating study, we examined pericyte alterations in the iBRB in DM, and in the BBB in DM and AD. To characterize pericytes in human retina and brain tissues, we performed immunofluorescence staining for neural/glial antigen 2 (NG2), platelet-derived growth factor receptor beta (PDGFRβ), and alpha smooth muscle actin (αSMA). Apart from our previous investigations [20, 21], no studies have systemically analysed NG2, PDGFRβ, and αSMA expression in pericytes of the adult human retina and brain. NG2 and PDGFRβ are receptors on the pericyte membrane; upon their activation, intracellular signalling pathways facilitate pericyte proliferation, and pericyte recruitment to newly formed vessels [8, 20, 22]. Interactions with endothelial cells enable maturation of the iBRB and BBB [12]. αSMA is a contractile protein found in smooth muscle cells and pericytes, which likely mediates pericyte contraction to regulate capillary diameter and blood flow in response to neural activity [23, 24]. Our analyses included retinal samples from donors with type 2 DM, with or without DR, and rare brain tissues from donors with type 2 DM, AD, or

both conditions. This comprehensive approach enabled quantitative comparisons of pericyte cellular density and vascular staining coverage based on these pericyte markers, as well as assessment of the marker expression patterns in neurovascular pathological conditions affecting both the retina and brain.

Materials and methods

Retinal tissue

Human post-mortem retina tissue samples were processed as previously described [20]. Retinal tissues were obtained from three donor groups: donors with type 2 DM without DR (mean age of 67 ± 2.3 years), donors with type 2 DM and DR (mean age of 65 ± 8.1 years), and non-diabetic controls (mean age of 67 ± 0.8 years) (n=4 for all groups). The male-to-female ratio was 2:2 (DM no DR), 1:3 (DR), and 1:3 (controls). Table 1 summarizes the donors' characteristics. The current research performed on human eyes is in accordance with all requirements stated in the Dutch law "Wet op orgaandonatie" that describes the use of donor material for research purposes. According to this law, donors provide written informed consent for donation with an opt out of left-over material for related scientific research purposes. Specific requirements for the use for scientific research of left-over material originating from corneal grafting have been described in an additional document formulated by the Ministry of Health, Welfare, and Sport and the Bio Implant Services (BIS) Foundation (Eurotransplant; Leiden, the Netherlands, July 21, 1995; 6714.ht). The eyes were stored anonymously and, therefore, approval of their use by the Ethics Committee was not required by Dutch law.

Immunofluorescence staining of retinal tissue

Human retinal flatmounts were subjected to immunofluorescence double staining for NG2 and PDGFRβ, and for αSMA and PDGFRβ, which was performed after optimization, as recently described (Bakker et al., 2025). Retinal flatmounts were used instead of tissue sections, to enable 3D reconstruction of pericytes on capillaries and of their distribution across the vascular network, including their position relative to arteries, veins, and microvascular branches. Table 2 lists the primary antibodies used in this study. Flatmounts stained for laminin, NG2, and PDGFRβ were incubated with the following secondary antibodies: donkey anti-goat Cy3, donkey anti-rabbit Alexa Fluor™ 488, and donkey anti-mouse Alexa Fluor™ 647 (Table 3). Flatmounts stained for laminin, αSMA, and PDGFRβ were incubated with the following secondary antibodies: donkey anti-goat Cy3, donkey anti-rabbit Alexa Fluor™ 488, and donkey anti-mouse Alexa Fluor™ 647 (Table 3).

Brain tissue

Post-mortem samples of the human frontal cortex were provided by the Netherlands Brain Bank, Amsterdam, The Netherlands (NBB project 1345S). Frontal cortex samples were selected, because pathological features, including vascular pathology [25, 26], appear in the frontal cortex during early stages of dementia [27-29]. All donors or their relatives provided written informed consent for brain autopsy and the use of brain tissue for research purposes. This usage was in accordance with the Declaration of Helsinki on the use of human material for scientific research. Brain tissues were collected within several hours post-mortem, dissected, snap frozen in liquid nitrogen, and stored at −80°C until sectioning. Donors were

Table 1. Information about retinal tissue donors.

Case	Laser yes/ no	Sex (F/M)	Age at death (y)	Post-mortem delay (h)	Age at diabetes onset (y)	Insulin use (yes/no)	Diagnosis	Cause of death
Control								
1	No	F	68	14		No	Stomach cancer	Cancer (stomach)
2	No	F	68	17		No	Myocardial infarction	Myocardial infarction
3	No	F	67	12		No	Atherosclerotic disease, chronic kidney failure, narrowed coronary arteries	Atherosclerotic disease
4	No	M	66	9		No	Lung embolism	Melanoma
Mean ± SD			*67 ± 0.8*	*13.0 ± 2.9*				
DM no DR								
5	No	M	67	15	Unknown	No	Vascular disease, leg amputation	Aortic aneurysm
6	No	M	65	11	63	No	COPD, acute bronchitis, hyperthyroidism	Lung condition
7	No	F	66	13	Unknown	No	Brain metastasis	Brain metastasis
8	No	F	71	10	Unknown	No	Breast carcinoma, alcohol abuse, hepatocellular carcinoma	Hepatic coma, liver failure
Mean ± SD			*67 ± 2.3*	*12.3 ± 1.9*				
DM + DR								
9	Yes	F	66	19	Unknown	No	Heart failure	Heart failure
10	Yes	F	61	13	<49	Yes	Heart failure	Heart failure
11	Yes	M	77	18	62	Yes	Heart failure, kidney stones, hypertension, cerebral hematoma	Heart failure
12	Unknown	F	55	10	41	No	Hypertension, adiposity, high cholesterol, lipid disorder, fatty liver	Heart failure
Mean ± SD			*65 ± 8.1*	*15.0 ± 3.7*				

DM, diabetes mellitus; *DR*, diabetic retinopathy

Table 2. Primary antibodies used in this study.

Antigen	Host species	Source	Working dilution
Laminin	Rabbit	Abcam, Ab11575	1:1000
NG2	Mouse	Merck Life Science, MAB2029	1:100 (retina)/1:200 (brain)
PDGFRβ	Goat	R&D Systems, AF385	1:100
αSMA	Mouse	DAKO, M0851	1:500

R&D systems (Minneapolis, MI); DAKO (Santa Clara, CA)

Table 3. Secondary antibodies used in this study.

Antibody	Conjugate	Source	Working dilution
Donkey anti-rabbit IgG	Alexa Fluor™ 488	Invitrogen, A-21206	1:400
Donkey anti-mouse IgG	Alexa Fluor™ 488 plus	Invitrogen, A-32766	1:1000
Donkey anti-goat IgG	Cy3	Jackson, 705-165-147	1:200
Donkey anti-rabbit IgG	Alexa Fluor™ 647	Invitrogen, A-31573	1:500
Donkey anti-mouse IgG	Alexa Fluor™ 647	Invitrogen, A-31571	1:200

Invitrogen (Waltcam, MA); Jackson ImmunoResearch Laboratories (West Grove, PA)

classified into four groups: donors with type 2 DM (mean age of 72 ± 9.6 years) (n=4), donors with AD (mean age of 74 ± 7.6 years) (n=4), donors with type 2 DM and AD (mean age of 74 ± 6.6 years) (n=4), and non-diabetic non-AD controls (mean age of 70 ± 12.2 years) (n=3). Clinical diagnoses were confirmed by autopsy findings. The male-to-female ratio was 2:2 (DM), 3:1 (AD), 3:1 (DM + AD), and 1:2 (controls). Table 4 summarizes the donors' characteristics. The subject groups were age-matched to the controls, to account for age-dependent loss of BBB integrity [30].

Immunofluorescence staining of brain tissue

Brain tissue specimens were cut into 20-µm-thick sections at −20°C, using an Microm Cryo Star HM 560 cryostat (Thermo Fisher Scientific), which were stored at −80°C until further use. These thick brain sections enabled 3D visualization of pericytes. In preparation for immunofluorescence staining, the tissue sections were air dried at RT for 20 min. Next, the sections were fixed with 4% formaldehyde (28908; Thermo Fisher Scientific) for 20 min, and then washed once in 3× PBS for 10 min. Non-specific fluorescence was blocked following an adaptation of the methods described by Ma et al (Ma et al., 2018). The sections were blocked and permeabilized by incubation in PBS supplemented with 0.2% BSA, 0.3% T-X, and 5% normal donkey serum, at RT for 1 h. Directly after incubation with blocking buffer, the sections were incubated with primary antibodies (Table 2) diluted in 0.2% BSA in PBS, overnight at 4°C. Subsequently, the sections were washed three times with PBS for 10 min each. To reduce lipofuscin autofluorescence, the sections were incubated in Trueblack (Zhang et al., 2022; Stillman et al., 2023) (23007; Biotium, Fremont, CA) diluted 20× in 70% ethanol for 30 sec, and were then washed three times in PBS for 10 min each. Next, the sections were incubated for 1 h at RT in the dark with the following secondary antibodies: donkey anti-mouse Alexa Fluor™ plus 488, donkey anti-goat Cy3, and donkey anti-rabbit Alexa Fluor™ 647 (Table 3). Following this incubation, the sections were washed three times with PBS for 10 min each. Finally, the sections were mounted with Vectashield antifading mounting medium containing DAPI (H-1200-10; Vector Laboratories), covered with a cover glass, and sealed with transparent nail varnish.

Table 4. Information about brain tissue donors.

Case	Sex (F/M)	Age at death (y)	Post-mortem delay (h)	Age at disease onset (y)	Braak stage (0–6)	Vascular pathology in frontal cortex	Neuropathology in frontal cortex	Cause of death
Control								
1	F	66	6.3		1	Slight atherosclerosis	Myelin pallor, only MS plaques, no AD plaques	Cancer
2	M	58	7.7		0	Slight atherosclerosis	Partly absent myelination, no amyloid plaques	Myocardial ischemia
3	F	87	4.6		2	Slight atherosclerosis	No CAA, moderate number of amyloid diffuse plaques, a few classic plaques, no tangles	Pneumonia
Mean ± SD		*70 ± 12.2*	*6.2 ± 1.3*					
DM								
4	F	70	6.0	50	2	Slight atherosclerosis, perivascular oedema, some iron pigment	Few diffuse plaques, no CAA, no tangles	Kidney failure
5	M	67	9.0	61	1	Slight atherosclerosis	No CAA, moderate-to-large number of diffuse plaques, no tangles, slight perivascular oedema	Aortic aneurysm, asystole
6	M	65	7.2	Unknown	2	Slight atherosclerosis	No plaques or tangles, some tau-positive cells	Fever, neuroleptic malignant syndrome
7	F	86	7.5	Unknown	2	Slight atherosclerosis, severe perivascular oedema	No CAA; moderate number of plaques, equal numbers of diffuse and classic types; no tangles	Cancer
Mean ± SD		*72 ± 9.6*	*7.4 ± 1.2*					

Table 4. Information about brain tissue donors (continued).

Case	Sex (F/ M)	Age at death (y)	Post-mortem delay (h)	Age at disease onset (y)	Braak stage (0–6)	Vascular pathology in frontal cortex	Neuropathology in frontal cortex	Cause of death
AD								
8	F	78	7.5	71	5	Slight atherosclerosis	Moderate CAA; no dyshoric angiopathy; no striking capillary angiopathy; moderate-to-many amyloid plaques, especially diffuse; many tangles	Dehydration
9	M	75	6.3	66	5	Slight atherosclerosis	Slight CAA; many diffuse and classic plaques; presence of tangles, neuritic plaques, and Lewy bodies	Cachexia
10	M	63	9.8	56	6	Slight to severe atherosclerosis	Slight CAA with dyshoric angiopathy and no capillary angiopathy; many plaques, diffuse types and classic types; many tangles	Dehydration/ cachexia
11	M	80	5.5	79	6	No atherosclerosis	CAA present, many diffuse plaques and few classic plaques, presence of tangles and Lewy bodies	Dehydration and pneumonia
Mean ± SD		*74 ± 7.6*	*7.3 ± 1.9*					
DM + AD								
12	M	67	5.4	DM and Dem: unknown	5	Slight atherosclerosis	Many senile plaques, neurofibrillary tangles and many neuropil threads; moderate number of plaques, mainly "classic" plaques with large cores	Cerebral infarction
13	M	71	4.0	DM: 57; Dem: 64	6	Slight atherosclerosis	Large plaques with coarse fibrils of weakly staining amyloid, few diffuse plaques, many neuritic plaques, and a moderate amount of tangles	Dementia, delirium, and dehydration
14	M	82	8.5	DM: unknown; Dem: 80	5	Perivascular oedema	Many amyloid beta depositions, including diffuse plaques, classic plaques, and small depositions; many neuropil threads, tangles, and dispersed neuritic plaques; myelination is normal	Heart failure
15	F	77	3.8	DM: 73; Dem: 73	5	Moderate atherosclerosis	Slight to moderate CAA, mostly diffuse plaques, few-to-moderate neuritic plaques, moderate number of tangles, many Lewy inclusions, many Lewy threads	Infection and dehydration
Mean ± SD		*74 ± 6.6*	*5.4 ± 2.2*					

AD, Alzheimer's disease; *CAA*, cerebral amyloid angiopathy; *DM*, diabetes mellitus; *Dem*, dementia

Microscopical analysis of pericyte staining in 3D

Imaging was performed as previously described [20]. Images of at least 10 randomly selected areas in a section were analysed for quantification for each patient group (n=3–4 donors per group). For each marker, the exposure time and laser intensity were maintained constant for each section, among all patient groups. Three-dimensional confocal images were projected with maximum intensity projection from 5.89-µm-thick z-stacks for the retinal flatmounts, and from 4.5-µm-thick z-stacks for brain samples, each with a step size of 0.346 µm.

Quantification

Pericyte staining was quantified using ImageJ software (National Institutes of Health). Relative vascular staining coverage was calculated as % pericyte marker+ area/total vessel area, as determined by laminin immunofluorescence staining. Regions of interest (ROIs) were drawn manually (brain samples) or automatically (retina samples) around the vasculature, using ImageJ running macro script 1. Details are provided in Supplementary Figure 1. To select for capillaries and avoid small fragments of blood vessels, respectively, we excluded blood vessels with a diameter of >10 µm and those with a length of <20 µm.

Before quantifying vascular staining coverage, we determined the background intensity for each pericyte marker in three equally-sized square regions, outside of blood vessels, in every image. The mean intensity from these background regions was used as the threshold for background subtraction using the ImageJ macro script 2 (Supplementary Figure 2).

Vascular staining coverage was quantified as the percentage of pericyte area colocalized with vascular ROI, as determined by laminin immunofluorescence staining, using ImageJ Area Fraction measurement. The results were averaged across all images per donor.

Pericyte cellular density was quantified by manually counting the NG2-positive pericyte bodies (identified based on their characteristic nodular or bump-shaped morphology) per mm of capillary length. To obtain vascular area measurements, laminin-positive blood vessels were traced in ImageJ, generating ROIs for each image. To measure capillary length in the laminin channel, a line was manually drawn through the central axis of each blood vessel in ImageJ. Finally, pericyte cellular density was calculated as the average number of pericyte bodies per mm capillary length for each donor.

Statistical analysis

Statistical tests were performed using GraphPad Prism v10 (GraphPad Software, La Jolla, USA). A Kruskal-Wallis test was used for comparison between patient groups (n=4). Data are presented as mean ± standard deviation. Statistical significance was set at $p<0.05$.

Results

Pronounced pericyte degeneration and alterations in the diabetic human retina

NG2/PDGFRβ double immunofluorescence staining of retinal flatmounts yielded detailed comprehensive 3D reconstructions of the pericyte morphology (Figure 1A; Figure 2). Confocal microscopy tile scans from each patient group revealed the pericyte distributions in all disease states, with fine morphological details captured by high-resolution imaging [FiglinQ-link-NG2].

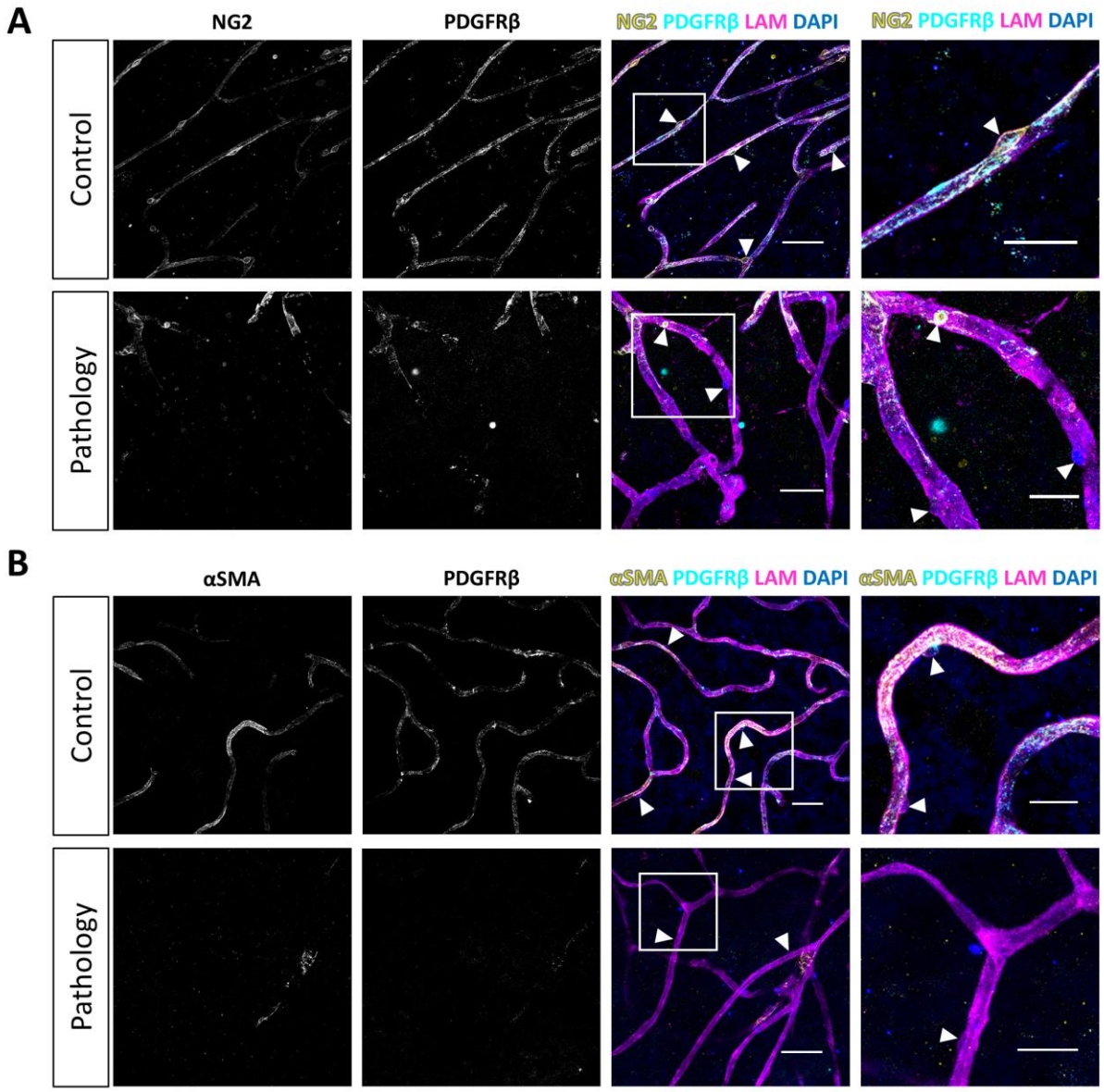

Figure 1. Loss of pericyte markers from capillaries in retina samples from donors with type 2 diabetes mellitus. Immunofluorescence 3D images of NG2 (yellow) and PDGFRβ (cyan) staining (**A**), and of αSMA (yellow) and PDGFRβ (cyan) staining (**B**). Images show expression in the human retina under physiological control conditions, and the loss of pericyte marker expression under pathological conditions. The basal lamina of blood vessels is stained for laminin (LAM, magenta), and nuclei are stained with DAPI (blue). White arrowheads indicate examples of pericytes. Scale bars: 50 µm. Images on the far right show higher magnification of the boxed region; scale bars: 25 µm.

NG2 staining robustly labelled pericyte cell bodies, and distinctly outlined their processes along capillaries in all patient groups. NG2-positive pericytes with spherical somata were predominantly localized at the branching points of blood vessels. PDGFRβ expression exhibited a granular pattern, showing diffuse distribution across most of the vasculature in all patient groups. Overall, the NG2 and PDGFRβ signals showed substantial, although not complete, colocalization in the retinas of all patient groups. Notably, compared to control retinas, type 2 DM and DR retinas exhibited a higher prevalence of capillaries lacking expression of both markers.

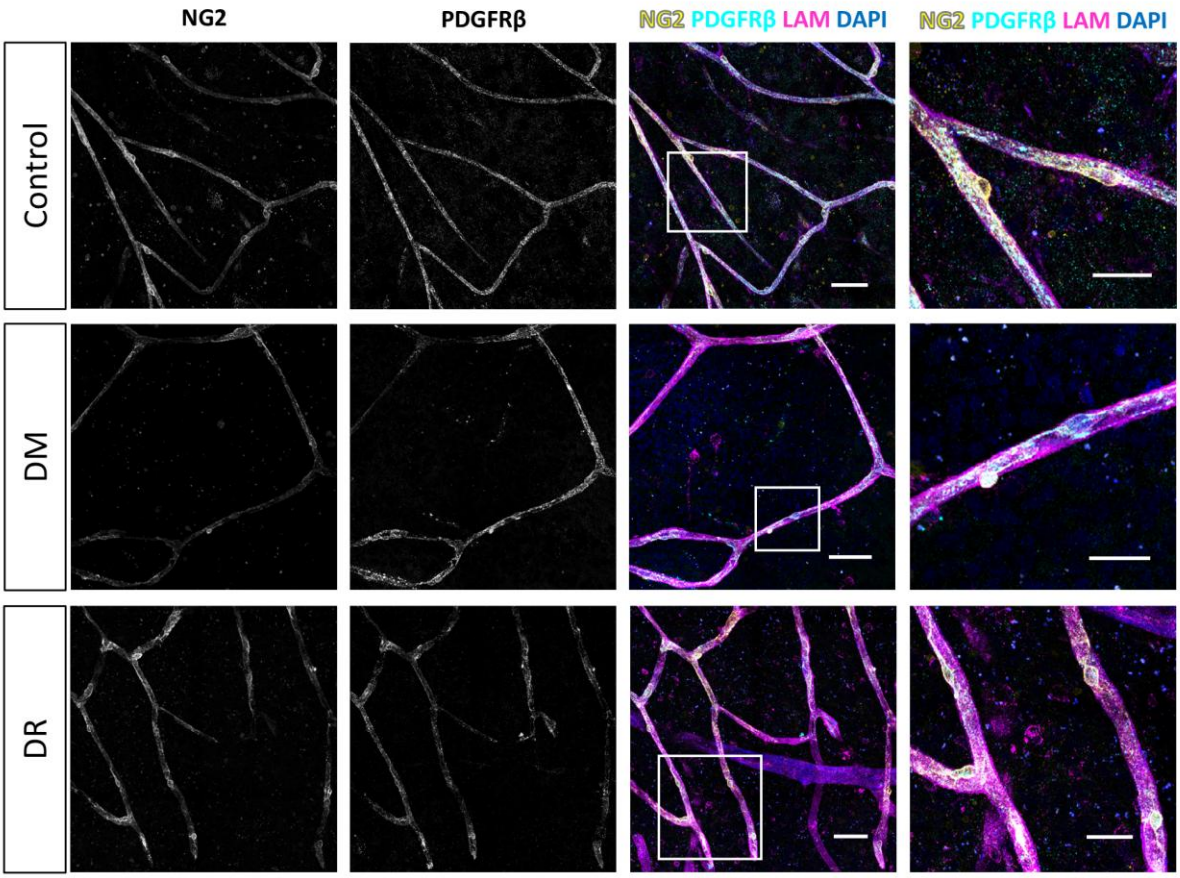

Figure 2. Immunofluorescence staining of NG2 and PDGFRβ in the human retina. Representative 3D confocal microscopy images of NG2 (yellow) and PDGFRβ (cyan) immunofluorescence staining on capillaries in retinal flatmounts from non-diabetic donors (Control), donors with type 2 diabetes mellitus (DM) without diabetic retinopathy (DR), and donors with DR. The basal lamina of blood vessels is stained for laminin (LAM, magenta), and nuclei are stained with DAPI (blue). Scale bars: 50 µm. Images on the far right show higher magnification of the boxed region; scale bars: 25 µm.

We also performed αSMA/PDGFRβ double immunofluorescence staining in human retinas from the same donors. Confocal microscopy tile scans of αSMA/PDGFRβ co-stained human retinal flatmounts were obtained from each patient group [FiglinQ-link-aSMA]. In contrast to the ubiquitous NG2 and PDGFRβ expression, αSMA immunoreactivity was predominantly localized in arteriolar smooth muscle cells, with only segments of capillaries being positive for αSMA, across all patient groups (Figure 1B; Figure 3). αSMA expression was consistently colocalized with PDGFRβ expression. Capillaries lacking both pericyte markers were observed in some regions in most DM and DR retinas, and in one control retina sample (Figure 1B). Retina samples from two DR donors exhibited reduced αSMA staining, compared to retina samples from both control and DM donors.

Both double staining experiments revealed that total PDGFRβ expression in the retinal vasculature was generally lower in DR donors, compared to both control and DM donors.

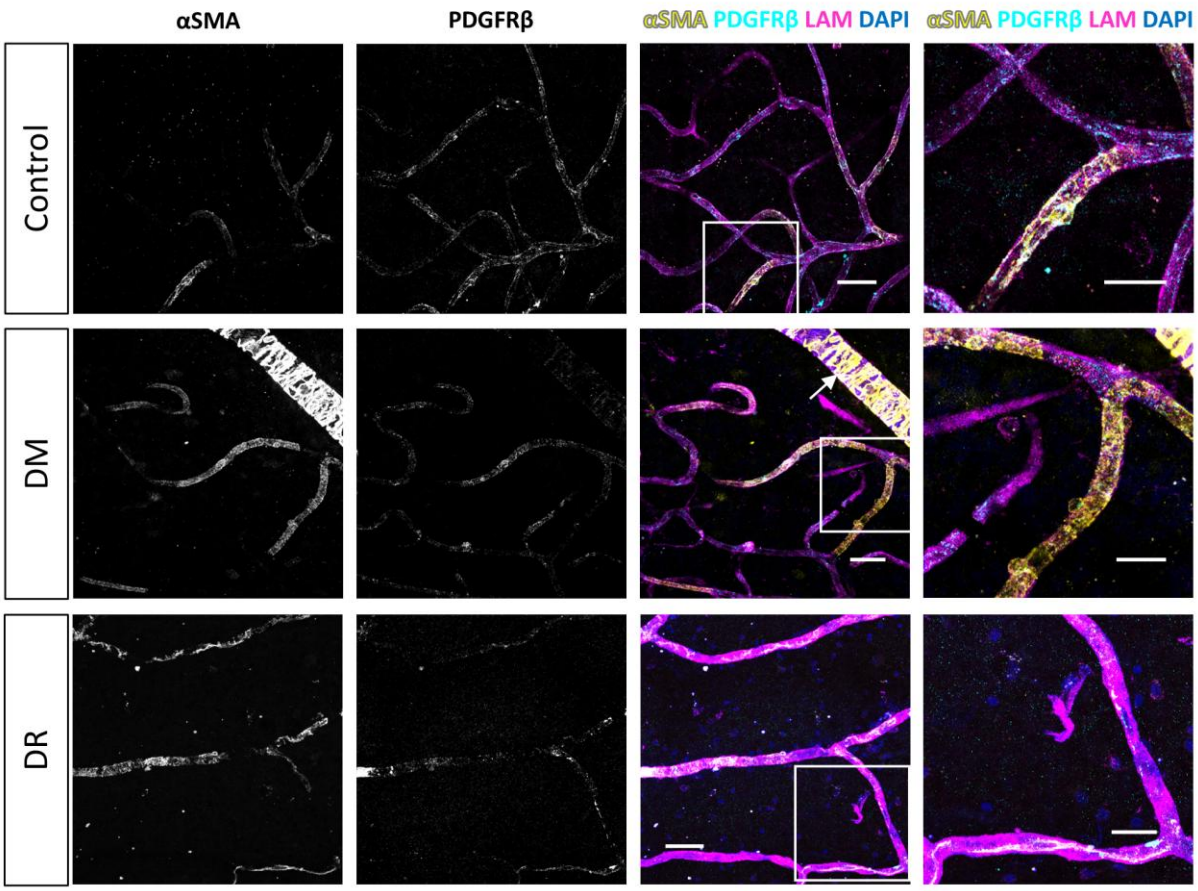

Figure 3. Immunofluorescence staining for αSMA and PDGFRβ in human retina samples. Representative 3D confocal microscopy images of αSMA (yellow) and PDGFRβ (cyan) immunofluorescence staining in retinal flatmounts from non-diabetic control donors (Control), donors with type 2 diabetes mellitus (DM), and donors with diabetic retinopathy (DR). The basal lamina of blood vessels is stained for laminin (LAM, magenta), and nuclei are stained with DAPI (blue). Arrow indicates arteriole. Scale bars: 50 µm. Images on the far right show higher magnification of the boxed region; scale bars: 25 µm.

Based on the presence or absence of NG2, PDGFRβ, and αSMA, we identified distinct pericyte subpopulations in retinal flatmounts from all donors. These subpopulations showed similar overall distributions across patient groups, except that pericytes positive for both PDGFRβ and αSMA were presented at lower proportions in the DM and DR groups, compared to controls.

Apart from pericyte-specific alterations, both control and DM retinas generally exhibited well-organized vasculature. In contrast, immunofluorescence staining revealed regional vascular disorganization in all retina samples from DR donors, characterized by disrupted vessel alignment or, for some donors, the presence of microaneurysms (Supplementary Figure 3), which are hallmarks of DR [1].

The immunofluorescence staining results were used to quantify the vascular staining coverage of these markers and the pericyte cellular density along retinal capillaries. Among

non-diabetic controls, NG2-positive pericytes covered approximately 80% of retinal capillaries (Figure 4A), while PDGFRβ-positive pericytes covered approximately 70% (Figure 4B), indicating that pericytes covered nearly the entire abluminal surface area of retinal capillaries. Compared to controls, diabetic retinas, with and without DR, showed reduced vascular staining coverage based on NG2 expression, although substantial variability was observed among diabetic donors (Figure 4A). Additionally, PDGFRβ coverage was significantly reduced to 45% in DR retinas, compared to non-diabetic controls (p=0.043) (Figure 4B). All groups showed consistently low vascular staining coverage of αSMA. Approximately 25% of capillaries displayed αSMA-positive pericytes, with no significant differences between groups (Figure 4C). Based on previous reports [17], we anticipated that pericyte deficiency may be associated with high variability in vascular diameter. However, compared to areas with normal pericyte marker expression, the retinal areas with reduced pericyte marker expression showed no major globally-detectable differences in blood vessel diameter. Pericyte density was calculated to be 7 pericytes/mm capillary length in the non-diabetic retinas, and was reduced to 4 pericytes/mm capillary length in both DM and DR retinas

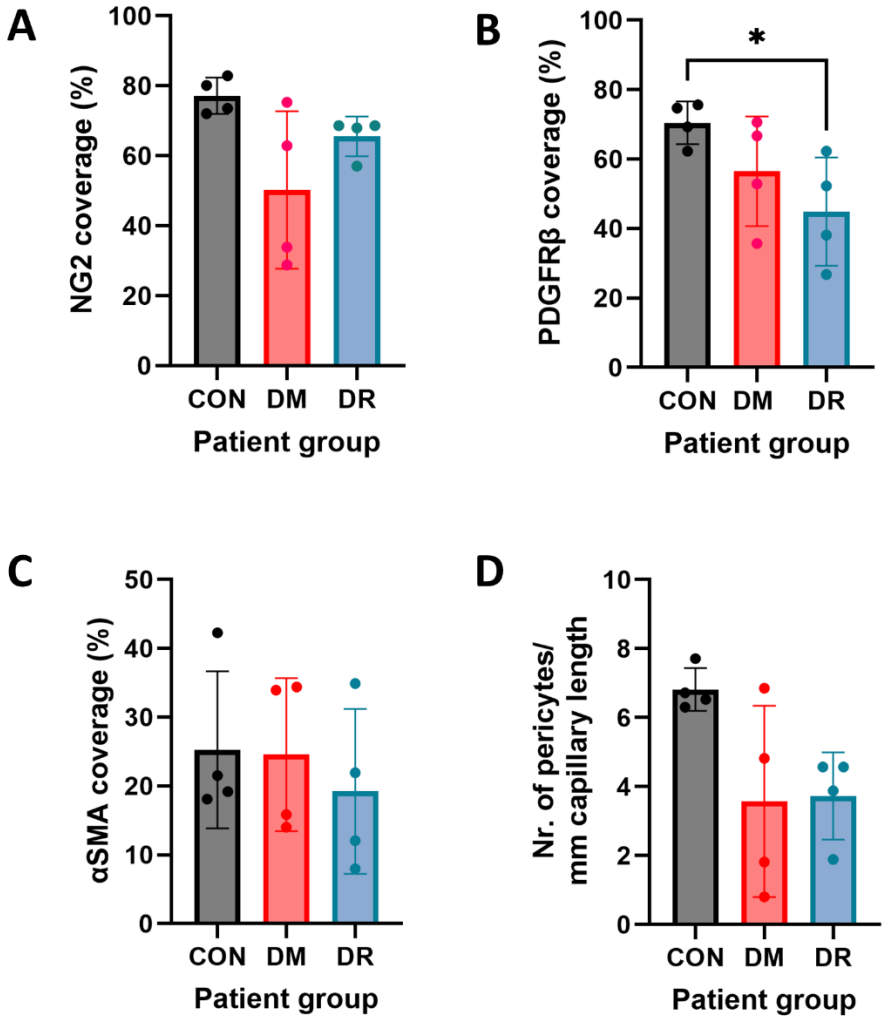

Figure 4. Quantification of retinal vascular staining coverage, and pericyte cellular density, based on pericyte markers. Quantification of NG2 (**A**), PDGFRβ (**B**), and αSMA (**C**) vascular coverage in human retina samples from non-diabetic controls (CON), donors with type 2 diabetes mellitus (DM), and donors with diabetic retinopathy (DR) (*n*=4). Quantification of NG2 pericyte cell number in the retina

was normalized to laminin (LAM)-positive capillary length (**D**). Each dot represents an individual donor. Data are expressed as the mean ± SD. *p<0.05.

(Figure 4D). These results are in accordance with previous reports of early pericyte loss in DM, prior to DR onset [1, 22]. Across all groups, we observed thin laminin-positive tubular structures bridging capillaries that lacked pericyte marker expression (Figure 5), with a predominance among control donors.

In summary, quantitative immunofluorescence analysis revealed substantial reductions of NG2-postive pericyte density, and vascular NG2 and PDGFRβ staining coverage, in diabetic retinas, both with and without DR, compared to non-diabetic controls. We did not observe any DM-induced alterations in αSMA coverage. These findings correspond to the known pericyte alterations in DM and DR during early disease stages, preceding clinically detectable DR.

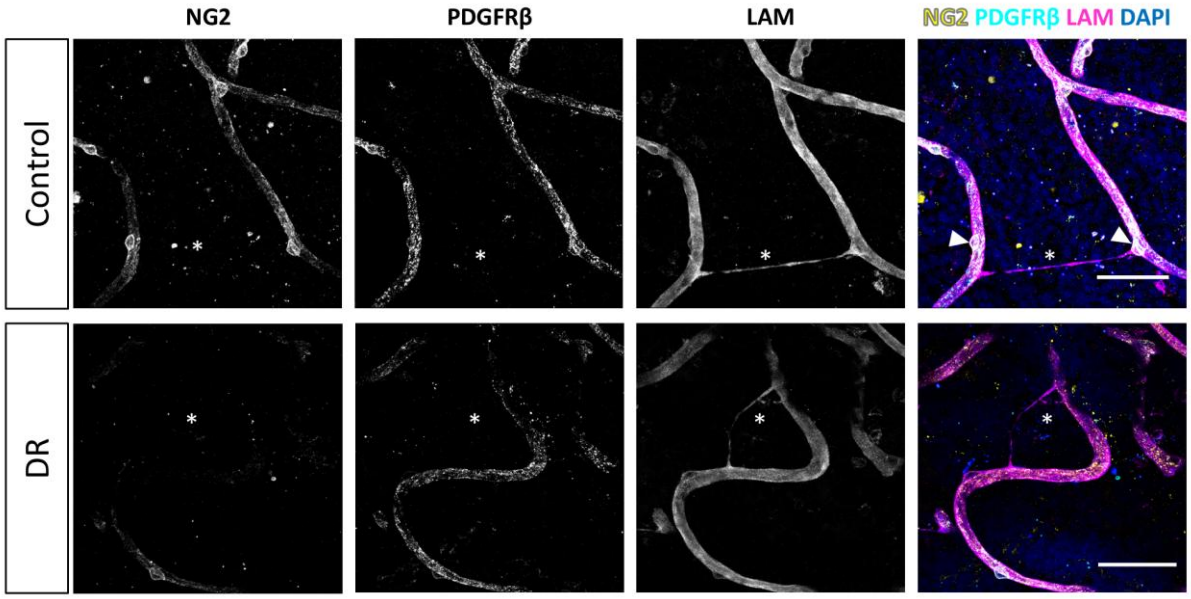

Figure 5. Basal lamina bridges in the human retina. Confocal microscopy images of basal lamina bridges in human retina samples from a non-diabetic (Control) donor and a donor with diabetic retinopathy (DR). Laminin (LAM, magenta) staining reveals the basal lamina of the microvasculature in the retina, including the basal lamina bridges. Pericytes are stained for NG2 (cyan) and PDGFRβ (yellow), and nuclei are stained with DAPI (blue). White asterisks indicate basal lamina bridges. White arrowheads indicate pericyte somata in close proximity to a basal lamina bridge. Scale bars: 50 µm.

Subtle reduction in the vascular staining coverage of pericyte markers in DM and AD brain samples, with unchanged pericyte density

Consistent with our observations in retina samples, NG2 expression in the frontal cortex was predominantly localized to pericyte cell bodies and, to a lesser extent, in the pericyte processes (Figure 6A; Figure 7). In contrast, PDGFRβ expression was diffusely and evenly distributed throughout the pericyte cell body and processes, exhibiting a very different pattern compared to the granular pattern observed in pericytes in the retina. We did not observe brain sample regions with complete loss of both pericyte markers in any patient

group. Some areas contained capillaries stained for PDGFRβ but lacking NG2 expression (Figure 6). Additionally, lower NG2 expression was generally observed in the patient groups compared to controls (Figure 7). Quantitative analysis demonstrated that approximately 70–80% of cortical capillaries were covered by NG2-positive and PDGFRβ-positive pericytes in

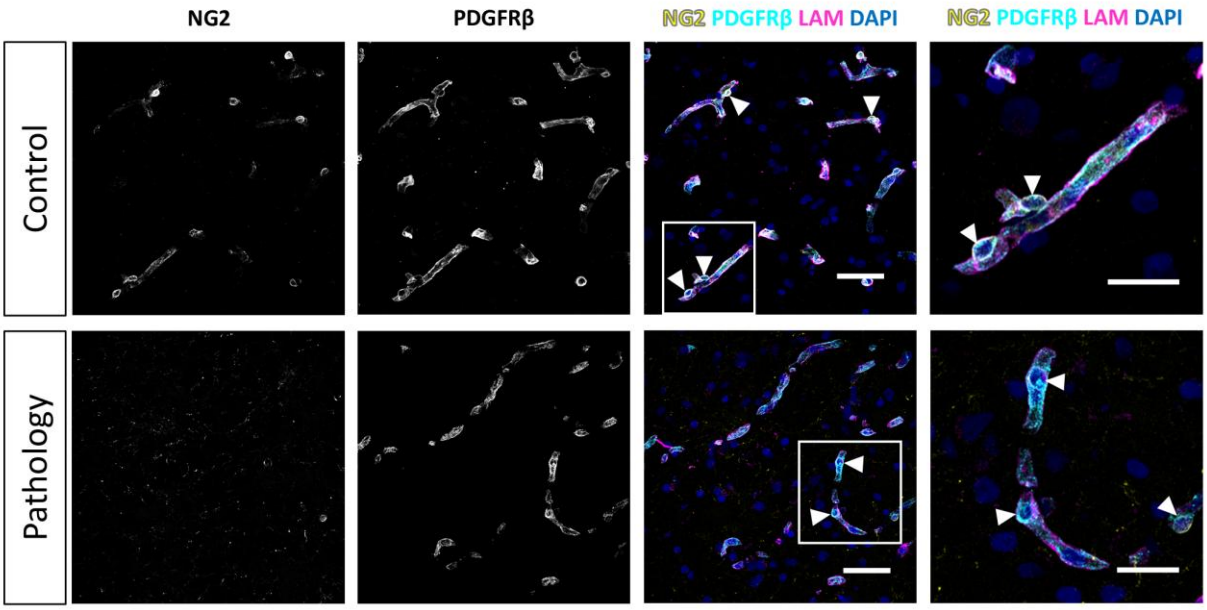

Figure 6. Immunofluorescence staining of NG2 and PDGFRβ in the human frontal cortex. Immunofluorescence images of NG2 (yellow) and PDGFRβ (cyan) staining in the human frontal cortex under physiological control conditions, and showing the loss of NG2 expression under pathological conditions. The basal lamina of blood vessels is stained for laminin (LAM, magenta) and nuclei are stained with DAPI (blue). White arrowheads indicate examples of pericytes. Scale bars: 50 µm. Images on the far right show higher magnification of the boxed region; scale bars: 25 µm.

control brain samples, which was comparable to our observations in control retina samples (Figure 8A, B). Compared to controls, all patient groups (type 2 DM, AD, and type 2 DM+AD) exhibited reduced vascular staining coverage of NG2 (Figure 8A) and PDGFRβ (Figure 8B), with the DM+AD group exhibiting the lowest NG2 coverage (44%) and PDGFRβ coverage (63%). Quantitative analysis revealed that the pericyte density was modestly higher in control brain tissue (9/mm) compared to control retinal tissue (7/mm) (Figure 8C). However, pericyte density did not significantly differ among diabetic, AD, DM+AD, and control brain samples.

We did not observe αSMA staining in human brain samples using the same antibody and fixation method that were applied to the retina samples.

Overall, our comparative analysis revealed subtle reductions in the vascular staining coverage of pericyte markers in frontal cortex samples from donors with DM and AD, without alterations of pericyte cellular density.

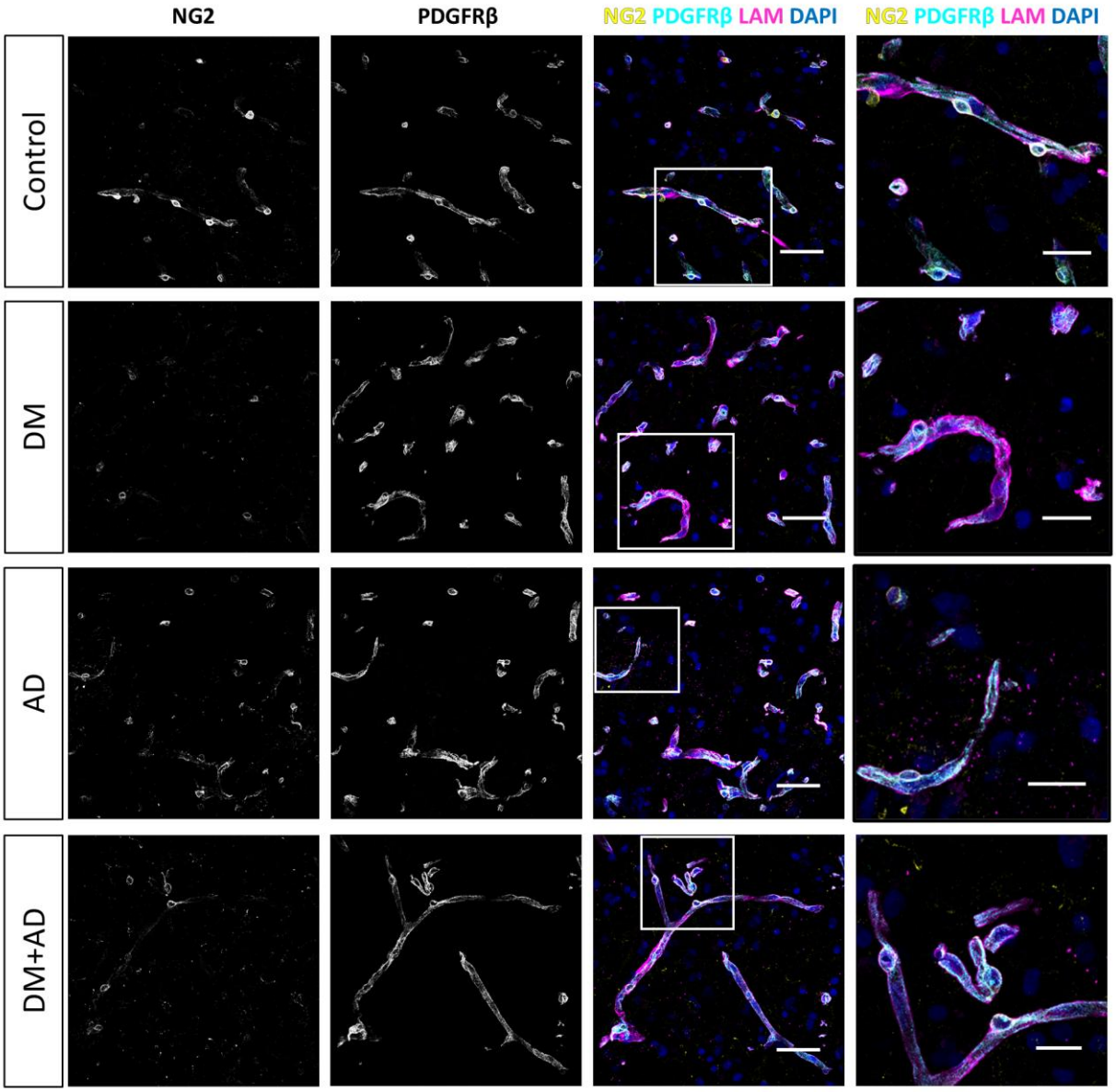

Figure 7. Immunofluorescence staining for NG2 and PDGFRβ in human brain samples from donors with type 2 diabetes mellitus (DM) and donors with Alzheimer's disease (AD). Representative confocal microscopy images of NG2 (yellow) and PDGFRβ (cyan) immunofluorescence staining in human frontal cortex cryosections (10 µm) from control donors, donors with DM, donors with AD, and donors with both DM+AD. The basal lamina of blood vessels is stained for laminin (LAM, magenta), and nuclei are stained with DAPI (blue). Scale bars: 50 µm. Images on the far right show higher magnification of the boxed region; scale bars: 25 µm.

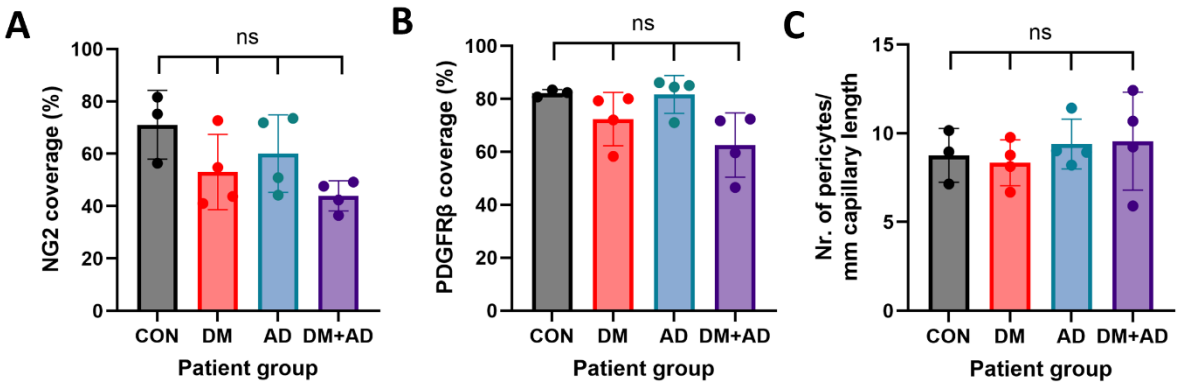

Figure 8. Quantification of cerebral vascular coverage, and pericyte density, based on pericyte markers. Immunofluorescence analysis of NG2 and PDGFRβ pericytes in the blood–brain barrier. Quantification of NG2 (A) and PDGFRβ (B) vascular staining coverage in human frontal cortex samples from control donors (CON) (n=3), donors with type 2 diabetes mellitus (DM) (n=4), donors with Alzheimer's disease (AD) (n=4), and donors with both DM+AD (n=4). Quantification of the NG2 pericyte cell number in the retina is normalized to CD31-positive capillary length (C). Each dot represents an individual donor. Data are expressed as the mean ± SD.

Discussion

The aim of this study was to explore pericyte characteristics of the BBB in cases of type 2 DM and AD, with comparison to those of the iBRB in cases of type 2 DM. Our study is the first explorative quantitative analysis of this subject, and revealed an estimated vascular staining coverage of 70–80%, based on NG2 and PDGFRβ, under non-diabetic conditions. Compared to the human retina, the human brain samples exhibited similar widespread expression of NG2 and PDGFRβ in the vasculature, reflected by similar vascular staining coverage of 70–80%. Among the examined markers, NG2 and PDGFRβ showed the highest vascular coverage, closely approximating the vascular coverage and density of the pericyte population. In contrast, αSMA showed lower staining coverage of around 25% in the retina. Although previous studies have reported αSMA detection in cerebral microvasculature [31-33], here we did not observe αSMA immunoreactivity in brain pericytes.

Our results revealed interesting trends in differential tissue-specific pericyte alterations between retina and brain tissue, related to pericyte cellular density in DM and AD. First, while both tissue types showed lower vascular staining coverage of pericyte markers in samples from donors with DM, quantitative assessment showed reduced pericyte cellular density only in diabetic retinas. The unchanged cerebral pericyte cellular density may indicate that although reduced expression of pericyte markers leads to decreased vascular staining coverage, the marker expression in the pericyte somata remains detectable. Alternatively, pericyte somata may be preserved despite alterations of cell processes. Our study could not resolve this issues in the absence of electron microscopy. Secondly, among the brain samples, the DM+AD group showed marked reductions of both NG2 and PDGFRβ vascular staining coverage, which were not observed in the donor groups with only DM or only AD. This finding may indicate that pericyte alterations play a role via diabetes-specific mechanisms, specifically in patients with DM who develop AD. There remains a need for further research using human AD tissue, to better understand how diabetes-induced vascular pathology contributes to the development and progression of AD in DM.

The visualization of pericytes using marker-independent techniques, such as 3D electron microscopy [34], offers superior resolution for defining pericyte morphology and spatial context; however, such approaches are often limited in human tissue studies by accessibility and practicality. Thus, here we employed immunofluorescence staining with commonly used pericyte markers, as a surrogate tool for assessing pericyte characteristics. These markers, including NG2, PDGFRβ, and αSMA, have been previously validated in retinal and brain tissues, through anatomical and morphological characterization and co-expression of pericyte markers [20, 35]. However, it must be noted that these markers are not entirely pericyte-specific, as they can also be expressed by other cell types. Moreover, their expression may not be uniform across all pericyte subpopulations or cellular compartments, potentially leading to underrepresentation. Despite their limitations, these markers remain the most valuable tools for approximating pericyte coverage and density in human tissue.

Our study is also subject to several other limitations. It was constrained by small sample sizes, due to the rarity of human brain and retina samples from donors with DM and/or AD. Additionally, there was high inter-patient variation, possibly due to comorbidities. Together, these limitations resulted in low statistical power. Therefore, the observed pathological differences should be regarded as trends, and may not reflect the true situation in the total patient population. There remains a need to increase the number of donors per patient group, to improve the statistical power. Another key limitation is the lack of matched eye and brain samples from the same donor, which prevents direct comparison of retinal and cerebral pathology. Furthermore, our analysis was confined to the frontal cortex, and pathological changes in AD vary according to region, e.g. with atrophy beginning in the hippocampus [36]. Additionally, it is possible that pericyte cellular density was underestimated because pericytes with a flat morphology, or with somata located on the underside of blood vessels, can be difficult to detect in post-mortem tissue, in contrast to the easily identifiable pericytes with a nodular shape. Discrepancies between our results and those in the literature may be attributed to post-mortem artifacts in our study, partial pericyte marker expression, or interspecies differences. Notably, previous reports have detected αSMA in brain pericytes, while this was not the case in our present study. This specific discrepancy may arise from antibody or fixation limitations; reduced αSMA expression in our aged donor cohort, consistent with reported age-related reductions of 20–30% [37]; or the expression of alternative actin isoforms, such as smooth muscle γ-actin [37, 38].

Despite these limitations, the observed trends regarding differences in pericyte pathology between the retina and brain may indicate that pericytes are differently affected, or play a different role in pathology, in the NVU of the brain versus the retina, in DM alone, AD alone, and in DM patients developing AD. Alternatively, the brain may be more protected by compensating mechanisms [39]. Notably, the distinct and well-characterized early pericyte pathology observed in the retina in DM may explain why the retina shows microvascular damage in DM at an earlier stage, compared to the cerebral microvasculature [1]. The presently observed reduction in cerebral vascular staining coverage of pericyte markers aligns with previous findings in the diabetic rat brain [40] and in the post-mortem human AD brain [41-43]. On the other hand, the currently reported preserved pericyte density contrasts with previous studies, which have reported significant decreases [41, 42, 44-46] or increases

[47, 48] of pericyte density in the human AD brain. Pericyte dysfunction and loss compromise the integrity of the BBB and iBRB, potentially affecting neural tissue homeostasis in the brain and retina, respectively [1, 12]. The contradictory findings regarding pericyte loss in brain capillaries in AD, in the literature together with our present findings, indicate that pericyte loss in the brain is not a consistent or universal feature of AD and DM. Alternatively, discrepancies may be explained by regional differences in cell bodies [46, 48], or by differences among quantification approaches. Beyond tissue-specific differences in pericyte pathology, previous studies have identified additional tissue-specific variations, including regulation of the amyloidogenic and non-amyloidogenic pathways, neuronal tissue thinning, ganglion cell loss, tau protein accumulation, and alterations in microglial gene expression [49, 50].

Our present findings, in a rare collection of human tissues, provide the first preliminary indication that there are distinct tissue-specific pathogenic mechanisms at play, which affect pericytes in the brain, as compared to the retina, in type 2 DM and AD. Moreover, our result suggest that retinal pericyte biomarkers may not be relevant as early predictors of cognitive impairment. Further work is needed to characterize these pericyte changes and other alterations in the BBB in type 2 DM and AD.

Ethics statement

The current research performed on human eyes is in accordance with all requirements stated in the Dutch law “Wet op orgaandonatie” that describes the use of donor material for research purposes. According to this law, donors provide written informed consent for donation with an opt out of left-over material for related scientific research purposes. Specific requirements for the use for scientific research of left-over material originating from corneal grafting have been described in an additional document formulated by the Ministry of Health, Welfare, and Sport and the Bio Implant Services (BIS) Foundation (Eurotransplant; Leiden, the Netherlands, July 21, 1995; 6714.ht). The eyes were stored anonymously and, therefore, approval of their use by the Ethics Committee was not required by Dutch law. All donors or their relatives provided written informed consent for brain autopsy and the use of brain tissue for research purposes. The use of human material was also in accordance with the Declaration of Helsinki on the use of human material for scientific research.

Conflict of interest

The authors declare that the research was conducted in the absence of any commercial or financial relationships that could be construed as a potential conflict of interest.

Author contributions

The authors have contributed to this article as follows: IK, NBVB, CJFVN, and ROS conceived and designed the study; AAC, EP, and NBVB performed immunofluorescence staining experiments, microscopical fluorescence imaging, and quantification scientific discussions; IK, NBVB, and CJFVN wrote the manuscript; all authors gave final approval of the manuscript; and IK, CJFVN, ROS, and NBVB supervised the entire study.

Funding

This study was supported by the RECOGNISED consortium grant (EU GA 847749), and The Encouraging European Research (EER) regulation of The Dutch Research Council (NWO, grant 200629). The study funders were not involved in the study design; the data collection, analysis, or interpretation; or the writing of the report; nor did they impose any restrictions regarding the publication of the report.

Acknowledgments

The authors acknowledge the Microscopy and Cytometry Core Facility - location AMC (MCCF-AMC) for their technical assistance.

Data availability statement

The data generated and analysed during the current study are available in interactive form via figlinq.com (https://create.figlinq.com/~iklaassen/141). The raw data supporting the conclusions of this article will be made available by the authors, without undue reservation.

References

[1] Little K, Llorian-Salvador M, Scullion S, Hernandez C, Simo-Servat O, Del Marco A, et al. (2022) Common pathways in dementia and diabetic retinopathy: understanding the mechanisms of diabetes-related cognitive decline. Trends Endocrinol Metab 33(1): 50–71. doi: 10.1016/j.tem.2021.10.008

[2] Bosma EK, van Noorden CJF, Klaassen I, Schlingemann RO (2019) Microvascular complications in the eye: diabetic retinopathy. In: Roelofs JJ, Vogt L (eds) Diabetic Nephropathy. Springer International Publishing AG, Cham, pp 305–321

[3] Feng L, Gao L (2024) The role of neurovascular coupling dysfunction in cognitive decline of diabetes patients. Front Neurosci 18: 1375908. doi: 10.3389/fnins.2024.1375908

[4] Dai J, Vrensen GF, Schlingemann RO (2002) Blood-brain barrier integrity is unaltered in human brain cortex with diabetes mellitus. Brain Res 954(2): 311–316. doi: 10.1016/s0006-8993(02)03294-8

[5] Santos GSP, Prazeres P, Mintz A, Birbrair A (2018) Role of pericytes in the retina. Eye (Lond) 32(3): 483–486. doi: 10.1038/eye.2017.220

[6] Villasenor R, Kuennecke B, Ozmen L, Ammann M, Kugler C, Gruninger F, et al. (2017) Region-specific permeability of the blood-brain barrier upon pericyte loss. J Cereb Blood Flow Metab 37(12): 3683–3694. doi: 10.1177/0271678X17697340

[7] Park DY, Lee J, Kim J, Kim K, Hong S, Han S, et al. (2017) Plastic roles of pericytes in the blood-retinal barrier. Nat Commun 8: 15296. doi: 10.1038/ncomms15296

[8] Trost A, Lange S, Schroedl F, Bruckner D, Motloch KA, Bogner B, et al. (2016) Brain and retinal pericytes: origin, function and role. Front Cell Neurosci 10: 20. doi: 10.3389/fncel.2016.00020

[9] Ogura S, Kurata K, Hattori Y, Takase H, Ishiguro-Oonuma T, Hwang Y, et al. (2017) Sustained inflammation after pericyte depletion induces irreversible blood-retina barrier breakdown. JCI Insight 2(3): e90905. doi: 10.1172/jci.insight.90905

[10] Little K, Singh A, Del Marco A, Llorian-Salvador M, Vargas-Soria M, Turch-Anguera M, et al. (2023) Disruption of cortical cell type composition and function underlies diabetes-associated cognitive decline. Diabetologia 66(8): 1557–1575. doi: 10.1007/s00125-023-05935-2

[11] Bogush M, Heldt NA, Persidsky Y (2017) Blood brain barrier injury in diabetes: unrecognized effects on brain and cognition. J Neuroimmune Pharmacol 12(4): 593–601. doi: 10.1007/s11481-017-9752-7

[12] Klaassen I, Van Noorden CJ, Schlingemann RO (2013) Molecular basis of the inner blood-retinal barrier and its breakdown in diabetic macular edema and other pathological conditions. Prog Retin Eye Res 34: 19–48. doi: 10.1016/j.preteyeres.2013.02.001

[13] Klaassen I, van Geest RJ, Kuiper EJ, van Noorden CJ, Schlingemann RO (2015) The role of CTGF in diabetic retinopathy. Exp Eye Res 133: 37–48. doi: 10.1016/j.exer.2014.10.016

[14] van Noorden CJF, Yetkin-Arik B, Martinez PS, Bakker N, Smallenburg MEV, Schlingemann RO, et al. (2024) New insights in ATP synthesis as therapeutic target in cancer and angiogenic ocular diseases. J Histochem Cytochem 72(5): 329–352. doi: 10.1369/00221554241249515

[15] El-Ghazawi K, Eyo UB, Peirce SM (2024) Brain microvascular pericyte pathology linking Alzheimer's disease to diabetes. Microcirculation 31(7): e12877. doi: 10.1111/micc.12877

[16] Li P, Fan H (2023) Pericyte loss in diseases. Cells 12(15): 1–19. doi: 10.3390/cells12151931

[17] Warmke N, Griffin KJ, Cubbon RM (2016) Pericytes in diabetes-associated vascular disease. J Diabetes Complications 30(8): 1643–1650. doi: 10.1016/j.jdiacomp.2016.08.005

[18] Benarroch E (2023) What are the roles of pericytes in the neurovascular unit and its disorders? Neurology 100(20): 970–977. doi: 10.1212/WNL.0000000000207379

[19] Ehtewish H, Arredouani A, El-Agnaf O (2022) Diagnostic, prognostic, and mechanistic biomarkers of diabetes mellitus-associated cognitive decline. Int J Mol Sci 23(11): 1–32. doi: 10.3390/ijms23116144

[20] Bakker N, Croes AA, Prevaes E, van Noorden CJF, Schlingemann RO, Klaassen I (2025) Development of immunostaining protocols for 3D visualization of pericytes in human retinal flatmounts. J Histochem Cytochem: 221554251323655. doi: 10.1369/00221554251323655

[21] Kuiper EJ, Witmer AN, Klaassen I, Oliver N, Goldschmeding R, Schlingemann RO (2004) Differential expression of connective tissue growth factor in microglia and pericytes in the human diabetic retina. Br J Ophthalmol 88(8): 1082–1087. doi: 10.1136/bjo.2003.032045
[22] van der Wijk AE, Vogels IMC, van Veen HA, van Noorden CJF, Schlingemann RO, Klaassen I (2018) Spatial and temporal recruitment of the neurovascular unit during development of the mouse blood-retinal barrier. Tissue Cell 52: 42–50. doi: 10.1016/j.tice.2018.03.010
[23] Girolamo F, Errede M, Bizzoca A, Virgintino D, Ribatti D (2022) Central nervous system pericytes contribute to health and disease. Cells 11(10): 1–30. doi: 10.3390/cells11101707
[24] Alarcon-Martinez L, Yilmaz-Ozcan S, Yemisci M, Schallek J, Kiliç K, Can A, et al. (2018) Capillary pericytes express α-smooth muscle actin, which requires prevention of filamentous-actin depolymerization for detection. Elife 7. doi: 10.7554/eLife.34861
[25] Thomas T, Miners S, Love S (2015) Post-mortem assessment of hypoperfusion of cerebral cortex in Alzheimer's disease and vascular dementia. Brain 138(Pt 4): 1059–1069. doi: 10.1093/brain/awv025
[26] Govindpani K, McNamara LG, Smith NR, Vinnakota C, Waldvogel HJ, Faull RL, et al. (2019) Vascular dysfunction in Alzheimer's disease: a prelude to the pathological process or a consequence of it? J Clin Med 8(5): 1–57. doi: 10.3390/jcm8050651
[27] Metaxas A, Thygesen C, Briting SRR, Landau AM, Darvesh S, Finsen B (2019) Increased inflammation and unchanged density of synaptic vesicle glycoprotein 2A (SV2A) in the postmortem frontal cortex of Alzheimer's disease patients. Front Cell Neurosci 13: 538. doi: 10.3389/fncel.2019.00538
[28] Beason-Held LL, Goh JO, An Y, Kraut MA, O'Brien RJ, Ferrucci L, et al. (2013) Changes in brain function occur years before the onset of cognitive impairment. J Neurosci 33(46): 18008–18014. doi: 10.1523/JNEUROSCI.1402-13.2013
[29] DeTure MA, Dickson DW (2019) The neuropathological diagnosis of Alzheimer's disease. Mol Neurodegener 14(1): 32. doi: 10.1186/s13024-019-0333-5
[30] Michalicova A, Majerova P, Kovac A (2020) Tau protein and its role in blood-brain barrier dysfunction. Front Mol Neurosci 13. doi: 10.3389/fnmol.2020.570045
[31] Ma Q, Zhao Z, Sagare AP, Wu Y, Wang M, Owens NC, et al. (2018) Blood-brain barrier-associated pericytes internalize and clear aggregated amyloid-beta42 by LRP1-dependent apolipoprotein E isoform-specific mechanism. Mol Neurodegener 13(1): 57. doi: 10.1186/s13024-018-0286-0
[32] Stillman JM, Lopes F, Lin JP, Hu K, Reich DS, Schafer DP (2023) Lipofuscin-like autofluorescence within microglia and its impact on studying microglial engulfment. Nature Communications 14(1). doi: 10.1038/s41467-023-42809-y
[33] Zhang H, Tan C, Shi X, Xu J (2022) Impacts of autofluorescence on fluorescence based techniques to study microglia. BMC Neurosci 23(1): 21. doi: 10.1186/s12868-022-00703-1
[34] Bandopadhyay R, Orte C, Lawrenson JG, Reid AR, De Silva S, Allt G (2001) Contractile proteins in pericytes at the blood-brain and blood-retinal barriers. J Neurocytol 30(1): 35–44. doi: 10.1023/a:1011965307612
[35] Hutter-Schmid B, Humpel C (2016) Alpha-smooth muscle actin mRNA and protein are increased in isolated brain vessel extracts of Alzheimer mice. Pharmacology 98(5-6): 251–260. doi: 10.1159/000448007
[36] Schlingemann RO, Rietveld FJ, de Waal RM, Ferrone S, Ruiter DJ (1990) Expression of the high molecular weight melanoma-associated antigen by pericytes during angiogenesis in tumors and in healing wounds. Am J Pathol 136(6): 1393–1405.
[37] Abdelazim H, Payne LB, Nolan K, Paralkar K, Bradley V, Kanodia R, et al. (2022) Pericyte heterogeneity identified by 3D ultrastructural analysis of the microvessel wall. Front Physiol 13: 1016382. doi: 10.3389/fphys.2022.1016382
[38] Armulik A, Genove G, Betsholtz C (2011) Pericytes: developmental, physiological, and pathological perspectives, problems, and promises. Dev Cell 21(2): 193–215. doi: 10.1016/j.devcel.2011.07.001

[39] Planche V, Manjon JV, Mansencal B, Lanuza E, Tourdias T, Catheline G, et al. (2022) Structural progression of Alzheimer's disease over decades: the MRI staging scheme. Brain Commun 4(3): fcac109. doi: 10.1093/braincomms/fcac109
[40] Gyori F, Meszaros A, Krecsmarik M, Molnar K, Balta C, Hermenean A, et al. (2025) Expression of alpha smooth muscle actin decreases with ageing and increases upon lumen obstruction in mouse brain pericytes. Geroscience 47(2): 2525–2540. doi: 10.1007/s11357-024-01429-0
[41] Grant RI, Hartmann DA, Underly RG, Berthiaume AA, Bhat NR, Shih AY (2019) Organizational hierarchy and structural diversity of microvascular pericytes in adult mouse cortex. J Cereb Blood Flow Metab 39(3): 411–425. doi: 10.1177/0271678X17732229
[42] Bobkova N, Vorobyov V (2015) The brain compensatory mechanisms and Alzheimer's disease progression: a new protective strategy. Neural Regen Res 10(5): 696–697. doi: 10.4103/1673-5374.156954
[43] Liu Y, Zhang H, Wang S, Guo Y, Fang X, Zheng B, et al. (2021) Reduced pericyte and tight junction coverage in old diabetic rats are associated with hyperglycemia-induced cerebrovascular pericyte dysfunction. Am J Physiol Heart Circ Physiol 320(2): H549–H562. doi: 10.1152/ajpheart.00726.2020
[44] Halliday MR, Rege SV, Ma Q, Zhao Z, Miller CA, Winkler EA, et al. (2016) Accelerated pericyte degeneration and blood-brain barrier breakdown in apolipoprotein E4 carriers with Alzheimer's disease. J Cereb Blood Flow Metab 36(1): 216–227. doi: 10.1038/jcbfm.2015.44
[45] Sengillo JD, Winkler EA, Walker CT, Sullivan JS, Johnson M, Zlokovic BV (2013) Deficiency in mural vascular cells coincides with blood-brain barrier disruption in Alzheimer's disease. Brain Pathol 23(3): 303–310. doi: 10.1111/bpa.12004
[46] Kirabali T, Rust R, Rigotti S, Siccoli A, Nitsch RM, Kulic L (2020) Distinct changes in all major components of the neurovascular unit across different neuropathological stages of Alzheimer's disease. Brain Pathol 30(6): 1056–1070. doi: 10.1111/bpa.12895
[47] Schultz N, Brannstrom K, Byman E, Moussaud S, Nielsen HM, Netherlands Brain B, et al. (2018) Amyloid-beta 1-40 is associated with alterations in NG2+ pericyte population ex vivo and in vitro. Aging Cell 17(3): e12728. doi: 10.1111/acel.12728
[48] Ding R, Hase Y, Ameen-Ali KE, Ndung'u M, Stevenson W, Barsby J, et al. (2020) Loss of capillary pericytes and the blood-brain barrier in white matter in poststroke and vascular dementias and Alzheimer's disease. Brain Pathol 30(6): 1087–1101. doi: 10.1111/bpa.12888
[49] Hase Y, Jobson D, Cheong J, Gotama K, Maffei L, Hase M, et al. (2024) Hippocampal capillary pericytes in post-stroke and vascular dementias and Alzheimer's disease and experimental chronic cerebral hypoperfusion. Acta Neuropathol Commun 12(1): 29. doi: 10.1186/s40478-024-01737-8
[50] Fernandez-Klett F, Brandt L, Fernandez-Zapata C, Abuelnor B, Middeldorp J, Sluijs JA, et al. (2020) Denser brain capillary network with preserved pericytes in Alzheimer's disease. Brain Pathol 30(6): 1071–1086. doi: 10.1111/bpa.12897
[51] Ding R, Hase Y, Burke M, Foster V, Stevenson W, Polvikoski T, et al. (2021) Loss with ageing but preservation of frontal cortical capillary pericytes in post-stroke dementia, vascular dementia and Alzheimer's disease. Acta Neuropathol Commun 9(1): 130. doi: 10.1186/s40478-021-01230-6
[52] den Haan J, Morrema THJ, Verbraak FD, de Boer JF, Scheltens P, Rozemuller AJ, et al. (2018) Amyloid-beta and phosphorylated tau in post-mortem Alzheimer's disease retinas. Acta Neuropathol Commun 6(1): 147. doi: 10.1186/s40478-018-0650-x
[53] Bloomfield CL, Gong J, Droho S, Makinde HM, Gurra MG, Stumpf CH, et al. (2024) Retinal microglia express more MHC class I and promote greater T-cell-driven inflammation than brain microglia. Front Immunol 15: 1399989. doi: 10.3389/fimmu.2024.1399989

Supplementary Material

Macro for drawing blood vessel ROI

```
if (bitDepth() != 16) {
   exit("This script requires a 16-bit image.");
}
setAutoThreshold("Default dark");
setOption("BlackBackground", false);
run("Analyze Particles...", "size=100-Infinity circularity=0.00-1.00 show=Nothing display clear
add");
count = roiManager("count");
for (i = count-1; i >= 0; i--) {
   roiManager("select", i);
   diameter = getValue("Feret");
   length = getValue("Major");
   if (diameter < 10 || length > 20) {
      roiManager("delete");
   }
}
roiManager("Show All");
```

Supplementary Figure 1. **ImageJ macro script 1 to automatically draw an ROI around blood vessels in immunofluorescence images.**

Macro to set threshold for pericyte marker channel

```
threshold = 1.000;
setThreshold(threshold, 255);
setOption("BlackBackground", false);
run("Measure");
```

Supplementary Figure 2. ImageJ macro script 2 to remove background signal from immunofluorescence images using a pre-defined threshold.

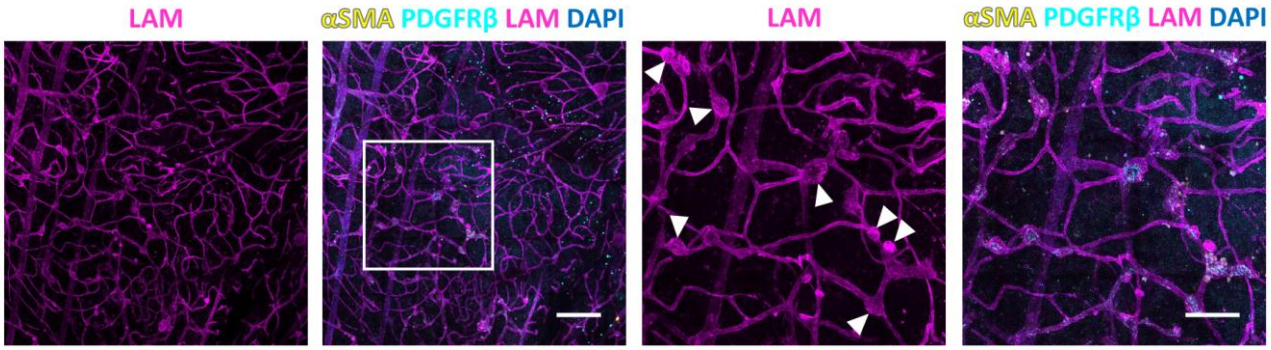

Supplementary Figure 3. Vascular disruptions in the human retinas from donors with diabetic retinopathy (DR). Immunofluorescence images of laminin (LAM, magenta), αSMA (yellow) and PDGFRβ (cyan) staining in the human DR retina. Nuclei are stained with DAPI (blue). White arrowheads indicate examples of microaneurysms. Scale bars: 200 µm. Images on the far right show higher magnification of the boxed region; scale bars: 100 µm.

Chapter 7

General discussion

The neurovascular unit (NVU) is a complex, multicellular structure composed of endothelial cells, surrounded by pericytes, macroglia, microglia, and neurons (Figure 1, **Chapter 1**), which facilitate homeostasis in the retina and brain in a concerted manner [1-5]. The NVU regulates blood flow in response to the metabolic demand of neuronal tissue in the retina and brain. Endothelial cells in the NVU form a barrier between the blood and surrounding tissue, thereby protecting neuronal tissue from potentially harmful compounds in the circulation. Such a stable and functional environment is required for proper neuronal functioning in these organs. A dysfunctional NVU can lead to an impaired barrier function, which results in vascular leakage and neuronal damage.

In this thesis, we aimed to study mechanisms involved in retinal and brain neurovascular impairment. Cellular and molecular alterations of the NVU in the retina and brain were investigated in the context of type 2 diabetes mellitus (DM) and Alzheimer's disease (AD) in human patient material and animal models (zebrafish and mice).

Animal models to study the neurovascular unit

Animal models as an *in vivo* model for human diseases allow for studying pathophysiology, disease progression, and potential treatment options in a living organism with complex biological systems. Animal models offer a controlled *in vivo* environment related to genetic, environmental, and lifestyle effects to study mechanisms underlying neurovascular diseases. Zebrafish are highly suitable as an *in vivo* model for studying interactions within the NVU. In general, the advantage of zebrafish models over mice is that they allow studies of the NVU in real-time within the living organism because of their optical transparency [6]. Zebrafish are small in size and are widely considered a more ethical alternative to larger animal models in scientific research. Additionally, zebrafish allow for genetic editing and they reproduce rapidly and have a short life cycle, allowing for high-throughput studies.

We developed a zebrafish multi-modal toolbox to study the blood-brain barrier (BBB) in the context of neurodegenerative diseases, as described in detail in **Chapter 2**. Zebrafish embryos were exposed to hyperglycaemia, which was used as a pathological stimulus to affect the BBB as proof of concept. Increased vascular diameters and tracer extravasation in the brain were identified *in vivo* in our zebrafish model as pathological responses. Contribution of the BBB to the tracer extravasation in the brain was confirmed by studying expression levels of proteins involved in the endothelial paracellular and transcellular transport pathways. Thus, this zebrafish embryo model allows for detailed studies of both BBB function and the role of proteins associated with barrier dysfunction. However, features of human adult neurodegenerative diseases, including protein aggregation and progressive neurodegeneration, are not fully recapitulated in embryonic stages. The zebrafish model would better reflect human diseases when zebrafish in fully matured stages are utilized and the time of exposure to pathological stimuli are prolonged. Nevertheless, our multi-model zebrafish toolbox is promising to study both the retina and brain.

Given the fact that the retina shares an embryonic origin with the brain [7], the retina may offer a non-invasive assessment of pathophysiological alterations common to the brain, often referred to as a "window to the brain". A link between retinal and brain abnormalities has also been suggested in AD, including thinning of neuronal tissue and presence of amyloid β

(Aβ) plaques [8-11]. Identifying measurable retinal indicators of brain pathology may offer new opportunities for the diagnosis, monitoring, and treatment of AD.

To study potential shared molecular mechanisms underlying NVU dysfunction in AD in both the eye and brain, we used an established animal model, the 5xFAD mouse model. This mouse model recapitulates characteristics of AD, including behavioural impairment and Aβ plaque formation, leading to microgliosis and inflammation as well as synaptic and neuronal loss [12]. In human AD, c-Jun N-terminal kinase (JNK) contributes to Aβ plaque formation, tau tangle pathology and synaptic dysfunction [13]. JNK activation has been suggested as a common pathogenic mechanism driving both retinal and cerebral neurodegeneration [14]. However, in **Chapter 3**, by means of a transgenic mouse model of AD, we provide data that do not support this hypothesis for this given model, as in the retina, early synaptic dysfunction and inflammation occurred without robust Aβ aggregation or widespread JNK activation.

Still, finding a shared pathway in future studies would enhance the retina's potential as a practical and accessible means of monitoring AD progression in the central nervous system. Other possible mechanisms shared by both tissues in AD, such as MAPK cascade activation induced by oxidative stress, mitochondrial dysfunction, dysregulated unfolded protein response pathways and impaired glial-cell mediated clearance need further study [15-18].

In general, animal models of eye complications and neurological disorders are suitable *in vivo* models to provide insight in the status of the NVU over time and at different stages of the human disease. Animal models can provide information on the sequence of events and whether neuronal damage occurs before or after vascular damage. However, despite animal models being able to replicate the features of human eye complications and neurovascular diseases, the results should be interpreted with caution, and their applicability to human disease should be considered carefully.

The human neurovascular unit in diabetes and Alzheimer's disease

There is a clear need for reliable retinal biomarkers that can effectively reflect structural and functional brain dysfunction. Early diagnosis and intervention based on these biomarkers may prevent the onset of neurodegenerative diseases. Therefore, understanding the precise pathophysiological nature of the complex cell-cell interactions in the brain and retina is required, especially pertaining to the NVU. Although the influence of DM on the retina and the inner blood-retinal barrier (iBRB) dysfunction has been extensively studied [3, 19-21], the effects of DM on the BBB remain underexplored and require additional research. In **Chapter 4**, we compared type 2 DM-induced pathology in the NVU of the human eye and brain by performing immunostaining to study cellular changes. The general structure and function of the NVU in the human retina and brain are similar, but in this study we found that there are differences in DM-induced NVU pathology between these organs. DM differentially affects vascular permeability, tight junction integrity, transcytosis, the expression of water and ion channels and vascular coverage of pericytes in the eye and brain. Not only differences, but also similarities in pathology were found as changes in macroglia activity and function were observed in both the eye and brain in DM. Based on our findings we could confirm the clinical notion that there is no equivalent of diabetic retinopathy (DR) in the brain.

Like in the retina and brain in type 2 DM, we also observed macroglial activation in the AD brain. Currently, there are no techniques available in the clinic to measure macroglia activation or function in the human eye or brain. There is a growing interest in astrocytes and their involvement in the pathophysiological processes underlying neurological diseases [22, 23]. Whereas initial macroglia activation provides neuroprotection, chronic activation can lead to neuroinflammation, synaptic dysfunction and impaired waste removal, driving neurodegeneration. Currently, positron emission tomography (PET) tracers, along with biomarkers in blood and cerebral spinal fluid, enable assessment of astrocyte functions [24]. The potential of astrocytes as a therapeutic target need further study given their involvement in neuroinflammation and Aβ clearance.

Dysfunction of the cerebral NVU has been suggested to be a critical event in AD [25], but current understanding regarding NVU dysfunction in AD is mostly based on findings in rodent models, and studies on the human NVU in the context of AD are often limited and/or have provided contradictory data. In our studies, using human post-mortem tissue samples of the frontal cortex, we found glial cell activation, lower vascular coverage of pericyte markers, altered localization of tight junction proteins, strong upregulation of the transcytosis inhibitor MFSD2A, and subtle changes in the expression of water and ion channels in AD. Thus, multiple cell types in the NVU appear affected in AD. However, we did not observe increased extravasation of the large plasma protein fibrinogen in AD alone. Fibrinogen might not be suitable to measure vascular leakage in the post-mortem brain. Given the previously reported vascular leakage in AD patients [26, 27], further validation using additional plasma proteins, such as immunoglobulin G (IgG) and albumin or smaller molecules, may be necessary as markers to identify vascular leakage.

The most striking differences were observed in the elevated vascular permeability in patients with a combination of DM and AD. In future studies, it would be valuable to examine alterations in the NVU at the level of individual vessels exhibiting vascular leakage. Microvascular impairment, together with neurodegeneration, is a main mechanism involved in AD [4]. It is not clear whether microvascular pathology is a cause or a consequence in AD [28, 29]. It is be possible that Aβ in AD primarily affects neurons rather than the microvasculature. Several studies suggest that hypoxia causes changes in the endothelial cells of the microvasculature, leading to vascular leakage [28, 30, 31]. The increased permeability could be attributed to a dysfunctional paracellular transport pathway, based on the observed alterations in tight junction protein expression. In general, in addition to the paracellular transport pathway, the transcellular transport pathway contributes to vascular permeability in barrier endothelia. However, in our studies, we identified biologically fundamental differences between the retina and brain in this context, in particular in the expression pattern of plasmalemma vesicle-associated protein (PLVAP). PLVAP is a protein associated with endothelial plasmalemmal vesicles involved in transcellular transport and the regulation of vascular permeability [32-34]. PLVAP is absent in microvasculature with intact barrier function and upregulation correlates inversely with barrier integrity. In the brain, PLVAP expression was absent in all patient groups, including the patients with both DM and AD, suggesting that PLVAP and possibly transcellular transport, do not contribute to the increased vascular permeability observed in this patient group. In contrast, PLVAP was expressed in retinal microvasculature of DR patients, indicating altered transcellular transport as reported earlier.

The human studies presented in this thesis provide only preliminary insights because of the limited sample sizes and cross-sectional nature of our studies. Nevertheless, the tissues prove to be useful for highlighting differences in the NVU between the retina and brain. Human studies with limited sample sizes may be more relevant for understanding human diseases than large-scale animal studies, due to the challenges in translating findings from the existing animal models to human conditions. However, human studies described in this thesis lack tissue samples from both the eyes and brains of the same donor due to the rarity of such specimens, preventing the assessment of simultaneous pathology in these organs. The simultaneous impairment of the NVU in retina and brain in DM patients remains to be elucidated. To assess whether the eye can serve as a window to the brain, it is essential to first confirm concurrent NVU pathology in the retina and brain from the same donors. Such correlations can be identified by analysing a large cohort of paired retinal and brain tissues.

Alterations in the NVU have not only been found in DM and AD, but have also been reported previously in the brain in other diseases, including Parkinson's disease, ischemic stroke, traumatic brain injury, amyotrophic lateral sclerosis [2, 35, 36]. Understanding the cellular and molecular alterations underlying NVU dysfunction may facilitate identification of potential therapeutic targets. However, non-invasive delivery of therapeutics to the eye and brain remains challenging because of the BRB and BBB [37]. The recent advancements in developing non-invasive delivery techniques show potential for clinical applications. Focused ultrasound in combination with microbubbles allow for localised increase in BBB permeability and the controlled breakdown of microbubbles to facilitate the release of therapeutic agents [38-43]. Likewise, electromagnetic fields can regulate BBB permeability and allow for drug delivery into the brain [44, 45]. Drug delivery can also be facilitated by modified extracellular vesicles [46, 47] or liposomes [48] that serve as a carrier across the BBB for therapeutic agents.

Localisation of pericytes in human retinal flatmounts

Retinal pericyte loss is an early event in DM, occurring prior to clinical DR onset [4, 49]. Pericyte loss has also been reported in the brain in experimental models of DM [50, 51]; however, corresponding human studies are lacking. Additionally, pericytes are considered to play a role in AD pathology, but findings regarding pericyte loss in the human AD brain remain contradictory [52-59]. Visualization of pericytes in retinal flatmounts provides a valuable tool for studying their role in retinal vascular health and disease.

To be able to study pericytes in 3D in the human post-mortem retina, we developed a novel immunostaining protocol using several markers. In **Chapter 5**, we described how the immunostaining protocol on human retinal flatmounts was optimized for reliable visualisation of pericytes in human post-mortem retinal tissue. The advantage of retinal flatmounts over retinal cryosections lies in their ability to enable 3D reconstruction of pericytes and enhances spatial information by visualisation of pericyte localisation across the entire network. Optimization of staining protocols is crucial as the methodology may not be applicable for other tissues or other species. Furthermore, it is important to note that there is no single, universal marker that is exclusively specific to pericytes within the NVU of the retina and brain. Our study supports this notion, demonstrating distinct variations in the expression of neural/glial antigen 2 (NG2), platelet-derived growth factor receptor beta

(PDGFRβ), and alpha smooth muscle actin (αSMA) in retinal pericytes. Consequently, we identified pericyte subpopulations based on differential marker expression.

Immunofluorescence staining is performed in all human studies described in the present thesis. Immunofluorescence staining was the preferred technique as it allows highly specific and sensitive detection and localisation of target antigens within cells or tissues [60]. This method offers detailed spatial information regarding protein expression and enables the visualization of multiple targets within the same sample using different fluorophores. This capability allows for the examination of NVU alterations of individual blood vessels. A limitation of immunofluorescence staining in human tissue is that the tissue is removed from its natural *in vivo* environment and subjected to fixation, possibly affecting the conformation and location of proteins [60, 61]. Whereas fluorophores enable high sensitivity, the fluorescence signal can diminish over time or during exposure to light [60]. Additionally, autofluorescence and nonspecific antibody binding can complicate the interpretation of staining results [61, 62]. Furthermore, the lack of consensus on standardized methods for quantifying NVU markers complicates comparisons across studies. Nevertheless, immunofluorescence staining provides detailed insights into the process of barrier loss, offering information that cannot be obtained through in vivo imaging of the human retina and brain. Furthermore, immunofluorescence staining has broad applicability for studying molecular and cellular processes in both research and diagnostics.

Pericyte pathology in the human neurovascular unit

By employing our optimized immunofluorescence protocol to visualize pericytes in the retinal vasculature, we confirmed that pericyte loss is an early hallmark of DR progression in type 2 DM, as shown in **Chapter 6**. Additionally, we visualised pericytes in the human frontal cortex using immunofluorescence staining. Comparing the pericyte pathology between the human retina and brain revealed differential tissue-specific pericyte alterations in pathology. In the retina, vascular staining coverage of both NG2 and PDGFRβ and pericyte density was lower in DM donors. In the brain, vascular staining coverage of NG2 was lower in donors with DM, whereas pericyte density remained unchanged. A possible explanation is that pericytes are differentially affected or play distinct roles in the pathology of the NVU in these two tissues. Alternatively, compensatory mechanisms in the brain may protect pericytes from dysfunction and loss. Elucidating the precise mechanisms by which pericyte loss or dysfunction contributes to the effects of DM and AD pathology remains an important goal.

Among the brain samples, the DM with AD group showed marked reductions in both NG2 and PDGFRβ vascular staining coverage, a pattern not observed in the DM only or AD only groups, suggesting that pericyte alterations may be driven by DM-specific mechanisms that are particularly active in patients with DM who develop AD. Individuals with DM have an increased risk of developing AD [63], but much remains unknown regarding the mechanisms through which DM-induced vascular pathology contributes to the onset and progression of AD in individuals with DM.

Notable differences were observed when comparing the vascular coverage by pericytes in retinal cryosections (**Chapter 4**) and retinal flatmounts (**Chapter 6**). Baseline pericyte coverage in non-DM controls was similar in both cryosections and flatmounts. However, cryosection analysis did not fully reflect the lowered coverage observed in type 2 DM retinas

in flatmounts. Specifically, retinal cryosections of type 2 DM donors exhibited only a subtle reduction in vascular coverage, in contrast to the more pronounced reduction that was detected in flatmounts. These findings suggest that retinal cryosections may not be the optimal method for studying pericytes in DM retinas and cannot be considered a reliable substitute for flatmounts.

Pericytes are not a homogeneous cell population. Pericyte subtypes can be identified based on their phenotype, expression of molecular markers, distribution, function and embryonic origin [64] and they differ between species [65]. Here, we have also demonstrated pericyte heterogeneity in both the retina and brain based on expression of NG2, PDGFRβ, and αSMA. Future studies should focus on better understanding of the contribution of pericyte subpopulations or altered marker expression patterns to pathology of the NVU. Single-cell sequencing techniques offer the potential for more precise subclassification based on gene expression profiles. Imaging modalities can be employed for subclassification of pericytes based on their morphological characteristics. These approaches allow for characterization of certain phenotypes in physiology and pathology. A pericyte subpopulation may be more or less prone to pathological stimuli or contribute to a larger extent to NVU dysfunction.

Since our studies, together with previous literature, show that pericytes in the NVU are affected in pathological conditions, therapeutical approaches aiming to restore pericytes have the potential to improve barrier integrity. Experimental studies of transplanting pericyte-like cells or stem cell-derived progenitors in the eye and brain have demonstrated promising results: integration into the vasculature, restoring barrier integrity and ameliorating retinal and cerebral function [66-68]. Cell-based therapy may be an attractive therapeutic option for improving barrier function. However, major hurdles need to be overcome, including costs, delivery approach, adverse effects of the therapy, and the technical, manufacturing and regulatory challenges. Furthermore, future therapeutic approaches may benefit from targeting multiple cell types within the NVU, rather than focusing on a single cell type, as neurological diseases often involve dysfunction of several cell types.

Concluding remarks

The studies presented in this thesis advance our understanding of the cellular mechanisms underlying NVU disruption and BRB and BBB dysfunction. The NVU relies on coordinated interactions among its cellular and intercellular components to support proper neuronal function. In both type 2 DM and AD, NVU integrity is compromised in the eye and the brain. However, our findings indicate distinct pathological patterns in these tissues, both in human post-mortem tissue and in a mouse model of AD. Notably, there is no cerebral equivalent of DR. Further investigations are needed for the understanding of cellular and molecular mechanisms underlying BRB and BBB dysfunction for optimal diagnosis, monitoring and treatment of eye diseases, such as DR, and neurovascular disorders. In this context, zebrafish provide a valuable *in vivo* model for dissecting the mechanisms of blood-barrier breakdown.

References

[1] Rowsthorn E, Pham W, Nazem-Zadeh MR, Law M, Pase MP, Harding IH (2023) Imaging the neurovascular unit in health and neurodegeneration: a scoping review of interdependencies between MRI measures. Fluids Barriers CNS 20(1): 97. doi: 10.1186/s12987-023-00499-0

[2] Yu X, Ji C, Shao A (2020) Neurovascular Unit Dysfunction and Neurodegenerative Disorders. Front Neurosci 14: 334. doi: 10.3389/fnins.2020.00334

[3] Klaassen I, Van Noorden CJ, Schlingemann RO (2013) Molecular basis of the inner blood-retinal barrier and its breakdown in diabetic macular edema and other pathological conditions. Prog Retin Eye Res 34: 19–48. doi: 10.1016/j.preteyeres.2013.02.001

[4] Little K, Llorian-Salvador M, Scullion S, Hernandez C, Simo-Servat O, Del Marco A, et al. (2022) Common pathways in dementia and diabetic retinopathy: understanding the mechanisms of diabetes-related cognitive decline. Trends Endocrinol Metab 33(1): 50–71. doi: 10.1016/j.tem.2021.10.008

[5] Nian S, Lo ACY, Mi Y, Ren K, Yang D (2021) Neurovascular unit in diabetic retinopathy: pathophysiological roles and potential therapeutical targets. Eye Vis (Lond) 8(1): 15. doi: 10.1186/s40662-021-00239-1

[6] Lu D, Ma R, Xie Q, Xu Z, Yuan J, Ren M, et al. (2021) Application and advantages of zebrafish model in the study of neurovascular unit. Eur J Pharmacol 910: 174483. doi: 10.1016/j.ejphar.2021.174483

[7] London A, Benhar I, Schwartz M (2013) The retina as a window to the brain-from eye research to CNS disorders. Nat Rev Neurol 9(1): 44–53. doi: 10.1038/nrneurol.2012.227

[8] Doustar J, Torbati T, Black KL, Koronyo Y, Koronyo-Hamaoui M (2017) Optical Coherence Tomography in Alzheimer's Disease and Other Neurodegenerative Diseases. Front Neurol 8: 701. doi: 10.3389/fneur.2017.00701

[9] Gaire BP, Koronyo Y, Fuchs DT, Shi H, Rentsendorj A, Danziger R, et al. (2024) Alzheimer's disease pathophysiology in the Retina. Prog Retin Eye Res 101: 101273. doi: 10.1016/j.preteyeres.2024.101273

[10] Jin Z, Wang X, Lang Y, Song Y, Zhan H, Shama W, et al. (2025) Retinal optical coherence tomography intensity spatial correlation features as new biomarkers for confirmed Alzheimer's disease. Alzheimers Res Ther 17(1): 33. doi: 10.1186/s13195-025-01676-z

[11] Parisi V, Restuccia R, Fattapposta F, Mina C, Bucci MG, Pierelli F (2001) Morphological and functional retinal impairment in Alzheimer's disease patients. Clin Neurophysiol 112(10): 1860–1867. doi: 10.1016/s1388-2457(01)00620-4

[12] Forner S, Kawauchi S, Balderrama-Gutierrez G, Kramar EA, Matheos DP, Phan J, et al. (2021) Systematic phenotyping and characterization of the 5xFAD mouse model of Alzheimer's disease. Sci Data 8(1): 270. doi: 10.1038/s41597-021-01054-y

[13] Priori EC, Musi CA, Giani A, Colnaghi L, Milic I, Devitt A, et al. (2023) JNK Activation Correlates with Cognitive Impairment and Alteration of the Post-Synaptic Element in the 5xFAD AD Mouse Model. Cells 12(6). doi: 10.3390/cells12060904

[14] Buccarello L, Sclip A, Sacchi M, Castaldo AM, Bertani I, ReCecconi A, et al. (2017) The c-jun N-terminal kinase plays a key role in ocular degenerative changes in a mouse model of Alzheimer disease suggesting a correlation between ocular and brain pathologies. Oncotarget 8(47): 83038–83051. doi: 10.18632/oncotarget.19886

[15] Wang L, Mao X (2021) Role of Retinal Amyloid-beta in Neurodegenerative Diseases: Overlapping Mechanisms and Emerging Clinical Applications. Int J Mol Sci 22(5). doi: 10.3390/ijms22052360

[16] Wijesinghe P, Hosseini A, Campbell M, Tejpal S, Haynes J, Xi J, et al. (2025) Decoding amyloid beta clearance systems at inner blood-retina barrier using three-dimensional ex vivo retinal imaging in Alzheimer's disease. Alzheimers Dement 21(9): e70592. doi: 10.1002/alz.70592

[17] Palacios AG, Zhang SX, Acosta ML (2025) Diabetic retinopathy and Alzheimer's disease: Convergence of the unfolded protein response in neurodegeneration. Alzheimers Dement 21(8): e70497. doi: 10.1002/alz.70497
[18] Rask-Madsen C, King GL (2013) Vascular complications of diabetes: mechanisms of injury and protective factors. Cell Metab 17(1): 20–33. doi: 10.1016/j.cmet.2012.11.012
[19] Frey T, Antonetti DA (2011) Alterations to the blood-retinal barrier in diabetes: cytokines and reactive oxygen species. Antioxid Redox Signal 15(5): 1271–1284. doi: 10.1089/ars.2011.3906
[20] Li M, Yang L, Zhai H, Qiao L, Wang Z, An X, et al. (2025) A new perspective on protecting the blood-retinal barrier against injury in diabetic retinopathy: mitophagy. Front Endocrinol (Lausanne) 16: 1617797. doi: 10.3389/fendo.2025.1617797
[21] Rudraraju M, Narayanan SP, Somanath PR (2020) Regulation of blood-retinal barrier cell-junctions in diabetic retinopathy. Pharmacol Res 161: 105115. doi: 10.1016/j.phrs.2020.105115
[22] Rodriguez-Giraldo M, Gonzalez-Reyes RE, Ramirez-Guerrero S, Bonilla-Trilleras CE, Guardo-Maya S, Nava-Mesa MO (2022) Astrocytes as a Therapeutic Target in Alzheimer's Disease-Comprehensive Review and Recent Developments. Int J Mol Sci 23(21). doi: 10.3390/ijms232113630
[23] Huang M, Long A, Hao L, Shi Z, Zhang M (2025) Astrocyte in Neurological Disease: Pathogenesis and Therapy. MedComm (2020) 6(8): e70299. doi: 10.1002/mco2.70299
[24] Kumar A, Fontana IC, Nordberg A (2023) Reactive astrogliosis: A friend or foe in the pathogenesis of Alzheimer's disease. J Neurochem 164(3): 309–324. doi: 10.1111/jnc.15565
[25] Soto-Rojas LO, Pacheco-Herrero M, Martinez-Gomez PA, Campa-Cordoba BB, Apatiga-Perez R, Villegas-Rojas MM, et al. (2021) The Neurovascular Unit Dysfunction in Alzheimer's Disease. Int J Mol Sci 22(4). doi: 10.3390/ijms22042022
[26] Nehra G, Bauer B, Hartz AMS (2022) Blood-brain barrier leakage in Alzheimer's disease: From discovery to clinical relevance. Pharmacol Ther 234: 108119. doi: 10.1016/j.pharmthera.2022.108119
[27] Wang N, Yang X, Zhao Z, Liu D, Wang X, Tang H, et al. (2023) Cooperation between neurovascular dysfunction and Abeta in Alzheimer's disease. Front Mol Neurosci 16: 1227493. doi: 10.3389/fnmol.2023.1227493
[28] Tarawneh R (2023) Microvascular Contributions to Alzheimer Disease Pathogenesis: Is Alzheimer Disease Primarily an Endotheliopathy? Biomolecules 13(5). doi: 10.3390/biom13050830
[29] De Silva TM, Faraci FM (2016) Microvascular Dysfunction and Cognitive Impairment. Cell Mol Neurobiol 36(2): 241–258. doi: 10.1007/s10571-015-0308-1
[30] Li HY, Yuan Y, Fu YH, Wang Y, Gao XY (2020) Hypoxia-inducible factor-1alpha: A promising therapeutic target for vasculopathy in diabetic retinopathy. Pharmacol Res 159: 104924. doi: 10.1016/j.phrs.2020.104924
[31] Gnanasambandam B, Prince J, Limaye S, Moran E, Lee B, Huynh J, et al. (2024) Addressing retinal hypoxia: pathophysiology, therapeutic innovations, and future prospects. Ther Adv Ophthalmol 16: 25158414241280187. doi: 10.1177/25158414241280187
[32] Bosma EK, van Noorden CJF, Schlingemann RO, Klaassen I (2018) The role of plasmalemma vesicle-associated protein in pathological breakdown of blood-brain and blood-retinal barriers: potential novel therapeutic target for cerebral edema and diabetic macular edema. Fluids Barriers CNS 15(1): 24. doi: 10.1186/s12987-018-0109-2
[33] Schlingemann RO, Hofman P, Andersson L, Troost D, vanderGaag R (1997) Vascular expression of endothelial antigen PAL-E indicates absence of blood-ocular barriers in the normal eye. Ophthalmic Res 29(3): 130–138. doi: Doi 10.1159/000268007
[34] Schlingemann RO, Hofman P, Vrensen GF, Blaauwgeers HG (1999) Increased expression of endothelial antigen PAL-E in human diabetic retinopathy correlates with microvascular leakage. Diabetologia 42(5): 596–602. doi: 10.1007/s001250051200
[35] Monsour M, Borlongan CV (2023) Neurovascular unit permeability in neuroinflammatory diseases: a common pathologic and therapeutic target? Neural Regen Res 18(8): 1715–1716. doi: 10.4103/1673-5374.363197
[36] Iadecola C (2004) Neurovascular regulation in the normal brain and in Alzheimer's disease. Nat Rev Neurosci 5(5): 347–360. doi: 10.1038/nrn1387

[37] Niazi SK (2023) Non-Invasive Drug Delivery across the Blood-Brain Barrier: A Prospective Analysis. Pharmaceutics 15(11). doi: 10.3390/pharmaceutics15112599
[38] Thevenot E, Jordao JF, O'Reilly MA, Markham K, Weng YQ, Foust KD, et al. (2012) Targeted delivery of self-complementary adeno-associated virus serotype 9 to the brain, using magnetic resonance imaging-guided focused ultrasound. Hum Gene Ther 23(11): 1144–1155. doi: 10.1089/hum.2012.013
[39] Raymond SB, Treat LH, Dewey JD, McDannold NJ, Hynynen K, Bacskai BJ (2008) Ultrasound enhanced delivery of molecular imaging and therapeutic agents in Alzheimer's disease mouse models. PLoS One 3(5): e2175. doi: 10.1371/journal.pone.0002175
[40] Nisbet RM, Van der Jeugd A, Leinenga G, Evans HT, Janowicz PW, Gotz J (2017) Combined effects of scanning ultrasound and a tau-specific single chain antibody in a tau transgenic mouse model. Brain 140(5): 1220–1230. doi: 10.1093/brain/awx052
[41] Kinoshita M, McDannold N, Jolesz FA, Hynynen K (2006) Noninvasive localized delivery of Herceptin to the mouse brain by MRI-guided focused ultrasound-induced blood-brain barrier disruption. Proc Natl Acad Sci U S A 103(31): 11719–11723. doi: 10.1073/pnas.0604318103
[42] Diaz RJ, McVeigh PZ, O'Reilly MA, Burrell K, Bebenek M, Smith C, et al. (2014) Focused ultrasound delivery of Raman nanoparticles across the blood-brain barrier: potential for targeting experimental brain tumors. Nanomedicine 10(5): 1075–1087. doi: 10.1016/j.nano.2013.12.006
[43] Woodworth G, Anastasiadis P, Bettegowda C, Chabros J, Chen CX, Ozair A, et al. (2025) Multicenter trial of microbubble-enhanced transcranial focused ultrasound (MB-FUS) with monthly adjuvant temozolomide for patients with high-grade gliomas. J Clin Oncol 43(16_Suppl): 2009–2009. doi: 10.1200/JCO.2025.43.16_suppl.2009
[44] Hjouj M, Last D, Guez D, Daniels D, Sharabi S, Lavee J, et al. (2012) MRI study on reversible and irreversible electroporation induced blood brain barrier disruption. PLoS One 7(8): e42817. doi: 10.1371/journal.pone.0042817
[45] Cuccurazzu B, Leone L, Podda MV, Piacentini R, Riccardi E, Ripoli C, et al. (2010) Exposure to extremely low-frequency (50 Hz) electromagnetic fields enhances adult hippocampal neurogenesis in C57BL/6 mice. Exp Neurol 226(1): 173–182. doi: 10.1016/j.expneurol.2010.08.022
[46] Zhu Z, Zhai Y, Hao Y, Wang Q, Han F, Zheng W, et al. (2022) Specific anti-glioma targeted-delivery strategy of engineered small extracellular vesicles dual-functionalised by Angiopep-2 and TAT peptides. J Extracell Vesicles 11(8): e12255. doi: 10.1002/jev2.12255
[47] Reynolds JL, Mahajan SD (2020) Transmigration of Tetraspanin 2 (Tspan2) siRNA Via Microglia Derived Exosomes across the Blood Brain Barrier Modifies the Production of Immune Mediators by Microglia Cells. J Neuroimmune Pharmacol 15(3): 554–563. doi: 10.1007/s11481-019-09895-6
[48] Ma F, Yang L, Sun Z, Chen J, Rui X, Glass Z, et al. (2020) Neurotransmitter-derived lipidoids (NT-lipidoids) for enhanced brain delivery through intravenous injection. Sci Adv 6(30): eabb4429. doi: 10.1126/sciadv.abb4429
[49] van der Wijk AE, Vogels IMC, van Veen HA, van Noorden CJF, Schlingemann RO, Klaassen I (2018) Spatial and temporal recruitment of the neurovascular unit during development of the mouse blood-retinal barrier. Tissue Cell 52: 42–50. doi: 10.1016/j.tice.2018.03.010
[50] Feng L, Gao L (2024) The role of neurovascular coupling dysfunction in cognitive decline of diabetes patients. Front Neurosci 18: 1375908. doi: 10.3389/fnins.2024.1375908
[51] El-Ghazawi K, Eyo UB, Peirce SM (2024) Brain Microvascular Pericyte Pathology Linking Alzheimer's Disease to Diabetes. Microcirculation 31(7): e12877. doi: 10.1111/micc.12877
[52] Halliday MR, Rege SV, Ma Q, Zhao Z, Miller CA, Winkler EA, et al. (2016) Accelerated pericyte degeneration and blood-brain barrier breakdown in apolipoprotein E4 carriers with Alzheimer's disease. J Cereb Blood Flow Metab 36(1): 216–227. doi: 10.1038/jcbfm.2015.44
[53] Sengillo JD, Winkler EA, Walker CT, Sullivan JS, Johnson M, Zlokovic BV (2013) Deficiency in mural vascular cells coincides with blood-brain barrier disruption in Alzheimer's disease. Brain Pathol 23(3): 303–310. doi: 10.1111/bpa.12004

[54] Kirabali T, Rust R, Rigotti S, Siccoli A, Nitsch RM, Kulic L (2020) Distinct changes in all major components of the neurovascular unit across different neuropathological stages of Alzheimer's disease. Brain Pathol 30(6): 1056–1070. doi: 10.1111/bpa.12895
[55] Schultz N, Brannstrom K, Byman E, Moussaud S, Nielsen HM, Netherlands Brain B, et al. (2018) Amyloid-beta 1-40 is associated with alterations in NG2+ pericyte population ex vivo and in vitro. Aging Cell 17(3): e12728. doi: 10.1111/acel.12728
[56] Ding R, Hase Y, Ameen-Ali KE, Ndung'u M, Stevenson W, Barsby J, et al. (2020) Loss of capillary pericytes and the blood-brain barrier in white matter in poststroke and vascular dementias and Alzheimer's disease. Brain Pathol 30(6): 1087–1101. doi: 10.1111/bpa.12888
[57] Hase Y, Jobson D, Cheong J, Gotama K, Maffei L, Hase M, et al. (2024) Hippocampal capillary pericytes in post-stroke and vascular dementias and Alzheimer's disease and experimental chronic cerebral hypoperfusion. Acta Neuropathol Commun 12(1): 29. doi: 10.1186/s40478-024-01737-8
[58] Fernandez-Klett F, Brandt L, Fernandez-Zapata C, Abuelnor B, Middeldorp J, Sluijs JA, et al. (2020) Denser brain capillary network with preserved pericytes in Alzheimer's disease. Brain Pathol 30(6): 1071–1086. doi: 10.1111/bpa.12897
[59] Ding R, Hase Y, Burke M, Foster V, Stevenson W, Polvikoski T, et al. (2021) Loss with ageing but preservation of frontal cortical capillary pericytes in post-stroke dementia, vascular dementia and Alzheimer's disease. Acta Neuropathol Commun 9(1): 130. doi: 10.1186/s40478-021-01230-6
[60] Im K, Mareninov S, Diaz MFP, Yong WH (2019) An Introduction to Performing Immunofluorescence Staining. Methods Mol Biol 1897: 299–311. doi: 10.1007/978-1-4939-8935-5_26
[61] Piña R, Santos-Díaz AI, Orta-Salazar E, Aguilar-Vazquez AR, Mantellero CA, Acosta-Galeana I, et al. (2022) Ten Approaches That Improve Immunostaining: A Review of the Latest Advances for the Optimization of Immunofluorescence. International Journal of Molecular Sciences 23(3). doi: 10.3390/ijms23031426
[62] Sicherre E, Favier AL, Riccobono D, Nikovics K (2021) Non-Specific Binding, a Limitation of the Immunofluorescence Method to Study Macrophages In Situ. Genes (Basel) 12(5). doi: 10.3390/genes12050649
[63] Zhang J, Chen C, Hua S, Liao H, Wang M, Xiong Y, et al. (2017) An updated meta-analysis of cohort studies: Diabetes and risk of Alzheimer's disease. Diabetes Res Clin Pract 124: 41–47. doi: 10.1016/j.diabres.2016.10.024
[64] Dias Moura Prazeres PH, Sena IFG, Borges IDT, de Azevedo PO, Andreotti JP, de Paiva AE, et al. (2017) Pericytes are heterogeneous in their origin within the same tissue. Dev Biol 427(1): 6–11. doi: 10.1016/j.ydbio.2017.05.001
[65] Bakker N, Croes AA, Prevaes E, van Noorden CJF, Schlingemann RO, Klaassen I (2025) Development of Immunostaining Protocols for 3D Visualization of Pericytes in Human Retinal Flatmounts. J Histochem Cytochem: 221554251323655. doi: 10.1369/00221554251323655
[66] Mendel TA, Clabough EB, Kao DS, Demidova-Rice TN, Durham JT, Zotter BC, et al. (2013) Pericytes derived from adipose-derived stem cells protect against retinal vasculopathy. PLoS One 8(5): e65691. doi: 10.1371/journal.pone.0065691
[67] D'Esposito F, Cappellani F, Visalli F, Capobianco M, Rapisarda L, Avitabile A, et al. (2025) Pericytes as Key Players in Retinal Diseases: A Comprehensive Narrative Review. Biology (Basel) 14(7). doi: 10.3390/biology14070736
[68] Lu MH, Ji WL, Chen H, Sun YY, Zhao XY, Wang F, et al. (2021) Intranasal Transplantation of Human Neural Stem Cells Ameliorates Alzheimer's Disease-Like Pathology in a Mouse Model. Front Aging Neurosci 13: 650103. doi: 10.3389/fnagi.2021.650103

Appendices

English summary

Exploring the divergence: the neurovascular unit in the eye and brain in diabetes and Alzheimer's disease

The retina and brain contain specialized blood vessels that form highly selective barriers, which restrict the free movement of molecules and cells. These barriers are essential for protecting and regulating the local microenvironment necessary for proper neuronal function. The properties of these barriers are regulated by the neurovascular unit (NVU), a complex multicellular structure composed of endothelial cells, pericytes, macroglia, microglia, and neurons. Disruption of the NVU can compromise barrier integrity, leading to vascular leakage and neuronal damage. Both diabetes mellitus (DM) and Alzheimer's disease (AD) are associated with vascular abnormalities and neurodegenerative processes involving the NVU in the eye and brain, respectively. Additionally, individuals with type 2 DM are at an increased risk of developing AD. However, the precise characteristics of these pathological structural and functional changes in the retina and brain and the mechanisms driving them remain poorly understood. While it is known that DM can lead to diabetic retinopathy (DR), the impact of DM on the brain NVU and its possible role in AD development in DM have yet to be fully explored. In this thesis, we aimed to investigate the alterations in the NVU within the retina and brain, especially focussing on DM and its associated increased risk of AD.

In **Chapter 2**, we present a newly developed *in vivo* pathological model designed to investigate blood-brain barrier (BBB) integrity, utilizing zebrafish larvae. As a proof of concept, we induced hyperglycaemia to trigger BBB leakage. The techniques employed to comprehensively assess BBB integrity include: 1) live imaging in *Tg(fli1:EGFP)* zebrafish to visualise the cerebral vasculature and quantify vascular permeability via fluorescent tracer extravasation; 2) fluorescent reporter imaging in transgenic zebrafish lines to examine the expression of the tight junction protein claudin-5, as well as PLVAP, a marker for immature and pathological barrier endothelium involved in transcellular transport; and 3) transmission electron microscopy to investigate tight junction structures. This methodological toolbox provides a valuable foundation for utilizing zebrafish models to dissect the molecular mechanisms of blood-barrier breakdown, with important implications for studying diabetic macular oedema and other neurovascular diseases.

In **Chapter 3**, we report retinal alterations in the 5xFAD mouse model of AD. In this model, both synaptic dysfunction and gliosis were observed in the retina. At 4 and 10 months of age, 5xFAD mice showed an increased thickness of both the total retina and the inner retinal layer, which may be indicative of Müller cell swelling and gliotic remodelling. In contrast to the amyloid pathology observed in the brain of 5xFAD mice, minimal accumulation of amyloid precursor protein (APP) and amyloid beta 42 (Aβ42) was found in the retina. Furthermore, while the c-Jun N-terminal kinase (JNK) signaling pathway is activated in the brain, no activation of this pathway was observed in the retinal tissue of 5xFAD mice. The weak JNK activation and amyloid pathology observed in the retinal tissue, in contrast to the pronounced pathology in the brain, suggests a divergence between retinal and cerebral AD pathologies.

In **Chapter 4**, we characterized and compared NVU alterations in the retina of type 2 DM and DR patients, and in the brain of type 2 DM and AD patients, using unique human tissue samples. We studied relevant surrogate markers of vascular parameters, including vascular permeability, tight junction integrity, transcytosis, and vascular coverage of pericytes, in both the human retina and brain. Our quantitative analysis revealed that DM affects vascular parameters differently in the brain compared to the retina. In AD, NVU alterations in the brain were similar to those observed in the DM retina for most of the NVU markers. NVU disruption was most severe in patients with both DM and AD, exceeding the damage observed in either condition alone. This was evidenced by the highest vascular permeability, the most pronounced alterations in endothelial paracellular and transcellular transport, and the greatest delocalization of astrocytic water channels. This explorative analysis in a small cohort also highlighted correlations between several altered NVU characteristics in the retina of DM patients and in the brain of DM and AD patients.

Chapter 5 outlines the development of an optimized immunofluorescence staining protocol to visualise pericytes in 3D in human retinal flatmounts. Human retinal pericytes express platelet-derived growth factor receptor beta (PDGFRβ), nerve/glial antigen 2 (NG2), and alpha smooth muscle actin (αSMA). The use of retinal flatmounts enables comprehensive 3D visualization of pericyte distribution across the entire retinal vascular network. Key refinements to the methodology included optimization of the fixation procedure, blocking buffer composition, antibody solvent, and the incorporation of jasplakinolide to enhance αSMA detection. These improvements were essential for establishing a reliable immunofluorescence staining approach to study pericyte characteristics in the retina.

This optimized protocol was then applied to examine pericyte coverage and density in human retinal flatmounts from individuals with type 2 DM and DR, as discussed in **Chapter 6**. Compared to non-DM controls, retinas from DM and DR patients showed significant reductions in pericyte density. In non-DR DM retinas, there was a notable decrease in the vascular coverage of NG2 and PDGFRβ. In DR retinas, reductions in PDGFRβ coverage were more pronounced, along with a decrease in αSMA staining. In addition to retinal analysis, we investigated pericyte characteristics in the human frontal cortex in DM and AD. We found subtle reductions in NG2 vascular coverage in frontal cortex samples from DM and AD donors, as well as from those with both DM and AD, though there were no statistically significant changes in pericyte density. Notably, PDGFRβ staining coverage was reduced in individuals with both DM and AD. We did not observe αSMA staining of pericytes in any of the brain samples. Taken together, these findings suggested distinct tissue-specific pathogenic mechanisms affecting pericytes in the brain in DM and AD, contrasting with the well-characterized pericyte loss observed in the retina of individuals with early pre-clinical DR in DM.

Conclusions and future perspectives

Finally, in **Chapter 7**, we present a broader discussion of the novel findings and hypotheses from this thesis, contextualized within the current body of research and the objectives and study questions of the RECOGNISED project. We discuss the use of zebrafish as an *in vivo* model to further investigate the molecular mechanisms involved in NVU disruption. Our work in human and mouse models demonstrates that the NVUs in the eye and brain are affected in both DM and AD. However, we identified differential pathologies in the retina and

brain in both human post-mortem tissues and in a mouse model of AD. Finally, in patients with both DM and AD, specific and more pronounced changes occurred. Future research should focus on elucidating the cellular and molecular processes driving dysfunction of the blood-retinal barrier and BBB in DM, DR and AD. Such insights will be crucial for understanding the pathophysiology of these diseases, but also for improving diagnostic strategies, monitoring disease progression, and expanding treatment.

Nederlandse samenvatting

Neurovasculaire Verschillen tussen Oog en Hersenen bij Diabetes en de Ziekte van Alzheimer

De retina en de hersenen hebben gespecialiseerde bloedvaten die zeer selectieve barrières vormen en die de vrije beweging van moleculen en cellen beperken. Deze barrières zijn essentieel voor het beschermen en reguleren van de lokale micro-omgeving die nodig is voor een goede neuronale functie. De eigenschappen van deze barrières worden gereguleerd door de neurovasculaire eenheid (NVE), een complexe multicellulaire structuur bestaande uit endotheelcellen, pericyten, macroglia, microglia en neuronen. Verstoring van de NVE kan de integriteit van de barrière aantasten, wat leidt tot vaatlekkage en neuronale schade. Zowel diabetes mellitus (DM) als de ziekte van Alzheimer (AD) worden geassocieerd met vasculaire afwijkingen en met neurodegeneratieve processen van de NVE in respectievelijk het oog en de hersenen. Bovendien hebben personen met DM type 2 een verhoogd risico om AD te ontwikkelen. De precieze kenmerken van deze pathologische structurele en functionele veranderingen in de retina en de hersenen en de onderliggende mechanismen, zijn echter nog steeds onvoldoende begrepen. Hoewel bekend is dat DM kan leiden tot diabetische retinopathie (DR), is de impact van DM op de NVE in de hersenen en de mogelijke rol in de ontwikkeling van AD in DM nog niet volledig onderzocht. In dit proefschrift was onze doelstelling om de veranderingen in de NVE in de retina en de hersenen te onderzoeken, met name in relatie tot DM en het daarmee samenhangende verhoogde risico op AD.

In **Hoofdstuk 2** presenteren we een nieuw *in vivo* pathologisch model, ontworpen om de integriteit van de bloed-hersenbarrière (BHB) te onderzoeken met behulp van zebravissenlarven. Als bewijs van concept induceerden we hyperglycemie om lekkage van de BHB te veroorzaken. De gebruikte technieken om de BHB-integriteit uitgebreid te beoordelen, zijn: 1) live imaging in *Tg(fli1:EGFP)* zebravissen om de cerebrale vasculatuur te visualiseren en de vasculaire permeabiliteit te kwantificeren via extravasatie van fluorescente tracers; 2) fluorescentie reporter imaging in transgene zebravissenlijnen om de expressie van het tight junction-eiwit claudine-5 te onderzoeken, evenals PLVAP, een marker voor immatuur en pathologisch barrière-endotheel dat betrokken is bij transcellulair transport; en 3) transmissie-elektronenmicroscopie om tight junction-structuren te onderzoeken. Deze methodologische toolbox biedt een waardevolle basis voor het gebruik van zebravismodellen om de moleculaire mechanismen van bloed-barrière afbraak te ontrafelen, met belangrijke implicaties voor het bestuderen van diabetisch macula-oedeem en andere neurovasculaire aandoeningen.

In **Hoofdstuk 3** beschrijven we retinale veranderingen in het 5xFAD-muismodel van AD. In dit model werden zowel synaptische disfunctie als activatie van gliale cellen (gliose) in de retina waargenomen. Bij 4 en 10 maanden oude 5xFAD-muizen was er een toegenomen dikte van zowel de totale retina als de binnenste retinale laag, wat mogelijk duidt op zwelling van de Müller-cellen en reactieve gliacelveranderingen. In tegenstelling tot de amyloïde pathologie in de hersenen van 5xFAD-muizen, werd er minimale ophoping van amyloïde precursorproteïne (APP) en amyloïde bèta 42 (Aβ42) in de retina gevonden. Bovendien, hoewel de c-Jun N-terminale kinase (JNK)-signaalroute geactiveerd is in de hersenen, zagen we geen activatie van deze route in het retinale weefsel van 5xFAD-muizen. De zwakke JNK-

activatie en amyloïde pathologie in het retinale weefsel, in tegenstelling tot de uitgesproken pathologie in de hersenen, suggereert een divergentie tussen retinale en cerebrale AD-pathologie.

Hoofdstuk 4 beschrijft de karakterisering en vergelijking van NVE-veranderingen in de retina van patiënten met DM type 2 en DR, en in de hersenen van patiënten met DM type 2 en AD, met behulp van unieke menselijke weefsels. We bestudeerden relevante surrogaatmarkers voor vasculaire parameters, waaronder vasculaire permeabiliteit, integriteit van tight junctions, transcytose en vasculaire bedekking van pericyten, in zowel de humane retina als de hersenen. Onze kwantitatieve analyse toonde aan dat DM vasculaire parameters anders beïnvloedt in de hersenen dan in de retina. Bij AD waren de NVE-veranderingen in de hersenen vergelijkbaar met die in de DM-retina voor de meeste NVE-markers. De verstoring van de NVE was het ernstigst bij patiënten met zowel DM als AD, en overtrof de schade die werd waargenomen bij elk van beide aandoeningen afzonderlijk. Dit bleek uit de hoogste vasculaire permeabiliteit, de meest uitgesproken veranderingen in het paracellulaire en transcellulaire endotheeltransport, en de sterkste verplaatsing van astrocytaire waterkanalen. Deze exploratieve analyse in een klein cohort bracht bovendien correlaties aan het licht tussen verschillende veranderde NVE-kenmerken in de retina van DM-patiënten en in de hersenen van DM- en AD-patiënten die in toekomstige studies nader dienen te worden onderzocht.

Hoofdstuk 5 beschrijft de ontwikkeling van een geoptimaliseerd immunofluorescentie kleuringsprotocol om pericyten in 3D te visualiseren in humane retinale flatmount preparaten. Humane retinale pericyten brengen de platelet-derived growth factor receptor bèta (PDGFRβ), nerve/glial antigen 2 (NG2), en alpha smooth muscle actin (αSMA) tot expressie. Het gebruik van retinale flatmounts maakt een uitgebreide 3D-visualisatie mogelijk van de verdeling van pericyten over het gehele retinale vaatnetwerk. Belangrijke verfijningen van de methodologie omvatten de optimalisatie van de fixatieprocedure, de samenstelling van de blokkeerbuffer, het antilichaam oplosmiddel en de incorporatie van jasplakinolide om de detectie van αSMA te verbeteren. Deze verbeteringen waren essentieel om een betrouwbare immunofluorescentiekleuring te ontwikkelen voor het bestuderen van pericyt kenmerken in de retina.

Dit geoptimaliseerde protocol werd vervolgens toegepast om de pericyt bedekking en -dichtheid te onderzoeken in humane retinale flatmount preparaten van individuen met DM type 2 en DR, zoals besproken in **Hoofdstuk 6**. Vergeleken met controles zonder DM vertoonden retina's van DM- en DR-patiënten een statistisch significante afname van de pericyten dichtheid. In retina's van patiënten met DM zonder DR was er een opmerkelijke afname van de vasculaire bedekking van NG2 en PDGFRβ. In retina's van patiënten met DR waren de afnames in PDGFRβ-bedekking meer uitgesproken, samen met een afname van de αSMA-kleuring. Naast de analyse van de retina onderzochten we ook pericyt kenmerken in de humane frontale cortex bij DM en AD. We vonden subtiele verminderingen in de NG2-vasculaire dekking in de frontale cortex van DM- en AD-donoren, net als van donoren met zowel DM als AD, terwijl de pericyten dichtheid onveranderd bleef. Opvallend was de vermindering van de PDGFRβ-kleuring in individuen met zowel DM als AD. We vonden geen αSMA-kleuring in de pericyten in de hersenen. Al met al wijzen deze bevindingen op verschillende weefselspecifieke pathogene mechanismen die pericyten in de hersenen bij

DM en AD beïnvloeden, in tegenstelling tot het goed gekarakteriseerde pericytenverlies in de retina van individuen met vroege preklinische DR in DM.

Conclusies en toekomstperspectieven

Tot slot presenteren we in **Hoofdstuk 7** een discussie over de nieuwe bevindingen en hypothesen uit dit proefschrift, geplaatst in de context van het huidige onderzoeksveld en de doelstellingen en onderzoeksvragen van het RECOGNISED-project. We bespreken het gebruik van zebravissen als *in vivo*-model om de moleculaire mechanismen verder te onderzoeken die betrokken zijn bij NVE-disruptie. Ons onderzoek met humane en muismodellen toont aan dat de NVE in het oog en de hersenen zowel bij DM als bij AD worden aangetast. We identificeerden echter verschillen in de pathologische veranderingen in de NVU tussen de retina en de hersenen, zowel in menselijke post-mortem weefsels als in een muismodel van AD. Ten slotte vonden we opvallend juist bij patiënten met zowel DM als AD specifieke en meer uitgesproken veranderingen in de NVE. Toekomstig onderzoek zou zich moeten richten op het ophelderen van de cellulaire en moleculaire processen die de disfunctie van de bloed-retina barrière en de BHB bij DM, DR en AD veroorzaken. Dergelijke inzichten zijn van cruciaal belang voor het begrijpen van de pathofysiologie van deze ziekten, maar ook voor het verbeteren van diagnostische strategieën, het monitoren van de ziekteprogressie en het uitbreiden van de behandelingsmogelijkheden.

List of publications

Publications included in this thesis

Bakker N, Croes AA, Prevaes E, van Noorden CJF, Schlingemann RO, Klaassen I. Development of immunostaining protocols for 3D visualization of pericytes in human retinal flatmounts. J Histochem Cytochem. 2025 Mar-Apr;73(3-4):147-170. doi: 10.1369/00221554251323655.

Bakker-van Bugnum N, Croes AA, Prevaes E, van Noorden CJF, Schlingemann RO and Klaassen I. Differential pericyte pathology in the human retina and brain in diabetes mellitus and Alzheimer's disease. Front. Neurosci. 2026 Feb;20:1749112. doi: 10.3389/fnins.2026.1749112.

Bakker-van Bugnum N, Snijders EE, Hogendorp FEE, van Noorden CJF, Lou L, Vanhollebeke M, Vanhollebeke B, Grootemaat AE, Van der Wel NN, Schlingemann RO, Klaassen I. A zebrafish multimodal toolbox to study the blood-brain barrier in health and disease. Sci Rep. 2026. doi: 10.1038/s41598-026-39616-y. *Accepted for publication.*

Giani A*, Musi CA*, Priori EC, Turchetti S, Passi M, Galbiati S, Viganò I, **Bakker N**, Klaassen I, Zerbini G, Borsello T, on behalf of the RECOGNISED consortium. Revealing subcellular retinal alterations in 5xFAD B6SJLF1/J mice. Exp Neurol. 2026. *Under revision.*

Other publications

Little K, Singh A, Del Marco A, Llorián-Salvador M, Vargas-Soria M, Turch-Anguera M, Solé M, **Bakker N**, Scullion S, Comella JX, Klaassen I, Simó R, Garcia-Alloza M, Tiwari VK, Stitt AW; RECOGNISED consortium. Disruption of cortical cell type composition and function underlies diabetes-associated cognitive decline. Diabetologia. 2023 Aug;66(8):1557-1575. doi: 10.1007/s00125-023-05935-2.

van Noorden CJF, Yetkin-Arik B, Serrano Martinez P, **Bakker N**, van Breest Smallenburg ME, Schlingemann RO, Klaassen I, Majc B, Habic A, Bogataj U, Galun SK, Vittori M, Erdani Kreft M, Novak M, Breznik B, Hira VVV. New Insights in ATP Synthesis as Therapeutic Target in Cancer and Angiogenic Ocular Diseases. J Histochem Cytochem. 2024 May;72(5):329-352. doi: 10.1369/00221554241249515.

van Noorden CJF, Breznik B, Novak M, van Dijck AJ, Tanan S, Vittori M, Bogataj U, **Bakker N**, Khoury JD, Molenaar RJ, Hira VVV. Cell Biology Meets Cell Metabolism: Energy Production Is Similar in Stem Cells and in Cancer Stem Cells in Brain and Bone Marrow. J Histochem Cytochem. 2022 Jan;70(1):29-51. doi: 10.1369/00221554211054585.

Rothgangl T, Dennis MK, Lin PJC, Oka R, Witzigmann D, Villiger L, Qi W, Hruzova M, Kissling L, Lenggenhager D, Borrelli C, Egli S, Frey N, **Bakker N**, Walker JA 2nd, Kadina AP, Victorov DV, Pacesa M, Kreutzer S, Kontarakis Z, Moor A, Jinek M, Weissman D, Stoffel M, van Boxtel R, Holden K, Pardi N, Thöny B, Häberle J, Tam YK, Semple SC, Schwank G. In vivo adenine base editing of PCSK9 in macaques reduces LDL cholesterol levels. Nat Biotechnol. 2021 Aug;39(8):949-957. doi: 10.1038/s41587-021-00933-4.

Cehofski LJ, Kojima K, Kusada N, Hansen MS, Muttuvelu DV, **Bakker N**, Klaassen I, Grauslund J, Vorum H, Honoré B. Central subfield thickness of diabetic macular edema: Correlation with the aqueous humor proteome. Mol Vis. 2024 Feb 10;30:17-35.

Curriculum Vitae

Noëlle Bakker werd geboren op 28 januari 1997 in Alkmaar. In 2009 ging zij naar de Gemeenschappelijke Scholengemeenschap (GSg) te Schagen, waar ze in 2015 haar VWO-diploma met de profielen Natuur en Gezondheid en Natuur en Techniek haalde. Datzelfde jaar startte zij met de opleiding Bio-Farmaceutische Wetenschappen aan de Universiteit Leiden, waar ze tijdens haar minor een paar maanden in Uppsala, Zweden, studeerde. In 2018 haalde ze haar bachelor cum laude, inclusief het Honoursprogramma. In hetzelfde jaar begon ze met de master Bio-Pharmaceutical Sciences aan de Universiteit Leiden. Tijdens deze master heeft zij twee stages gelopen. De eerste stage was bij het Leiden Academic Centre for Drug Research in de groep van Prof. Dr. Alireza Mashaghi, waar zij onderzoek deed naar de heterogeniteit en dysfunctie van mitochondriën in de context van de ziekte van Parkinson. In de zomer van 2019 nam ze deel aan een Summer School aan de China Pharmaceutical University als extracurriculaire activiteit. De tweede stage was aan de Universiteit Zürich in de groep van Dr. Gerald Schwank. Tijdens deze stage hield zij zich bezig met de ontwikkeling van CRISPR base editing als nieuwe therapie voor patiënten met familiale hypercholesterolemie. In 2020 heeft zij haar master cum laude behaald. Vanaf november 2020 begon zij met haar promotieonderzoek in de Oculaire Angiogenese Groep bij de Amsterdam Universitair Medisch Centrum, locatie Academisch Medisch Centrum, in Amsterdam, wat resulteerde in dit proefschrift. Na haar promotie is zij gestart als postdoc in de onderzoeksgroep van Dirk Bumann aan de Universiteit van Bazel in Zwitserland, waar zij onderzoek doet naar bacteriële infecties in menselijk weefsel.

Portfolio

PhD student:	Noëlle Bakker
PhD period:	November 2020 - June 2025
Promotor:	Prof. dr. R.O. Schlingemann
Co-promotores:	Dr. I. Klaassen
	Prof. dr. C.J.F. van Noorden

	Year	ECTS
Courses		
Laboratory safety	2020	0.1
AMC world of science	2021	0.7
Medical literature: PubMed basics and correct citation	2021	0.1
Medical literature: critical approach topics (CAT)	2021	0.1
Scientific writing in English for publication	2021	1.5
Models of the blood-brain barrier (BBB)	2021	0.6
From pixel to publication	2022	1.0
Didactical skills	2022	0.4
Practical biostatistics	2022	2.0
Laboratory animal science	2022	3.9
Advanced microscopy	2022	1.6
Advanced topics in biostatistics	2023	2.1
Basic microscopy	2023	1.5
Career management	2024	0.1
Seminars, workshops and master classes		
T2N lectures	2021-2022	0.5
Swammerdam lectures	2021-2022	0.1
Present like a boss (ASAP)	2021	0.1
PhD retreat	2022	0.6
Conferences and meetings		
ACS symposium microcirculation	2021-2024	0.3
3D-cember Mimetas symposium	2021	0.1
RECOGNISED WP2 meeting	2021	0.1
Ophthalmology department meeting	2021	0.1
Cold spring harbor laboratory barrier meeting	2021	0.9
JIM 17th key symposium: the BBB: key to brain health and disease	2021	0.2

Amsterdam cardiovascular sciences annual conference – Poster presentation	2021/2024	0.5
EASDec conference - poster and oral presentation	2021-2023	0.1
3rd organoplate symposium: 3D-cember	2021	0.1
Alzheimercyclus: risk factors and prevention of dementia	2022	0.1
Wetenschappelijke avond genootschap ter bevordering van natuur-, genees- en heelkunde	2022	0.1
Netherlands vascular biology meeting - oral presentation	2022	2.0
BBBNedwork - pitch presentation	2022	0.5
EASDec conference	2022	0.7
RECOGNISED WP2 meeting June	2022	0.3
BBBNedwork - pitch presentation	2023	0.5
EAsDEC conference - oral presentation	2023	0.7
BBB signaling meeting	2023	0.3
Cerebral vascular biology meeting - poster presentation	2023	1.0
RECOGNISED general meeting	2023	0.3
Netherlands vascular biology organization meeting - oral presentation	2023	1.0
Dutch ophthalmology PhD students meeting - poster presentation	2023	0.4
BBBNedwork - pitch presentation	2024	0.5
The association for research in vision and ophthalmology – poster presentation	2024	1.4
	2024	1.0
International vascular biology meeting - poster presentation	2025	0.2
Amsterdam vascular biology meeting - oral presentation		
BBBNedwork - pitch presentation	2025	0.4

Teaching

Wetlab Ophthalmology, Medicine, UvA	2020-2025	6.0
Mentor Amsterdam UMC mentoring program	2023-2025	0.1
Organising monthly department research meetings	2022-2025	0.3
Supervision Master Student, Cardiovascular Research, VU	2022	3
Supervision Bachelor Student, Medicine and Biomedical Sciences, UvA	2022	1.5
Supervision Master Student, Biomedical Sciences, VU	2023	2
Supervision HBO student, Laboratory Science, Saxion Deventer	2023	2
Supervision Master Student, Biomedical Sciences, UvA	2023-2024	2
Supervision Master Student, Biomedical Sciences, UvA	2023-2024	1.5

Supervision Master Student, Biomedical Sciences, Leiden University	2024	2
Supervision Bachelor Student, Biomedical Sciences, UvA	2024	0.5
Supervision Master Student, Medical Biology, Radboud University	2024-2025	3
Supervision Bachelor Student, Biomedical Sciences, VU	2025	1.5

Dankwoord

Daar is-ie dan! Mijn proefschrift! Na heel wat experimenten en vele uren achter de microscoop en computer heb ik mijn proefschrift afgerond. Ik wist al vrij snel dat onderzoek doen iets is wat echt bij mij past. Daarom kijk ik met veel plezier terug op mijn tijd als PhD-student, hoewel echt niet alles zonder slag of stoot ging. Dit proefschrift is het resultaat van teamwork. Ik wil graag iedereen bedanken die hieraan heeft bijgedragen.

Allereerst ben ik enorm dankbaar voor de kans die ik heb gekregen van mijn promotor Reinier en copromotoren Ingeborg en Ron. **Reinier**, bedankt voor jouw vertrouwen en het delen van jouw kennis over oogheelkunde en het schrijven van manuscripten. Jouw connectie met de kliniek was erg waardevol tijdens onze besprekingen. Met jouw stroom aan ideeën was er altijd iets om mee aan de slag te gaan. Je hebt mij geleerd onze bevindingen als waardevol te zien, ondanks dat ze tegen de huidige theorieën van de “maffia” ingingen. Je noemt jezelf dan ook de wetenschappelijke Robin Hood. Ook heb je de onderzoeksgroep een aantal keer ontvangen in jullie prachtige huis. Bedankt voor deze gastvrijheid.

Ingeborg, jij stond altijd voor mij paraat. Hoe druk je het ook had met het schrijven van manuscripten, subsidieaanvragen, subsidierapporten en de oneindige stroom aan mailtjes, jij maakte altijd tijd vrij om te kunnen overleggen. Jij vond het ook belangrijk dat er af en toe een sociale activiteit op het programma stond, buiten het onderzoek om. Het was heel gezellig om kerst met alle leden van de onderzoeksgroep te vieren en de meegebrachte gerechten te delen. Je bent een gedreven persoon, hebt een scherpe blik en mag trots zijn op jouw werk als PI.

Ron, bedankt voor jouw bijdrage aan mijn promotietraject. Je bent realistisch en hielp mij bij het doorhakken van knopen. Jouw duidelijke manier van communiceren viel me vanaf de eerste werkbespreking al op en dat zal ik meenemen in mijn verdere carrière. Jouw ervaring met het schrijven van manuscripten heeft mij geholpen bij het schrijven van mijn eigen manuscripten. Fijn dat je mij vaak snel van nuttige feedback kon voorzien. Je kunt al een tijdje van je pensioen genieten, maar je bent nog altijd zeer gedreven en gepassioneerd over je vak. Ook al had je soms je twijfels, ik vind dat je altijd nog een waardevolle toevoeging bent voor de groep. Ik hoop dat ik op jouw leeftijd ook nog zo actief ben in de wetenschap en zo goed van geest ben. Ik wens je veel mooie fietsritten en treinreizen, wellicht samen met Dylan.

Lieve (oud-)collega's van de OAG-groep, wat fijn om jullie te leren kennen tijdens mijn promotietraject. Ik heb genoten van de gezelligheid tijdens de lunchpauzes, het buiten zitten in de zon op het gras, onze uitjes met de groep en de congressen. Ook kon ik de katten- en hondenplaatjes zeer waarderen. **Yasmin**, het eerste jaar zaten we samen in het kantoor. Je was een prettige collega en als analist een fijne toevoeging aan de groep. We hebben niet lang een kantoor gedeeld, want je vond een mooie nieuwe uitdaging dichterbij huis. **Esmeralda**, in de eerste paar jaar konden wij onze ervaringen als PhD-student uitwisselen. Ik vond het gezellig om met z’n vieren op kantoor te zitten en jouw verhalen over de kat en de schildpad te horen. Regelmatig fietste je vanuit huis naar werk, sportief! **Maxime**, jij volgde Yasmin op als analist in onze groep. Je was een echte toevoeging voor de groep. Je was zo behendig in het kweken van de organoids en je kunt ook prachtige plaatjes maken met de microscoop. Het was gezellig met jou op kantoor. **Amber**, jij bent alweer een tijdje analist in

onze groep. Ik weet nog goed dat jij gelijk in je eerste week gezellig mee ging naar alle sociale activiteiten van de afdeling. Een goede start om iedereen te leren kennen. Bedankt voor jouw inspanningen in het lab voor de laatste kleuringen. **Mathilda**, ik vond het erg gezellig om met jou gewerkt te hebben. Jouw vermogen om collega's te verbinden kwam goed van pas tijdens het organiseren van sociale activiteiten op de afdeling. Als jij aan de lunchtafel zat, wist je dat het nooit saai was. Super dat jij jezelf hebt hervonden in een nieuwe werkomgeving. Ik wens je veel succes en voldoening in deze nieuwe fase. **Paola**, ik vond het erg gezellig om het kantoor en het lab met jou te delen. Je hebt een goed gevoel voor humor en je toverde regelmatig een lach op de gezichten. Je hebt veel Nederlandse lessen gehad en je voortgang vond ik bewonderingswaardig. Je bent ook zeker een getalenteerde en gedreven onderzoekster. Succes met je verdediging. Ik weet zeker dat je het fantastisch zult doen.

Verder wil ik iedereen van de afdeling Medische Biologie bedanken voor de prettige werksfeer op het lab en de gezelligheid daarbuiten. Ik ben begonnen in 2020, tijdens de coronapandemie, en het heeft daarom een tijd geduurd voordat ik jullie heb leren kennen. De jaarlijkse uitjes met de afdeling waren altijd erg geslaagd, net als de borrels, de excursie naar de kelder, filmavondjes en kerstvieringen. Ik heb ook genoten van de diners in Amsterdam en de random feitjes die werden gedeeld. Met activiteiten zoals Drawful kon iedereen zijn creativiteit kwijt. De 7-minute workout was een perfecte break om ook even lekker in beweging te zijn.

Iedereen bedankt voor het delen van jullie expertise, waaronder **Gabrielle** met haar kennis over de cryostaat en **Ron Hoebe** voor het analyseren van microscopieplaatjes. **Daisy**, je bent een spin in het web, gezellig, staat voor iedereen klaar en in mijn ogen onmisbaar voor onze afdeling. **Eric**, bedankt dat je mijn tv-carrière een kickstart hebt gegeven; wie had gedacht dat ik nog op tv zou komen voor onderzoek, en niet eens mijn eigen onderzoek? Bedankt voor de prettige communicatie om dingen voor de MB3-meeting te regelen. Ik kon lachen om jouw humor en verhalen van vroeger. Over de MB3-meeting gesproken, ook wel de "kroketmeeting"; **Sanne**, ik vond het erg leuk om samen met jou deze meetings te regelen. Ik heb vele inspirerende onderzoeken voorbij zien komen tijdens de meetings. **Anita, Nicole, Theo Verboom, Wilbert Bitter, Walbert Bakker, Kin Ki Jim**, en **leden van het Vanhollebeke-lab**, dank voor jullie bijdrage aan het zebraviswerk.

Ook wil ik alle leden van mijn promotiecommissie bedanken voor het lezen en beoordelen van mijn proefschrift en voor hun deelname aan de commissie. **Elga**, bedankt dat je mijn PhD-counselor wilde zijn en dat ik jullie interessante werkbesprekingen met betrekking tot hersenonderzoek mocht bijwonen.

I would like to thank all the coauthors that contributed to the papers included in this thesis.

Ik wil alle studenten, **Hinke, Alexander, Eva, Eloise, Emma, Sofia, Gwen, Sena, Aïcha en Theo**, bedanken voor hun bijdrage aan mijn onderzoeksprojecten. Ik heb ook veel van jullie mogen leren. Er staat jullie een mooie toekomst te wachten.

Ik heb met plezier wetlab-onderwijs gegeven voor geneeskundestudenten die bij oogheelkunde kwamen kijken. Iedere keer kon ik samen met Ingeborg onze denkbeeldige

bingokaart weer tevoorschijn halen. Daar stond bijvoorbeeld op: 'Spuit er niks uit het oog?', 'Wat is dat zwarte?' en 'Ik kom niet door de sclera heen.' **Armida**, bedankt voor het coördineren van het wetlab-onderwijs.

Lieve **pap, mam, Christiaan, Shannon, Rijn, Carina, Ilona, Pascal** en verdere **(schoon)familie**, dank jullie wel voor jullie interesse in mijn onderzoek, ook al strooide ik soms met moeilijke termen. Fijn dat ik alle hoogte- en dieptepunten met jullie kon delen. De arbeidsethos van mijn ouders was een inspiratie voor mij. Hard werken heeft mij ver gebracht, dank daarvoor. Jullie hebben altijd gezegd dat ik iets moet doen wat ik leuk vind. Dat is gelukt, ik heb mijn plek gevonden!

Lieve **vrienden en vriendinnen**, bedankt voor jullie interesse en steun. Jullie konden mij altijd aan het lachen maken, ook al waren de resultaten op werk soms om te huilen. Met jullie kon ik mijn blijdschap over mijn eerste artikel met eerste auteurschap delen en jullie hebben het zelfs geprobeerd te lezen. Ik heb genoten van de spelletjesavonden, de dansmoves en escaperooms.

Lieve **Maick**, woorden komen te kort om te vertellen wat jij voor mij betekent. Jij bent er altijd voor mij en daar ben ik onwijs dankbaar voor. In deze drukke tijd zorgde jij voor de nodige afwisseling. Ook waardeer ik jouw steun in mijn volgende carrièrestap. Met jou aan mijn zijde kijk ik vol vertrouwen uit naar de toekomst.